JAERI-Conf
99-015

PROCEEDINGS OF THE SYMPOSIUM ON FRONTIER NUCLEAR PHYSICS (FRONP99) AUGUST 2-4, 1999, JAERI, TOKAI, JAPAN

January 2000

(Ed.) Satoshi CHIBA

日本原子力研究所
Japan Atomic Energy Research Institute

本レポートは，日本原子力研究所が不定期に公刊している研究報告書です。
入手の問合わせは，日本原子力研究所研究情報部研究情報課（〒319-1195　茨城県那珂郡東海村）あて，お申し越しください。なお，このほかに財団法人原子力弘済会資料センター（〒319-1195　茨城県那珂郡東海村日本原子力研究所内）で複写による実費頒布をおこなっております。

This report is issued irregularly.
Inquiries about availability of the reports should be addressed to Research Information Division, Department of Intellectual Resources, Japan Atomic Energy Research Institute, Tokai-mura, Naka-gun, Ibaraki-ken, 319-1195, Japan.

編集兼発行　　日本原子力研究所

JAERI-Conf 99-015

Proceedings of the Symposium on Frontier Nuclear Physics (FRONP99)

August 2 - 4, 1999, JAERI, Tokai, Japan

(Ed.) Satoshi CHIBA

Advanced Science Research Center
(Tokai Site)
Japan Atomic Energy Research Institute
Tokai-mura, Naka-gun, Ibaraki-ken

(Received December 14, 1999)

The symposium on Frontier Nuclear Physics (FRONP99), organized by the Research Group for Hadron Science, Advanced Science Research Center, under close cooperation with the Research Center for Nuclear Physics, Osaka University and High Energy Accelerator Research Organization, was held at Tokai Research Establishment of JAERI on August 2 to 4, 1999. The symposium was devoted for discussions and presentations of research results in wide variety of fields such as hyper nuclear physics, lepton nuclear physics, quark nuclear physics, unstable nuclear physics, superheavy elements and heavy-ion physics. Three talks on the joint project between JAERI (Neutron Science Research Center) and KEK (JHF) were presented in a public session. Thirty three talks on these topics presented at the symposium aroused lively discussions among approximately 70 participants. This report contains 26 papers submitted from the lecturers.

Keywords: Proceedings, Joint Project, 50-GeV Accelerator, Hypernuclear Physics, Lepton Nuclear Physics, Quark Nuclear Physics, Unstable Nuclei, Superheavy Elements, Heavy-ion Physics

---

Organizers: H. Toki (RCNP), H. Horiuchi (Kyoto Univ.) , T. Otsuka (Tokyo Univ.), S. Sawada (KEK), A. Iwamoto (Department of Materials Science, JAERI) and S. Chiba (Research Group for Hadron Science, Advanced Science Research Center, JAERI)

JAERI-Conf 99-015

「最前線の原子核物理」研究会 (FRONP99) 報告集

1999 年 8 月 2 日～8 月 4 日、東海研究所、東海村

日本原子力研究所先端基礎研究センター
(編) 千葉　敏

(1999 年 12 月 14 日受理)

「最前線の原子核物理」研究会は、先端基礎研究センター第１６２回基礎科学セミナーとして原研先端基礎研究センター、大阪大学核物理研究センター及び高エネルギー加速器研究機構の協力のもと、1999 年 8 月 2～4 日にかけて、東海研究所にて行われた。内容はハイパー核物理、クォーク核物理、レプトン核物理、不安定原子核、超重元素、重イオン核物理等多岐に渡り、33 件の発表が行われた。そのうち 3 件は原研の中性子科学研究センターと KEK の JHF (Japan Hadron Facility) の統合計画に関する特別講演であった。参加総数は約 70 名で、盛況のうちに全日程を終えた。本レポートは、会議終了後提出された２６本の論文を含むその報告集である。

本研究会の世話人は、大阪大学　土岐　博、京都大学　堀内　昶、東京大学　大塚　孝治、高エネルギー加速器研究機構　澤田　真也、日本原子力研究所　岩本　昭、千葉　敏が担当した。

日本原子力研究所（東海駐在):〒 319-1195 茨城県那珂郡東海村白方白根 2-4

Contents

目 次

1. 「最前線の原子核物理」研究会 (FRONP99) プログラム

日時 : 平成１１年８月２日 (13:00) - ８月４日(15:10)
場所 : 先端基礎研究交流棟大会議室

<<<<<<<<<< ◆ ◆ ◆ ◆ ◆ Aug. 2 (Mon.) ◆ ◆ ◆ ◆ ◆ >>>>>>>>>>

10:00-13:00 Registration

13:00-13:15 Opening session
-Chairman H. Toki(RCNP)-
H. Yasuoka(JAERI) (8) Welcome address
A. Iwamoto(JAERI) (7) Welcome address

13:15-15:05 Hyper Nuclear Physics
-Chairman H. Toki(RCNP)-
H. Tamura(Tohoku) (30) Gamma spectroscopy in hypernuclei
T. Motoba(Osaka-E) (30) Excitement of hypernuclear physics
Y. Akaishi(KEK) (30) Exotic atoms and hypernuclei
E. Hiyama(RIKEN) (20) Few-body aspect of hypernuclear physics

15:05-15:35 Coffee break

15:35-17:45 Quark Nuclear Physics
-Chairman Y. Akaishi(KEK)-
A. Hosaka(Numazu) (30) Flavor SU(3) baryons and quark confinement
M. Oka(Tokyo IT) (30) Roles of quark substructures in hypernuclei
T. Maruyama(JAERI) (30) Color molecular dynamics for dense matter and nuclei
D. Jido (Kyoto) (20) Chiral symmetry in the baryon spectrum
S. Furui (Teikyo) (20) A lattice test of the Kugo-Ojima confinement criteria

18:00 Bus transportation to Akogigaura Club
18:15-20:00 Conference party (Akogigaura Club BC room)

<<<<<<<<<< ◆ ◆ ◆ ◆ ◆ Aug. 3 (Tue.) ◆ ◆ ◆ ◆ ◆ >>>>>>>>>>

9:00-10:30 Lepton Nuclear Physics
-Chairman M. Oka(TIT)-
Y. Kuno(KEK) (30) Lepton flavor violation and beyond standard model
O. Yasuda (TMU) (30) Neutrino mass and the quark-lepton symmetry
K. Suzuki(RCNP) (30) Roles of pions for neutrinoless double beta decay in nuclei

10:30-11:00 Coffee break

11:00-12:00 Quark-lepton nuclear physics
-Chairman T. Otsuka(Tokyo)-
T. Hatsuda(Kyoto) (30) QCD spectral function
T. Inagaki (KEK) (30) Precise Measurement of K->pi,nu,nu decay at JHF

12:00-13:30 Lunch

13:30-14:30 Special session (public)
-Chairman A. Iwamoto(JAERI)-
S. Nagamiya(KEK) (30) Joint Project between KEK and JAERI on High Intensity Accelerators + Thoughts on Exciting Physics
H. Toki (RCNP) (30) Quark Nuclear Physics with JHF
14:30-15:00 Coffee
15:00-15:30 Special session (continued)
T. Mukaiyama(JAERI) (30) Transmutation of long-lived nuclides in nuclear waste

15:30-17:00 Unstable Nuclear Physics
-Chairman Y. Abe (Kyoto-Kiken) -
T. Otsuka(Tokyo) (30) Monte-Carlo shell model for nuclear physics
H. Horiuchi(Kyoto) (30) Anti-symmetrized quantum molecule theory
K. Kato(Hokkaido) (30) Light unstable nuclei in the continuum

17:00-18:30 Superheavy nuclei
-Chairman H. Horiuchi (Kyoto)-
Y. Abe (Kyoto) (30) Theory of synthesis of superheavy elements
T. Wada(Konan) (30) Fission dynamics of heavy and superheavy nuclei
H. Ikezoe(JAERI) (30) Heavy-ion fusion for synthesis of superheavy nuclei

<<<<<<<<<< ◆ ◆ ◆ ◆ ◆ Aug. 4 (Wed.) ◆ ◆ ◆ ◆ ◆ >>>>>>>>>>

9:00-10:30 Atomic Nuclear Physics
-Chairman T. Hatsuda(Kyoto)-

S. Hirenzaki(Nara W)	(30)	Deeply bound pionic states and modifications of hadrons
T. Kishimoto(Osaka)	(30)	Kaonic nuclei and kaon condensation in neutron star
A. Hayashigaki (Kiken)	(30)	Charmed mesons in hadronic matter

10:30-11:00 Coffee

11:00-12:00 Theoretical Quark Nuclear Physics
-Chairman A. Hosaka(Numazu)-

H. Suganuma(RCNP)	(30)	Confinement and color monopoles in QCD
K. Itakura(RCNP)	(30)	Light front quantization and its application

12:00-13:00 Lunch

13:00-15:00 Heavy Ion Nuclear Physics
-Chairman K.Oyamatsu (Aichi)-

Y. Nara (JAERI)	(30)	Relativisitc heavy ion physics
T. Kunihiro(Ryukoku)	(30)	Roles of the sigma meson in QCD and possible experiments to observe it
T. Kido (JAERI)	(20)	Nuclear matter in neutron star crust
T. Maruyama (Nihon)	(20)	Study of in-medium hadronic properties in high energy reactions
G. Mao (JAERI)	(20)	Bound states of negative-energy nucleons in finite nuclei

15:00-15:10 Concluding session

Y. Akaishi(KEK)	(10)	Concluding remark

15:30 Bus transporation to Tokai Station

2. ハイパー核のγ線分光

Gamma Spectroscopy in Hypernuclei

田村 裕和
東北大学 大学院理学研究科

H.Tamura
Department of Physics, Tohoku University, Sendai 980-8578, Japan

Abstract

We have started a project of high-resolution hypernuclear γ-spectroscopy using a recently-constructed germanium detector system (Hyperball). In the first experiment (KEK E419), we observed two γ transitions in ${}^{7}_{\Lambda}$Li, the spin-flip $M1(\frac{3}{2}^{+}\rightarrow\frac{1}{2}^{+})$ at $691.7\pm0.6^{stat}\pm1.0^{sys}$ keV and the $E2(\frac{5}{2}^{+}\rightarrow\frac{1}{2}^{+})$ at $2050.4\pm0.4^{stat}\pm0.7^{sys}$ keV. The former gives unambiguous information on the strength of the ΛN spin-spin interaction. $B(E2)$ of the latter transition was measured to be $3.6\pm0.5^{stat}\ {}^{+0.5}_{-0.4}\ {}^{sys}e^2\mathrm{fm}^4$. In the second experiment (BNL E930), we observed the $E2(\frac{5}{2}^{+},\frac{3}{2}^{+}\rightarrow\frac{1}{2}^{+})$ transitions of ${}^{9}_{\Lambda}$Be at around 3.05 MeV, which suggests a small ΛN spin-orbit interaction. Such studies for various p-shell Λ hypernuclei are being continued to determine all the ΛN spin-dependent interactions. Intense beams at JHF 50 GeV PS allow us γ-spectroscopy of heavier hypernuclei, neutron rich hypernuclei, and double Λ hypernuclei, etc.

1 はじめに

ハイパー核の研究は、これまで磁気スペクトロメーターを用いて(K^-,π^-), (π^+,K^+)反応によって行なわれてきたが、1GeV/c領域の2次ビームを使用するためにエネルギー分解能は最良でも2 MeV FWHM程度に制限されてしまう。この制限のもとでも、Λがs,p,d,f等の軌道のそれぞれに入った単一粒子状態が観測され、Λのポテンシャルが浅いことやLS力が小さいことなど、大雑把な構造からいくつかのハイパー核の重要な性質が明らかになってきた。しかし、さらにハイパー核の詳細なレベル構造を調べるには、圧倒的な分解能の向上が不可欠である。ゲルマニウム(Ge)検出器を用いたγ線分光を導入すれば、分解能は3桁も向上し2 keV FWHMが実現される。通常の原子核物理において、精密γ線分光が果たした役割は非常に大きい。同様に、ハイパー核においても精密γ線分光が可能になれば画期的な進歩が期待できる。正確なレベルエネルギーの決定ばかりか、遷移確率の測定、角相関、偏光の測定によるスピン・パリティの決定などによって、核構造にとって決定的な情報が得られる。しかし、中間子ビームのハローや散乱による強烈なバックグラウンドのためハイパー核実験の環境では通常のGe検出器は動作せず、ハイパー核の生成断面積及びGe検出器の効率が小さいこととあいまって、これまで実験は不可能とされていた。実際、ハイパー核のγ遷移の観測例は過去に5例のみあるが、すべて分解能の悪いNaIシンシレーションカウンターを用いており、統計精度も低い。

我々は、特殊な高速の回路系を用いて技術的問題を解決し、ハイパー核専用の高効率大立体角ゲルマニウム検出器システムを建設して、これまで行なわれていなかったハイパー核の精密γ線分光の開拓に取り組んでいる[1]。最近建設されたGe検出器システム(Hyperball)は、図1のように、相対効率60%のn型Ge検出器14台と、それぞれを取り囲むBGOカウンターから成る。Ge検出器は、全体で約15%の立体角と1 MeVで約3%のピーク効率を持ち、超高計数率用のリセット型プリアンプとgated integrator内蔵のメインアンプが接続されている。BGOカウンターは、Compton suppression及びπ^0や高エネルギー荷電粒子のバックグラウンドの除去のため用いられる。なお、高計数用の特殊な回路系を使用したにもかかわらず、以下に述べるKEKの実験ではGe検出器のdeadtimeは40-50%であり、動作限界ギリギ

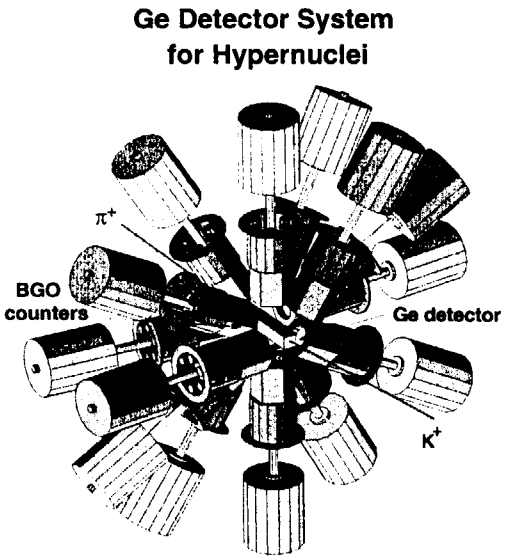

図 1: ハイパー核分光用ゲルマニウム検出器システム Hyperball の概略図。相対効率60%のゲルマニウム検出器 14 台と Compton suppression 用の BGO カウンターからなる。

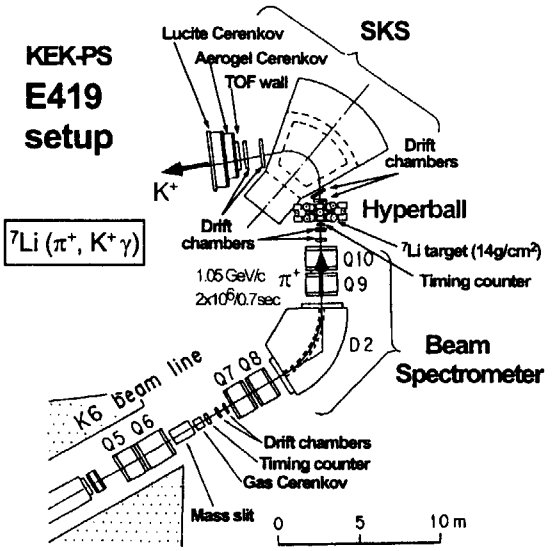

図 2: KEK E419 実験のセットアップ。K6 ビームラインの 1.05 GeV/c の π^+ は粒子ごとにビームスペクトロメータで運動量分析され、^{7}Li 標的でのハイパー核生成反応で発生する K^+ は SKS で分析される。標的の位置に Hyperball が設置され、γ 線を検出する。

リであった。そのため、実験中にそれぞれの Ge 検出器の性能 (deadtime と分解能) を beam on 時/off 時で比較しながら常時モニターするシステムを開発し使用している。

2 最初の実験 — $^7_\Lambda$Li の γ 線分光 (KEK E419)

我々は、98 年 5,6 月に KEK-PS において Hyperball を用いた最初のハイパー核 γ 線分光実験 (E419) を行なった。K6 ビームライン、SKS(超電導 K 中間子スペクトロメーター) を用いて、(π^+,K^+) 反応によって $^7_\Lambda$Li の束縛状態を生成し、そこからの γ 線のスペクトルを同時計測した (図 2 参照)。この実験で Ge 検出器によって初めてハイパー核 γ 遷移を検出することに成功した。

図 3 は $^7_\Lambda$Li の束縛状態を選んだときの γ 線スペクトルである。0.69MeV, 2.05 MeV に現れたピークは、非束縛状態を選んだ時には現れず、$^7_\Lambda$Li ハイパー核の γ 遷移であることがわかる。ドップラー効果によって広がったピークの形状から、前者は M1 遷移、後者は E2 遷移であることがわかり、そのエネルギーや強度から、それぞれ M1$(\frac{3}{2}^+\rightarrow\frac{1}{2}^+)$ および E2$(\frac{5}{2}^+\rightarrow\frac{1}{2}^+)$ と同定された (図 4 参照)。M1 のピークは Doppler shift 補正をすると図 3 内左上図のように細くなり、明らかに $^7_\Lambda$Li から発生していることがわかる。

M1 のエネルギー $691.7 \pm 0.6^{stat} \pm 1.0^{sys}$ keV は $^7_\Lambda$Li の基底状態の二重項 $(\frac{3}{2}^+,\frac{1}{2}^+)$ の間隔を示す。この間隔はほぼ Λ と核子間のスピンスピン相互作用のみによって決まることが分かっているので、今回の測定からスピンスピン相互作用の大きさの情報が得られた。スピンスピン相互作用に直接関係するデータとしては、これまで NaI によって測られた γ 線によって知られていた A=4 ハイパー核 ($^4_\Lambda$H,$^4_\Lambda$He) の基底状態二重項の間隔 (1.1MeV)[2] が唯一のものであったが、スピンスピン力以外に 3 体力の効果が大きいと予想されたことや、A=4 のデータと矛盾する $^{10}_\Lambda$B の実験結果 (基底状態二重項間の M1 遷移が観測されなかったことからこの間隔が非常に小さいと結論した) のために s-shell で得られたスピンスピン力を他の核に適用することの妥当性が疑われていたことから、p-shell ハイパー核での測定が不可欠とされていた。肥山らのクラスターモデル計算 [3] や、Millener らの shell model 計算 [4] によって、今回得られた

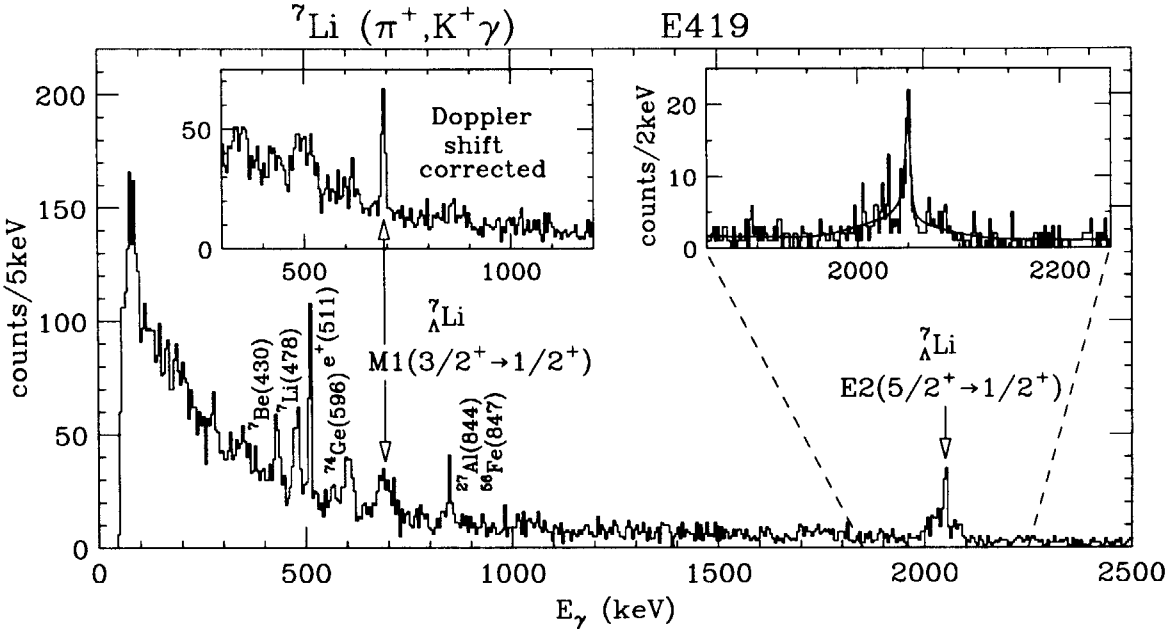

図 3: KEK E419 実験で測定された $^7_\Lambda$Li の γ 線スペクトル。$M1(\frac{3}{2}^+\rightarrow\frac{1}{2}^+)$ 遷移と $E2(\frac{5}{2}^+\rightarrow\frac{1}{2}^+)$ 遷移が観測された。Doppler shift の補正によって、M1 のピークは左上図のように細くなる。また、Doppler シフトで部分的に広がった E2 のピークは、右上図のようにフィットされ、$\frac{5}{2}^+$ 状態の寿命が決められた。

$^7_\Lambda$Li の二重項間隔が A=4 の二重項間隔と consisitent に説明できることが既に示されているため、今回の実験結果によって ΛN 間のスピンスピン力が確立したといえる。

一方、$2050.4\pm0.4^{stat}\pm0.7^{sys}$ keV に観測された E2 遷移は、過去に BNL で NaI を用いて検出されているが [6]、今回は Ge 検出器の高分解能のおかげでピークの形状から Doppler shift attenuation method によって $\frac{5}{2}^+$ 状態の寿命が得られ、これから遷移確率 $B(E2)$ がハイパー核として初めて測定された。反跳を受けた $^7_\Lambda$Li が標的物質中で静止する前に γ 線を放出する事象は、ドップラー効果で広がった裾を作り、静止してから γ 線が放出された事象は細いピークを形作るため、裾とピークの数の比が $^7_\Lambda$Li の寿命に敏感であり、図 3 内の右上図のように、種々の寿命を仮定して simulation により計算されたピーク形状を用いてデータをフィットすることで、$\frac{5}{2}^+$ の寿命として $5.8^{+0.9}_{-0.7}\pm0.7$ ps が得られた。この遷移の分岐比が 94%と考えられることを用いると、この寿命から $B(E2)=3.6\pm0.5^{stat}\ ^{+0.5}_{-0.4}\ ^{sys}e^2\mathrm{fm}^4$ が得られる。これは対応するコア核 ^{6}Li の $3^+\rightarrow1^+$ 遷移の $B(E2)=10.9\pm0.9\ e^2\mathrm{fm}^4$ [7] の 1/3 であり、この違いは $^7_\Lambda$Li のサイズが ^{6}Li のサイズより約 19±4%縮んでいるためと解釈できる [5]。これはパウリ効果を受けない Λ が 0s 状態に入って ^{6}Li のように緩く束縛した核子群を引き付けるためで、15 年前に元場、坂東、池田によって予言されていながらこれまで実験的に検証されていなかった、ハイパー核特有の現象である [8]。

3 γ 線分光による ΛN 間のスピン依存相互作用の研究 — BNL E930

ハイパー核の精密 γ 線分光の最も重要な目的は、ハイパー核の詳細なレベル構造から ΛN 間の相互作用を調べることである。NN 相互作用の場合と異なり、ΛN 間では Λ の寿命の短さのため二体の散乱実験は難しい。一方、Λ が核内でパウリ効果を受けないことと、ΛN 間の相互作用が一般に NN より弱く核内の多体効果が小さいことにより、G-matrix 計算を通じて ΛN 間の相互作用とその核内有効相互作用を定量的に対応させることができる。ΛN 間の有効相互作用は、Λ ハイパー核のレベル構造から調べるこ

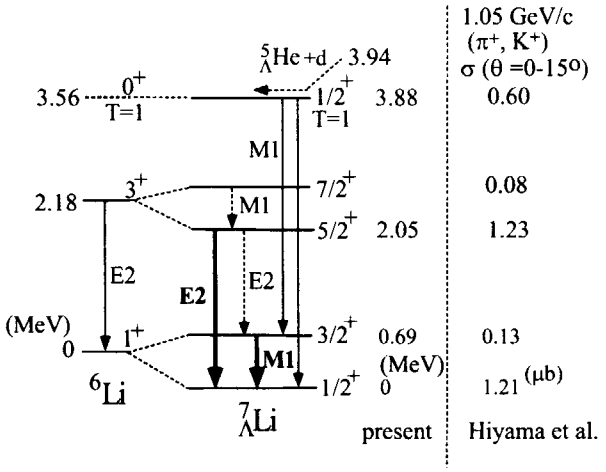

図 4: ${}^{7}_{\Lambda}$Li のレベル図。"present" は KEK E419 で決められたレベルエネルギーであり、観測された γ 線は太い矢印で書かれている。左側には肥山らによる生成断面積の計算値 [5] も示されている。

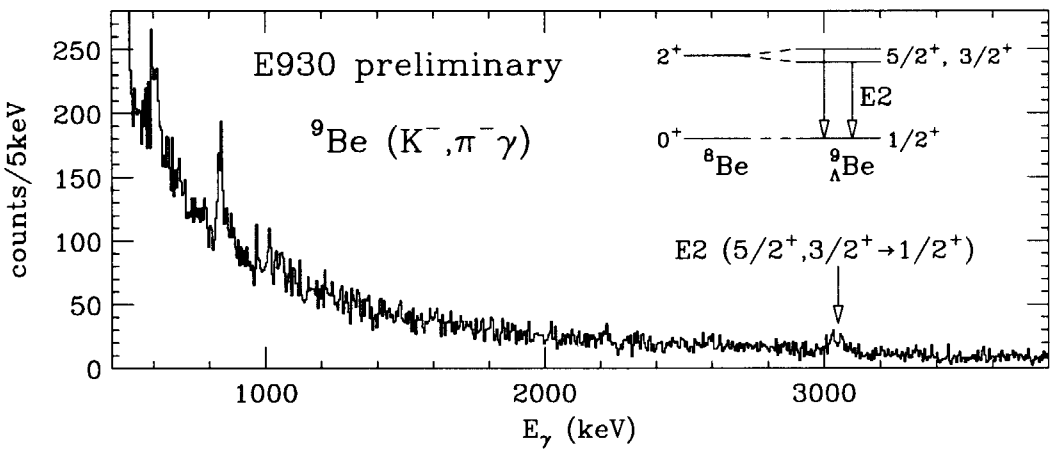

図 5: BNL E930 で得られた ${}^{9}_{\Lambda}$Be の束縛状態を選んだ時の γ 線スペクトル (preliminary)。3.05MeV 付近の構造は、Doppler shift から計算されるピークの形状 (破線) を用いると 2 本の γ 線からなることがわかり、E2($\frac{5}{2}^{+}\rightarrow\frac{1}{2}^{+}$, $\frac{3}{2}^{+}\rightarrow\frac{1}{2}^{+}$) に assign される。

とが出来る。

Λ 核子間の核内有効相互作用は

$$V_{\Lambda N} = V_0(r) + V_\sigma(r)\mathbf{s}_N\mathbf{s}_\Lambda + V_\Lambda(r)\mathbf{l}_{N\Lambda}\mathbf{s}_\Lambda + V_N(r)\mathbf{l}_{N\Lambda}\mathbf{s}_N + V_T(r)[3(\mathbf{s}_N\mathbf{r})(\mathbf{s}_\Lambda\mathbf{r}) - \mathbf{s}_N\mathbf{s}_\Lambda]$$

と書ける。それぞれの項はスピン平均した中心力、スピンスピン力、Λ スピンに依存するスピン軌道力、核子スピンに依存するスピン軌道力、テンソル力である。p-shell のハイパー核のレベルから、それぞれの項の"強さ"（各々の $V_X(r)$ について p-shell の波動関数で radial integral を取った量）を知ることができる [4]。第一項以外のスピン依存力はこれまで良くわかったいなかった。前述の ${}^{7}_{\Lambda}$Li の実験では、基底状態二重項の間隔にほぼスピンスピン力の項のみが寄与しているので、692 keV の M1 のエネルギーか

らこの項の強さ (Δ=0.50 MeV) がわかったことになる。

我々はKEKの実験後、いくつかのp-shellハイパー核のレベル構造からこれらΛ核子間のスピン依存相互作用のすべてを定量的に求めることを目的とした実験(E930)を米国ブルックヘブン国立研究所(BNL)で行なった。Hyperballを BNL AGS D6ラインに設置し、0.9 GeV/cのK^-ビームによる(K^-,π^-)反応を用いてハイパー核を生成した。ビームタイムの都合により1998年12月に${}^{9}_{\Lambda}$Beのデータのみを収集した。${}^{9}_{\Lambda}$Beでは、2つのE2($\frac{5}{2}^+\rightarrow\frac{1}{2}^+$, $\frac{3}{2}^+\rightarrow\frac{1}{2}^+$)を分離して検出し、$\frac{5}{2}^+$,$\frac{3}{2}^+$のエネルギー差がΛのspin-orbit力のみから決まっていることを利用してΛのスピン軌道力を決めることができる。

図5は、${}^{9}_{\Lambda}$Be束縛状態に対するγ線スペクトル(preliminary)である。3.05 MeV付近の構造は非束縛状態を選んだ時には現れないため、${}^{9}_{\Lambda}$Beのγ線であることがわかり、過去のBNLのNaIによる実験で観測されたエネルギー3.079±0.040 MeV [6]にも一致している。このγ線の構造は特殊な形をしているが、Doppler shiftの効果をsimulateして計算したピーク形状と比較すると、同じ強度の2つのピークが100 keV以下(数十keV程度)の狭い間隔で存在するとするとよく説明できる。すなわち、$\frac{5}{2}^+$,$\frac{3}{2}^+$のエネルギー差は100keVよりずっと小さい可能性がある。

ΛのLS力とこのレベルのエネルギー差を関連付ける${}^{9}_{\Lambda}$Beの構造計算[9]によると、ΛのLS力として、Nijmegen D, F, SC98などのバリオンバリオン相互作用の中間子交換モデルの予言する値(核子の場合の1/3-1/5程度)を用いると、この間隔は100 keV以上になる。解析は進行中でありまだ結論を出すことはできないが、もし数十keV程度の間隔がこの実験で確定すれば、現在の中間子交換モデルへの深刻な疑問を提起することになるであろう。一方、クォーク·グルオンの交換をLS力の起源と考えると、ΛのLS力(V_Λ)は非常に小さくなることが知られているので、我々のデータは核力のLS力の起源をどう考えるかという重大な問題に関係してくる。

BNLでは2001年よりAGSの運転が再開され、E930の残りの実験(${}^{16}_{\Lambda}$O, ${}^{12}_{\Lambda}$C, および1.1 GeV/cの(K^-,π^-)反応を用いた${}^{7}_{\Lambda}$Liの分光)を行うことになっている。これらの実験では、特に${}^{16}_{\Lambda}$Oの基底状態二重項の間隔からΛN間のテンソル力の情報が得られ、${}^{7}_{\Lambda}$Liの$\frac{7}{2}^+\rightarrow\frac{5}{2}^+$遷移の観測により核子スピン依存LS力($V_N$)の強さがわかるはずである。$\Lambda N$間のテンソル力は、one pion exchangeが禁止されるため小さいと期待されるが、Σを経由する2 pion exchangeの効果が現れるので興味深い。また、核子スピン依存LS力がわかると、${}^{9}_{\Lambda}$Beから得られるΛスピン依存LS力(V_Λ)と合わせて、symmetric LS力($\propto \mathbf{l}_{\Lambda N}(\mathbf{s}_\Lambda+\mathbf{s}_N)$)、anti-symmetric LS力($\propto \mathbf{l}_{\Lambda N}(\mathbf{s}_\Lambda-\mathbf{s}_N)$)のそれぞれを求めることができる。前者は$NN$のLS力からflavor SU(3)対称性を使って予想することが出来るが、後者はNN間にはないためまったく未知である。それぞれについて中間子交換モデルやクォークモデルの予言と比較することがLS力の起源を知る上で必要である。

こうして、様々なp-shellハイパー核の分光を進めることにより、ΛN間の相互作用のすべてを実験的に確立することができる。これらは、Nijmegen modelなどのバリオン間力のモデルの良否の判定に決定的な役割を果たすとともに、これらを改良するための指針ともなる。バリオン間力を中間子交換模型で統一的に説明できるのか、クォーク·グルオンの描像が必要になるのかが、いずれ明らかになるかも知れない。

4 JHFでのハイパー核γ線分光

ハイパー核の精密γ線分光は、JHFにおける主要な研究テーマのひとつとされている。K-arena実験室に建設予定の最大1.1 GeV/cのビームラインに、増強·改良したHyperballを設置して実験を行なう。ビーム強度は現在の2桁も向上するので、pile upの分離機能を持ったより高速の回路系を開発するとともに、検出器を増やして標的から遠ざけて配置する必要がある。

大強度のK^-ビームを用いて、(K^-,π^-)反応によってsd shellから${}^{208}_{\Lambda}$Pbにいたる様々な質量数領域のハイパー核のγ分光を行なうことができるようになる。ここでは、$\gamma\gamma$同時計数が可能になり、角相関や偏光の情報も用いてレベルスキームが詳細に決定できる。$B(M1)$,$B(E2)$などの遷移確率の測定も様々

なハイパー核について可能になる。Λが入ることによって原子核が受けるサイズや変形、殻/クラスター構造、集団運動などの変化を系統的に調べることが目的である。また、重い核での $B(M1)$ の測定から核内のΛの磁気モーメントを求めることで、核内でのバリオンの性質変化が見えるかも知れない。

一方、(K^-,π^-) 反応ばかりでなく、(K^-,π^0), (π^+,K^0) 反応によって ${}^{7}_{\Lambda}$He, ${}^{11}_{\Lambda}$Be など、さらに生成断面積は非常に小さいが 2 step の (K^-,π^+) 反応によって ${}^{11}_{\Lambda}$Li などの中性子過剰ハイパー核を調べることも考えている。Λによって中性子のハロー構造がどう変化するかが興味深い。

JHF でのみ可能な重要な研究として、ダブルΛハイパー核のγ分光がある。ダブルΛハイパー核は、1.8 GeV/c のビームラインにおいて、(K^-,K^+) 反応によってΞ$^-$ 吸収またはΞ$^-$ ハイパー核経由で作られる。ΛΛ 間の相互作用は、H ダイバリオンの存在や中性子星内部のハイペロン物質の問題と関連した重要なテーマであるが、これまでほとんどわかっていない。例えば、${}^{13}_{\Lambda\Lambda}$B のγ分光により、$(p_{1/2})_\Lambda(s)_\Lambda \to (s)_\Lambda(s)_\Lambda$, $(p_{3/2})_\Lambda(s)_\Lambda \to (s)_\Lambda(s)_\Lambda$ の両方を観測すれば、ΛΛ 間の中心力だけでなく、LS 力やテンソル力の情報も得られる。やはり Hyperball を用いて実験を予定しているΞ$^-$-atom の X 線のシフトの測定や、Ξハイパー核自身の (K^-,K^+) 分光実験によって明らかになるΞN 相互作用と併せることにより、核内でのΛΛ $-$ ΞN mixing や可能性が指摘されている核内の H ダイバリオン的な相関も明らかにすることができるであろう。また、Λが 2 つ入ることで原子核がより大きく縮んだり、構造が大きく変化したりする可能性もあり、興味が持たれる。

5 まとめ

我々は、ハイパー核の新しい研究手法である精密γ線分光を開拓してきた。専用の Ge 検出器システム Hyperball が建設され、KEK-PS において最初の実験(E419)では Ge 検出器による初めてのハイパー核γ線の観測に成功した。ここではスピン反転 M1 遷移からΛN 間のスピンスピン力が明らかになり、また $B(E2)$ の測定からΛによる核の縮み効果が観測された。BNL-AGS での E930 実験では、${}^{9}_{\Lambda}$Be の preliminary なγ線スペクトルに E2($\frac{5}{2}^+,\frac{3}{2}^+ \to \frac{1}{2}^+$) が観測され、ΛのLS力が非常に小さいことが示唆されている。さらに今後も p-shell ハイパー核のγ分光を続けΛN 間のスピン依存力をすべて決定する予定である。JHF K-arena では様々なΛハイパー核やΛΛハイパー核のγ分光を行ないたい。

参考文献

[1] H. Tamura, Nucl. Phys. **A639**, 83c (1998)

[2] M. Bedjidian *et al.*, Phys. Lett. **62B**, 467 (1976); M. Bedjidian *et al.*, Phys. Lett. **83B**, 252 (1979)

[3] E. Hiyama, M. Kamimura, T. Motoba, T. Yamada and Y. Yamamoto, Phys. Rev. **C53**, 2075 (1996); Nucl. Phys. **A639** 173c (1998)

[4] D.J. Millener, A. Gal, C.B. Dover, R.H. Dalitz, Phys. Rev. **C31**, 499 (1985)

[5] E. Hiyama, M. Kamimura, K. Miyazaki and T. Motoba, Phys. Rev. **C59**, 2351 (1999)

[6] M. May *et al.*, Phys. Rev. Lett. **51**, 2085 (1983)

[7] R. B. Firestone, "Table of Isotopes" (8th edition). A Wiley-Interscience Publication 1996.

[8] T. Motoba, H. Bandō and K. Ikeda, Prog. Theor. Phys. **80**, 189 (1983)

[9] E. Hiyama *et al.*, to be published.

3. Light Hypernuclei and Exotic Atoms

Yoshinori Akaishi

Institute of Particle and Nuclear Studies, KEK, Tanashi, Tokyo 188-8501, Japan

It is found that the suppression due to two-body ΛN-ΣN coupling solves the overbinding problem in ${}^{5}_{\Lambda}$He but it causes a severe underbinding in the four-body systems. The shortage of this binding is overcome by introducing the Λ-Σ coupling explicitly which is equivalent to the ΛNN three-body force. This three-body force becomes strong in the 0^+ state of ${}^{4}_{\Lambda}$H and ${}^{4}_{\Lambda}$He according to the coherent enhancement. In the strangeness -2 sector there is a possibility that the lightest double-Λ hypernucleus ${}^{4}_{\Lambda\Lambda}$H is abundantly populated via an exotic atom by stopping Ξ^- on ^{4}He. An excited state with strangeness halo appears in a double-strangeness five-body system.

1 Λ-Σ coupling in *s*-shell hypernuclei

There is a long standing problem of fitting the experimental Λ-separation energies of ${}^{3}_{\Lambda}$H, ${}^{4}_{\Lambda}$H, ${}^{4}_{\Lambda}$He and ${}^{5}_{\Lambda}$He consistently. Dalitz *et al.*[1] determined a reasonable ΛN central force that produce the correct Λ-separation energies in ${}^{3}_{\Lambda}$H and ${}^{4}_{\Lambda}$H. Then this potential is found to be so strong for ${}^{5}_{\Lambda}$He that it gives the binding energy value B_Λ of 5.46 MeV which is much larger than the experimental value of 3.12 ± 0.02 MeV. We show that some of realistic YN interactions will reproduce all the *s*-shell hypernuclear data by solving the overbinding problem with ΛNN three-body force due to the Λ-Σ coupling.

In order to find some key to solve the overbinding problem we prepare various types of potentials simplified from realistic hyperon-nucleon (YN) interactions. The potential D0 has only central part of ΛN interaction and D2 has central parts of both ΛN and ΣN channels. All central and tensor parts of the both channels are included in D3. These D0~3 potentials give identical phase shifts which are equivalent to the Nijmegen D interaction [2]. The potentials SC89(S) and SC97f(S) are obtained in a same way as D3 from the Nijmegen soft-core SC89 [3] and SC97f [4] interactions. The Λ separation energies of four-body and five-body hypernuclei are calculated by the Brueckner-Hartree-Fock method on Gaussian basis.

Now let's see results obtained when the hyperon wave function is restricted in the Λ space. The D0 potential gives a good result of $B_\Lambda = 2.44$ MeV for ${}^{4}_{\Lambda}$He compared to the experimental one 2.39 ± 0.03 MeV, but causes the overbinding of 6.66 MeV in ${}^{5}_{\Lambda}$He as it was shown by Dalitz *et al.* [2] By employing the D2 potential which includes the ΛN-ΣN coupling of central type, the binding energy in the five-body system is reduced to 3.01 MeV which is well close to the experimental one. This is due to the large suppression of the ΛN-ΣN coupling in the nucleus.

While this coupling remedies the overbinding problem in ${}^{5}_{\Lambda}$He, the suppression effect in turn causes a serious underbinding problem in the four-body systems, that is, $B_\Lambda = 1.04$ MeV for ${}^{4}_{\Lambda}$He which is short by 1.35 MeV.

How to solve this underbinding problem of ${}^{4}_{\Lambda}$He? Gibson *et al.* [5] firstly introduced Σ-space components explicitly into the wave function as

$$|{}^{4}_{\Lambda}\mathrm{He}>=\Phi_\Lambda(\vec{r})|{}^{3}\mathrm{He}>+\sqrt{\frac{2}{3}}\Phi_{\Sigma^+}(\vec{r})|{}^{3}\mathrm{H}>-\sqrt{\frac{1}{3}}\Phi_{\Sigma^0}(\vec{r})|{}^{3}\mathrm{He}>. \quad (1)$$

We adopt this idea in order to take into account ΛNN three-body force effects due to the Λ-Σ coupling. Then, the hyperon-nucleus potential has a Λ-Σ coupling term, to which the two-body ΛN-ΣN coupling interaction contributes as follows [6];

$$\begin{aligned}&\frac{3}{2}{}^{3}g_{\Sigma N,\Lambda N}-\frac{1}{2}{}^{1}g_{\Sigma N,\Lambda N} \quad \text{for } 0^+,\\ &\frac{1}{2}{}^{3}g_{\Sigma N,\Lambda N}-\frac{1}{2}{}^{1}g_{\Sigma N,\Lambda N} \quad \text{for } 1^+.\end{aligned} \quad (2)$$

Since the ΛN-ΣN coupling strength is much stronger in the spin-triplet state than in the spin-singlet state, the Λ-Σ coupling effect on B_Λ in the 0^+ state becomes by about one order of magnitude larger than that in the 1^+ state. This is due to coherent enhancement in the 0^+ state where contributions from each pair of YN coupling are added constructively. On the other hand, contributions from the two pairs are cancelled out in the 1^+ state and the resulting spin-triplet weight is 1/3 of that in the 0^+ state. Therefore, the attractive effect due to the Λ-Σ coupling in the 0^+ state is $3^2 = 9$ times as large as that in the 1^+ state. In this respect the 0^+ state is an extraordinary state.

Figure 1 summarizes the results calculated for ${}^{4}_{\Lambda}$He together with the experimental data. The left part and the right part for each interaction are the cases without and with the Σ-space component of eq. (1), respectively. The level splitting at the left part is due to the ΛN spin-spin interaction, and the level shifts seen at the right part are the ΛNN three-body force effect due to the Λ-Σ coupling. The Σ admixture is given in the figure for the 0^+ state and it is negligibly small for the 1^+ state. By using the potential D2 the three-body force effect due to the Λ-Σ coupling is estimated to be 1.23 MeV attraction with 1.9% Σ-mixing for the 0^+ state and only 0.01 MeV attraction with 0.01% Σ-mixing for the 1^+ state. In the D2 case the 0^+-1^+ splitting in ${}^{4}_{\Lambda}$He comes not from the ΛN spin-spin interaction but from the ΛNN three-body force. This confirms Gibson's statement that the 0^+-1^+ energy difference is not a measure of the ΛN spin-spin interaction [7]. However, the D3 potential which simulates most faithfully the original Nijmegen D potential brings only a small 0^+-1^+ splitting energy of 0.13 MeV in contrast to the D2 potential. This is due to the difference of ΛN-ΣN potential type, which is of central type for D2 but is mainly of tensor type for D3. The success of D2 in solving the four-body underbinding problem does not apply to the Nijmegen D potential. The SC97f(S) potential [4] fits rather well all the experimental Λ binding energies of *s*-shell hypernuclei. In order to understand the nature of interaction we divide the ΛN-ΣN coupling interaction into its central and tensor parts. The three-body effect on the 0^+-1^+ splitting is due to the ΛN-ΣN central coupling, while the large

suppression is mainly due to the ΛN-ΣN tensor coupling. The binding B_Λ of ${}^{5}_{\Lambda}$He is calculated to be 2.38 MeV for SC97f(S) and 3.57 MeV for SC97e(S). Since the experimental value 3.12 $\pm$ 0.02 MeV is in between them, the result for SC97f(S) is not bad and would be adjusted so as to reproduce the data without difficulty. A proper ratio of the ΛN-ΣN central coupling and tensor coupling is significant in the hyperon-nucleon interaction. It is found that the Nijmegen SC97f potential meets this requirement. The 0^+-1^+ spin doublet splitting in ${}^{4}_{\Lambda}$He is half due to the ΛN spin-spin interaction and half due to the Λ-Σ coupling in SC97f(S).

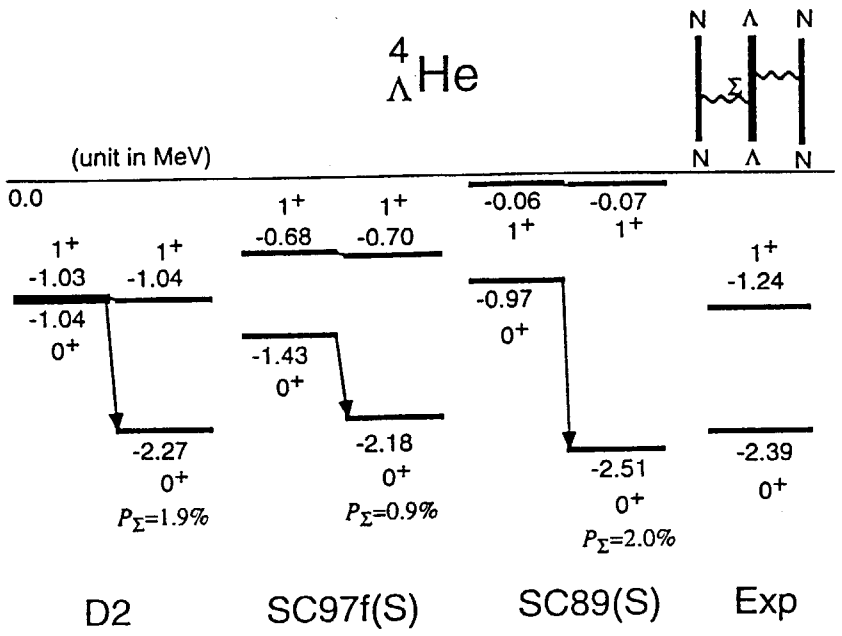

Fig. 1. The Λ energy levels calculated with the D2, SC97f(S) and SC89(S) potentials. The level shift shown by the arrow is mainly due to the ΛNN three-body force.

2 Exotic atom and formation of double-Λ hypernuclei

Double-strangeness ($S = -2$) hypernuclei are of particular interest: What nature would be revealed about the $\Lambda\Lambda$ and ΞN interaction? Since two-body scattering data are not available in the $\Lambda\Lambda$ sector, double-Λ hypernuclei are unique sources of information concerning the $S = -2$ interaction.

Is there any way to produce abundantly double-Λ hypernuclei? Suppose the case where a Ξ^- hyperon stops on a nucleus and then forms a double-Λ hypernucleus via the elementary reaction process;

$$\Xi^- + p \rightarrow \Lambda + \Lambda + 28.33\ \mathrm{MeV}. \tag{3}$$

This reaction Q value of 28.33 MeV is accidentally very close to the binding energy of the alpha particle, 28.30 MeV. If an alpha particle is broken by absorbing Ξ^- stopped on its atomic orbit, the released Q-value energy is almost exhausted and two produced Λ's cannot get enough energy to escape a hypernucleus. Then, there occurs a large chance for the hyperons to form a double-Λ hypernucleus.

The possible lightest double-Λ hypernucleus is predicted to be ${}^{4}_{\Lambda\Lambda}\mathrm{H}$ [8]. The formation rate of ${}^{4}_{\Lambda\Lambda}\mathrm{H}$ via stopped Ξ^- on ^{4}He is estimated by Kumagai-Fuse *et al.* [9]. Table 2 shows the formation rate and branching ratio of each process calculated for atomic s-orbit and p-orbit absorptions of Ξ^-. The branching ratios of the four-body and five-body breakup processes are negligibly small due to the small phase volume. In the case of the ${}^{4}_{\Lambda\Lambda}\mathrm{H}$ formation, the rate is suppressed by the final-state interaction for the s-orbit absorption while it is enhanced for the p-orbit absorption. This situation is explained in relation to the existence of a bound state. When the system of ${}^{4}_{\Lambda\Lambda}\mathrm{H}$ $+n$ has a bound state ${}^{5}_{\Lambda\Lambda}\mathrm{H}$ which concentrates in it the neutron s-wave strength, the formation rate is largely suppressed in the s-orbit absorption case. On the other hand, when the distortion potential becomes stronger but still has no bound state, the maximum of the formation rate moves toward the threshold and becomes higher. The ${}^{4}_{\Lambda\Lambda}\mathrm{H}$ formation rate from the p-orbit absorption is greatly enhanced and amounts to 20%. Now we consider the atomic cascade process of Ξ^- in ^{4}He. The Ξ^- capture fractions from atomic s orbit and from p orbit are estimated to be 25% and 73%, respectively [9]. Thus, a large branching ratio of 15% is obtained for the ${}^{4}_{\Lambda\Lambda}\mathrm{H}$ formation.

Table 2. The formation rate and branching ratio [%] from Ξ^- stopped on ^{4}He.

Process	s−orbit absorp.$(10^{18}/\mathrm{s})$	p−orbit absorp.$(10^{15}/s)$
${}^{4}_{\Lambda\Lambda}\mathrm{H} + n$	0.04 [1.5%]	0.73 [20.1%]
$\Lambda + {}^{4}_{\Lambda\Lambda}\mathrm{H}$	0.41 [15.2%]	0.61 [16.9%]
$\Lambda + {}^{4}_{\Lambda\Lambda}\mathrm{H}*$	1.27 [46.7%]	1.89 [52.2%]
$\Lambda + \Lambda + {}^{3}\mathrm{H}$	0.94 [34.7%]	0.39 [10.8%]
$\Lambda + {}^{3}_{\Lambda}\mathrm{H} + n$	0.05 [1.9%]	0.00 [0.05%]

The $S = -2$ five-body system is composed of ${}^{5}_{\Xi}\mathrm{H}$ and ${}^{5}_{\Lambda\Lambda}\mathrm{H}$ [10]. An interesting feature of this system is that the $p\Xi^-$ channel comes closer to the $\Lambda\Lambda$ channel due to the large binding energy of the alpha particle. The threshold difference is reduced to 8.51 MeV in this case from the mass difference 28.33 MeV between $p\Xi^-$ and $\Lambda\Lambda$. In the system a Ξ-hypernuclear state exists at 6.8 MeV above the $t + \Lambda + \Lambda$ threshold, that is, at -1.7 MeV below the $\alpha + \Xi^-$ threshold. Its binding mechanism is interesting. In the $\alpha\Xi^-$ system there exists the atomic $1s$ state with 24.0 fm rms distance. The Coulomb interaction gives binding energy of 0.1 MeV for Ξ^-. The strong interaction between α and Ξ^- brings about a shallow bound state with 0.5 MeV binding energy and 5.3 fm rms distance. When both the strong and Coulomb interactions are combined, the binding energy increases to 1.6 MeV but the rms distance remains still large to be 4.0 fm due to the long-range nature of the Coulomb interaction. This bound state ${}^{5}_{\Xi}\mathrm{H}$ has a strangeness halo as seen in Fig. 2. The Coulomb interaction ensures the existence of this state while the

strong interaction maintains the nature of a nuclear state. Both the Coulomb and strong interactions play important roles in forming this exotic state.

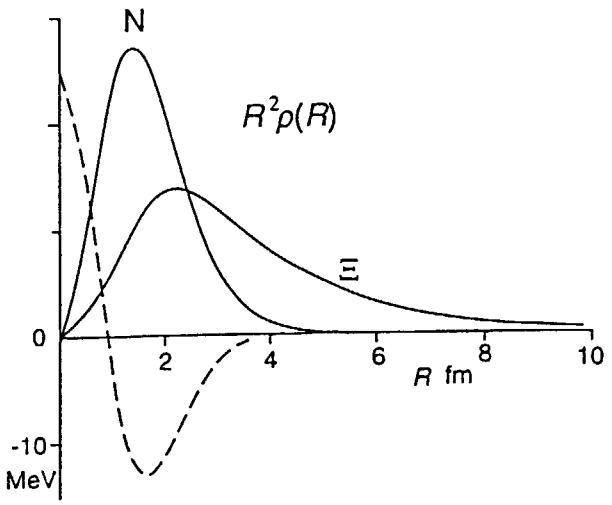

Fig.2. The density distribution of Ξ^- in the $\alpha\Xi^-$ system. The dashed curve denotes the α-Ξ^- potential.

In summary, the breakup of an alpha particle by Ξ^- absorption benefits the formation of double-Λ hypernuclei. The conversion reaction to $\Lambda\Lambda$ from $p\Xi^-$ via the exotic atom after Ξ^- stopping on ^{4}He produces the lightest double-Λ hypernucleus, ${}^{4}_{\Lambda\Lambda}$H, with a high branching ratio of 15%. The ${}^{5}_{\Xi}$H state is bound by the cooperation of the Coulomb and the strong interactions as an atom-nucleus hybrid state with strangeness halo.

References

1. R.H. Dalitz, R.C. Herndon and Y.C. Tang, *Nucl. Phys.* **B47** (1972) 109.
2. M.M. Nagels, T.A. Rijken and J.J. de Swart, *Phys. Rev.* **D12** (1975) 744.
3. P.M.M. Maessen, Th.A. Rijken and J.J. de Swart, *Phys. Rev.* **C40** (1989) 2226.
4. Th.A. Rijken, V.G.J. Stoks and Y. Yamamoto, *Phys. Rev.* **C59** (1999) 21.
5. B.F. Gibson, A. Goldberg and M.S. Weiss, *Phys. Rev.* **C6** (1972) 741.
6. J. Dabrowski, *Phys. Rev.* **C8** (1973) 835.
7. B.F. Gibson, *Proc. U.S.-Japan Seminar, Maui,* (1993) 55.
8. S. Nakaichi-Maeda and Y. Akaishi, *Prog. Theor. Phys.* **84** (1990) 1025.
9. I. Kumagai-Fuse, T. Koike and Y. Akaishi, *Nucl. Phys.* **A585** (1995) 367c.
10. Khin Swe Myint and Y. Akaishi, *Prog. Theor. Phys. Suppl.* **117** (1994) 251.

4. Few-Body Aspect of Hypernuclear Physics

E. Hiyama

Institute for Physical and Chemical Research (RIKEN), Wako, Saitama 351-0198, Japan

Abstract

We have carried out four-body calculationals of ${}^{4}_{\Lambda}$H and ${}^{4}_{\Lambda}$He taking both the $3N$+Λ and $3N$+Σ channels explicitly with the use of realistic NN and YN interactions. The Σ-channel component plays an important role in binding energies of the $A = 4$ hypernuclei though the admixture is approximately 1%. The $\Lambda N - \Sigma N$ coupling is found to be of central-force type in the Nijmegen model D and of tensor type in the model F.

One of our purpose to study is to develop the calculational method to study three- and four-body systems. In order to solve three- and four-body problems accurately, we employed a variational method with the use of Jacobian coordinate Gaussian basis functions [1,2]. This method has been successfully applied to the bound states of various three- and four-body systems[1-8]. The basis functions work excellently in describing both the short-range correlations and the long-range tail behaviour.

Recently, we have proposed a new type of Gaussian basis function [x]. This basis function is called Infinitesimally-Separated Gaussian Lobe (ISGL) besis function. This basis function makes much easier to calculate the matrix element. Therefore, variational method with ISGL basis function is applicable to various types of three- and four-body systems even with complicated interactions (quadratic spin orbit force and momentum dependent force).

In this paper, we focus attention to the four-body structure study of ${}^{4}_{\Lambda}$H and ${}^{4}_{\Lambda}$He. One of the main goals of the hypernuclear study is to obtain useful information on the hyperon-nucleon (YN) interaction. Although several types of YN interactions have been

proposed, these interactions have a lot of ambiguity due to little information from the YN scattering experiments. Therefore, the study of hypernuclear structure should be helpful in elucidating the YN interaction properties. As is well known, the study of ${}^{4}_{\Lambda}$H and ${}^{4}_{\Lambda}$He is very useful to examine the YN interactions because both of the spin-doublet states have been observed. Especially, it is expected to obtain information on the role of $\Lambda N - \Sigma N$ coupling in the binding mechanisum of the $A = 4$ hypernuclei. In this work, we report four-body calculations of ${}^{4}_{\Lambda}$H and ${}^{4}_{\Lambda}$He taking the $\Lambda N - \Sigma N$ channel coupling into account explicitly.

We consider explicitly both the $3N + \Lambda$ and $3N + \Sigma$ channels explicitly and solve the four-body problem taking the $\Lambda N - \Sigma N$ conversion into account. we employ a variational method with the use of Jacobian coordinate Gaussian basis functions [1, 2] which span over all the rearrangement channels in Fig. 1. The four-body wavefunctions are written [6, 8] as

$$\Psi_{JM}({}^{4}_{\Lambda}\mathrm{H},{}^{4}_{\Lambda}\mathrm{He}) = \sum_{Y=\Lambda,\Sigma}\sum_{c=1}^{4}\sum_{I,j}\sum_{l,L,\lambda}\sum_{s_0,s,S,t_0,t_0}\sum_{n,N,\nu} A^{(c)}_{Y,nlNL\nu\lambda Ijs_0sSt_0t}$$
$$\times\mathcal{A}_N\left\{\left[\left[[\phi^{(c)}_{nl}(\mathbf{r}_c)\psi^{(c)}_{NL}(\mathbf{R}_c)]_I\xi^{(c)}_{\nu\lambda}(\boldsymbol{\rho}_c)\right]_j\left[[[\chi^{(\sigma)}_{1/2}(N_1)\chi^{(\sigma)}_{1/2}(N_2)]_{s_0}\chi^{(\sigma)}_{1/2}(N_3)]_s\chi^{(\sigma)}_{1/2}(Y)\right]_S\right]_{JM}\right.$$
$$\left.\times\left[[[\chi^{(\tau)}_{1/2}(N_1)\chi^{(\tau)}_{1/2}(N_2)]_{t_0}\chi^{(\tau)}_{1/2}(N_3)]_t\chi^{(\tau)}_{t_Y}(Y)\right]_{T=1/2}\right\},$$

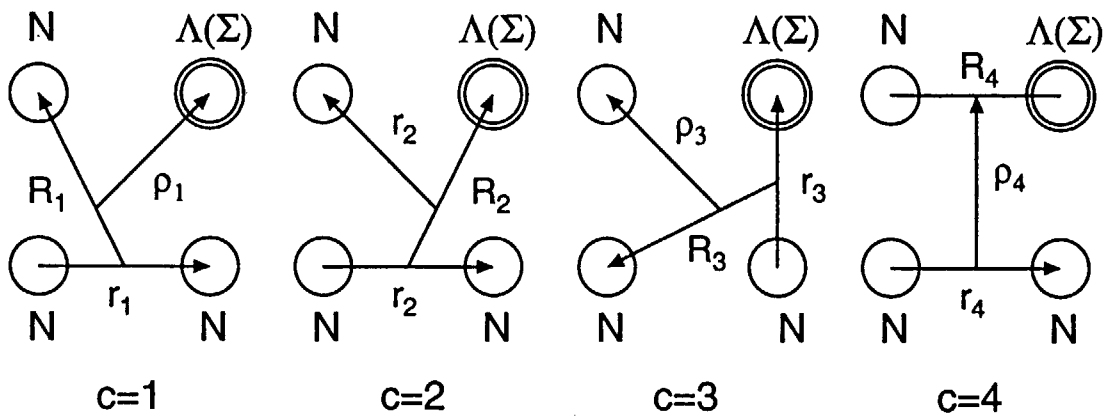

Figure 1. Jacobian coordinates for all the rearrangement channels of $3N + \Lambda(\Sigma)$ of ${}^{4}_{\Lambda}$H and ${}^{4}_{\Lambda}$He. The three nucleons are to be antisymmetrized.

where $\mathcal{A}_N$ are the three-nucleon antisymmetrization operator and the isospin $t_Y = 0$ for $Y = \Lambda$ and $t_Y = 1$ for $Y = \Sigma$. Here, n, N and ν denote the size of the Gaussian basis functions for four-body systems which are explicitly given in Ref. [6]. The eigenenegies of Hamiltonian and coefficients C are determined by Rayleigh-Litz variational method. Calculation of the interaction matrix elements between the four-body basis functions can be performed rather easily with the use of the infinitesimally-shifted- Gaussian-Lobe representation of the basis functions [9,4].

As for the YN interaction with $\Lambda N - \Sigma N$ coupling terms, we consider those of Nijmegen model D and model F, but we simulate them by using soft-core potentials with central and tensor terms [10] which reproduce the scattering phase shifts obtained by the original interactions. In the following, we refer to the phase-shift equivalent soft-core potentials as ND and NF. We employ the AV8 potential as the NN interaction.

All the calculations shown below have been done both for ${}^{4}_{\Lambda}\mathrm{H}$ and ${}^{4}_{\Lambda}\mathrm{He}$, but we present only the case of the former since the result for the latter is very similar to that for the former. Calculated energies of the 0^+ ground state and the 1^+ excited state are illustrated in Fig. 2 together with the observed values. The energies are measured from the ${}^3\mathrm{H} + \Lambda$ threshold. In the case of only the $3N + \Lambda$ channel included in the calculation, the 0^+ state is barely bound and the 1^+ state is unbound. When the $(3N)_{t=1/2} + \Sigma$ channel is further adopted, both of the two states become bound evidently. Finally, further inclusion of the $(3N)_{t=3/2} + \Sigma$ channel makes the 1^+ state significantly more bound but with the 0^+ state almost unchanged. We understand that the Σ-channel component plays a very important role both in the energy gain and the relative splitting of the 0^+ and 1^+ states. However, the calculated binding energy of the 0^+ state is some 0.5 MeV smaller and hence the $0^+ - 1^+$ splitting is about a half of the observed value. The level structure calculated with NF is similar to the case of ND. The calculated energies of the 0^+ and 1^+ state are -0.99 and -0.44 MeV, respectively.

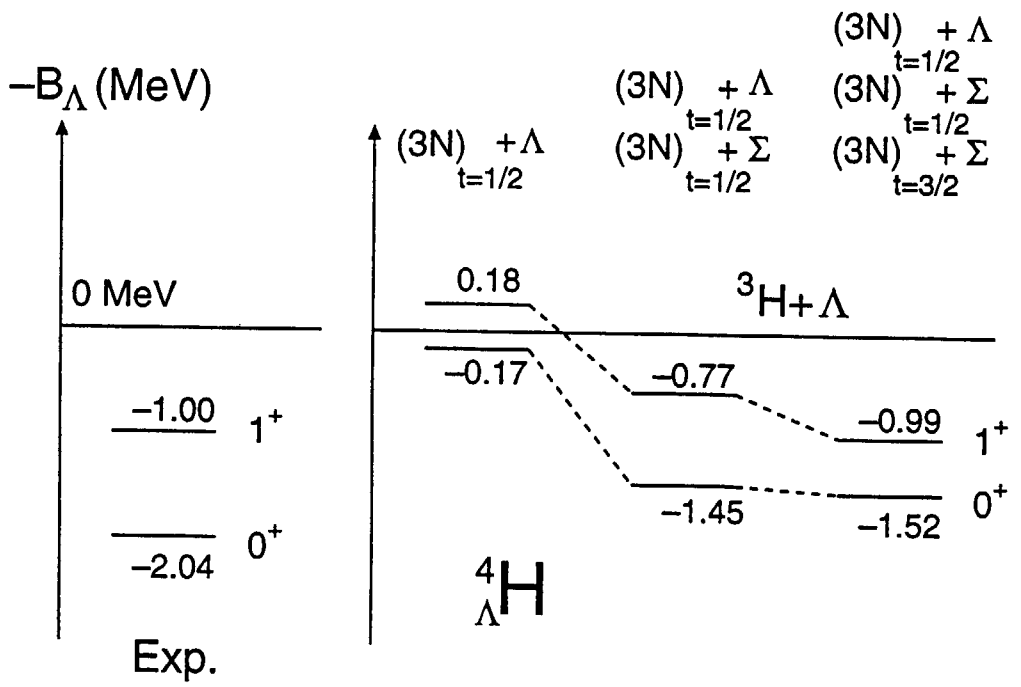

Figure 2. Calculated energy levels of ${}^{4}_{\Lambda}$H with the use of ND for three cases of the Λ and Σ channels.

We calculated the probability of the $3N + \Sigma$-channel admixture in ${}^{4}_{\Lambda}$H with the use of ND and NF. Tendency of the admixture is different between the two cases. In the case of ND, the probability is $\sim$1 % for the 0^+ state and $\sim$0.5 % for the 1^+ state. But, in the case of NF, it is $\sim$0.7 % for the both states. Precise percentage of the Σ-channel component is listed in Table 1. In the 0^+ state, the probability of the $(3N)_{t=1/2} + \Sigma$ channel is much larger than that of the the $(3N)_{t=3/2} + \Sigma$ channel, but, in the 1^+ state, they are nearly the same. We therefore understand that $(3N)_{t=3/2} + \Sigma$ channel is specially important in the 1^+ state. This tendency holds in the case of NF, too.

Also listed in Table 1 are the S-state and D-state probabilities of the channels. As long as the $3N + \Sigma$ channel in the 0^+ and 1^+ states is concerned, the S-state component is dominant in the case of ND while the D state is dominant in the case of NF. Therefore, we understand that the $\Lambda N - \Sigma N$ coupling is central-force type in ND, but is tensor-force type in NF. This is verified, as seen in Table 2, from the expectation value of the $\Lambda N - \Sigma N$

Table 1
Probabilities of the $(3N)_{t=1/2}+\Lambda$, $(3N)_{t=1/2}+\Sigma$ and $(3N)_{t=3/2}+\Sigma$ channels in the 0^+ and 1^+ states of ${}^4_\Lambda$H. The S-state and D-state probabilities are also listed. The numbers with no parentheses are for the interaction ND and those in the parentheses are for NF.

	$(3N)_{t=1/2}+\Lambda$	$(3N)_{t=1/2}+\Sigma$	$(3N)_{t=3/2}+\Sigma$
0^+	98.8 (99.3) %	1.11 (0.69) %	0.03 (0.03) %
S-state	90.9 (91.8)	0.91 (0.10)	0.02 (0.02)
D-state	7.9 (7.5)	0.20 (0.59)	0.01 (0.01)
1^+	99.5 (99.3) %	0.24 (0.33) %	0.23 (0.40) %
S-state	91.5 (91.5)	0.18 (0.01)	0.17 (0.01)
D-state	8.0 (7.8)	0.06 (0.32)	0.06 (0.39)

Table 2
Expectation values of the central and tensor terms of the $\Lambda N-\Sigma N$ coupling potential, $2\times\langle\, V_{\Lambda N-\Sigma N}\,\rangle$, in ${}^4_\Lambda$H with ND and NF

	ND		NF	
$2\times\langle\, V_{\Lambda N-\Sigma N}\,\rangle$ (MeV)	0^+	1^+	0^+	1^+
Central	−3.20	−2.19	−0.33	−0.11
Tensor	−0.62	−0.59	−5.54	−6.74

coupling potential. Namely, the central-force contribution is dominant in the case of ND, while the tensor-force one is dominant in NF.

In summary, we have developed the calculational method of four-body bound-state problems so that it becomes possible to make complicated four-body calculation of ${}^4_\Lambda$H and ${}^4_\Lambda$He taking both the $(3N+\Lambda)$ and $(3N+\Sigma)$ channels explicitly with the use of realistic NN and YN interactions. We are now able to investigate precisely the role of the $\Lambda N-\Sigma N$ coupling in ${}^4_\Lambda$H and ${}^4_\Lambda$He. However, the observed binding energies of the 0^+ and 1^+ states were not well reproduced with the use of ND and NF. Therefore, we are much interested in using a new version of Nijmegen soft-core YN interaction, NSC97 and in examining this interaction by the four-body calculation of ${}^4_\Lambda$H and ${}^4_\Lambda$He including the $\Lambda N-\Sigma N$ coupling explicitly. This calculation is in progress.

REFERENCES

[1] M. Kamimura, Phys. Rev. A38 (1988) 621.

[2] H. Kameyama, M. Kamimura and Y. Fukushima, Phys. Rev. C40 (1989) 974.

[3] M. Kamimura and H. Kameyama, Nucl. Phys. A508 (1990) 17c.

[4] E. Hiyama and M. Kamimura, Nucl. Phys. A588 (1995) 35c.

[5] E. Hiyama *et al.*, Phys. Rev. C53 (1996) 2075.

[6] E. Hiyama *et al.*, Prog. Theor. Phys. 97 (1997) 881.

[7] Y. Kino, M. Kamimura and H. Kudo Nucl. Phys. A631 (1998) 649c.

[8] E. Hiyama *et al.*, Nucl. Phys. A639 (1998) 169c and 173c.

[9] E. Hiyama, RCNP Physics Report RCNP-P-132 (1994) 35.

[10] Y. Yamamoto, private communications (1998).

5. Flavor SU(3) Baryons and quark confinement [1]

A. Hosaka [2]
Numazu College of Technology
3600 Ooka, Numazu 410-8501 Japan

Abstract

We study properties of baryons in the light flavor SU(3) sector. After a brief description for the ground state nucleon where the role of the pion is emphasized, we discuss excited states where we point out a very simple systematics in the mass spectrum. We show that the systematics can be well explained by a quark model with a deformed confining potential. Further investigations on electromagnetic couplings are discussed.

Hadron physics is a rich source of interesting non-perturbative phenomena of low energy QCD. Although QCD is the theory of interacting quarks and gluons, actually observed degrees of freedom are hadrons. The mechanism of generating hadrons from quarks and gluons at low energy is a very difficult matter and is not yet fully understood theoretically. In such a situation, one might attempt a description in terms of appropriate effective degrees of freedom. From an effective theory point of view, one should recall the successful current algebra based on chiral symmetry [1, 2] and quark models for hadron structure [3, 4]. In the former the pion appears as the Nambu-Goldstone boson, while in the latter the constituent quarks are the main constituents of hadrons.

There are many examples in which we can not simply ignore the pions. They include the nucleon-nucleon interaction [5], exchange currents in nuclei [6], proton and neutron charge radius and so on. If we turn to nucleon structure, a simple quark model is not sufficient to describe all the details of the structure. For instance, the failures in the quark model for the neutron charge radius and the spin content of the nucleon can be, at least partially, resolved by introducing the pion. Indeed, a detailed study of the chiral bag model has shown that an optimal description for nucleon properties can be achieved at an intermediate bag radius $R \sim 0.6$ fm, where both the quarks and pions share their significant roles [7].

Therefore, we can draw an intuitive picture for the ground state nucleon: confined constituent quarks with the pion cloud around them. When we turn to excited states, however, the situation starts to change. Within the information available up to date, there is a strong evidence in the excited mass spectrum that many states can be consistently explained in a quark model by introducing one dynamical assumption of spatial deformation [8]. This assumption is not only simple but also applies to essentially all flavor SU(3) baryons, independent of flavor quantum numbers. Due to its flavor independence, one may expect that it might reflect the nature of quark confinement.

Let us now look at experimental masses of excited baryons. We take 49 states out of 50 states of three and four stars, and several more states with one and two stars [9]. We

[1] Talk given by AH at the workshop FRONP99 at JAERI, August 1999.

[2] e-mail address: hosaka@la.numazu-ct.ac.jp

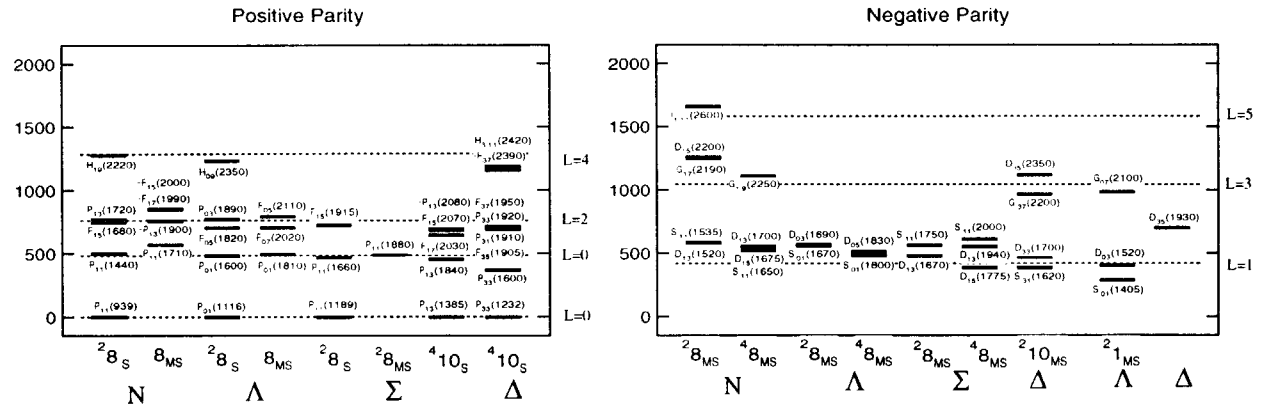

Figure 1: Observed baryon masses as compared with the prediction of the DOQ model with intruder states.

arrange experimental data as follows: (1) Masses are measured from the ground states of the corresponding spin-flavor states. By doing so we expect that spin-flavor dependence of excited states is dictated by the Gell-Mann-Okubo mass formula. (2) Masses of ${}^2 8_{MS}$, ${}^4 8_{MS}$ for positive parity, and of ${}^4 8_{MS}$ for negative parity are reduced by 200 MeV. Here we have just introduced this prescription simply by phenomenological point of view.

Now the resulting mass spectra show up with a very simple systematics for all spin-flavor states as shown in Figs. 1 [8]. In the figures, we would like to emphasize the structure of level spacings which become larger for higher L. Also we note that the level spacings of negative parity states are larger than those of the positive parity states. These are the features which remind us of the properties of deformed nuclei.

Hence we consider a simple quark model which we call the deformed oscillator quark (DOQ) model, whose hamiltonian is given by

$$H_{DOQ} = \sum_{i=1}^{3} \left[\frac{p_i^2}{2m} + \frac{1}{2} m(\omega_x^2 x_i^2 + \omega_y^2 y_i^2 + \omega_z^2 z_i^2) \right] . \tag{1}$$

Here we ignore interactions due to gluons and mesons not only for simplicity but also due to the expectation that important dynamics can be described by that simple hamiltonian. The only dynamical content is anisotropic oscillator potential, $\omega_x \neq \omega_y \neq \omega_z$.

After removing the center of mass motion, we find an intrinsic energy

$$E_{int}(N_x, N_y, N_z) = (N_x + 1)\omega_x + (N_y + 1)\omega_y + (N_z + 1)\omega_z , \tag{2}$$

where N_x, N_y, N_z are the sum of principal quantum numbers for the internal degrees of freedom for the ρ and λ coordinates. If we consider prolate deformation along the z-direction when $N_x = N_y = 0, N_z \equiv N$, one obtains the minimum energy and deformation under the volume conservation condition $\omega_x \omega_y \omega_z = \omega^3$,

$$E_{int}(N) = 3(N + 1)^{1/3}\omega , \quad \omega_x/\omega_z = N + 1 . \tag{3}$$

For $N > 0$ the minimum energies are significantly smaller than the corresponding energies of spherical shapes ($(N+3)\omega$).

Physical excited states are obtained by rotating the deformed intrinsic states, whose energies are given by the standard cranking formula [10]

$$E_{rot} = E_{int} - \frac{\langle L^2 \rangle}{2I} + \frac{L(L+1)}{2I} . \tag{4}$$

Here the moment of inertia I and the expectation value of the angular momentum fluctuation $\langle L^2 \rangle$ are given in literatures [8]. We note the presence of the second term which reduces the energy. This is crucially important to bring the mass of the $1/2^+$ excited states down close to the observed values, the aspect which the spherical quark model does not possess.

The rigid rotor formula of (4) may not be good for actual baryonic system. We can improve this by considering the so called intruder states which accounts for the softness of the intrinsic state [11]. There is only one parameter in the DOQ model ω which is determined by the average of the excitation energies of the first $1/2^+$ excited states in the $^2 8$ multiplet. The resulting value is $\omega = 644$ MeV. In this way theoretical predictions are made which are shown by the dashed lines in Figs. 1. It is remarkable to see that the predicted energy levels agree with observed levels. At the same time, in Figs. 1 there are many missing states in the region of $L = 4$ and $L = 3$. It would be interesting if those states are observed in experiments.

Further study can be made by various transition amplitudes. Here we discuss electromagnetic couplings of nucleon excited states whose experimental data are well compiled [12]. Experimentally, electromagnetic couplings of excited states are extracted from the pion photoproduction [13]. Using a resonance dominant model, we can learn not only the magnitude but also the sign ϵ of the combination

$$\langle N|H_\pi|N^*\rangle \cdot \langle N^*|H_\gamma|N\rangle \equiv \epsilon |\langle N|H_\pi|N^*\rangle \cdot \langle N^*|H_\gamma|N\rangle| , \tag{5}$$

where H_π and H_γ are the interaction hamiltonian for the pion and photon couplings. In the data table the sign ϵ is included in photon couplings [9]. Therefore, in a model calculation, both the electromagnetic and strong (pion) couplings have to be calculated simultaneously. Ignorance of the strong coupling part sometimes leads to incorrect results for the sign [14].

We adopt the non-relativistic form for the γNN and πNN couplings:

$$\begin{aligned} H_\gamma &= -e\vec{J}\cdot\vec{A}, \quad \vec{J} = \frac{1}{2m}\left(u_f^\dagger (i\overleftarrow{\nabla} - i\overrightarrow{\nabla}) u_i + \overrightarrow{\nabla}\times(u_f^\dagger \vec{\sigma} u_i)\right)\tau_\mu , \\ H_\pi &= \frac{g_{\pi qq}}{2M_N}\vec{\sigma}\cdot\overrightarrow{\nabla} . \end{aligned} \tag{6}$$

Matrix elements are then computed between the ground state and excited states of $N = 1, 2$. Results for proton helicity amplitudes $A^p_{1/2}$ and $A^p_{3/2}$ are summarized in Table 1, where the DOQ results are compared with the conventional quark model results by Koniuk-Isgur (KI) [14] and with experimental data [9]. We note that the identification of the model states with physical states is only tentative, where possible mixing effects are ignored.

We have found that in many channels, theoretical results of the DOQ and KI are similar to each other and consistent with experimental data within uncertainties; there is rather weak

Table 1: Proton helicity amplitudes in units of $GeV^{-1/2} \times 10^{-3}$. The column indicated as DOQ is for the present results of the DOQ model, while the column indicated as KI is for the conventional results of Koniuk-Isgur. [14]

Proton		$A_p^{1/2}$			$A_p^{3/2}$			
		DOQ	KI	Exp	DOQ	KI	Exp	
$1/2^+$	$^2S'_S$	109	22.6	-68± 5	–	–	–	$P_{11}(1440)$
	$^2S_{MS}$	-14.6	-15.9	+5±16	–	–	–	$P_{11}(1710)$
$3/2^+$	^2D_S	70.9	111	52±39	-23.5	-36.7	-35±24	$P_{13}(1720)$
$5/2^+$	^2D_S	-3.8	-5.9	-17±10	47.0	73.5	127±12	$F_{15}(1680)$
$1/2^-$	$^2P_{MS}$	151	156	74±11	–	–	–	$S_{11}(1535)$
	$^4P_{MS}$	0	0	48±16	–	–	–	$S_{11}(1650)$
$3/2^-$	$^2P_{MS}$	24.8	25.6	-23±9	138	143	163±8	$D_{13}(1520)$
	$^4P_{MS}$	0	0	-22±13	0	0	0±19	$D_{13}(1700)$
$5/2^-$	$^4P_{MS}$	0	0	19 ± 12	0	–	19 ± 12	$D_{15}(1675)$

dependence on the deformation d. One exception, however, is the coupling of the Roper; even the sign is not correctly reproduced. In the DOQ model, the absolute values increase but with the wrong sign remaining. This problem was first discussed by Kubota and Ohta who considered relativistic corrections [15].

Here instead of discussing the effect of the relativistic corrections, we consider a limitation of the non-relativistic method. Since the orbital wave functions of both the Roper and the nucleon are the S-state, matrix elements of H_γ and H_π reduce to the same spin matrix element:

$$\langle N^*|H_\gamma|N\gamma\rangle \sim \langle \pi N|H_\pi|N^*\rangle \to \langle L=0|\sigma|L=0\rangle\,.$$

Therefore, we can not change the sign of (5), since it is the square of the same matrix elements. Hence we can not reproduce the sign of the photon-Roper coupling as long as we use the non-relativistic hamiltonian. We need more delicate treatment to explain transition amplitudes for more information on the structure of baryons.

In the end of this report, we would like to mention further extensions of the present work. If we look at Figs. 1 in detail, observed states of the negative parity sector fluctuate more than those of positive parity. This implies that some important dynamics might be missing there. In fact, the success of the recent chiral unitary approach for the particular state $\Lambda(1405)$ suggests the important role of chiral mesons [16]. Another problem is the limitation of the non-relativistic treatment. Apparently, for excited states around GeV region relativistic treatment should become indispensable. Establishing reliable theoretical methods and their comprehensive application to various phenomena will be needed for a better understanding of hadron physics.

References

[1] J.J. Sakurai, *Currents and mesons*, Chicago Univ. Press, Chicago (1969);

[2] S. Coleman, *Aspects of Symmetry*, Cambrige University Press, Cambrige (1985).

[3] F.E. Close, *An Introduction to Quarks and Partons*, Academic Press, London (1979).

[4] N. Isgur and G. Karl, Phys. Rev. D18 (1978) 4187; *ibid.* D20 (1979) 1191.

[5] R. Machleidt, K. Holinde and C. Elster, Phys. Reports 149 (1987) 1.

[6] *Mesons in Nuclei*, editted by M. Rho and D.W. Wilkinson, North-Holland (1979).

[7] A. Hosaka and H. Toki, Phys. Reports, 277 (1996) 65.

[8] A. Hosaka, M. Takayama and H. Toki, Mod. Phys.Lett. A13 (1998) 1699; M. Takayama, H. Toki and A. Hosaka, Prog. Theor. Phys. 101 (1999) 1271.

[9] C. Caso et al. (Particle Data Group), Euro. Phys. J. C3 (1998) 1;
R.M. Barnett et al. (Particle Data Group), Phys. Rev. D54 (1996) 1.

[10] A. Bohr and B. Mottelson, "Nuclear Structure", Benjamin Inc. (1975).

[11] M. Takayama, H. Toki and A. Hosaka, Proceedings of PANIC99, Uppsala, Sweden, May 1999.

[12] A. Hosaka, M. Takayama and H. Toki, Preprint (1999).

[13] *"Electromagnetic excitation and decay of hadron resonances"*, in *Electromagnetic interactions of hadrons, Ch.2*, edited by A. Donnachie and G. Shaw, Plenum (1978).

[14] R. Koniuk and N. Isgur, Phys. Rev. D21 (1980) 1868.

[15] T. Kubota and K. Ohta, Phys. Lett. B65, (1976) 374.

[16] E. Oset and A. Ramos, Nucl. Phys. A635 (1998) 99.

6. Roles of Quark Substructures in Hypernuclei

Makoto Oka
Department of Physics, Tokyo Institute of Technology
Meguro, Tokyo 152-8551, JAPAN
email: oka@th.phys.titech.ac.jp

In this talk, we discuss several interesting aspects of hypernuclear physics, which represent the roles of explicit quark content of the baryons. Both the strong and weak interactions in the YN systems show characteristic features of the quark substructure of the baryons. It is in contrast to the NN system, where most phenomena can be accounted either with or without explicit quarks. It is our hope that the YN system can distinguish and enlighten the effects of quark substructure much more clearly.

First, the short range parts of the strong hyperon-nucleon interactions are examined in the quark cluster model of the baryon-baryon interaction. We find that the short-range part of the ΣN interaction depends strongly on the spin-isospin quntum numbers. We also emphasize that the spin-orbit YN forces give characteristic behaviors, which are distinct from the meson exchange forces.

Secondly, the weak decays of Λ in hypernuclei are studied in detail. We find that the direct quark mechanism provides significant short-range contribution to the process. It is pointed out that the neutron induced nonmesonic decay is enhanced due to the direct quark transition. Importance of the $\Delta I = 3/2$ decay amplitudes is emphasized both for the nonmesonic weak decays and the π^+ emission in the Λ decay.

We refer the details of the discussion to another article[1].

[1] M. Oka, Y. Tani, T. Inoue and K. Sasaki, in *Proc. the 7th Conference Mesons and Light Nuclei '98*, ed. by J. Adam, et al. p.146 (World Scientific, 1999)

7. カラー分子動力学による高密度物質と原子核のシミュレーション

丸山敏毅[1]、初田哲男[2]
1 原研・先端基礎研究センター
2 京都大学・大学院理学研究科

Abstract

We propose a microscopic simulation for quark many-body system based on a molecular dynamics. Using confinement potential, one-gluon exchange potential and meson exchange potentials, we can construct color-singlet nucleons, nuclei and also an infinite nuclear/quark matter. Statistical feature and the dynamical change between confinement and deconfinement phases are studied with this molecular dynamics simulation.

1 はじめに

クォークは物質を構成する最も基本的な粒子の1つであるが、通常は3つのクォークまたは1対のクォーク反クォークとグルーオンからなる、カラーが中性のハドロン状態でしか存在しない(カラーの閉じ込め)。最近クォークに関連した研究が理論的にも実験的にも盛んに行われていが、特に高温または高密度状態においてカラーの閉じ込めが解けたクォーク・グルーオンプラズマ(QGP)[1]が理論的に予言されてからは超高エネルギーでの重イオン衝突実験の計画が進んでいる。また天体物理の分野でも、中性子星内部でクォーク物質が存在するのではないかという予測がされ、さらに、それが球状や棒状などの特殊な構造を持つのではないかという議論がされる[2]など、様々な形で注目されている。

近年計算機の進歩にともない、微視的シミュレーションによる物質の構造、反応の研究が盛んである。原子核物理の分野でもQMD[3]やAMD[4]、FMD[5]などの分子動力学による核反応計算や、天体に於ける核物質の構造計算[6]が行われ、反応機構や物質構造の仮定に依らない新しい結果が得られるようになった。我々はこの核子多体系に於ける分子動力学の成果に着目し、クォーク多体系にも同様のシミュレーションを行う事を考えた。しかしクォーク系はSU(3)カラー力学に支配されるため、分子動力学としては新しい手法の開発が必要になる。

クォークの状態は空間的な波動関数だけでなくスピン、フレーバー、カラーで決まる。クォーク間相互作用の特徴はカラー交換力であり、そのためカラー座標の時間変化を分子動力学に取り入れた。今回はスピン、フレーバーを固定(無視)し空間座標、カラー座標におけるconstituentクォーク多体系の分子動力学を構築した。これは微視的シミュレーションとしては初めてダイナミカル(自動的)に閉じ込め-非閉じ込めの効果を扱うことが出来るものである。ここではこのモデルを無限系クォーク物質や有限系に適用し、QGP相転移や、クォーク物質の統計的性質を研究する手段としての有効性を確かめる。

2 クォーク系の分子動力学

通常の温度や密度ではクォークが単体の粒子として取り出すことは出来ない。これはカラーに依存した強い閉じ込めポテンシャルによって理解されている。このカラー自由度を取り扱う事がクォーク系の分子動力学を作る上で必要になる。ここでは簡単のためスピンとフレーバーを無視し、座標空間とカラー空間での時間発展の記述を行う。

全系の波動関数Ψを1粒子波動関数ψ_iの直積で表す。反対称化はここでは無視する。

$$\Psi = \prod_i \psi_i, \tag{1}$$

$$\psi_i = \phi_i(\mathbf{r})\chi_i, \tag{2}$$

$$\phi_i(\mathbf{r}) \equiv \exp[-(\mathbf{r}-\mathbf{R}_i)^2/2L^2 - i\mathbf{P}_i\mathbf{r}], \tag{3}$$

$$\chi_i \equiv \begin{pmatrix} \cos\alpha_i\ e^{-i\beta_i}\ \cos\theta_i \\ \sin\alpha_i\ e^{+i\beta_i}\ \cos\theta_i \\ \sin\theta_i\ e^{i\varphi_i} \end{pmatrix}. \tag{4}$$

ここでϕ_iは座標空間における波動関数で幅を固定したガウス波束とし、χ_iはカラーSU(3)のcoherent stateである。

系の時間発展は$\{\mathbf{R}_i, \mathbf{P}_i, \alpha_i, \beta_i, \theta_i, \varphi_i\}$の運動方程式を解くことで決まる。系のラグランジアンを計算すると、

$$\mathcal{L} = \langle\Psi|i\hbar\frac{d}{dt} - \hat{H}|\Psi\rangle \tag{5}$$

$$= \sum_i \langle\phi_i|i\hbar\frac{d}{dt}|\phi_i\rangle + \sum_i \langle\chi_i|i\hbar\frac{d}{dt}|\chi_i\rangle - \langle\Psi|\hat{H}|\Psi\rangle \tag{6}$$

$$= \sum_i [-\dot{\mathbf{P}}_i\mathbf{R}_i + \hbar\dot{\beta}_i\cos 2\alpha_i\ \cos^2\theta_i - \hbar\dot{\varphi}_i\sin^2\theta_i] - H \tag{7}$$

となり、時間依存変分原理

$$\frac{\partial\mathcal{L}}{\partial q} = \frac{d}{dt}\frac{\partial\mathcal{L}}{\partial\dot{q}} \tag{8}$$

から次のような運動方程式を得る。

$$\dot{\mathbf{R}}_i = \frac{\partial H}{\partial\mathbf{P}_i}, \tag{9}$$

$$\dot{\mathbf{P}}_i = -\frac{\partial H}{\partial\mathbf{R}_i}, \tag{10}$$

$$\dot{\beta}_i = -\frac{1}{2\hbar\sin 2\alpha_i\ \cos^2\theta_i}\frac{\partial H}{\partial\alpha_i}, \tag{11}$$

$$\dot{\theta}_i = \frac{1}{2\hbar\sin\theta_i\ \cos\theta_i}\frac{\partial H}{\partial\varphi_i}, \tag{12}$$

$$\dot{\alpha}_i = \frac{1}{2\hbar\sin 2\alpha_i\ \cos^2\theta_i}\frac{\partial H}{\partial\beta_i} - \frac{\cos 2\alpha_i}{2\hbar\sin 2\alpha_i\ \cos^2\theta_i}\frac{\partial H}{\partial\varphi_i}, \tag{13}$$

$$\dot{\varphi}_i = -\frac{1}{2\hbar\sin\theta_i\ \cos\theta_i}\frac{\partial H}{\partial\theta_i} + \frac{\cos 2\alpha_i}{2\hbar\sin 2\alpha_i\ \cos^2\theta_i}\frac{\partial H}{\partial\alpha_i}. \tag{14}$$

カラーがcoherent stateで連続的に変化するのは、rgbのいずれかのカラー状態にあるクォークが他の粒子と相互作用しながら時事刻々カラーを変えていく事象の重ね合わせを表していると解釈できる。

クォーク間の相互作用には1グルーオン交換力とリニアな閉じ込めポテンシャル、核子間の中間子交換力をクォーク間に焼き直した斥力と引力を用いる。カラーの閉じ込めポテンシャルは3体力の取り扱いが難しいため2体力のみを用いている。ハミルトニアンは以下のように書ける。

$$\hat{H} = \sum_i \sqrt{m^2 + \mathbf{p}_i^{\,2}} + \frac{1}{2}\sum_{i,j\neq i}\hat{V}_{ij} \tag{15}$$

$$\hat{V}_{ij} = -\sum_{a=1}^{8}\frac{\lambda_i^a\lambda_j^a}{4}[V_{\mathrm{S}}(\hat{r}_{ij}) + V_{\mathrm{L}}(\hat{r}_{ij})] + V_{\mathrm{M}}(\hat{r}_{ij}) \tag{16}$$

$$V_{\mathrm{S}}(r) \equiv -\frac{\alpha_{\mathrm{S}}}{r} \tag{17}$$

$$V_{\rm L}(r) \equiv Kr \tag{18}$$

$$V_{\rm M}(r) \equiv -\frac{g_{\sigma q}^2}{4\pi}\frac{e^{-\mu_\sigma r}}{r} + \frac{g_{\omega q}^2}{4\pi}\frac{e^{-\mu_\omega r}}{r} \tag{19}$$

$$\lambda^a = \text{Gell-Mann matrices.} \tag{20}$$

ここで$V_{\rm S}$はグルーオン交換力 [7]、$V_{\rm L}$は閉じ込め [7] $V_{\rm M}$は中間子交換力 [8] である。また、$V_{\rm L}(r)$ には有限の距離$r_{\rm cut}$でのカットオフを入れる。ハミルトニアン第1項の運動エネルギーからは、1粒子波動関数にガウス波束を用いていることに因る運動量分散項が現れるが、今は波束の幅を固定しているためこの運動量分散項はspuriousになり、運動エネルギーからは差し引いている。この計算で用いるクォーク質量及びその他のパラメータの値は以下のものを用いる。$m = 320$ MeV, $L = 0.35$ fm, $\alpha_{\rm S} = 1.25$, $K = 750$ [MeV/fm], $r_{\rm cut} = 3$ [fm], $g_{\sigma q} = 10.6/3$, $\mu_\sigma = 550$ [MeV], $g_{\omega q} = 17.55/3$, $\mu_\omega = 782$ [MeV].

ここで補足する点が2つある。まず、我々の模型は反対称化を取り入れていないため、カラー1重項状態での交換項の寄与が抜けていて、しかもその寄与は無視できないほど大きい。例えば、カラー1重項のrgbの、rgの$\lambda\lambda$ 行列要素は

$$\langle rg|\lambda\lambda|rg - gr\rangle = 4\langle rg|\lambda\lambda|rg\rangle \tag{21}$$

となり、交換項の寄与を入れると強度が4倍になる。そこでカラー依存の相互作用パラメータを4倍して以下のものを用いる。

$$\alpha_{\rm S}^{\rm eff} = 4\alpha_{\rm S} \tag{22}$$

$$K^{\rm eff} = 4K \tag{23}$$

また、中間子交換力の計算では、核子間の相互作用をクォーク間の相互作用に焼き直したものであるため、核子の拡がりが反映されるようにLの代わりに多少大きめの波束幅で計算する。

$$L^{\rm eff} = 0.7 \text{ [fm]} \tag{24}$$

3 核子 (3クォーク系) の性質

これまでのところ反クォーク$\bar{q}$の自由度は入れていないので、一番簡単な多体系は3つのクォークからなる核子である。カラー中性 (White) な核子をシミュレートする手順としてはじめに3クォーク系のカラーをWhiteにする。すなわち

$$\sum_{i=1}^{3}\langle\chi_i|\lambda^a|\chi_i\rangle = 0 \qquad (a = 1, \cdots, 8) \tag{25}$$

となるようなχ_iのパラメータを探す。具体的には、はじめχ_iのパラメータとしてランダムな値を採り、$\sum_{i,j\neq i}\sum_{a=1}^{8}\langle\chi_i|\lambda^a|\chi_i\rangle\langle\chi_j|\lambda^a|\chi_j\rangle$ に単調に依存する引力を与えた上でカラー空間に於ける摩擦冷却を行う。これによって3クォーク系がトータルでWhiteになる。次に核子内運動に相当する運動を与える。

このようにして得られた核子の性質を挙げると、全エネルギー1269 [MeV]、運動エネルギー74 [MeV/q]、Lを用いてfoldした平均自乗半径0.46 [fm]、$L^{\rm eff}$を用いてfoldした平均自乗半径0.87 [fm]、となる。

4 クォーク無限系の性質

次にクォーク無限系について考察する。無限系は実際には周期的境界条件を課した箱の中の有限系で近似する。まず上で説明した3クォークからなるカラー中性の核子を多数作り、これを空間にランダムに

ばらまく。この段階では系は「励起状態」にある。この系のエネルギー最低状態を作るには摩擦冷却を行うが、核子内での運動を許したまま冷却すると核子内運動も無くなってしまうため、核子内での運動やカラーの時間変化を凍結しておいて、「核子」の重心運動のみの空間で摩擦冷却を行う。「核子」重心運動の空間での冷却を行った系は、「核子」は静止しているが核子内ではクォークが運動している。「核子」のフェルミ運動は今は無視する。エネルギー最低状態まで冷却しても、$V_{\rm M}$に含まれる斥力が働いているため、系がつぶれてしまうことはない。このエネルギー最低状態の系に「核子」のランダムな運動をさせる事で系に励起エネルギーを与える。適当な時間放っておくとやがて平衡状態に達し、「閉じ込め」「非閉じ込め」状態の判定や、系の温度その他の統計的な量を議論することが出来る。

この系の初期条件はクォークが「閉じ込め」状態にある核子からなっているが平衡に達した時点でクォークが閉じ込められているかどうかを次のように判定する。

$$\begin{cases} |\mathbf{R}_i - \mathbf{R}_j| < d_{\rm cluster} \quad (i,j=1,2,3), \\ \left| \sum_i^3 \langle \chi_i | \lambda^a | \chi_i \rangle \right| < \varepsilon. \end{cases} \tag{26}$$

つまり、「3クォークがある距離内に存在し、それが3つでWhiteになっている」というのを「閉じ込め」状態にある条件とする。この判定を全てのクォークについて順次行っていくが、「閉じ込め」状態にあると判定された組の3クォークは別の組と共有しないよう次の判定では除外する。

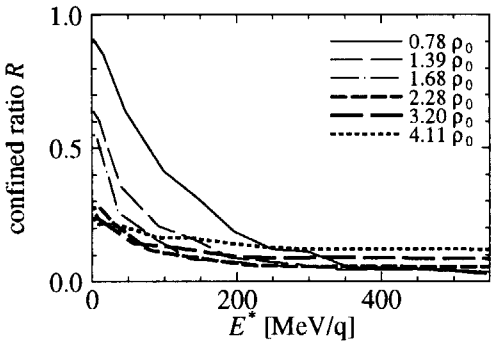

図1. 密度及び励起エネルギーに対する閉じ込め率(閉じ込められているクォークの割合)の変化。表示されている密度はバリオン密度。

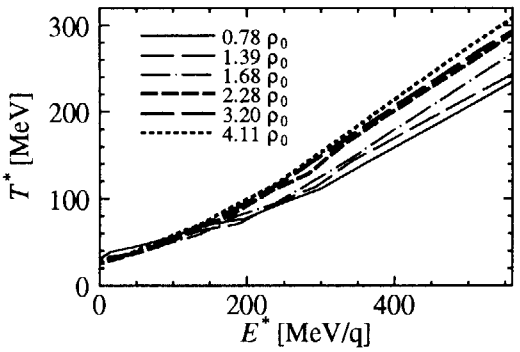

図2. クォークの運動エネルギー分布から求めた系の温度。運動エネルギー分布はボルツマン分布でフィットされる。

図1は密度及び励起エネルギーを変化させたときのクォークの閉じ込め率の変化の様子である。低密度、低励起ではクォークの閉じ込め率は高いが、励起エネルギーを上げていったり密度を高くすると閉じ込められているクォークの割合は減っていく。ここで得られた結果では、常識的な相転移の密度よりもかなり低い密度で非閉じ込め状態になってしまっている。用いている相互作用パラメータを調整する必要がある。

いま扱っている系の熱力学的性質かを調べるためにクォークの運動エネルギー分布を見ると、特に高エネルギーではボルツマン分布で非常に良くフィットされる。従ってこの系は古典ガスとして振る舞っていることが分かる。ボルツマン分布のフィットから系の温度を求めたのが図2である。高密度の場合は励起エネルギーに対してほぼ直線的に温度が依存しているが、低密度の場合低励起の領域で温度の上昇が緩やかになっている(比熱が大きい)。これはちょうど図1の閉じ込め率の変化する領域であり、核子クラス

ターが解けるのにエネルギーが使われたためと思われる。これがはっきりした相転移を示しているのかは今の所明らかでない。また、この枠組みには$q\bar{q}$の対生成過程が取り入れられていないので、系が高温でボルツマンガスの振る舞いをするが、対生成の過程を取り入れることで系の統計性は別のものになると思う。

5 有限系 (原子核)

この分子動力学を原子核衝突のシミュレーションに用いるには、まず衝突させる原子核をつくる。無限系のエネルギー最低状態を作るときと同様に、"3q 核子" を空間にばらまき、核子内自由度を凍結した上で摩擦冷却により、系を安定させるとほぼ球形の束縛系 (原子核) ができる。これを 2 つ boost し時間発展させることで原子核衝突のシミュレーションが出来る。

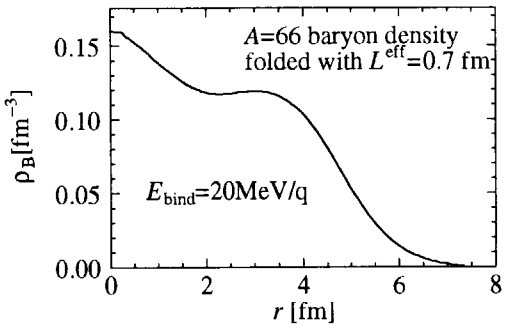

図 3. 得られた質量数 66 の "原子核" の密度分布。

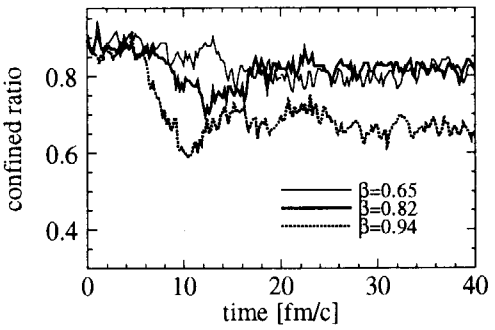

図 4. クォークの閉じ込め率の時間変化。

図 3 はクォーク 198 体系 (バリオン数 66) の原子核の密度分布である。密度は L^{eff} で fold して求めた。束縛エネルギーがクォーク当たり 20MeV と深すぎる。これは相互作用の調整を行っていないのと、核子のフェルミ運動を入れてないのが原因である。将来的には改善したい。

図 3 の原子核同士を衝突させたときのクォークの閉じ込め率の時間発展を示したのが図 4 である。β_{CM} は重心系での原子核の速度を表している。衝突とともに非閉じ込めのクォークが現れ、時間と共に減衰しているのがわかる。高エネルギーの衝突 (β_{CM}=0.94) の方が非閉じ込めクォークがより多く現れる。また、非閉じ込め」クォークの存在する時間が常識的な QGP のタイムスケールに比べて長続きしすぎるが、$q\bar{q}$ 対生成過程が取り入れられていないのと、閉じ込めポテンシャルにカットオフを用いているのが原因と思われる。これらを改善すればより早く非閉じ込め状態は減衰するだろう。

6 まとめ

我々は座標空間とカラー空間における分子動力学をつくり、クォーク系のシミュレーションを行った。これはクォークの閉じ込め非閉じ込めのダイナミカル (自動的) な記述が可能な初めての分子動力学である。まだ定性的な議論の段階だがこれによって分子動力学によるクォーク物質の研究が可能になった。

周期的境界条件の下でのクォーク無限系にこの枠組みを適用し密度、励起エネルギーに対する系の応答を調べたところ、低密かつ度低エネルギーではクォークの閉じ込めが実現しているが、高密度や高エネルギーになると閉じ込め状態に無いクォークが現れることが分かった。また系の温度と励起エネルギーとの関係からは、系が高温や高密度で古典ガスとして振る舞うこと、低密度では励起エネルギーが上がるときに温度の上昇が抑えられる領域があり、相転移的な様相を示すことなどが分かった。

有限系にこの分子動力学を適用しクォークからなる核子が束縛系をつくることを確かめた。定量的にはまだ不十分だが、原子核衝突のシミュレーションにこの分子動力学を適用することが出来ることが分かった。原子核衝突のシミュレーションでは、衝突とともに閉じ込め状態から非閉じ込め状態への転移や、ここでは示さなかったが、衝突のエネルギーに応じた核物質のフロー、原子核のすり抜けなどの現象が定性的に記述できることも分かった。

今後は相互作用の調節や、$q\bar{q}$対生成過程の導入等によって無限系の計算、原子核衝突の計算ともにある程度定量的な議論が可能になるのではないかと思う。

参考文献

[1] J. Harris and B. Müller, Ann. Rev. Nucl. Part. Sci. **46** (1996) 71; W. Greiner and D. Rischke, Phys. Rep. **264** (1996) 183; C. Y. Wong, *Introduction to High-Energy Heavy-Ion Physics*, World Scientific Publ. Singapore, 1994.

[2] G. Baym, Nucl. Phys. **A590** (1995) 233.

[3] J. Aichelin and H. Stöcker, Phys. Lett. B **176** (1986) 14; J. Aichelin, Phys. Rep. **202** (1991) 233; D. H. Boal and J. N. Glosli, Phys. Rev. C **38** (1988) 1870; T. Maruyama, A. Ohnishi and H. Horiuchi, Phys. Rev. **C42** (1990), 386.

[4] A. Ono, H. Horiuchi, T. Maruyama and A. Ohnishi, Phys. Rev. Lett **68** (1992) 2898, Prog. Theor. Phys. **87** (1992) 1185, Phys. Rev. C **47** (1993) 2652.

[5] H. Feldmeier, Nucl. Phys. **A515** (1990) 147.

[6] T. Maruyama, K. Niita, K. Oyamatsu, T. Maruyama, S. Chiba and A. Iwamoto, Phys. Rev. **C57** (1998) 655.

[7] T. Hatsuda, Prog. Theor. Phys. **70** (1983) 1685.

[8] K. Saito, K. Tsushima and A.W. Thomas, nucl-th/9901084; and references therein.

8. Chiral Symmetry in the Baryon Spectrum

京都大学理学研究科物理学第二教室
慈道 大介

Baryon resonances with even and odd parity are collectively investigated from the viewpoint of chiral symmetry(ChS). We propose a quartet scheme where Δ's and N*'s with even and odd parity form a chiral multiplet. This scheme gives model-independent constraints on the baryon masses in the quartet, which are consistent with observed masses with spin 1/2,3/2,5/2. The scheme also gives selection rules in the one-pion decay.

§ 1.序論

ハドロン物理の目的の一つとして、ハドロンの諸性質をＱＣＤから理解することがあげられる。低エネルギーのハドロンの性質を考えるうえで、カイラル対称性とその動的破れはＱＣＤの重要な性質である。ハドロンは、原理的に、カイラル群の既約表現に分類することができ、質量や相互作用はカイラル対称性により制約を受ける。

今まで、バリオンは主にカイラル群の非線形表現を使って研究がなされてきて、chiral perturbation theoryとしてまとめられ多くの成功をおさめている[1]。核子の非線形表現は、商群 $SU(N_f)_L \times SU(N_f)_R/SU(N_f)_V$ の座標と核子へ $SU(N_f)_V$ の既約表現を与えることで、ユニークに決まる[2]。しかし、近年、ハドロン物理の興味はゼロ温度でのハドロンの性質にとどまらず、有限温度や有限密度でのハドロンの振る舞いにもある。そのような特殊な状況下では、動的に破れていたカイラル対称性は回復すると考えられており、そこでは、カイラル対称性が破れていることを前提に導かれた非線形表現は使えなくなる。

一方、線形表現は、軸性ベクトル変換も含めた $SU(N_f)_L \times SU(N_f)_R$ の既約表現を与えることで決まり、ハドロンはカイラル群の既約表現によって分類される。線形表現を用いたバリオンの記述の最初の例は、Gell-Mann Levy のσモデルである[3]。そこでは、核子がカイラル群 $SU(2)_L \times SU(2)_R$ の下で線形に変換する。DeTar と Kunihiro はこのモデルを、正のパリティーを持つ核子 N_+ とそのパリティーパートナー N_- を含めたモデルに一般化した[4]。このモデルの特徴的なところは、カイラル対称な質量項を導入できるところである。このモデルでは、$N\pm$ はお互いに反対符号の軸性電荷をもつ N_1 と N_2 の線形結合であらわされ、お互いがカイラルパートナーとなる。これは"mirror assignment"と呼ばれ、N_1 と N_2 が同符号の軸性電荷を持つ"naive assignment"とは区別される[5]。

本研究の目的は、カイラル対称性とその破れがどのように現れているかを、群論的な立場から調べることにある。そのためには、バリオンをカイラル群の既約表現によって分類し、その既約表現に基づく線形σ模型を用いてカイラル対称性が破れた世界に移行し、現象論的な性質を見る。ここでは励起状態 (Δ, N^*) に注目し、mirror assignment に従うとする。以下に見るように、Δ と N^* は同じ既約表現に分類され、結果として、４つの粒子 $\Delta+$, $\Delta-$, N^*+, N^*-（下付き添え字はパリティーを表す）が同一既約表現に属する枠組みに至る。これを"quartet scheme"と呼ぶことにする。この quartet scheme は、quartet menber の質量に対してパラメターに依らない関係式を与える。これらは、実際に観測されている質量と良く合っている。

本報告書は[6]を元に書かれており、そちらも参考にしていただきたい。

§ 2．Δの変換性と線形σ模型

$\Delta(1232)$ (J=3/2) を例として議論する。まずはじめに、$\Delta(I=3/2)$ にどのカイラル群の表現に割り当てるかを選ぶ必要がある。クォークがカイラル群の基本表現 $\chi_{1/2} \equiv (1/2,0) \oplus (0,1/2)$ に属していて、バリオンがクォーク３つ $[(1/2,0) \oplus (0,1/2)]^3$ からできていることに留意すると、$I=3/2$ を持つ $\chi_{1,1/2} \equiv (1,1/2) \oplus (1/2,1)$ 表現と $\chi_{3/2} \equiv (3/2,0) \oplus (0,3/2)$ 表現が候補となる。ここで、括弧の中の左側（右側）

は、$SU(2)_L(SU(2)_R)$ の表現を表す。ところが、$\Delta(1232)$ は核子と π 粒子の強い共鳴状態であり、$N\times\pi=\chi_{1/2}\times(1/2,1/2)$ には $\chi_{3/2}$ が含まれないので、Δ の属する規約表現として $\chi_{1,1/2}$ を選ぶのが適当である。

この $\chi_{1,1/2}$ はアイソスピン 3/2 と 1/2 の両方を含んでいる。後者は N^* を表すのに用いることにする。したがって、$\chi_{1,1/2}$ 表現を用いて Δ をカイラル対称に考えるには、必然的に N^* も導入する必要があり、それらは同じ規約表現の中に入る。さらに mirror assignment を取ると、それぞれ正と負のパリティーを持つ二つの場 ψ_1 と ψ_2 を導入する必要がある。したがって、ここで扱いたい粒子は $\Delta_+(P_{33})$, $\Delta_-(D_{33})$, $N^*_-(P_{13})$, $N^*_+(D_{13})$ の 4 つである。

mirror assignment では、ψ_{1l} と ψ_2 は (1,1/2) 表現に属する場、ψ_{1r} と ψ_{2l} は (1/2,1) 表現に属する場である。これらの場は $(\psi_{1,2})^{\alpha\beta}_\gamma$ のように 3 つの足 α,β,γ=1,2 を持つ。(α,β) は 3 重項の、γ は 2 重項の足である。成分表示で書けば、

$$(\psi_{1,2})^{\alpha\beta}_\gamma=\sum_{A=1\,2\,3}(\tau^A)^{\alpha\beta}(\psi_{1.2})^A_\gamma\ , \tag{1}$$

となる。ここで τ^A はパウリ行列である。

$SU(2)_L\times SU(2)_R$ の下での $\psi_{1,2}$ の変換則は以下のように与えられる。

$$\begin{aligned}(\tau^A)_{\alpha\beta}(\psi_{1l.2r})^{A,\gamma}&\rightarrow(L\tau^AL^\dagger)_{\alpha\beta}(R\psi_{1l.2r})^{A,\gamma}\ ,\\(\tau^A)_{\alpha\beta}(\psi_{2l.1r})^{A,\gamma}&\rightarrow(R\tau^AR^\dagger)_{\alpha\beta}(L\psi_{2l.1r})^{A,\gamma}\ ,\end{aligned} \tag{2}$$

対応する無限小変換は

$$\begin{aligned}[Q^A_L,\psi^{Ba}_{1l.2r}]&=i\epsilon^{ABC}\psi^{C.a}_{1l.2r}\ ,\\[Q^A_R,\psi^{Ba}_{1l.2r}]&=-\frac{1}{2}(\tau^A)^a_b\psi^{B.b}_{1l.2r}\ ,\\[Q^A_L,\psi^{Ba}_{2l.1r}]&=-\frac{1}{2}(\tau^A)^a_b\psi^{B.b}_{1r.2l}\ ,\\[Q^A_R,\psi^{Ba}_{2l.1r}]&=i\epsilon^{ABC}\psi^{C.a}_{1r.2l}\ ,\end{aligned} \tag{3}$$

となる。メソン場 $M\equiv\sigma+i\vec{\pi}\cdot\tau$ は (1/2,1/2) 表現に属するので、$M\rightarrow LMR^\dagger$ と変換をする。

上記のようなカイラル変換に対し不変なラグランジアンを考える：

$$\begin{aligned}\mathcal{L}&=(\text{Kinetic Terms})+m_0(\bar\psi^A_2\gamma_5\psi^A_1-\bar\psi^A_1\gamma_5\psi^A_2)\\&+a\bar\psi^A_1\tau^B(\sigma-i\vec\pi\cdot\vec\tau\gamma_5)\tau^A\psi^B_1\\&+b\bar\psi^A_2\tau^B(\sigma+i\vec\pi\cdot\vec\tau\gamma_5)\tau^A\psi^B_2+\mathcal{L}_M\ ,\end{aligned} \tag{4}$$

ここで a,b,m_0 はカイラル対称性と無関係なパラメーターである。また、$\mathcal{L}_M$ はメソンに対するラグランジアンで、カイラル対称性を自発的に破りさえすれば、具体的な形は必要なく以下の結論は変わらない。このラグランジアンは $\chi_{1/2}$ 表現の chiral doublet model[4] から $\chi_{1,1/2}$ 表現の chiral quartet model への自然な拡張である。

既に指摘したように、$\psi^{A,\gamma}_i$ はアイソスピン 3/2 の場 $\Delta_{M,i}$ (M=3/2, 1/2, -1/2, -3/2) と 1/2 の場 $N^*_{i,m}$ (m=1/2, -1/2) を含む。これらは、以下のように分離できる。

$$\psi^{A,\gamma}_i=\sum_M(T^A_{3/2})_{\gamma M}\Delta_{i.M}+\sum_m(T^A_{1/2})_{\gamma m}N^*_{i.m}\ , \tag{5}$$

ここで、アイソスピン射影行列 $T_{3/2}{}^A$ と $T_{1/2}{}^A$ は Clebsh-Gordon 係数によって定義される：

$$\begin{aligned}(T^A_{3/2})_{aM}&=\sum_{r=1.0.-1}(1r\tfrac{1}{2}a|\tfrac{3}{2}M)\epsilon^A_r\\(T^A_{1/2})_{am}&=\sum_{r=1.0.-1}(1r\tfrac{1}{2}a|\tfrac{1}{2}m)\epsilon^A_r\end{aligned} \tag{6}$$

またベクトル $\vec{\epsilon}_r$ は 3 重項の足 A=(1,2,3) 基底と r=(+1,0,-1) 基底を関係づけるものである。

§3. 結果

σ 粒子が真空期待値を持つことにより、カイラル対称性を自発的に破る。そのときに、(i) Δ や N^* の質量がどのように与えられるか、(ii) Δ と N^* の崩壊パターンがどうなるかを見ていく。

§3.1 質量

質量項に非対角な成分があるので、質量行列を対角化する物理的な基底 $\Delta\pm$ と $N^*\pm$ に書き直す。それらは

$$\begin{pmatrix}\Delta_+\\\Delta_-\end{pmatrix}=\frac{1}{\sqrt{2\cosh\xi}}\begin{pmatrix}e^{\xi/2}&\gamma_5e^{-\xi/2}\\\gamma_5e^{-\xi/2}&-e^{\xi/2}\end{pmatrix}\begin{pmatrix}\Delta_1\\\Delta_2\end{pmatrix}$$

で与えられ、N^* についても同様で ξ を η に置き換える。混合角 ξ, η は $\sinh\xi=-(a+b)\sigma_0/m_0$ ないし $\sinh\eta=(a+b)\sigma_0/(2m_0)$ で決まる。

このようにして最終的に以下の質量公式を得る。

$$\begin{aligned}m_{\Delta\pm}&=\sqrt{(a+b)^2\sigma_0^2+m_0^2}\mp\sigma_0(a-b),\\m_{N^*_\pm}&=\sqrt{(\frac{a+b}{2})^2\sigma_0^2+m_0^2}\pm\frac{\sigma_0}{2}(a-b).\end{aligned} \tag{7}$$

これらの質量公式から、カイラル対称性の破れによって、パリティーパートナー間 (Δ_+ vs Δ_-、と N^*_+ vs N^*_-) の質量差が生じ、同時にアイソスピン間 (Δ vs N^*) の質量の縮退もとけることがわかる。また、m_0=0 と取ったときが naive assignment に対応するが、そのとき、$m_{\Delta\pm}=2m_{N^*_\mp}$, となり現実にそぐわない。そのために、mirror assignment を取った。

このモデルで一番重要な結論は、これらの質量

公式から得られる、パラメーターa, b, m_0に無関係な次の3つの関係式である。

1) パリティーパートナー間の質量順はN^*とΔとで常に逆である：

$$\mathrm{sgn}\left[m_{\Delta_+} - m_{\Delta_-}\right] = -\,\mathrm{sgn}\left[m_{N_+^*} - m_{N_-^*}\right] . \quad (8)$$

2) 二つのパリティー2重項の質量差は固定されている：

$$\frac{1}{2}(m_{\Delta_-} - m_{\Delta_+}) = m_{N_+^*} - m_{N_-^*} . \quad (9)$$

3) Δのパリティー2重項の質量平均はN*の2重項の質量平均以上である：

$$\frac{1}{2}(m_{\Delta_+} + m_{\Delta_-}) \geq \frac{1}{2}(m_{N_+^*} + m_{N_-^*}) . \quad (10)$$

今まで、スピン3/2に限って話を進めてきたが、実は、$\chi_{1,1/2}$表現を考えるかぎり、上記の結論はスピンによらないものである。

このように得た結果(8, 9, 10)と観測されているスペクトラムとの比較を行う。そのために、現実の世界での4重項の候補を、それぞれのスピンーパリティーで、軽いものから取ってくることにする。ただし、$N(940)$は例外で$\chi_{1/2}$表現に属すると考える。さらに、$\chi_{1/2}$表現でもmirror assignmentが実現していると、$N(940)$のカイラルパートナーが必要になり、その候補としては$N(1535)$か$N(1650)$かそれらの線形結合が考えられる[5]。ここでは、case 1として$N(1535)$が4重項メンバーの場合と、case 2として$N(1650)$が4重項メンバーの場合と、二つの場合について調べる。図1には、上記の条件によって選ばれた励起状態が図示されている。

カイラル対称性から得られた質量関係式(8, 9, 10)と実験データとの比較は表1に示されている。観測されている質量はどのスピンでも(8, 9)をよく満たしている。(10)に関しては、スピン1/2, 5/2ではよく満たしていて、3/2では少し破れているが、定性的にはどのスピンでも満たしていると言える。

さて、このようにパラメーターに依存せず、観測されている質量をよく再現しているので、議論をさらにすすめ、それぞれのスピンセクターでパラメーターa, b, m_0を決めることを試みる。ここでは、4つの質量をインプットとしてもちいて最小二乗法でパラメーターを決めた。また$\sigma_0 = f_\pi$=93MeVを用いる。結果は表1の下2行に示されている。スピン3/2では、結論(10)の若干の破れを補うために、$a=-b$を仮定した。決めたパラメーターを元に計算した質量は図1に示した。どの値も10%以内で実験を再現している。

興味深いことに、どのスピンセクターにおいても、おおよそm_0～1500 MeVを得た。この値はDeTar-Kunihiro modelの場合の値(m_0= 270 MeV)と比べて比較的大きな値である。m_0の起源は、今後、ＱＣＤにおけて理解される必要のある課題である。また、m_0の値、表現による違いが物理的にどのような意味があるのかも今後の課題である。カイラル対称性が回復した世界で、バリオン的な励起モードの存在を調べることは、このモデルのチェックとなりうる。

§3.2 崩壊モード

スピン3/2の話にもどる。一つのπを放出して同じ4重項間の崩壊モードを調べてみる。πと$\psi\pm$の相互作用ラグランジアンは$a=b$=1.2のとき、

$$\mathcal{L}_{1\pi} = (\bar{\psi}_+^A, \bar{\psi}_-^A) \begin{pmatrix} 0 & -a \\ a & 0 \end{pmatrix} \tau^B (i\vec{\pi}\cdot\vec{\tau}) \tau^A \begin{pmatrix} \psi_+^B \\ \psi_-^B \end{pmatrix} ,$$

と与えられる。ここで、$\psi_+ = \frac{1}{\sqrt{2}}(\psi_1 + \gamma_5\psi_2)$ $\psi_- = \frac{1}{\sqrt{2}}(\gamma_5\psi_1 - \psi_2)$である。混合角$\xi, \eta$は、$a+b=0$であるため、等しくて0である。$\mathcal{L}_{1\pi}$は対角成分を持っていないので、パリティーを変えるような結合$\pi\Delta\pm\Delta\pm$, $\pi N^*\pm N^*\pm$, $\pi\Delta\pm N^*\pm$はtree levelでは許されない。

実際に、実験で見えている崩壊モードも上のような選択則があるように見える。$N+(1720)\rightarrow\pi\Delta+(1232)$の崩壊モードは、位相空間が十分大きいにもかかわらず全く見えていない。($N+(1720)$の主要な崩壊モードは$\pi\pi N$で、その$\pi\pi$はρから来る。)一方、$N-(1520)\rightarrow\pi\Delta+(1232)$と$\Delta-(1700)\rightarrow\pi\Delta(1232)$のＳ波の崩壊モードは、部分崩壊率としてそれぞれ5～12%と25～50%をもって観測されている[7]。その他の崩壊モードや結合定数に関しても、上記の選択則をチェックする必要がある。$\pi\Delta(1232)\Delta(1232)$結合に関しては、やや古い報告[8]ではあるが、$\pi N\rightarrow\pi\pi N$過程の解析によって、その結合は、クォーク模型から予言である$g_{\pi\Delta\Delta}=4/5\, g_{\pi NN}$の半分より小さいと報告されている。

上で議論してきた選択則は、原理的に、今回考えなかったカイラル対称な項によって変更を受け

る。これは線形σ模型における核子の軸性電荷g_Aに対する状況と全く同じである。線形σ模型でg_A、tree levelでは、1となるが、ループの寄与や高次の微分を含む項はその値を1.25にずらすことができる[9]。したがって、今後、そのような項について詳細な議論が必要である。

§4. まとめ

バリオンの励起状態(Δ, N^*)において、カイラル対称性がどのように見てるいるかをしらべた。ΔとN^*が$SU(2)_L \times SU(2)_R$の既約表現$(1, \frac{1}{2}) \oplus (\frac{1}{2}, 1)$に属する枠組みをとり、mirror assignmentを仮定した。その結果として、4つのバリオン$\Delta+$, $\Delta-$, N^*+, N^*-を同一に扱うquartet schemeを提唱するに至った。この枠組みは、モデルのパラメータに依存せずに質量に対する条件を与えた。この条件は、広いスピンセクターで、現実に観測されているバリオンの質量の傾向と一致している。また、スピン3/2では、一つのπを放出して崩壊する過程に対する選択則を得た。スピン3/2でパリティーを変えない遷移が見えないことを確かめることが、このモデルのテストになり、バリオンでのカイラル対称性の役割を調べるのに情報を与える。

本研究は、初田哲男氏（京都大学）と国広悌二氏（龍谷大学）との共同研究である。また、私は日本学術振興会特別研究員として補助を受けている。

参考文献

[1] S. Weinberg, *Physica* **96A**, 327 (1979). J. Gasser and H. Leutwyler, *Annals Phys.* (N.Y.) **158**, 142 (1984). S. Weinberg, *Nucl. Phys.* **B363**, 3 (1991).
[2] S. Weinberg, *Phy. Rev.* **166**, 1568 (1968).
[3] M. Gell-Mann and M. Levy, *Nuovo Cim.* **16**, 705 (1960). J. Schwinger, *Ann. Phys.* (N.Y.) **2**, 407 (1958).
[4] C. DeTar and T. Kunihiro, *Phys. Rev.* **D39**, 2805, (1989).
[5] D. Jido, Y. Nemoto, M. Oka and A. Hosaka, hep-ph/9805306.
[6] D. Jido, T. Hatsuda, T. Kunihiro, hep-ph/9910375.
[7] Particle Data Group, C. Caso *et. al.*, *Eur. Phys. J.* 3,1 (1998).
[8] R.A. Arndt *et. al.*, *Phys. Rev.* **D20**, 631 (1979).
[9] B. W. Lee, *Chiral Dynamics*, (Gordon and Breach, New York, 1972).

表1. quartet scheme (QS)の結果と実験との比較。case 1はquartet menberとして$N(1535)$を取った場合で、case 2は$N(1650)$を取った場合。最後の2行は実験データから決めたモデルのパラメータを表す。

	QS	$J=\frac{1}{2}$ case 1	$J=\frac{1}{2}$ case 2	$J=\frac{3}{2}$	$J=\frac{5}{2}$
$sgn\begin{pmatrix} m_{N^*_+}-m_{N^*_-} \\ m_{\Delta_+}-m_{\Delta_-} \end{pmatrix}$	−	−	−	−	−
$\frac{m_{N^*_+}-m_{N^*_-}}{m_{\Delta_+}-m_{\Delta_-}}$	−0.5	−0.33	−0.72	−0.43	−0.2
$\frac{m_{N^*_+}+m_{N^*_-}}{m_{\Delta_+}+m_{\Delta_-}}$	≤ 1	0.84	0.88	1.1	0.87
m_0 (MeV)		1380	1460	1540	1590
$(a,\ b)$		(5.2, 6.6)	(4.4, 6.1)	(1.2, −1.2)	(5.8, 5.7)

図1. スピン1/2, 3/2, 5/2を持ったquartet menber。それぞれのスピンで右側は観測されている質量を表し、左側はquartet schemeで再現されたものを表す。実線と破線は、それぞれ、正のパリティーと負のパリティーを持つバリオンを表す。

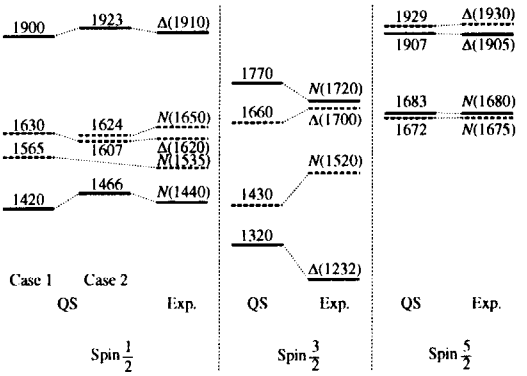

9. A lattice test of the Kugo-Ojima confinement criteria

Hideo Nakajima[1]
Department of Information science, Utsunomiya University
Sadataka Furui [2]
School of Science and Engineering, Teikyo University

Abstract

We present the first results of numerical test of the Kugo-Ojima confinement criterion in the lattice Landau gauge. The Kugo-Ojima criterion of color confinement in the BRS formulation of the continuum gauge theory is given by $u_b^a(0) = -\delta_b^a$, where

$$\int dx e^{ip(x-y)} \langle 0|TD_\mu c^a(x) g(A_\nu \times \bar{c})^b(y)|0\rangle = (g_{\mu\nu} - \frac{p_\mu p_\nu}{p^2}) u_b^a(p^2).$$

We measured the lattice version of $u_b^a(0)$ in use of $1/(-\partial D(A))$ where $D_\mu(A)$ is a lattice covariant derivative in the new definition of the gauge field as $U = e^A$. We obtained that $u_b^a(0)$ is consistent with $-c\delta_b^a$, $c = 0.7$ in $SU(3)$ quenched simulation, $\beta = 5.5$, on 8^4 and 12^4. We report the β dependence and finite-size effect of c.

1 Introduction

The colour confinement problem in the continuum gauge theory was extensively analysed in use of the BRS formulation by Kugo and Ojima[1]. A sufficient condition of the colour confinement given by them is that u_b^a defined by the two-point function of the FP (Faddeev-Popov) ghost fields, $c(x), \bar{c}(y)$, and $A_\nu(y)$,

$$\int e^{ip(x-y)} \langle 0|TD_\mu c^a(x) g(A_\nu \times \bar{c})_b(y)|0\rangle dx = (g_{\mu\nu} - \frac{p_\mu p_\nu}{p^2}) u_b^a(p^2) \tag{1}$$

satisfies $u_b^a = -\delta_b^a$.

Brief survey of Kugo-Ojima's argument that $u_b^a = -\delta_b^a$ is a sufficient condition of the colour confinement is the following.

The QCD lagrangian is invariant under the BRS transformation δ_B which is realized by replacing the parameter of the gauge transformation $\theta^a(x) \to \lambda c^a(x)$ where λ is the imaginary Grassmann number and $c^a(x)$ is the ghost field.

Putting $C(x) = gc^a(x)\Lambda_a$ where Λ_a is antihermitian such that $[\Lambda_a, \Lambda_b] = f_{abc}\Lambda_c$ and $\delta_B = \lambda \boldsymbol{\delta}_B$, and antihermitian matrix $A_\mu(x) = gA_\mu^a(x)\Lambda_a$, the BRS transformation reads

$$\boldsymbol{\delta}_B \phi = -C\phi, \quad \boldsymbol{\delta}_B A_\mu = D_\mu(A)C = \partial_\mu C + [A_\mu, C].$$

The nilpotency requirement of $\boldsymbol{\delta}_B$ derives, $\boldsymbol{\delta}_B C = -C^2$.

For each $c^a(x)$, one introduces an anti-ghost $\bar{c}^a(x)$, and similarly the matrix $\bar{C}$, and defines, $\boldsymbol{\delta}_B \bar{C} = iB$, then the nilpotency gives $\boldsymbol{\delta}_B B = 0$.

[1]e-mail nakajima@is.utsunomiya-u.ac.jp
[2]e-mail furui@dream.ics.teikyo-u.ac.jp

The total lagrangian $\mathcal{L}+\mathcal{L}_{GF+FP}$, where $\mathcal{L}=-\frac{1}{4}F^{\mu\nu}F_{\mu\nu}+\mathcal{L}_{matter}$ is BRS invariant due to the nilpotency $\boldsymbol{\delta}_B{}^2=0$. The corresponding conserved charge is

$$Q_B=\int d^3x\Big[B^aD_0c^a-\partial_0B^a\cdot c^a+\frac{i}{2}g\partial_0\bar{c}^a\cdot(c\times c)^a\Big]$$

where $(F\times G)^a=f_{abc}F^bG^c$. Thus the physical space is specified as the one that satisfies the condition $\mathcal{V}_{phys}=\{|phys\rangle\}$

$$Q_B|phys\rangle=0.$$

The BRS algebra is given by BRS charge, Q_B, and FP ghost charge, Q_c, as

$$Q_B^2=0,\quad [iQ_c,Q_B]=Q_B,\quad [Q_c,Q_c]=0.$$

Since these Q_B,Q_c are commuting with other conserved charge, all asymptotic one particle states can be classified by irreducible representations. Due to the nilpotency of BRS charge, Q_B, there only exist BRS singlets and doublets. From hermiticity of ghosts, Q_c is defined as a generator of scale transformation of FP ghosts. It is to be noted that while Q_c being hermite, FP ghost number is counted by $N_{FP}=iQ_c$, and that among FP ghost number eigenstates, $\langle M|N\rangle\neq 0$ only if $M=-N$. Due to this metric structure, BRS doublets always appear in pair of opposite sign FP ghost numbers, and this pair is called a BRS quartet. Under the assumption that **BRS singlets have positive metric**, it is proved that $\mathcal{V}_{\mathbf{phys}}$ has positive semidefinite in such a way that **BRS quartet particles appear only in zero norm.**

The Ward-Takahashi identity can be expressed as

$$\begin{aligned}0&=\langle 0|\{Q_B,T(A_\mu{}^a(x),\bar{c}(y)\}|0\rangle\\&=\langle 0|TA_\mu^a(x)B^b(y)|0\rangle-i\langle 0|TD_\mu c^a(x)\bar{c}^b(y)|0\rangle.\end{aligned}\tag{2}$$

Its Fourier transform

$$\begin{aligned}F.T.[\langle 0|TD_\mu c^a(x)\bar{c}^b(y)|0\rangle&=-i\langle 0|TA_\mu^a(x)B^b(y)|0\rangle]\\&=i\delta^{ab}\frac{p_\mu}{p^2},\end{aligned}\tag{3}$$

indicates that the Heisenberg operators, $D_\mu c^a,\bar{c}^a,A_\mu^a,B^a$ necessarily have in the $x_0\to\pm\infty$ massless asymptotic fields,

$$A_\mu^a(x)\to\partial_\mu\chi^a(x)+\cdots,\quad B^a(x)\to\beta^a(x)+\cdots,$$

$$D_\mu c^a(x)\to\partial_\mu\gamma^a(x)+\cdots,\quad \bar{c}^a(x)\to\bar{\gamma}^a(x)+\cdots.$$

One finds from the BRS transformation that for each colour a, a set of the above massless asymptotic fields form a BRS quartet.

The Noether current corresponding to the conservation of the colour symmetry is $gJ_\mu^a=\partial^\nu F_{\mu\nu}^a+\{Q_B,D_\mu\bar{c}\}$, where its ambiguity by divergence of antisymmetric tensor should be understood, and this ambiguity is utilised so that massless contribution may be eliminated for the charge, Q^a, to be well defined.

Denoting $g(A_\mu \times \bar{c})^a \to u^a_b \partial_\mu \bar{\gamma}^b$, and then $D_\mu \bar{c}^a \to (1+u)^a_b \partial_\mu \bar{\gamma}^b$, one obtains that

$$F.T.\langle 0|TD_\mu c^a(x) g(A_\nu \times \bar{c})^b(y)|0\rangle = (g_{\mu\nu} - \frac{p_\mu p_\nu}{p^2}) u^a_b(p^2),$$

provided A_μ has a vanishing expectation value. The current $\{Q_B, D_\mu \bar{c}\}$ contains the massless component, $(1+u)^a_b \partial_\mu \beta^b(x)$. We can modify the Noether current for colour charge Q^a such that

$$gJ'^a_\mu = gJ_\mu - \partial^\nu F^a_{\mu\nu} = \{Q_B, D_\mu \bar{c}\}.$$

In the case of $\mathbf{1+u=0}$, massless component in gJ'_0 is vanishing and the colour charge

$$Q^a = \int d^3x \{Q_B, g^{-1} D_0 \bar{c}^a(x)\} \tag{4}$$

becomes **well defined**.

The physical state condition $Q_B \mathcal{V}_{phys} = 0$ together with the equation (4) implies that all BRS singlet one particle states $|f\rangle \in \mathcal{V}_{phys}$ are colour singlet states. This statement implies that all coloured particles in $\mathcal{V}_{phys}$ belong to BRS quartet and have zero norm. This is the **colour confinement**.

In the course of their derivation, they assume Lorentz invariance and that the colour symmetry is not broken. They also proved that if the vector massless asymptotic field is missing in a channel a, and if the channel a belongs to the image of $1+u$ then the massless quartet in j^a_μ can not be cancelled, and the colour symmetry with charge Q^a, is spontaneously broken. (Inverse Higgs mechanism theorem)

2 Lattice calculation of u^a_b

The Faddeev-Popov operator is

$$\mathcal{M}[U] = -(\partial \cdot D(A)) = -(D(A) \cdot \partial), \tag{5}$$

where the new definition of the gauge field is adopted as $U = e^A$, and the lattice covariant derivative $D_\mu(A) = \partial_\mu + Ad(A_\mu)$ is given in [2].

The inverse, $\mathcal{M}^{-1}[U] = (M_0 - M_1[U])^{-1}$, is calculated perturbatively by using the Green function of the Poisson equation $M_0^{-1} = (-\partial^2)^{-1}$ whose zero-mode is eliminated.

$$\begin{aligned} \mathcal{M}^{-1} &= \{(-\partial^2)(1 - (-\partial^2)^{-1}\partial_\mu Ad(A_\mu(x))\}^{-1} \\ &= M_0^{-1} + \sum_{k=0}^{N_{end}} (M_0^{-1} M_1)^k M_0^{-1}. \end{aligned} \tag{6}$$

In use of colour source $|\lambda^a x\rangle$ normalized as $Tr\langle \lambda^a x|\lambda^b x_0\rangle = \delta^{ab}\delta_{x,x_0}$, the ghost propagator is given by

$$G^{ab}(x,y) = \langle Tr\langle \lambda^a x|(\mathcal{M}[U])^{-1}|\lambda^b y\rangle\rangle \tag{7}$$

where the outmost $\langle\rangle$ specifies average over samples U.

The ghost propagators of $\beta = 5.5$ and $\beta = 5$ are almost the same and they are infrared divergent which can be parametrized as $\frac{1}{p^{2.2}}$ and its finite-size effect is small[3].

In the similar way, one can calculate the Kugo-Ojima parameter as

$$(g_{\mu\nu} - \frac{p_\mu p_\nu}{p^2})u_b^a(p^2) = \langle Tr\langle \lambda^a k|D_\mu(A)(\mathcal{M}[U])^{-1}(Ad(A_\nu))|\lambda^b k\rangle\rangle \tag{8}$$

3 Numerical results of the u_b^a

We observed that off-diagonal element of u_b^a is consistent to zero, but there are statistical fluctuations. The projection operator $g_{\mu\nu} - \frac{p_\mu p_\nu}{p^2}$ in equation (1) is treated such that it has an expectation value $\frac{3}{4}$ in the limit of $p_\mu \to 0$.

Making the accuracy of the covariant Laplacian equation solver higher, we observe the tendency that the expectation value of $|u_a^a|$ increases.

	$diag$	$off-diag$	$diag_1$	$diag_2$	$diag_3$	$diag_4$
$\beta = 5.5, 8^3 \times 16$	-0.739(135)	0.002(60)	-0.776(109)	-0.779(105)	-0.818(118)	-0.581(49)
$\beta = 5.5, 12^4$	-0.715(46)	0.003(32)	-0.729(60)	-0.713(43)	-0.705(39)	-0.712(38)
$\beta = 5.5, 8^4$	-0.664(69)	0.002(45)	-0.669(71)	-0.656(70)	-0.667(67)	-0.664(67)
$\beta = 6.0, 12^4$	-0.548(133)	-0.015(85)	-0.555(123)	-0.561(107)	-0.508(133)	-0.566(159)
$\beta = 6.0, 8^4, w\ Z_3$	-0.303(80)	0.002(29)	-0.286(76)	-0.307(66)	-0.325(81)	-0.293(91)
$\beta = 6.0, 8^4, w\ Z_3, min$	-0.308(88)	-0.000(35)	-0.312(123)	-0.311(78)	-0.317(75)	-0.292(59)
$\beta = 6.0, 8^4, no\ Z_3$	-0.354(176)	-0.001(76)	-0.339(130)	-0.347(161)	-0.378(239)	-0.353(151)
$\beta = 8.0, 8^4, w\ Z_3$	-0.183(74)	0.002(20)	-0.177(71)	-0.197(77)	-0.221(83)	-0.138(19)
$\beta = 8.0, 8^4, no\ Z_3$	-0.338(513)	0.0116(251)	-0.264(278)	-0.359(553)	-0.334(610)	-0.394(536)

Table 1: Kugo-Ojima parameter u_a^a. $w\ Z_3$ means that Z_3 symmetry twist is performed for each sample such that the concentration occurs in $-60° \leq \theta \leq 60°$ and then the Landau gauge fixing is performed, and $no\ Z_3$ means without Z_3 symmetry twist. $w\ min$ means that minimal Landau gauge fixing is performed for each sample. (All data of 8^4 are the averages of 100 samples.)

As shown in the figure, for $\beta = 8$, direct measurement of u_b^a gives a large fluctuation, but suitable Z_3 twisting treatment for each sample so that the Polyakov scatter plot should be concentrated around $\arg z = 0$, suppresses the fluctuation and makes the data better. We consider that this treatment is indispensable in the simulation where Z_3 symmetry persists and the Z_3 factor affects the observed quantity. The similar behaviour is observed in $\beta = 6, 8^4$ lattice.

The absolute value of u_a^a is plotted as the function of the spatial extent of the lattice aL where a is calculated by assuming $\Lambda_{\overline{MS}} = 100MeV$. We find for $aL < 2fm$, there exists large finite-size effect. We expect that by making L large and a small, such that $aL > 2fm$, the absolute value of u_a^a becomes closer to 1.

For calculation in the deconfinement phase, one usually adopts non-symmetric lattice, but we avoided the tuning and used the symmetirc lattice.

We observe that in the confinement phase($\beta = 5.5$), the Polyakov loop distribution is uniform and the gauge fields are highly Z_3 randomised. While in the deconfinement phase($\beta = 6, 8$), the Polyakov loop distribution is concentrated in one of the three regions

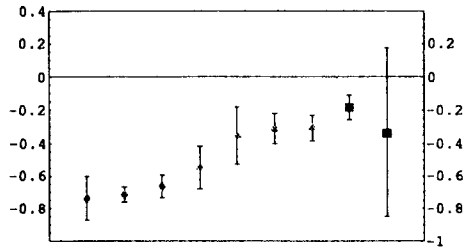

Figure 1: The dependence of space and colour diagonal part of the Kugo-Ojima parameter u_a^a on β and lattice size. (An average over the four directions and eight adjoint representations.) The data points are $\beta = 5.5, 8^3 \times 16; \beta = 5.5, 12^4; \beta = 5.5, 8^4; \beta = 6, 12^4; \beta = 6, 8^4(no\ Z_3); \beta = 6, 8^4(with\ Z_3); \beta = 6, 8^4(with\ Z_3, minimal\ Landau); \beta = 8, 8^4(with\ Z_3); \beta = 8, 8^4(no\ Z_3)$ respectively from left to right.

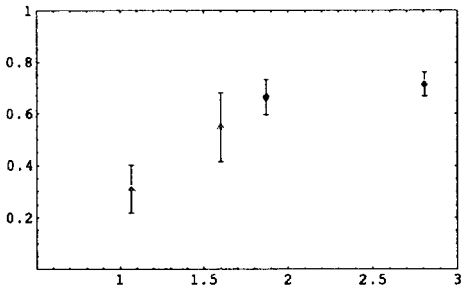

Figure 2: The finite-size effect of the Kugo-Ojima parameter $|u_a^a|$ as the function of the spatial extent of the lattice $aL(fm)$. When the spatial extent of the lattice is larger than 2 fm, the value of $|u_a^a|$ is about 0.7 in the case of $\beta = 5.5$. Finite size effect is large in the case of $\beta = 6$.

$-60° \leq \theta \leq 60°, 60° \leq \theta \leq 180°$, or $-180° \leq \theta \leq -60°$. The weight is roughly 2.5 : 1 : 1 in the case of $\beta = 8$ and roughly 1.5 : 1 : 1 in the case of $\beta = 6$. The distribution of $\beta = 6(12^4)$ can be regarded as uniform.

4 Summary and discussion

Proof of Kugo-Ojima colour confinement is accomplished successfully only in case of $u_b^a = -\delta_b^a$, and this condition is suggested to be a necessary condition as well. We did the first numerical tests of this criterion by the nonperturbative dynamics of lattice Landau gauge. Simulations were done on $8^3 \times 16, 8^4$, and 12^4. The quantity in question,

$$\langle Tr\langle \lambda^a k|D_\mu(A)(\mathcal{M}[U])^{-1}(Ad(A_\mu))|\lambda^b k\rangle\rangle.$$

requires no parameter tuning on the symmetric lattice, and is suitable for the numerical test. In the confinement region, $\beta = 5.5$, we found that the quantity is diagonal both in space indices and colour indices, and the value is around -0.7. Its absolute value decreases as β increases.

We observed the gluon propagator is infrared finite and the ghost propagator is infrared divergent, suggested to be more singular than $\frac{1}{p^2}$, but less singular than $\frac{1}{p^4}$. These results qualitatively agree with the Gribov-Zwanziger's conjecture[4, 5], and are consistent with the results of Dyson-Schwinger equation [6]. It is nice to observe that the infrared finiteness of the gluon propagator is in accordance with the Kugo-Ojima colour confinement. As stated in the inverse Higgs mechanism theorem, if we have no massless vector poles in all channels of the gauge field, A_μ^a, and if the colour symmetry is not broken at all, it follows that $1+u = 0$[7].

The real part of the complex mass of the gluon is about 600 MeV in our finite lattice simulation, which is consistent with[8].

For calculation of the deconfinement phase, we adopted a symmetric lattice with large β, and a suitable twisted Z_3 boundary conditions to eliminate the artificial fluctuation of the data.

This work is supported by High Energy Accelerator Research Organization, KEK Supercomputer Project(Project No.99-46), and by Japan Society for the Promotion of Science, Grant-in-aid for Scientific Research(C) (No.11640251).

References

[1] T. Kugo and I. Ojima, Prog. Theor. Phys. Supp. **66** (1979) 1

[2] H.Nakajima and S. Furui, Lattice 98 contribution, Bouldar(1998), hep-lat/9809080,9809081; Confinement III proceedings, June 1998, Jefferson Lab, NewPort. hep-lat/9809078

[3] H. Suman and K. Schilling, Phys. Lett. **B373** (1996) 314.

[4] V.N. Gribov, Nucl. Phys. **B139** (1978) 1.

[5] D. Zwanziger, Nucl. Phys. **B364** (1991) 127, Nucl. Phys. **B412** (1994) 657.

[6] von Smekal, A. Hauck, R. Alkofer, Ann. Phys.**267**(1998) 1, hep-ph/9707327.

[7] K.I. Izawa, hep-th/9411010.

[8] J.E. Mandula and M. Ogilvie, Phys. Lett. **B185** (1987) 127.

10. ニュートリノの質量とクォーク·レプトン対称性

Neutrino mass and the quark–lepton symmetry

都立大理学研究科 (Dept. of Physics, Tokyo Metropolitan Univ.)
安田 修 (Osamu Yasuda)

Recent status of neutrino oscillation experiments is briefly summarized. The case of just-so is discussed in the K2K experiment. It is shown that we get useful information on the allowed region of Δm^2 by looking at events of various channels.

この講演ではν振動の最近の話題のうちのいくつかについて触れた。

1. 太陽ニュートリノ問題

太陽ニュートリノは、ガリウム (GALLEX·SAGE) · 塩素 (Homestake) · 水 (Kamiokande·Superkamiokande) を標的とする三種類の実験で測定されており、以下のような結果がでている [1]。

Experiment	measured flux	SSM(BP98)	ratio exp/BP98	threshold energy
Homestake	2.56±0.16±0.16	$7.7\ ^{+1.2}_{-1.0}$	0.33±0.029	0.814 MeV
Kamiokande	2.80± 0.19± 0.33	$5.15\ ^{+1.0}_{-0.7}$	0.54± 0.07	7.5 MeV
Gallex	$77.5\pm 6.2\ ^{+4.3}_{-4.7}$	$129\ ^{+8}_{-6}$	0.60± 0.06	0.233 MeV
SAGE	$66.9\ ^{+7.1}_{-6.8}\ ^{+5.4}_{-5.7}$	$129\ ^{+8}_{-6}$	0.52±0.06	0.233 MeV
Superkamiokande	2.45± 0.04± 0.07	$5.15\ ^{+1.0}_{-0.7}$	0.475± 0.015	6.5 MeV

いずれの実験も理論より小さな値を出していることと、異なるエネルギーしきい値の実験がそれぞれ異なる実験値/理論値の比を出していることが太陽ニュートリノ問題であり、現在の所その解釈としてニュートリノ振動が最も有力視されている。その際、真空振動で説明する場合にはΔm^2が $10^{-10}\mathrm{eV}^2$ 程度、物質効果が本質的な MSW 解の場合にはΔm^2は $10^{-5}\mathrm{eV}^2$ 程度になる。

太陽ニュートリノ問題については鈴木洋一郎氏 [2] と南方久和氏 [3] による解説があるのでそちらを参照して頂きたい。

2. 大気ニュートリノ問題

大気ニュートリノは、一次宇宙線と大気中の核子が衝突して出来る粒子とその派生物の崩壊から出てくる$\nu_\mu + \bar{\nu}_\mu$と$\nu_e + \bar{\nu}_e$ であるが、その数の比はおおざっぱに 2:1 であると期待される。これまで NUSEX, Frejus, IMB, Kamiokande, Soudan2, Superkamiokande で大気ニュートリノの観測が行われているが、NUSEX と Frejus ではほぼ理論通りの結果が出ているのに対し、IMB, Kamiokande, Soudan2, Superkamiokande では ($\nu_\mu + \bar{\nu}_\mu$の数)/($\nu_e + \bar{\nu}_e$の数) はむしろ 1 に近い値が報告されている。NUSEX と Frejus の結果をどう解釈するかは微妙な問題であるが、他の四者に関しては理論と実験の間に食い違いがあり、大気ニュートリノ問題と呼ばれている。特に、Kamiokande と Superkamiokande のいわゆる multi-GeV のデータ (1

GeV $\lesssim E_\nu \lesssim$ 100GeV) では、測定器の上方で出来て大気の厚さの距離ほどしか飛んで来なかったニュートリノに対して (ν_μの数)/(ν_eの数) の実験値/理論値が 1 に近いのに比べ、地球の裏側で出来て地球の直径の長さだけ飛んで来るニュートリノに対しては実験値/理論値が 1 よりかなり小さくなっていることが報告されている (実験値/理論値の顕著な天頂角依存性)。この現象はニュートリノ振動で解釈でき、その best fit が$\Delta m^2 \sim$ 数 $10^{-3}\mathrm{eV}^2$となることが報告されている。

大気ニュートリノに関しては南方久和氏による前述の解説 [3] と梶田隆章氏による記事 [4] があるのでそちらを参照して頂きたい。

3. hot dark matter

ニュートリノ振動とは直接関係はないが、ニュートリノの質量を示唆しているかもしれないものに HDM(hot dark matter) がある。宇宙における大規模構造の形成理論において、CDM(cold dark matter) 成分 (axion 等の重い粒子) と HDM(hot dark matter) 成分 (ニュートリノ) が共存するという mixed dark matter シナリオが観測されている密度ゆらぎのスペクトルを説明するのに都合が良いと指摘されており、もし確立されればニュートリノに数 eV 程度の質量があるということになる。mixed dark matter シナリオが観測事実を良く説明すると主張している解析としては [5] があるが、一方遠くの超新星の最近の観測データを説明するには宇宙の平均密度全体が小さい方が良く、その場合には数 eV 程度の質量の HDM の入る余裕はないという主張がある [6]。宇宙論の観測では系統誤差が未知であるため、宇宙論の観測データからどれだけの信頼レベルでニュートリノの質量を議論出来るかは不明であり、結論を出すのはまだ時期早尚であると思われる。

4. ニュートリノ振動から予想される K2K 実験における事象数の期待値

preliminary な K2K 実験の結果 (1 event のみ) が当初の期待に比べてずっと少ないということから、どのような状況で実際の事象の数が少なくなるかを考察した [7]。

二世代の$\nu_\mu \leftrightarrow \nu_\tau$の枠組では disappearance の確率は

$$P(\nu_\mu \to \nu_\mu) = 1 - \sin^2 2\theta \sin^2\left(\Delta m^2 L/4E\right)$$

となり、最新のスーパーカミオカンデのデータから

$$2 \times 10^{-3}\mathrm{eV}^2 \lesssim \Delta m^2 \lesssim 8 \times 10^{-3}\mathrm{eV}^2$$
$$0.84 \lesssim \sin^2 2\theta \leq 1$$

ということがわかっている。特に best fit は$\Delta m^2 = 3.5 \times 10^{-3}\mathrm{eV}^2$, $\sin^2 2\theta = 1$ である。最大混合 ($\sin^2 2\theta = 1$) の場合に各チャンネルの事象数をΔm^2の関数としてプロットすると Fig. 1 のようになる (すべてニュートリノ振動がない場合の事象数との比を取ってある)。ここで、各チャンネルの散乱断面積は [8] のものを用いた。又、quasielastic の事象数とその他の事象数の比をプロットすると Fig. 2 のようになり、各チャンネルの事象数の比を見ることによりΔm^2に関する情報が増える可能

性がある。

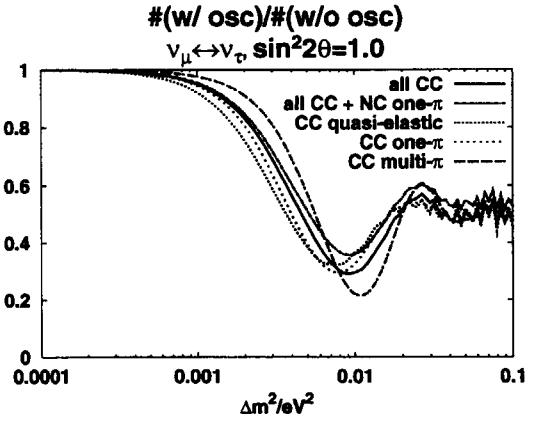

Fig.1

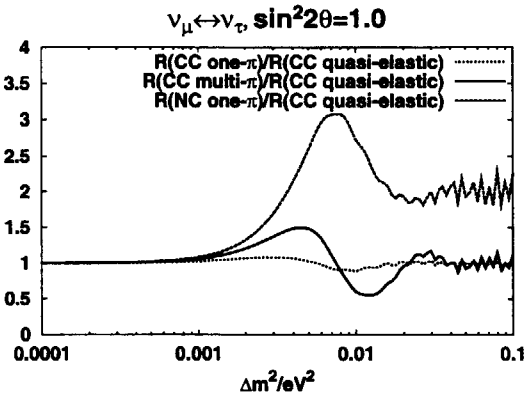

Fig.2

一方、さらに事象数が小さくなる例として sterile neutrino を入れて (3+1) 世代間でニュートリノ振動を考える。これは太陽ニュートリノ·大気ニュートリノ·LSND の結果をすべてニュートリノ振動によるものとするシナリオで、

$$U \equiv \begin{pmatrix} U_{e1} & U_{e2} & U_{e3} & U_{e4} \\ U_{\mu 1} & U_{\mu 2} & U_{\mu 3} & U_{\mu 4} \\ U_{\tau 1} & U_{\tau 2} & U_{\tau 3} & U_{\tau 4} \\ U_{s1} & U_{s2} & U_{s3} & U_{s4} \end{pmatrix}$$

という一般の混合を考えると、disappearance の確率は

$$\begin{aligned} P(\nu_\mu \to \nu_\mu) &= 1 - 4|U_{\mu 3}|^2|U_{\mu 4}|^2 \sin^2\left(\Delta m^2_{43} L/4E\right) - 2\left(|U_{\mu 3}|^2 + |U_{\mu 4}|^2\right)\left(1 - |U_{\mu 3}|^2 - |U_{\mu 4}|^2\right) \\ &= 1 - c^2_{23} \sin^2 2\theta_{24} \sin^2\left(\Delta m^2_{43} L/4E\right) - 2 s^2_{23} c^2_{24}(1 - s^2_{23} c^2_{24}) \end{aligned}$$

となる。最後の式では [9] で導入された 4×4 の行列の混合角を使った。又、$m^2_1 \simeq m^2_2 \ll m^2_3 \simeq m^2_4$で$\Delta m^2_{21}$は太陽ニュートリノのスケール ($\sim 10^{-5}\mathrm{eV}^2$ 又は$\sim 10^{-10}\mathrm{eV}^2$)、Δm^2_{43}は大気ニュートリノのスケール ($\sim 10^{-2.5}\mathrm{eV}^2$)、$\Delta m^2_{32}$は LSND のスケール ($\sim 1\mathrm{eV}^2$) と仮定する。[9] における$\theta_{34}$は、$\theta_{34} = 0$ であれば$\nu_\mu \leftrightarrow \nu_\tau$を、又、$\theta_{34} = \pi/2$ であれば$\nu_\mu \leftrightarrow \nu_s$を表すことがわかる。最新のスーパーカミオカンデのデータにより $\nu_\mu \leftrightarrow \nu_s$がほとんど否定されているので、ここでは$\theta_{34} = 0$ とおき、又、二世代の混合角に対応するθ_{24}は最大混合 ($\sin^2 2\theta_{24} = 1$) としてθ_{23}に関して事象数がどのように振舞うかを考察すると Fig. 3 のようになる。大気ニュートリノのデータには$\theta_{23} \lesssim 30°$ 程度までなら許容される fit を与えるので、$0 \le \theta_{23} \le 30°$の範囲でプロットしてある。あまり如実な効果とは言えないが、二世代の場合よりもさらに少ない事象数を与えることがわかる。現在までまだ 1 事象しか観測されていないので、ニュートリノ振動がない場合に期待される事象数の算出とともにさらに実験データがたまるの

を待つ必要がある。

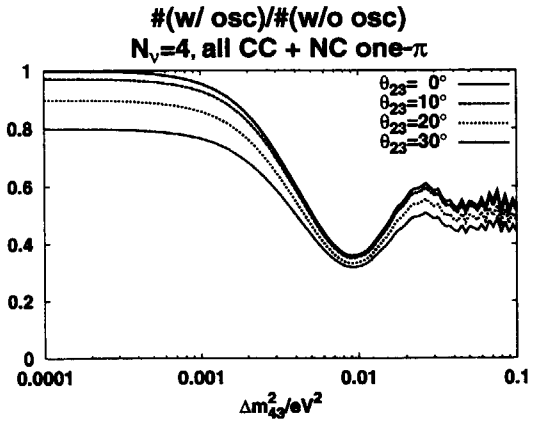

Fig.3

参考文献

[1] J.N. Bahcall, P.I. Krastev and A.Yu. Smirnov, Phys. Rev. **D58** (1998) 96016.

[2] 鈴木洋一郎, 太陽ニュートリノ問題, 日本物理学会誌 **51** (1996) 95.

[3] 南方久和, ニュートリノ振動研究の現状, 日本物理学会誌 **53** (1998) 743.

[4] 梶田隆章, スーパーカミオカンデにおけるニュートリノの観測, 日本物理学会誌 **52** (1997) 840; ニュートリノ振動の証拠–スーパーカミオカンデにおける大気ニュートリノの観測から–, 日本物理学会誌 **53** (1998) 783.

[5] E. Gawiser and J. Silk, Science **280** (1998) 1405.

[6] J. R. Primack and M. A. K. Gross astro-ph/9810204.

[7] H. Minakata and O. Yasuda, in preparation.

[8] M. Nakahata et. al., J. Phys. Soc. Japan, **55** (1986) 3786.

[9] N. Okada and O. Yasuda, Int. J. Mod. Phys. **A12** (1997) 3669.

11. Roles of pions for neutrinoless double β decay in nuclei

Katsuhiko Suzuki
Research Center for Nuclear Physics (RCNP), Osaka University,
Osaka 567-0047, Japan
E-mail: ksuzuki@rcnp.osaka-u.ac.jp

Abstract

We study the roles of pions for neutrinoless double β decay in nuclei, which provides constraints on the physics beyond the Standard Model such as neutrino masses and R-parity violation SUSY parameters. The effective meson-nucleon Lagrangian which describes the neutrinoless double β decay is constructed, assuming the $0\nu\beta\beta$ decay is driven by the heavy particle exchange between quarks. In addition to the conventional two-nucleon contact interaction which is suppressed by the NN hard core potential, we consider the pion-nucleon Yukawa term and the pion exchange current term. Making use of the soft pion theorem, it is found that dominant contribution comes from the pion-nucleon Yukawa term. The pion exchange current gives a negligible contribution in the case of the heavy Majorana neutrino exchange, while it provides a crucial contribution within the R-parity violating SUSY.

Introduction

There exist several possible mechanisms to generate the neutrinoless double β decay ($0\nu\beta\beta$) beyond the Standard Model. Most popular process is induced by the exchange of the massive (Majorana) neutrinos[1] shown in Fig.1. In this scenario, both light and heavy neutrinos contribute to the $0\nu\beta\beta$ decay, and their masses and mixing angles can be extracted from the experiments. Another one originates from the R-parity violating supersymmetric extension of the Standard Model (SUSY) [2], in which the $0\nu\beta\beta$ is mediated by the superparticles illustrated in Fig.2. If the R-parity is conserved, for example, the lightest superparticle could be a good candidate of the dark matter. Thus, the experimental test for the R-parity conservation is of great interest.

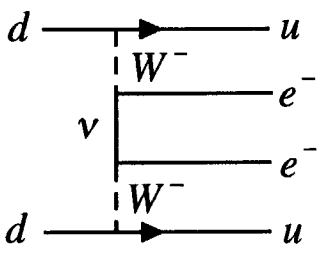

Figure 1: $0\nu\beta\beta$ decay in massive Majorana neutrino mechanism

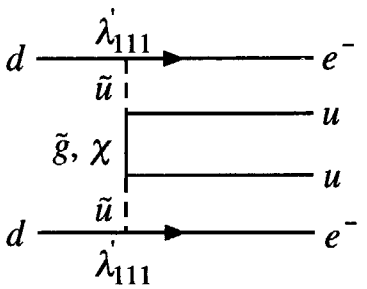

Figure 2: Typical diagram for $0\nu\beta\beta$ decay in R-parity violating SUSY

In this work, we consider only the exchange of the heavy particles between quarks to generate the $0\nu\beta\beta$ decay. To make theoretical predictions to be compared with the

experiment, we need the following steps. First, we construct the low energy effective Lagrangian for quarks and gluons by integrating out the heavy particles degrees of freedom such as the heavy Majorana neutrino or the superparticles. Then, the effective Lagrangian at the hadronic level in terms of baryons and mesons are constructed by taking into account the quark-gluon structure of the hadrons. Finally, we apply the resulting hadronic Lagrangian to the nuclear many body system, and evaluate the transition matrix elements in nuclei, ${}^{A}_{Z}X \rightarrow {}^{A}_{Z+2}Y + 2e^{-}$. We try to construct a possible effective Lagrangian for the hadrons, dealing with the pion-nucleon dynamics and the $0\nu\beta\beta$ interaction consistently. We remark the procedure presented here is rather general and can be applied to any model beyond the Standard Model.

Construction of the effective Lagrangian

Integrating out the heavy neutrino or the superparticles degrees of freedom, one can find that the effective quark-lepton Lagrangian is given by the local interaction between 4-quarks and 2-electrons. The low energy effective Lagrangian, in which the $0\nu\beta\beta$ decay is caused by the subprocess $dd \rightarrow uu + 2e^{-}$, can be written as,

$$\mathcal{L}_{quark} = \frac{G_F^2}{2m_p} C_{ij} \left[e\,\Gamma\,e^c\right] \left[\left(\bar{u}\,\Gamma^i\,d\right)\,\left(\bar{u}\Gamma^j\,d\right)\right] \tag{1}$$

where Γ denote the gamma matrices determined by the original theory. For the massive neutrino exchange model, it has the standard $(V-A)$ Dirac structure, while S, P and T structure appear within the R-parity violating SUSY. C_{ij} are expressed by the coupling constants of the original models, for example neutrino masses or the R-parity violating coupling λ'_{111}.

We then construct the effective meson-nucleon Lagrangian to describe the $dd \rightarrow uu + 2e^{-}$ process shown in Fig.1 and 2. The general from of the Lagrangian to induce $nn \rightarrow pp + 2e^{-}$ can be written as

$$\mathcal{L}_{Had} = \mathcal{L}_{2N} + \mathcal{L}_{N\pi} + \mathcal{L}_{2\pi} \tag{2}$$

The first term represents the 6-point interaction between nucleons and electrons shown in Fig.3, which can be obtained by simply replacing u and d quarks with p and n, respectively;

$$\mathcal{L}_{2N} = A_{2N} \frac{G_F^2}{2m_p} \left[\bar{p}\Gamma_i n\ \bar{p}\Gamma_j n\right] \left[\ e\Gamma e^c\right] \tag{3}$$

where Γ is againn the appropriate gamma matrices. Contributions of this term to nuclear decay matrix elements can be evaluated[1, 2]. However, this transition would be suppressed very much by the nucleon-nucleon hard core potential [3], although the transition matrix element does not vanish due to the finite size of nucleons.

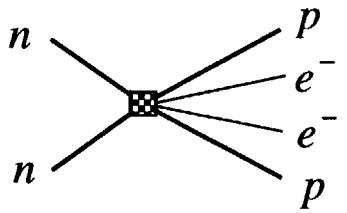

Figure 3: $\mathcal{L}_{2N}$

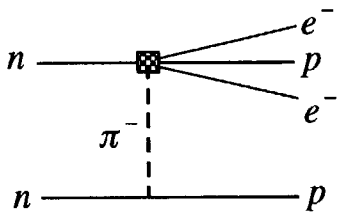

Figure 4: $\mathcal{L}_{N\pi}$

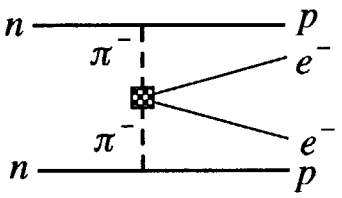

Figure 5: Pion exchange current $\mathcal{L}_{2\pi}$

We emphasize here that the short range nature of the $0\nu\beta\beta$ interaction at the quark level never means the short range interaction between nucleons. It is possible to introduce other degrees of freedom, namely, mesons. Considering only the pions which plays the most important roles at the low energy, one can add two possible contributions $\mathcal{L}_{N\pi}$ and $\mathcal{L}_{2\pi}$ as

$$\mathcal{L}_{N\pi} = \frac{G_F^2}{2m_p} m_\pi^2 \, e\Gamma e^c \left[A_{N\pi} \, \bar{p} n \, \pi^- + B_{N\pi} \bar{p} \, i\gamma^5 n \, \pi^- \right] \tag{4}$$

$$\mathcal{L}_{2\pi} = -A_{2\pi} \frac{G_F^2}{2m_p} m_\pi^4 \, e\Gamma e^c \, (\pi^-)^2 \tag{5}$$

These contributions are schematically shown in Fig.4 and 5, respectively. In order to fix unknown coupling constants, $A_{N\pi}, B_{N\pi}, A_{2\pi}$, of the effective hadronic Lagrangian, we exploit the matching conditions;

$$\left\langle p\, 2e^- | \mathcal{L}_{quark} | n \, \pi^- \right\rangle = \left\langle p\, 2e^- | \mathcal{L}_{N\pi} | n \, \pi^- \right\rangle \tag{6}$$

$$\left\langle \pi^+ 2e^- | \mathcal{L}_{quark} | \pi^- \right\rangle = \left\langle \pi^+ 2e^- | \mathcal{L}_{2\pi} | \pi^- \right\rangle \tag{7}$$

where $\mathcal{L}_{quark}$ stands for the Lagrangian eq. (1) which involves quark and lepton fields explicitly. These equations relate the coupling constants of the effective hadronic Lagrangian with the coupling constants of the original Lagrangian, for example R-parity violating coupling or the heavy neutrino mass. Our task here is to calculate the left hand side of eqs. (6,7) using some non-perturbative method based on QCD, and determine the values of the coupling constants, A_i, B_i.

We make use of the soft pion theorem based on the current algebra which is proved to work very well for the pionic hyperon decay process of the standard weak theory. Using the reduction formula and the PCAC relation, one gets

$$\begin{aligned} \langle p \, \pi_a | \mathcal{O} | n \rangle &= \int d^4x \, e^{-iqx} (\partial^2 + m_\pi^2) \langle p | T \{ \pi^a(x), \mathcal{O} \} | n \rangle \\ &= \frac{-1}{f_\pi} \left\langle p \left| \left[i \int d^3x \, A_a^0(x), \mathcal{O} \right] \right| n \right\rangle \\ &\quad + \frac{iq_\mu}{f_\pi} \int d^4x \, e^{-iqx} \langle p | T \{ A_a^\mu(x), \mathcal{O}(0) \} | n \rangle \end{aligned} \tag{8}$$

where $\mathcal{O} = [\bar{u}\Gamma^i d\ \bar{u}\Gamma^j d]$ is the any 4-quark operator appeared in the quark level Lagrangian of eq. (1). One can see that the first term of eq. (8) corresponds to the so called commutator term. The second one provides the baryon pole contribution by inserting the intermediate baryon states between $A_\mu(x)$ and $\mathcal{O}(0)$. In the present case, the intermediate states are assumed to be identified with Δ resonances. We note that the $\Delta I = 1/2$ enhancement of the non-leptonic weak hyperon decay is well reproduced within the same approximation scheme.

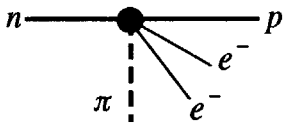

Figure 6: First term of eq. (8)

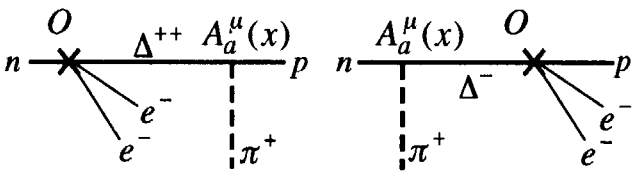

Figure 7: Second term of eq. (8). Intermediate baryon states are assumed to be Δ.

Matrix elements of eq. (8) can be evaluated by employing the wave function of the quark models. By doing so, we can relate the coupling constants of the hadronic Lagrangian with the fundamental parameters of the theory, and calculate thee $0\nu\beta\beta$ decay transition matrix elements using the suitable nuclear physics technique. For example, the coupling constants in the R-parity violating SUSY is given in ref. [4]. It was found that the pion-nucleon term $\mathcal{L}_{N\pi}$ is enhanced very much compared with the previous calculations. This difference could change the upper bound of the λ'_{111} considerably.

We also point out that the pion exchange current $\mathcal{L}_{2\pi}$ provides the large contribution in the case of the S, P interaction (e.g. in SUSY), while its contribution is negligible when the interaction is the $V - A$ type. This is simply due to the partial conservation of the axial-vector current in QCD. The matrix element of the axial-vector current between the pion states is proportional to the pion momentum q, which is small. For the S or P interaction, such an *accidental* suppression does not happen, and the pion exchange current contributions are comparable with others.

Conclusions

We have studied the meson-nucleon effective interaction in order to describe the $0\nu\beta\beta$ decay in nuclei. We generally construct the effective Lagrangian with the pion and nucleon, which is divided into three parts, two nucleon contact term, pion-nucleon Yukawa term and the two pion contact term. We have developed the method to calculate the transition matrix elements using the technique based on the current algebra which is proved to provide a reasonable description for the non-leptonic weak decay of hyperons. Our treatment can be applicable to any model that generates the $0\nu\beta\beta$

decay. To carry out the realistic calculation of the $0\nu\beta\beta$ matrix elements in nuclei, all the processes arising from $\mathcal{L}_{2N}, \mathcal{L}_{N\pi}$ and $\mathcal{L}_{2\pi}$ should be consistently taken into account in any model.

References

[1] For example, see W. Haxton and G. Stephenson, Prog. Part. Nucl. Phys. **12** 409 (1984)

[2] J.D. Vergados, Phys. Lett. **B184** 55(1987)
M. Hirsch, H. Klapdor-Kleingrothaus, S. Kovalenko, Phys. Rev. **D53** 1329 (1996).

[3] A. Faessler, S. Kovalenko, F. Simkovic, Phys. Rev. **D58** 115004 (1998)

[4] K. Suzuki and H. Toki, talk presented at International Symposium on Nuclear Electro-weak Spectroscopy, March 1999, Osaka, Japan, to be published in proceedings

12. Spectral Functions of Hadrons in Lattice QCD

Y. Nakahara[a], M. Asakawa[a], and T. Hatsuda[b]

[a]Department of Physics,Nagoya University, Nagoya 464 - 8602, Japan

[b]Physics Department, Kyoto University, Kyoto 606-8502, Japan

Using the maximum entropy method, spectral functions of the pseudo-scalar and vector mesons are extracted from lattice Monte Carlo data of the imaginary time Green's functions. The resonance and continuum structures as well as the ground state peaks are successfully obtained. Error analysis of the resultant spectral functions is also given on the basis of the Bayes probability theory.

1. Introduction

The spectral functions (SPFs) of hadrons play a special role in physical observables in QCD (See the examples in [1,2]). However, the lattice QCD simulations so far have difficulties in accessing the dynamical quantities in the Minkowski space, because measurements on the lattice can only be carried out for discrete points in imaginary time. The analytic continuation from the imaginary time to the real time using the noisy lattice data is highly non-trivial and is even classified as an ill-posed problem.

Recently we made a first serious attempt to extract SPFs of hadrons from lattice QCD data without making a priori assumptions on the spectral shape [3]. We use the maximum entropy method (MEM), which has been successfully applied for similar problems in quantum Monte Carlo simulations in condensed matter physics, image reconstruction in crystallography and astrophysics, and so forth [4,5]. In this report, we present the results for the pseudo-scalar (PS) and vector (V) channels at $T = 0$ using the continuum kernel and the lattice kernel of the integral transform. The latter analysis has not been reported in [3].

2. Basic idea of MEM

The Euclidean correlation function $D(\tau)$ of an operator $\mathcal{O}(\tau, \vec{x})$ and its spectral decomposition at zero three-momentum read

$$D(\tau) = \int \langle \mathcal{O}^\dagger(\tau, \vec{x}) \mathcal{O}(0, \vec{0}) \rangle d^3x = \int_0^\infty K(\tau, \omega) A(\omega) d\omega, \quad (1)$$

where $\tau > 0$, ω is a real frequency, and $A(\omega)$ is SPF (or sometimes called the *image*), which is positive semi-definite. The kernel $K(\tau, \omega)$ is proportional to the Fourier transform of a free boson propagator with mass ω: At $T = 0$ in the continuum limit, $K = K_{cont}(\tau, \omega) = \exp(-\tau\omega)$.

Monte Carlo simulation provides $D(\tau_i)$ on the discrete set of temporal points $0 \leq \tau_i/a \leq N_\tau$. From this data with statistical noise, we need to reconstruct the spectral function $A(\omega)$ with continuous variable ω. This is a typical ill-posed problem, where the number of data is much smaller than the number of degrees of freedom to be reconstructed. This makes the standard likelihood analysis and its variants inapplicable [6] unless strong assumptions on the spectral shape are made. MEM is a method to circumvent this difficulty through Bayesian statistical inference of the most probable *image* together with its reliability [4].

MEM is based on the Bayes' theorem in probability theory: $P[X|Y] = P[Y|X]P[X]/P[Y]$, where $P[X|Y]$ is the conditional probability of X given Y. The most probable image $A(\omega)$ for given lattice data D is obtained by maximizing the conditional probability $P[A|DH]$, where H summarizes all the definitions and prior knowl-

edge such as $A(\omega) \geq 0$. By the Bayes' theorem,

$$P[A|DH] \propto P[D|AH]P[A|H], \tag{2}$$

where $P[D|AH]$ ($P[A|H]$) is called the likelihood function (the prior probability).

For the likelihood function, the standard χ^2 is adopted, namely $P[D|AH] = Z_L^{-1}\exp(-L)$ with

$$L = \frac{1}{2}\sum_{i,j}(D(\tau_i) - D^A(\tau_i)) \times C_{ij}^{-1}(D(\tau_j) - D^A(\tau_j)). \tag{3}$$

Z_L is a normalization factor given by $Z_L = (2\pi)^{N/2}\sqrt{\det C}$ with $N = \tau_{max}/a - \tau_{min}/a + 1$. $D(\tau_i)$ is the lattice data averaged over gauge configurations and $D^A(\tau_i)$ is the correlation function defined by the right hand side of (1). C is an $N \times N$ covariance matrix of the data with N being the number of temporal points to be used in the MEM analysis. The lattice data have generally strong correlations among different τ's, and it is essential to take into account the off-diagonal components of C.

Axiomatic construction as well as intuitive "monkey argument" [7] show that, for positive distributions such as SPF, the prior probability can be written with parameters α and m as $P[A|H\alpha m] = Z_S^{-1}\exp(\alpha S)$. Here S is the Shannon-Jaynes entropy,

$$S = \int_0^\infty \left[A(\omega) - m(\omega) - -A(\omega)\log\left(\frac{A(\omega)}{m(\omega)}\right)\right] d\omega. \tag{4}$$

Z_S is a normalization factor: $Z_S \equiv \int e^{\alpha S}\mathcal{D}A$. α is a real and positive parameter and $m(\omega)$ is a real function called the default model.

In the state-of-art MEM [4], the output image A_{out} is given by a weighted average over A and α:

$$A_{out}(\omega) = \int A(\omega)\ P[A|DH\alpha m]P[\alpha|DHm]\ \mathcal{D}A\ d\alpha \simeq \int A_\alpha(\omega)\ P[\alpha|DHm]\ d\alpha. \tag{5}$$

Here $A_\alpha(\omega)$ is obtained by maximizing the "free-energy"

$$Q \equiv \alpha S - L, \tag{6}$$

for a given α. Here we assumed that $P[A|DH\alpha m]$ is sharply peaked around $A_\alpha(\omega)$. α dictates the relative weight of the entropy S (which tends to fit A to the default model m) and the likelihood function L (which tends to fit A to the lattice data). Note, however, that α appears only in the intermediate step and is integrated out in the final result. Our lattice data show that the weight factor $P[\alpha|DHm]$, which is calculable using Q [4], is highly peaked around its maximum $\alpha = \hat{\alpha}$. We have also studied the stability of the $A_{out}(\omega)$ against a reasonable variation of $m(\omega)$.

The non-trivial part of the MEM analysis is to find a global maximum of Q in the functional space of $A(\omega)$, which has typically 750 degrees of freedom in our case. We have utilized the singular value decomposition (SVD) of the kernel to define the search direction in this functional space. The method works successfully to find the global maximum within reasonable iteration steps.

3. MEM with mock data

To check our MEM code and to see the dependence of the MEM image on the quality of the data, we made the following test using mock data. (i) We start with an input image $A_{in}(\omega) \equiv \omega^2\rho_{in}(\omega)$ in the ρ-meson channel which simulates the experimental e^+e^- cross section. Then we calculate $D_{in}(\tau)$ from $A_{in}(\omega)$ using eq.(1). (ii) By taking $D_{in}(\tau_i)$ at N discrete points and adding a Gaussian noise, we create a mock data $D_{mock}(\tau_i)$. The variance of the noise $\sigma(\tau_i)$ is given by $\sigma(\tau_i) = b \times D_{in}(\tau_i) \times \tau_i/a$ with a parameter b, which controls the noise level [8]. (iii) We construct the output image $A_{out}(\omega) \equiv \omega^2\rho_{out}(\omega)$ using MEM with $D_{mock}(\tau_{min} \leq \tau_i \leq \tau_{max})$ and compare the result with $A_{in}(\omega)$. In this test, we have assumed that C is diagonal for simplicity.

In Fig.1, we show $\rho_{in}(\omega)$, and $\rho_{out}(\omega)$ for two sets of parameters, (I) and (II). As for m, we choose a form $m(\omega) = m_0\omega^2$ with $m_0 = 0.027$, which is motivated by the asymptotic behavior of A in perturbative QCD, $A(\omega \gg 1\text{GeV}) = (1/4\pi^2)(1+\alpha_s/\pi)\omega^2$. The final result is, however, insensitive to the variation of m_0 even by factor 5 or 1/5. The calculation of $A_{out}(\omega)$ has been done by discretizing the ω-space with an equal sepa-

ration of 10 MeV between adjacent points. This number is chosen for the reason we shall discuss below. The comparison of the dashed line (set (I)) and the dash-dotted line (set (II)) shows that increasing τ_{max} and reducing the noise level b lead to better SPFs closer to the input SPF.

We have also checked that MEM can nicely reproduce other forms of the mock SPFs. In particular, MEM works very well to reproduce not only the broad structure but also the sharp peaks close to the delta-function as far as the noise level is sufficiently small.

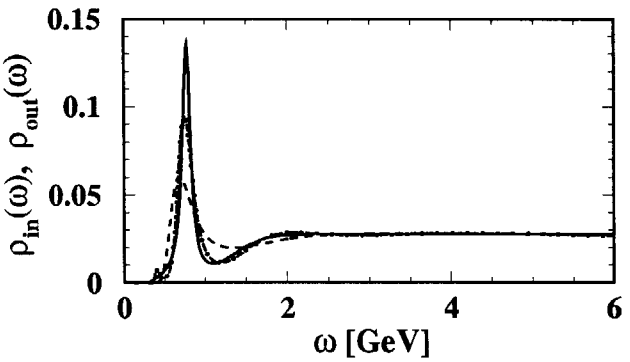

Figure 1. The solid line is $\rho_{in}(\omega)$. The dashed line and dash-dotted line are $\rho_{out}(\omega)$ obtained with parameter set (I) $a = 0.0847$ fm, $1 \leq \tau/a \leq 12$, $b = 0.001$ and set (II) $a = 0.0847$ fm, $1 \leq \tau/a \leq 36$, $b = 0.0001$, respectively.

4. MEM with lattice data

To apply MEM to actual lattice data, quenched lattice QCD simulations have been done with the plaquette gluon action and the Wilson quark action by the open MILC code with minor modifications [9]. The lattice size is $20^3 \times 24$ with $\beta = 6.0$, which corresponds to $a = 0.0847$ fm ($a^{-1} = 2.33$ GeV), $\kappa_c = 0.1571$ [10], and the spatial size of the lattice $L_s a = 1.69$ fm. Gauge configurations are generated by the heat-bath and over-relaxation algorithms with a ratio 1 : 4. Each configuration is separated by 1000 sweeps. Hopping parameters are chosen to be $\kappa = 0.153$, 0.1545, and 0.1557 with $N_{conf} = 161$ for each κ. For the quark propagator, the Dirichlet (periodic) boundary condition is employed for the temporal (spatial) direction. We have also done the simulation with periodic boundary condition in the temporal direction and obtained qualitatively the same results. To calculate the two-point correlation functions, we adopt a point-source at $\vec{x} = 0$ and a point-sink averaged over the spatial lattice-points.

We use data at $1 \leq \tau_i/a \leq 12(24)$ for the Dirichlet (periodic) boundary condition in the temporal direction. To avoid the known pathological behavior of the eigenvalues of C [4], we take $N_{conf} \gg N$.

We define SPFs for the PS and V channels as

$$A(\omega) = \omega^2 \rho_{PS,V}(\omega), \tag{7}$$

so that $\rho_{PS,V}(\omega \rightarrow \text{large})$ approaches a finite constant as predicted by perturbative QCD. For the MEM analysis, we need to discretize the ω-integration in (1). Since $\Delta\omega$ (the mesh size) $\ll 1/\tau_{max}$ should be satisfied to suppress the discretization error, we take $\Delta\omega = 10$ MeV. ω_{max} (the upper limit for the ω integration) should be comparable to the maximum available momentum on the lattice: $\omega_{max} \sim \pi/a \sim 7.3$ GeV. We have checked that larger values of ω_{max} do not change the result of $A(\omega)$ substantially, while smaller values of ω_{max} distort the high energy end of the spectrum. The dimension of the image to be reconstructed is $N_\omega \equiv \omega_{max}/\Delta\omega \sim 750$, which is in fact much larger than the maximum number of Monte Carlo data $N = 25$.

In Fig.2 (a) and (b), we show the reconstructed images for each κ in the case of the Dirichlet boundary condition. Here we use the continuum kernel $K_{cont} = \exp(-\tau\omega)$ in the Laplace transform. In these figures, we have used $m = m_0\omega^2$ with $m_0 = 2.0(0.86)$ for PS (V) channel motivated by the perturbative estimate of m_0 (see eq.(9) and the text below). We have checked that the result is not sensitive, within the statistical significance of the image, to the variation of m_0 by factor 5 or 1/5. The obtained images have a common structure: the low-energy peaks corresponding to π and ρ, and the broad struc-

ture in the high-energy region. From the position of the pion peaks in Fig.2(a), we extract $\kappa_c = 0.1570(3)$, which is consistent with 0.1571 [10] determined from the asymptotic behavior of $D(\tau)$. The mass of the ρ-meson in the chiral limit extracted from the peaks in Fig.2(b) reads $m_\rho a = 0.348(15)$. This is also consistent with $m_\rho a = 0.331(22)$ [10] determined by the asymptotic behavior. Although our maximum value of the fitting range $\tau_{max}/a = 12$ marginally covers the asymptotic limit in τ, we can extract reasonable masses for π and ρ. The width of π and ρ in Fig.2 is an artifact due to the statistical errors of the lattice data. In fact, in the quenched approximation, there is no room for the ρ-meson to decay into two pions.

As for the second peaks in the PS and V channels, the error analysis discussed in Fig.4 shows that their spectral "shape" does not have much statistical significance, although the existence of the non-vanishing spectral strength is significant. Under this reservation, we fit the position of the second peaks and made linear extrapolation to the chiral limit with the results, $m^{2nd}/m_\rho = 1.88(8)(2.44(11))$ for the PS (V) channel. These numbers should be compared with the experimental values: $m_{\pi(1300)}/m_\rho = 1.68$, and $m_{\rho(1450)}/m_\rho = 1.90$ or $m_{\rho(1700)}/m_\rho = 2.20$.

One should remark here that, in the standard two-mass fit of $D(\tau)$, the mass of the second resonance is highly sensitive to the lower limit of the fitting range, e.g., $m^{2nd}/m_\rho = 2.21(27)(1.58(26))$ for $\tau_{min}/a = 8(9)$ in the V channel with $\beta = 6.0$ [10]. This is because the contamination from the short distance contributions from $\tau < \tau_{min}$ is not under control in such an approach. On the other hand, MEM does not suffer from this difficulty and can utilize the full information down to $\tau_{min}/a = 1$. Therefore, MEM opens a possibility of systematic study of higher resonances with lattice QCD data.

As for the third bumps in Fig.2, the spectral "shape" is statistically not significant as is discussed in Fig.4, and they should rather be considered a part of the perturbative continuum instead of a single resonance. Fig.2 also shows that SPF decreases substantially above 6 GeV; MEM automatically detects the existence of the momentum cutoff on the lattice $\sim \pi/a$. It is expected that MEM with the data on finer lattices leads to larger ultraviolet cut-offs in the spectra. The height of the asymptotic form of the spectrum at high energy is estimated as

$$\rho_V(\omega \simeq 6\mathrm{GeV}) = \frac{1}{4\pi^2}\left(1+\frac{\alpha_s}{\pi}\right)\left(\frac{1}{2\kappa Z_V}\right)^2 \simeq 0.86. \quad (8)$$

The first two factors are the $q\bar{q}$ continuum expected from perturbative QCD. The third factor contains the non-perturbative renormalization constant for the lattice composite operator. We adopt $Z_V = 0.57$ determined from the two-

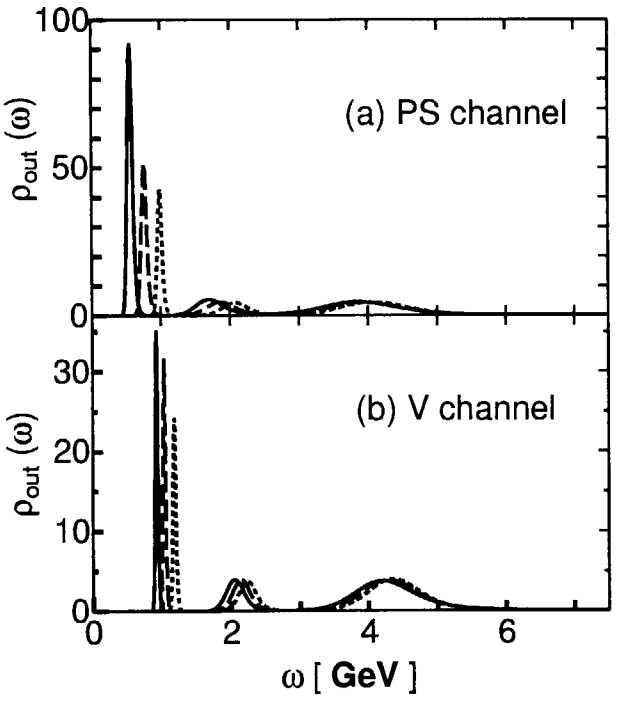

Figure 2. Reconstructed image $\rho_{out}(\omega)$ for the PS (a) and V (b) channels. The solid, dashed, and dotted lines are for $\kappa = 0.1557$, 0.1545, and 0.153, respectively. For the PS (V) channel, m_0 is taken to be 2.0 (0.86). ω_{max} is 7.5 GeV in this figure and Fig.3.

point functions at $\beta = 6.0$ [11] together with $\alpha_s = 0.21$ and $\kappa = 0.1557$. Our estimate in eq.(9) is consistent with the high energy part of the spectrum in Fig.2(b) after averaging over ω. We made a similar estimate for the PS channel using $Z_{PS} = 0.49$ [12] and obtained $\rho_{PS}(\omega \simeq 6\text{GeV}) \simeq 2.0$. This is also consistent with Fig. 2(a). We note here that an independent analysis of the imaginary time correlation functions [2] also shows that the lattice data at short distance is dominated by the perturbative continuum.

In Fig.3(a) and (b), the results using the lattice kernel K_{lat} are shown. K_{lat} is obtained from the free boson propagator on the lattice. It reduces to K_{cont} when $a \to 0$. The other parameters and boundary conditions are the same with Fig.2(a,b). The difference of Fig.2 and Fig.3 can be interpreted as a systematic error due to the finiteness of the lattice spacing a.

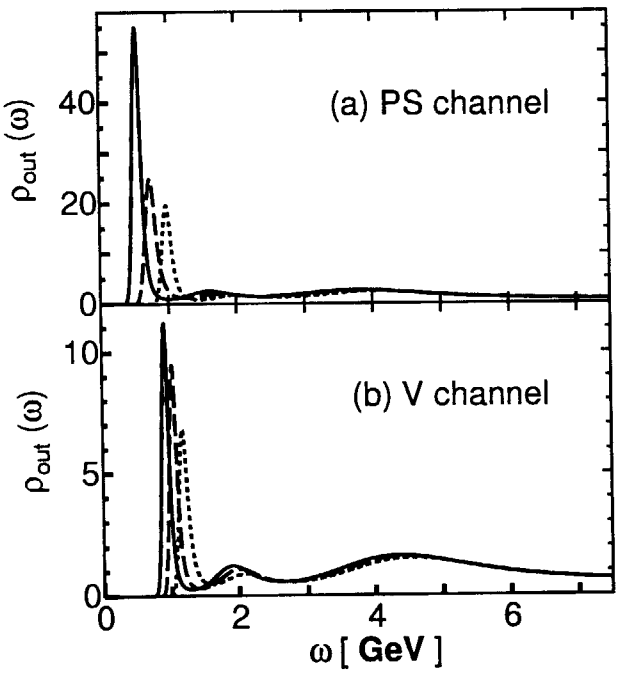

Figure 3. Same with Fig.2 except for the use of the lattice kernel K_{lat}.

5. Error analsis

The statistical significance of the reconstructed image can be studied by the following procedure [4]. Assuming that $P[A|DH\alpha m]$ has a Gaussian distribution around the most probable image $\hat{A}$, we estimate the error by the covariance of the image, $-\langle(\delta_A\delta_A Q)^{-1}\rangle_{A=\hat{A}}$, where δ_A is a functional derivative and $\langle\cdot\rangle$ is an average over a given energy interval. The final error for A_{out} is obtained by averaging the covariance over α with a weight factor $P[\alpha|DHm]$. Shown in Fig.4 is the MEM image in the V channel for $\kappa = 0.1557$ with errors obtained in the above procedure. The height of each horizontal bar is $\langle\rho_{out}(\omega)\rangle$ in each ω interval. The vertical bar indicates the error of $\langle\rho_{out}(\omega)\rangle$. The small error for the lowest peak in Fig.4 supports our identification of the peak with ρ. Although the existence of the non-vanishing spectral strength of the 2nd peak and 3rd bump is statistically significant, their spectral "shape" is either marginal or insignificant. Lattice data with better quality are called for to obtain better SPFs.

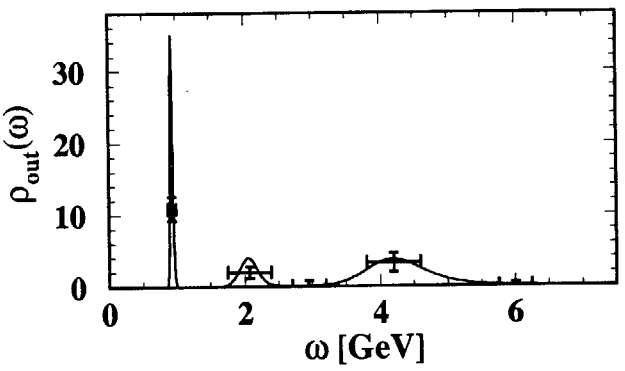

Figure 4. $\rho_{out}(\omega)$ in the V channel for $\kappa = 0.1557$ with error attached.

6. Summary

We have made a first serious attempt to reconstruct SPFs of hadrons from lattice QCD data. We have used MEM, which allows us to study SPFs without making a priori assumption on the spectral shape. The method works well for the mock data and actual lattice data. MEM produces resonance and continuum-like structures in addition to the ground state peaks. The statistical significance of the image can be also analyzed. Better data with finer and larger lattice will produce better images with smaller errors, and our study is a first attempt towards this goal.

There are many problems which can be explored by MEM combined with lattice QCD data. Some of the applications in the baryon excited states, hadrons at finite temperature, and heavy quark systems will be reported in future publications [13].

We appreciate MILC collaboration for their open codes for lattice QCD simulations, which has enabled this research. Our simulation was carried out on a Hitachi SR2201 parallel computer at Japan Atomic Energy Research Institute. M. A. (T. H.) was partly supported by Grant-in-Aid for Scientific Research No. 10740112 (No. 10874042) of the Japanese Ministry of Education, Science, and Culture.

REFERENCES

1. E. V. Shuryak, Rev. Mod. Phys. **65**,1 (1993).
2. M. -C. Chu, J. M. Grandy, S. Huang, and J. W. Negele, Phys. Rev. D **48**, 3340 (1993).
3. Y. Nakahara, M. Asakawa and T. Hatsuda, hep-lat/9905034 (Phys. Rev. D in press).
4. See the review, M. Jarrell and J. E. Gubernatis, Phys. Rep. **269**, 133 (1996).
5. R. N. Silver et al., Phys. Rev. Lett. **65**, 496 (1990); W. von der Linden, R. Preuss, and W. Hanke, J. Phys. **8**, 3881 (1996); N. Wu, *The Maximum Entropy Method*, (Springer-Verlag, Berlin, 1997).
6. D. B. Leinweber, Phys. Rev. D **51**, 6369 (1995); D. Makovoz and G. A. Miller, Nucl. Phys. **B468**, 293 (1996); C. Allton and S. Capitani, Nucl. Phys. **B526**, 463 (1998); Ph. de Forcrand et al., Nucl. Phys. B (Proc. Suppl.) **63A-C**, 460 (1998).
7. See e.g., J. Skilling, in *Maximum Entropy and Bayesian Methods*, ed. J. Skilling (Kluwer, London, 1989), pp.45-52; S. F. Gull, ibid. pp.53-71.
8. This formula is motivated by our lattice QCD data.
9. The MILC code ver. 5, http://cliodhna.cop.uop.edu/~hetrick/milc .
10. Y. Iwasaki et al., Phys. Rev. D **53**, 6443 (1996); T. Bhattacharya et al., ibid. 6486.
11. L. Maiani and G. Martinelli, Phys. Lett. **B178**, 265 (1986).
12. M. Göckeler et al., Nucl. Phys. **B544**, 699 (1999).
13. M. Asakawa, T. Hatsuda and Y. Nakahara, in preparation.

13. Precise Measurement of $K_L \rightarrow \pi^0 \nu \nu$ Decay at 50-GeV PS

Takao INAGAKI

High Energy Accelerator Research Organization, KEK
1-1 Oho, Tsukuba, Ibaraki 305-0801, Japan

Abstract

The $K_L \rightarrow \pi^0 \nu \nu$ decay is one of the processes whose experimental studies will have to be performed at the 50-GeV proton synchrotron (PS) of the Joint Project. The decay is a CP-violating process purely through $\Delta S=1$ transition with little having a theoretical ambiguity due to QCD corrections. The precise measurement of the branching ratio of $K_L \rightarrow \pi^0 \nu \nu$ decay will provide a clean determination of a basic parameter in the present particle-physics. A uniquely important chance will open to look for new-physics and to understand the CP-violation phenomena profoundly. After a kind of pilot experiment at the present KEK 12-GeV PS, a high sensitivity experiment is planned at the 50-GeV PS.

1. 始めに

１９８０年代以降、素粒子物理学では標準理論 almighty の時代が続いている。 標準理論を構成するクオーク・レプトン（フェルミオン）やゲージボソンが殆ど過不足無く観測されて、わずかにヒグス粒子と重力子の観測を残すだけである。 その他の実験事実も殆ど、標準理論に基づく計算によって定性的のみならず定量的に説明されている。 一方で、標準理論にはフェルミオンの質量やその混合等といった起源が説明できないパラメーターが多すぎるとか、左右非対称であるとか、重力を含めた相互作用の統一に達していないとかがあって、決して究極の理論とはよべない。 しかし、これらの根本的問題に access する実験は容易ではない。 それらを調べるには余りにも高エネルギーでの実験を要請されるからである。

それでも、我々素粒子物理実験屋は、次の２つの推論をもとに、次のステップ：100GeV-数 TeV 領域に問題を解き明かす鍵があると考えている。 １つ目は、ウィークボゾンに質量(100GeV)を与える為に導入されたヒグス粒子が輻射補正によって非常に大きな質量を持

ってしまうという事実から出発する。 その輻射補正を抑えて自然な形で、100GeV を与える為には、ヒグス粒子やフェルミオンが 100GeV-数 TeV 領域で溶ける複合粒子であることで輻射補正の増加を抑えるか、100GeV-数 TeV 領域に超対称粒子が存在して輻射補正の発散を相殺させるかが考えられている。 2つ目は、標準理論の根幹をなすくりこみ理論によって生じる強・弱・電磁相互作用の結合定数のエネルギー依存性である。 1980 年代までの実験で低エネルギー領域（現在の加速器エネルギー）で得られた3つの相互作用定数を外挿すると、誤差の範囲で 10^{16}GeV 付近の1点に収束し、大統一理論の根拠を与えていた。 逆に言えば、現状から大統一まで切れ目無く続く研究者にとって「砂漠」があると見られていた。 90 年になってＬＥＰ実験等で高精度になったデータを使うと、この収束にずれがあることが有意に見えてきた。 それぞれの外挿線をわずかに曲げる効果（即ち未知の物理）が、現状から大統一の間に必要になった。 ここでも、曲げる効果を与える最も有力なシナリオは 100GeV-数 TeV 領域の超対称性粒子の存在である。

これらは、現在我々の居る 100GeV からそう遠くない 100GeV-数 TeV 領域で、新粒子を含む多くの新現象がある事を示唆する。 我々がＳＳＣ、ＬＨＣ、ＪＬＣ等の超高エネルギー加速器の建設を多くの困難を乗り越えて進めようとするのもこの示唆に基づく。一方で、カナダの KAON プロジェクトや今回の 50GeV-PS 等の大強度ビームを使ったＫ中間子崩壊実験も、これら新現象を明らかにする上でユニークで重要な場を提供する。

２．Ｋ中間子崩壊実験の意義

まず、何故崩壊現象を見るのかを考えたい。 ここで言う粒子の崩壊は質量約 100GeV のウイークボゾンを交換する弱い相互作用を通して起こる。 即ち、相互作用の時空的な広がりが $1/100\text{GeV}^{-1}$ で、メソンやバリオン等のハドロンの典型的な広がり（クオーク間の距離）である 1GeV^{-1} に比べて極めて小さい。 崩壊は、自然界にはハドロンの構成粒子としてのみ存在する点状粒子・クオークの反応そのものを見ている。 一方、ハドロン散乱等の実験では、クオークを内部に束縛している相互作用と散乱で持ち込まれる相互作用が同じ QCD 相互作用なので、多体クオーク間の反応が重なりあった効果を見ている。 多体効果の物理の意義を否定するものではないが、基本粒子であるクオークの反応を裸で取り出すと言う点では、崩壊現象の観測は素粒子的課題に直接的な情報を与える。 それでも、崩壊現象を理論計算と突き合わせてクリティカルな比較をするのは実際は難しい。 親または娘のハドロンをクオークの束縛状態として記述する厳密な QCD に基づく計算が出来ない。 QCD では 1GeV^{-1} より遠方では非摂動性が顕著になる為である。 この QCD 効果を巧みに相殺させる測定量が実は非常に重要になる。

広がりについて言えば、崩壊頻度の少なさ（小さい分岐比）を相互作用の広がりが小さいこと（交換粒子の質量（M）が大きいこと）に対応させることも出来る。 そうすると頻度は、M^{-4} に比例する。 例えば弱い相互作用で崩壊する粒子のあるモードの分岐比が１０^{-12}であると、そのモードの観測は 100GeV の 1000 倍、100TeV の粒子交換効果を

見ていることとなる。 正に素粒子物理学上ホットなエネルギー領域をカバーする。 そして現在のK中間子崩壊実験は大体その当たりの分岐比を測っている。

次に、何故Kかであるが、その前に、弱い相互作用は左巻きヘリシティーのクオーク・レプトンに作用し、それらは対になって（(u,d),(c,s),(t,b)の様に）フレーバーという量子数をもち、そのフレーバーを変える(FC)反応が抑制されていることにふれたい。 その中で荷電を変える(CC)反応（s→u 等）は抑制されつつも通常のフレーバを変えない反応（d→u 等）の 1/10-1/1000 程度の強さで起こりうる（クオーク混合）が、荷電を変えない(NC)反応の直接過程は禁止されている。 現実の FCNC 反応は FCCC を含む second-order 反応(GIM 機構)で生じ、8桁以上抑制されている。

これまで測定されたクオーク質量を見ると、Kを構成するｓクオークとBのｂクオークが、相方のｃ、ｔよりも軽く、フレーバーを変えない反応がエネルギー的に起こり難いことがわかる。 即ち、K、B中間子は崩壊そのものが抑制されている（崩壊全巾が小さい）ので、同じ分岐比で例えばｃクオークを含むD中間子の崩壊を見た時より、更に高エネルギーの現象に到達しやすい。 これがK、B崩壊に実験の精力が集中している理由の一つである。

さて、我々の主な興味は崩壊頻度が抑制されより高エネルギーに到達しうるという理由で FCNC にあるが、先に述べた様に FCNC は second-order 反応である GIM 機構によって生じる。 その中でｔクオークがｄクオークに転化する（Vtd）等の未定の値が、ダイアグラムの内線に入ってくるｔクオークを使って求められる。 興味深いことには、GIM 機構では、内線のクオークとしてフレーバーの異なるクオークが入ってくるが、それらの質量が等しければクオーク混合のユニタリー性によって寄与が相殺することである。 結果的には内線クオークの質量差の二乗に比例したものが残る。 即ち FCNC では、三番目のフレーバーが特に重く他との質量差が大きいこともあって、特に t クオークの寄与を選択的に見るのに適している。

一方、KとBでは次の様な違いがある。 Bではｂとｔクオークが同じフレーバーである為に転化が容易で、内線にｔクオークが入る割合が大きい。 しかし、実験的に得られる親のKの数はBに比べて5桁以上多い。 それで、おおまかには、Bはクオーク混合等の測定が得意で、Kはより高エネルギー現象の発見学的アプローチに向いていると言える。 しかし、クオーク混合の測定でもKには特徴がある。 クオーク混合を測定する当面の目標はユニタリー性のチェックであり、ユニタリティ三角形の是非にあるが、Bの観測は角度の測定に対応し、Kの場合は辺の長さになる。 こういった相補的な特徴から、世界的にもK、Bの実験が進められている。

K、B中間子崩壊の大きな研究目標の一つにＣＰ非保存の理解がある。 ＣＰ非保存の理解は素粒子物理学上の課題であると同時に、Baryon Asymmetry といわれる宇宙創生の謎を解き明かすテーマでもある。 1960 年代に ε の測定によって $\Delta s = 2$ 振幅でＣＰ非保存が発見されて以来、最近ようやく $\Delta s = 1$ 振幅でのＣＰ非保存の存在が確認されたが、

Bファクトリーでの$\Delta b=1,2$振幅のCP非保存の測定や、50GeV 加速器の大強度ビームを使っての$\Delta s=1$振幅の定量的測定によって理解が飛躍的に深まることが期待されている。

3．JOINT-PROJRECT で取り組みたい実験：$K_L\to\pi^0\nu\nu$崩壊の分岐比の測定

50GeV 加速器での実験の特徴はテーマの多様性であるといわれている。 K崩壊物理においてもFCNC 過程を中心に多くの実験が検討されているが、その中で特にすぐにでも立ち上げたいテーマとして、$K_L\to\pi^0\nu\nu$崩壊の分岐比の測定がある。 $K_L\to\pi^0\nu\nu$はFCNC 過程であるが、非摂動的なQCD 計算の不定さを、分岐比の大きな$K\to\pi e\nu$との比をとることで相殺することが出来る。 クオーク混合の Vtd の虚数部を、理論計算の不定さが3％以下の精度で、求め得る。 又、$K_L\to\pi^0\nu\nu$はCP非保存過程で、直接CP非保存と言われる$\Delta s=1$振幅が支配的なpureな崩壊モードである。 そして、$K_L\to\pi^0\nu\nu$は、同じくCP非保存で、不定さの小さいB→ψKs崩壊での$\Delta b=2$振幅、それにεと呼ばれる$\Delta s=2$振幅等と合わせて、ユニタリティー三角形の是非を調べ、かつCP非保存の起源を解き明かす鍵となり得るものといわれている。 (εの場合は既に実験値は精密で理論計算の不定さが大きいが、それを最近Lattice-QCD 計算の発展に期待している。)

この様に$K_L\to\pi^0\nu\nu$崩壊の分岐比の測定はBファクトリーでの主たる測定に匹敵する意義を持つテーマであるが、実験的にはこれまで、予言値3×10^{-11}に対して10^{-6}の上限値が得られているだけである。 K_Lが中性で飛跡を観測できないし、π^0も2γに崩壊して同じく飛跡の観測が容易でない、しかも2つのνが観測不能である3体崩壊なので、π^0を測定しても運動学的に崩壊の同定が出来ない等々、今まで専用の実験を躊躇させるに十分な理由があった。 ここでは詳しく述べないが、私たちは初めて、ペンシル状の細いビームを使い、隙間無くカロリメーターを設置することでこの困難な測定が可能であることを示してきた。 大強度の50GeV 加速器を使うと、この測定法では理論計算上の不定さと同じ3％の統計誤差を与える約1000個の$K_L\to\pi^0\nu\nu$崩壊を観測することが不可能ではない。

しかし、一気に8桁の前進は容易くないので、私たちは、50GeV が稼働する前までに現存のKEK－12GeV 加速器を使って徹底的なパイロット実験 (実験番号E391a) を行いたいと考えている。 現在2001年度内の実験開始に向けて、実験装置の建設をすすめている。

JAERI-Conf 99-015

14. Quark Nuclear Physics at JHF

H. Toki

[1]*Research Center for Nuclear Physics(RCNP), Osaka University*
Ibaraki, Osaka 567-0047, Japan

Abstract

We discuss the research fields to be studied by the Japan Hadron Facility being planned in the site of JAERI as a joint project with Neutron Science Project. We would expect to reveal the most microscopic structure of matter using the intensity frontier proton machine. In particular, we would like to develope Quark Nuclear Physics to describe hadrons and nuclei in terms of quarks and gluons.

1 Introduction

The accelerator parameters of the JHF machine complex are $E_p \leq 50GeV$ and the intensity of $I_p \leq 15\mu A$. This high intensity frontier machine could produce as the secondary beams; pion, kaon, muon, neutrino and even heavy ions in addition to the primary proton. Hence, the possibilities of interesting physics program are great and in such a case a good idea is most welcome.

In fact, there are many programs being discussed with JHF. They are neutrino mixing, kaon rare decay, color transparency, hypernuclei, lepton flavor mixing, kaonic atom, meson spectroscopy, baryon spectroscopy, heavy ion collision and so on. These subjects could be discussed in terms of the hadron- meson degrees of freedom. At the same time, it is possible to discuss in terms of the quark-gluon degrees of freedom.

Hence, the JHF project would reveal the structure of the microscopic matter in terms of the most fundamental particles with the intensity frontier machine.

We would like to discuss what are the frontier projects to be performed with the JHF accelerator complex. Particularly, we would like to emphasize the interesting research field to be performed with the JHF machine as Quark Nuclear Physics.

2 Quark Nuclear Physics

Quark Nuclear Physics (QNP) is the research field of describing hadrons and nuclei in terms of quarks and gluons. Here, confinement and chiral symmetry breaking are the most essential phenomena for QNP. QCD is supposed to provide the dynamics of quarks and gluons. In fact, QCD is able to describe the above essential phenomena using the lattice QCD. On the other hand, the perturbative description of QCD provides the high momentum phenomena.

Although this is the case, we would like to develope the basic picture of QNP. We should understand why various interesting phenomena happen. This is very important for the motivation of development of various kinds of physics related with quarks and gluons. For nuclear physics, it was the shell model, which changed the situation of physics associated with nucleus completely. Suppose we want to describe a nucleus with about 100 nucleons. Such a system was impossilbe to solve. However, once physicists noticed the magic number and the important degrees of freedom for the description of the excitation spectra as those nucleons in the valence orbits, they were able to describe nuclear excitations, which are caused by about 100 particles. The shell model played a key role for the developement of nuclear physics.

What is the basic picture (model) then for QNP? There are various candidates; Dual Ginzburg-Landau (DGL) theory, Instanton model, QCD sum rule, $1/q^4$ model and so on. All these models have some truth in describing the low energy observables. Here we shall focus on the DGL theory, which has been studied in various directions. The DGL theory is demonstrated to describe both confinement and chiral symmetry breaking and at the same time has a strong connection to QCD.

3 Dual Ginzburg-Landau Theory

The DGL theory is based on the assumption that our vacuum is in the superconductor like state; dual superconductor. In the superconductor, the magnetic field H is disliked by the superconducting matter due to the Meissner effect. Hence, if the magnetic field is stronger than the critical amount, and the superconductor is the second-kind, then the magnetic field does not spread over the matter, but rather is confined in a vortex like

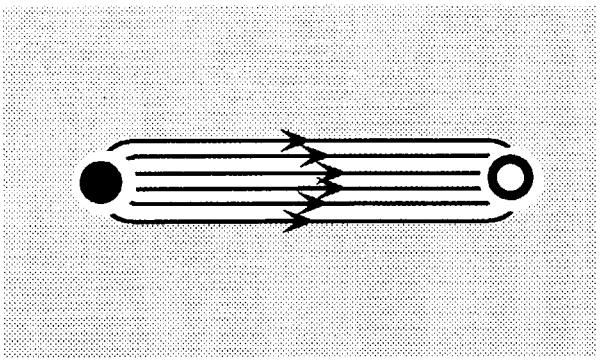

Figure 1: The schemtic view of quark confinement.

configuration as shown in Fig.1. We assume that our vacuum does not like the (color) electric field. Hence, when a quark and an anti-quark are placed in the dual superconductor, the color electric field produced by the quark cannot spread over the space but rather flows into the anti-quark in the vortex like configuration without disturbing much the dual superconductor. This property causes confinement of quarks, since quarks cannot exist alone but need a partner.

This dual superconductor picture is very attractive. However, there should be two important ingredients in this picture. One is the abelian dominance and the other is the color monopole. On the other hand, the fundamental theory of strong interaction, QCD, is a non-abelian gauge theory. QCD has non-abelian gluons and does not have color monopoles.

A miracle happens in QCD by the choice of a special gauge. 't Hooft is the one who introduced the abelian gauge by fixing the gauge of the non-abelian gluons and showed that in this case there appear color monopoles[1]. The lattice QCD demonstrates the appearance of monopoles and the signature of their condensation as the appearance of long and complicated monopole trajectries in the abelian gauge. The abelian dominance needs the study of the correlations of charged gluons and those of the non-charged gluons (abelian gluons) in the abeilan gauge. The recent lattice QCD calculations showed that the correlation length is very short for the charged gluons, while it is large for the abelian gluons in the maximally abelian (MA) gauge[2]. These facts indicate that the picture of quark confinement in terms of the dual-superconductor could have support from QCD.

This consideration then provides the effective lagrangian, where the color monopole couples with dual gluon fields and the quarks interact with abelian gluons. The Higgs

term provides condensation of color monopoles. The resulting lagrangain has a similarity to the Ginzburg-Landau theory and hence the name dual Ginzburg-Landau theory (DGL) is used for this model[3, 4].

The DGL theory provides clear predictions as

1. There should appear color monopole glueball around 1.5GeV. This is a Higgs particle of strong interaction.
2. The string tention for gluons is 3 times more than that for quark-antiquark string tention due to the abelian property of the long range physics.
3. We get the probabilities of hadronization with respect to the quark masses.
4. Various others.

4 Photon-nucleon collision

I first discuss the case of real photon in order to learn the nature at intermediate and high energies. What happens when a GeV photon collides with a nucleon? My favorite figures show the total cross sections for vastly different systems being plotted as functions of the squar root s; $\sqrt{s}$. All the cross sections could be described with just two energy dependent terms;

$$\sigma = As^{0.08} + Bs^{-0.45} \tag{1}$$

It is amazing to see that the photon-proton cross section also follows the same s dependence. This fact convinces the importance of the virtual vector mesons in photon beam.

These two s dependence is described in terms of two Regge trajectories, one is made of vector mesons constituted with quarks and the other made of glueballs of gluons. The slope of the vector mesons is well known from the meson spectra. This information provides the string tention between quark and anti-quark. On the other hand, we do not know the glueball states at all. Hence, the determination of the glueball states is important to get the regge slope and hence the string tention between gluons.

GeV photons may provide this information by studying carefully the s dependence and the t dependence. In particular, if we observe ϕ meson, which consists mainly of s quarks, we can emphasize the gluon exchange process due to the OZI suppression

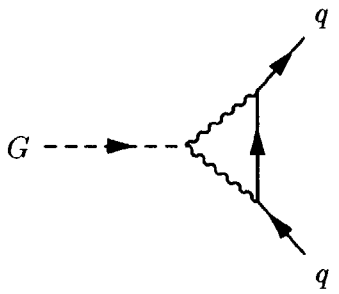

Figure 2: The simplest diagram of the glueball coupling to quark.

of the mesons made of quarks. The precise measurement of the t dependence should provide the slope of the glueball trajectory. It would be nice then to extract the string tention from this information. In addition, we can predict the position of the 2^+ glueball state. In addition, the energy dependence of the phi production around 2GeV may have contributions of the 0^+ glueball[5].

There is an interesting candidate for the 0^+ glueball at $1500MeV$ identified as $f_0(1500)$. The glueball filter being discussed in PLB is a possible argument for this state to be a glueball. However, the decay of $f_0(1500)$ is not flavor blind and the identification of this state to a glueball is in quesion. Recently, Koma et al. calculate the decay vertex of the glueball, the Higgs particle of the strong interaction to lead to quark confinement, and find that the glueball-quark coupling is not flavor blind. This is because the glueball of the DGL theory couples first to the dual gluon field and then couple to the gluon, which couple to quark. The simplest diagram of the glueball coupling to quark is shown in Fig.2. The results will be published soon[6].

It would be very important to search for glueballs with the intensity frontier machine. The use of various flavor beams should be used with screening purpose for the important glueball search with the JHF beams.

5 Baryon Spectra

Let us look now at the baryon spectrum. The baryon spectrum, which includes all the known SU(3) baryons, seems to show no regularity in the spectrum. The ground state baryons have been studied by Gell-Mann and Okubo. The Gell-Mann-Okubo mass formula provided the existence of the SU(3) quarks, which leads to the quark model.

It would be then very interesting to measure the excited states with respect to these ground states. This is done in Fig.3. Those states without the corresponding ground state baryons are shifted downward by 200MeV to consider the spin effect, which is seen as the mass difference between $\Sigma(1189)$ and $\Sigma(1385)$. Surprisingly the spectra show very good systematics as seen in Fig.3.

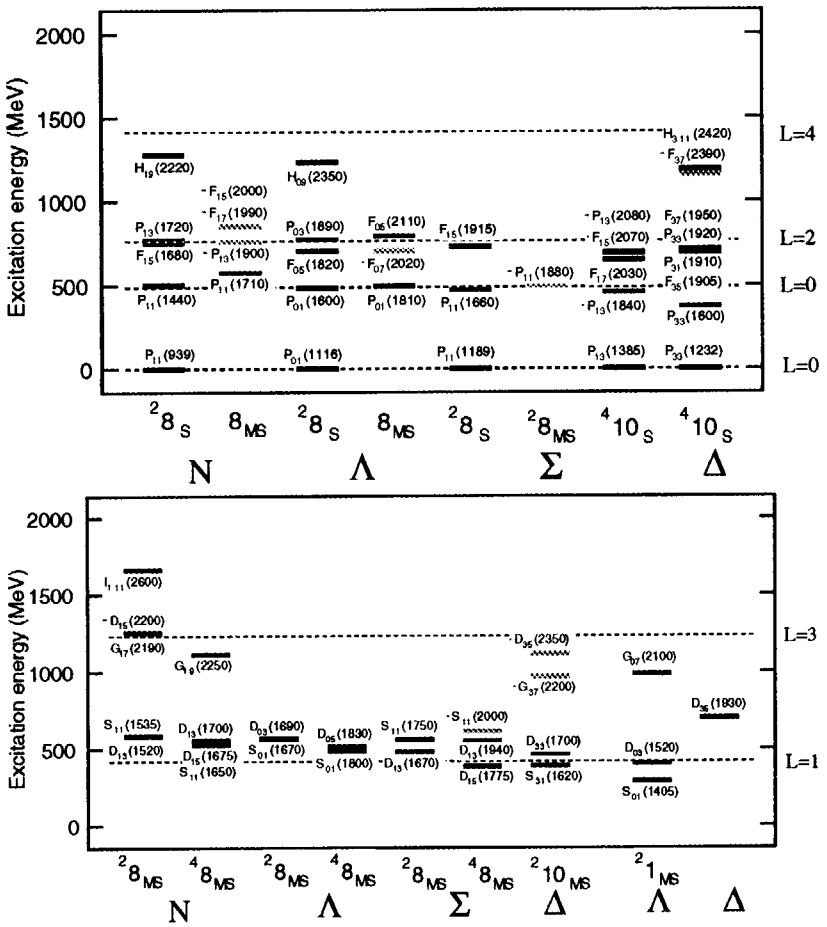

Figure 3: SU(3) flavor baryon spectra for even parity states (upper) and odd parity states (lower). The dashed lines with the angular momentum L are the predictions of the DOQ model[7].

These simple spectra indicate rather a simple dynamics is acting for the excitation of quarks. In fact, when we take a deformed oscillator quark model, we find the ground state is sphenical and the first and the second excited state are deformed. Once a state is deformed, there should appear a rotational band on top of the intrinsic deformed state. This was demonstrated by Hosaka et al.[7] and the results are indicated by dashed lines

in Fig.3.

If the baryon spectra are determined by the quark confinement dynamics, we need further experimental data. There are many states being missed in the systematics in Fig.4. On top, it is important to study the decay properties of these states to identify if they belong to some band or to another band. The electro-magnetic transitions are important in this respect.

6 Hadronization and Spin Polarization

When the struck quark with another quark try to leave out from the nucleon, a color vortex is formed between the struck quark and the remaining diquark. The pair creation, which could be $q\bar{q}$ or $q^2\bar{q}^2$, may lead to hadronization. When a antiquark or diquark try to form a hadron with the leading quark, these quarks are subject to be pulled from each other. This confining force could be the source of spin-polarization. At the same time, it is very important to learn how this hadronization takes place by slowly varying the proton energy at JHF.

This mechanism has been discussed phenomenologically by DeGrand and Miettinen [8] and formulated by using the scalar confining force by Yamamoto et al. [9] for the case of high energy hadron-hadron collisions. They have shown clearly the appearance of the spin polarization in accordance with the experimental spin observables.

The same mechnism is supposed to be responsible for spin polarization in the electron induced reaction. In fact, Suzuki et al. demonstrate some polarization to occur in the gamma induced production of Λ and Σ[10].

7 Conclusion

The JHF is the exciting accelerator complex to perform important experiments to extract fundamental informations of the subatomic world.

We can learn

1. Hadronization, which is very important by itself and as applications for Big-bang and RHIC physics.

2. Baryon, Meson spectroscopy

3. Glueball spectroscopy
4. Hadron polarization phenomena

We would like to mention at this place that QNP is a very special research field. Generally, experiments and/or observations provide motivations to develope theories/models to describe the phenomena. Theories then predict new experiments, which check the validity of the theories. In this way we can find the true picture of the phenomena. In QNP in addition to this excersize, we have QCD which tells which theory is correct. Hence, QNP provides an unique oppotunity for us to understand the microscopic world from the most fundamental theory from first principle.

We would like to mention at this place then how we construct nuclei in QNP. The quark and gluon degrees of freedom are used explicitely to describe hadrons; masses, sizes and their interactions. We use these informations as inputs to meson-baryon many body lagrangains as the chiral unitary model due to the strong residual interactions caused by the Goldstone bosons as pions and kaons. The meson-baryon dynamics should provide the baryon-baryon interactions, which are then used for the inputs of the nuclear many body scheme as the Brueckner-Hartree-Fock theory. Using nucleons as the fundamental degrees of freedom, we would like to describe nuclei and hypernculei and even stars and supernova.

H.T. wants to express his sincere thanks to the organizers of this conference at JAERI and at KEK. This meeting was truly an exciting meeting to reveal the important and exciting physics to be performed at JHF.

References

[1] G. 't Hooft, *Nucl. Phys.* **B190** (1981) 455.

[2] K. Amemiya and H. Suganuma, Proc. Int. Symp. on *Innovative Computational Methods in Nuclear Many-Body Problems (INNOCOM 97)*, World Scientific (1998) 284.

[3] H. Suganuma, S. Sasaki and H. Toki, *Nucl. Phys.* **B435** (1995) 207.

[4] S. Sasaki, H. Suganuma and H. Toki, *Prog. Theor. Phys.* **94** (1995) 373.

[5] T. Nakano and H. Toki, Proc. Int. Work. on *Exciting Physics with New Accelerator Facilities (EXPAF)*, World Scientific (1998) 48.

[6] Y. Koma, H. Suganuma and H. Toki, to be published.

[7] A. Hosaka, M. Takayama and H. Toki, *Mod. Phys. Lett.* **A13**(1998) 1699.

[8] T.A. DeGrand and H.I. Miettinen, *Phys. Rev.* **D23** (1981) 1227.

[9] Y. Yamamoto, K.-I. Kubo and H. Toki, *Prog. Theor. Phys.* **98** (1997) 95.

[10] K. Suzuki, N. Nakajima, H. Toki and K.-I. Kubo, to be published.

15. Light Unstable Nuclei in the Continuum

Kiyoshi Katō
Division of Physics, Graduate School of Science, Hokkaido University

November 25, 1999

Abstract

It is discussed that the complex scaling method is one of the most available frameworks to solve many body resonances. As the recent developments of the complex scaling method, we present several ways to analyse the properties of resonant states; the matrix elements associated with resonant states, the extended completeness relation and partial widths of resonances. We also show the discusions on the binding mechanism and excited resonant structure of the Borromean systems ^{4}He+n+n and ^{9}Li+n+n. It is shown that the pairing correlation between valence neutrons and among core neutrons plays an important role in neutron-rich nuclei.

1 はじめに

短寿命核ビームを用いた最近の実験の進展によって、安定線から遠く離れたドリップ・ライン近傍核についての研究の新たな局面が開かれつつある。核密度分布、魔法数など安定核に関する最も基本的な性質さえもドリップ・ライン近傍核において異なっていることが明らかになってきた。例えば、核半径についてよく知られた"(質量数)$^{1/3}$則"はもはやドリップ・ライン核では成立していないことが指摘されている [1]。そのような典型的な例を中性子過剰核の"ボロミーン系"において見ることが出来る。それらの柔結合系は中性子ハローのエキゾティックな構造を示し、どの二体部分系も結合状態を持たない"コア + n + n" 三体模型を用いてこれまで理論的に研究されてきた。そのようなエキゾティックな柔結合状態を調べるために、極端な弱結合状態と共に二体および三体系の非束縛状態あるいは共鳴状態を解きあげなければならない。そのような問題を扱うために、複素座標スケーリング法 [2] が有効であることが論じられてきた [3]。

複素座標スケーリング法では、束縛状態と同時に共鳴状態のエネルギーと幅をスケールされたハミルトニアンを対角化することによって求めることが出来る。この報告では、共鳴状態の性質を分析するための複素座標スケーリング法の最近の発展について報告し、次に複素座標スケーリング法を用いた不安定核（He および Li-アイソトープ）の研究を報告する。

複素座標スケーリング法の 1 つの発展として、スケーリングされて得られる共鳴状態の波動関数を用いて共鳴状態の分析を行う枠組みの作成である。まず、共鳴状態の行列要素の計算について論じ [4]、それを用いて電磁遷移確率の強度分布を議論する [5]。遷移強度については、共鳴状態を含む拡張された完全系の関係を用いて、共鳴状態、連続状態に分けて表すことが出来ることを示す。もう一つの発展として、共鳴状態の部分幅の計算法の確立がある。この報告で、我々は部分幅を計算する有効な方法を提案する [6]。

次に、^{6}He核について、^{4}He+n+n 模型と複素座標スケーリング法を適用して, 結合エネルギーや中性子ハロー構造など結合機構、および三体励起共鳴状態を分析した結果について報告する [7]。そこで、$J^\pi = 0^+$ 基底状態の結合機構を説明するために、外郭中性子間の対相関が重要であることを示す。基底状態について観測される性質をよく説明する枠組みで、励起状態についても同時に計算し、p-軌道配位で予想されるすべての J^π 共鳴状態が得られることを示す。それらの中で比較的幅の狭い 2^+ 状態が最近実験的に観測されたという報告を得ている [8]。

"コア+n+n" 模型計算は、はじめ、^{9}Li+n+n 系について行われた。しかし、^{11}Li の結合エネルギーが再現できず、その問題は、^{10}Li に関する最近の実験データ [9] に基づいて得られたより引力的な ^{9}Li-n 相互作用を用いても解決されないことが論じられてきた。そこで、我々は、もう一度 ^{9}Li-n

相互作用の問題に戻り、^{10}Li 核における低エネルギー s-軌道状態を説明する新たらしい考えを検討する。その考えの本質的な点は ^{9}Li 内の中性子の対相関を考慮し、奇数個の外郭中性子が付け加わることによってパウリ・ブロッキングが生じる得ることを考えるところにある。このような効果を考慮して得られる ^{9}Li-n 相互作用について議論する。

2 複素座標スケーリング法の発展

複素座標スケーリング法は多体系の共鳴状態のエネルギーおよび共鳴幅を求める非常に有効な方法である。さらに、共鳴状態のエネルギー・幅以外のさまざまな物理量についても分析できるならば、より優れた方法になるであろう。複素座標スケーリング法では、複素固有エネルギー値に対する固有関数として共鳴状態の波動関数が得られている。ここで波動関数は複素座標スケーリング $U(\theta)$: $r = r \cdot e^{i\theta}$ でスケール変換されているので、同じく変換された演算子 $\hat{O}(\theta) = U(\theta)\hat{O}U(\theta)^{-1}$ の行列要素を計算すれば θ に依存しない物理量の行列要素が得られる [4, 10]。

そのようにして計算された共鳴状態の行列要素を用いれば、共鳴状態の遷移確率の強度を調べることが出来る。すなわち、共鳴状態と連続状態からの遷移強度分布への寄与をそれぞれ分離して求められる。そのような目的のために、これまでグリーン関数の極展開など多くの研究が行われきた [11]。しかし、極展開法では、どのような展開するか、どのような極の集め方をするか、極以外の連続状態から寄与をどう評価するかなどが具体的な問題にあたって、問題になる。一方、複素座標スケーリング法では与えられたスケーリング・パラメータ θ に対して、結語状態、共鳴状態、θ-線上の連続状態の分離がユニークに行われる。そして、それらの状態を用いて、拡張した完全系

$$1 = \sum_{B}^{n_B} |\Phi_B^\theta(r,k_B)\rangle\langle\tilde{\Phi}_B^\theta(r',k_B)| + \sum_{R}^{n_R(L_\theta)} |\Phi_R^\theta(r,k_R)\rangle\langle\tilde{\Phi}_R^\theta(r',k_R)| + \int_{L_\theta} dk_\theta |\Phi^\theta(r,k_\theta)\rangle\langle\tilde{\Phi}^\theta(r',k_\theta)|.$$

をつくることができる [5]。

共鳴状態がどんな構造を持つか見るために、共鳴崩壊幅の部分幅は重要な物理情報である。しかし、複素座標スケーリング法では、通常、全共鳴幅しか求まらない。そこで、全共鳴幅だけでなく、部分幅についても複素座標スケーリング法の枠組みの中で求める新たな方法の開発が望まれてきた。我々は、ここで、Sofianos − Rakityansky[12] によって提案された「ヨースト関数の方法」を用いたチャンネル結合系における部分幅の計算方法を紹介する。ヨースト関数に対するチャンネル結合方程式は次のように与えられる：

$$\frac{\partial F_{nm}^{(\pm)}(E,r)}{\partial r} = \pm\frac{\mu_n}{i\hbar^2 k_n} H_n^{(\mp)} \sum_{n'=1}^{N} V_{nn'} \left(H_{n'}^{(+)} F_{n'm}^{(+)}(E,r) + H_{n'}^{(-)} F_{n'm}^{(-)}(E,r) \right), \tag{1}$$

ただし、$H_n^{(\mp)}(k_n,r)$ は n-番目のチャンネル（運動量 k_n）の斉次解である。そして、共鳴エネルギーは共鳴状態に対する "outgoing" の境界条件から以下の方程式を解いて求められる：

$$det\|F^{(-)}(E,r=\infty)\| = 0. \tag{2}$$

ヨースト関数が求められると、共鳴状態の部分幅は共鳴エネルギー（$E_{res} = E_r - i\Gamma/2$）での S-行列の留数で与えられるので、部分幅の比が次の式で求めることが出来る：

$$\frac{\Gamma_n}{\Gamma_{n'}} = \left\| \frac{\sum_m F_{nm}^{(+)}(E_{res},\infty) G_{mn}(E_{res})}{\sum_m F_{n'm}^{(+)}(E_{res},\infty) G_{mn'}(E_{res})} \right\|, \tag{3}$$

ここで、$G_{mn}(E_{res})$ は行列 $F_{nm}^{(-)}(E_{res},\infty)$ の余因子行列である。一方、全共鳴幅 $\Gamma = \sum_n \Gamma_n$ はエネルギーの虚数部として求められているので、部分幅の比とから部分幅の絶対値が得られる。

部分幅の比は、また、各チャンネルから崩壊する確率流の密度比でも与えられる [13]。すなわち、

$$\frac{\Gamma_n}{\Gamma_{n'}} = \left| \frac{A_n}{A_{n'}} \right|^2, \tag{4}$$

ただし、共鳴状態 $\psi_{res} = \sum_{n=1}^{N} \phi_n(r)$ で表され、各チャンネル波動関数の漸近形が、

$$\phi_n(r) \xrightarrow[r\to\infty]{} A_n j_n(r), \qquad j_n(r) = \sqrt{\frac{\mu_n}{k_n}} H_n^{(+)}(k_n, r). \tag{5}$$

で与えられる。

3 ボロミーン 系 : ^{6}He および ^{11}Li

3.1 模型と計算の枠組み

ここでは、次のような理由で半微視的 "コア＋中性子群 " 模型を用いる。すなわち、(1) その閾値近傍の束縛状態の性質を調べるうえで、各構成クラスターの結合エネルギーを再現しなければならない。(2) 三体クラスター間の相対運動について重要な相関に注目して解くために、そのような相関を容易に表現できる模型を用いる。どの二体部分系も結合状態を持たないボロミーン系に対するコア・プラス・中性子対模型で、まず、コアと中性子間の相互作用を用意しなければならない。その際、結合状態を持たないコアと中性子間の相互作用は散乱データあるいは共鳴状態の解析を通じて得られなければならない。そこで、共鳴状態の解析に複素座標スケーリング法を用いることが出来る。

最初に、コア・プラス・中性子対模型の有効性を見るために、コア－中性子間相互作用がよく調べられている ^{4}He+n+n 模型 [7] を用いて、^{6}He核を調べる。コアから外殻中性子に対する平均場の作用と外殻中性子間の対相関に注目して^{4}He+n+n 系の結合機構を調べるため、V－座標型クラスター軌道殻模型 (COSM)[14] と T-座標型拡張クラスター模型 (ECM)[15] のハイブリッド－ TV 模型 [15] を用いた計算を行う。そこでの結果を踏まえて、次に、^{9}Li+n+n 模型を^{11}Li 核に適用する。しかしながら、^{9}Li+n+n 系は ^{4}He+n+n 系の場合のように単純ではない。^{9}Li+n+n 系が ^{4}He 系と異なる重要な点は、外殻中性子がコア核の中性子と同じ p-殻配位を主要成分に持つことにある。我々は、外殻中性子と同様の^{9}Liコアの中性子間の対相関を考慮して三体クラスター系の結合機構を考える。そのために、まず、^{9}Liコアの中性子間の対相関を考慮した^{9}Li-n 相互作用を分析する。

3.2 ^{6}He=^{4}He+n+n

^{4}He+n+n 模型計算で、我々は ^{4}He-n 相互作用として KKN-ポテンシャル [16] を採用し、外殻中性子間の相互作用として Minnesota ポテンシャル [17] を用いることにする。^{4}He+n+n の基底状態の結合エネルギーについての結果を Fig.1 に示す。そこで、外殻中性子間の対相関の効果を見るために、クラスター軌道殻模型（COSM）計算とハイブリッド－ TV 模型計算の結果を比較する。COSM 計算結果は基底関数（チャンネル数 $[n]=[(l_n j_n)^2]_{J^\pi=0^+}$）の増加と共に非常にゆっくりした収束 を示す。

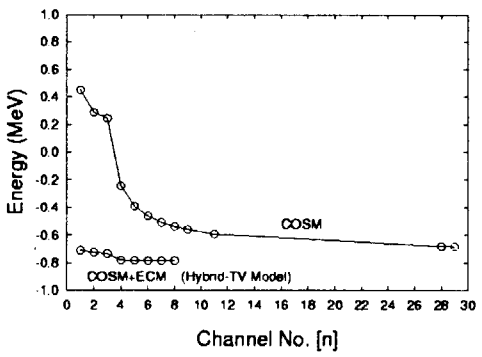

Figure 1: Bindind energy convergences of COSM and hybrid-TV model calculations of the ^{4}He+n+n system.

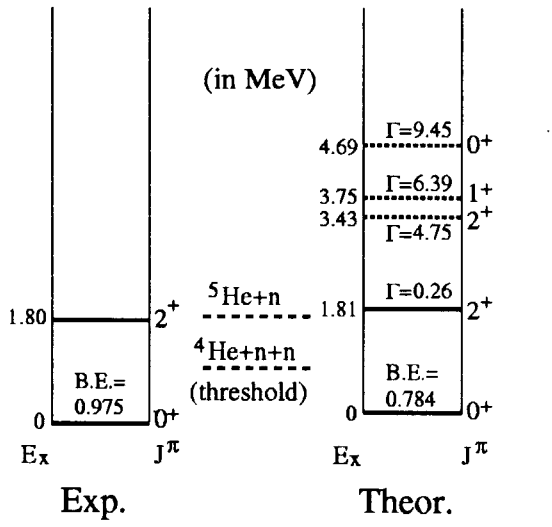

Figure 2: Energy levels of ^{6}He.

他方、ハイブリッド－TV模型で、0^+-ペアリング・タイプ $[l=0, L=0]_{J^\pi=0^+}$ のECM基底を付け加えると、非常に急速なエネルギー収束性を得る。この結果は外殻中性子の対相関が ^{4}He+n+n 系の結合機構において重要な役割を演じていること意味している。

^{4}He+n+n の結合エネルギーは 0.784 MeV と計算され, 観測結果 0.975 MeV と比べても満足すべき結果が得られる。しかし、およそ 0.2 MeV ほど計算値が観測と比べて結合エネルギーが不足していることも注意しておく必要がある。このわずかな不足エネルギーは ^{4}He コアの励起成分の寄与を示唆している [18, 19]。一方、後で示すように、この ^{4}He コアの励起の効果は ^{9}Li+n+n 系の ^{9}Li コアの励起に比べ非常に小さい。

この^{4}He+n+n 模型に複素座標スケーリング法を適用して、^{6}He の励起状態を求める。^{6}Heの励起状態は全て共鳴状態で、しかも三体共鳴状態である。結果は Fig. 2 に示される。その重要な結果は外殻二中性子の $(p)^2$- 配位で予想される全ての J^π が共鳴状態として求められるということである。最初の 2_1^+ 以外の状態は、幅がかなり大きく、一つ一つの共鳴状態として観測されることは困難かと思われたが、最近、幅が比較的小さな 2 番目の 2_2^+ 状態が観測されたという報告がなされている [8]。

3.3 ^{11}Li=^{9}Li+n+n

1990 年, Tosaka 等 [20] によって、先駆的な ^{9}Li+n+n 模型研究が行われたとき、コアと中性子間の相互作用に関する知識を与えてくれる^{10}Li 核の分光学的観測データは Wilcox 等 [23] による古い実験結果しかなかった。その Wilcox 等データに基づいて決められた ^{9}Li-n 相互作用を用いて計算された Tosaka 等の結果は、観測される ^{11}Li の結合エネルギーに対して全く足りないことを示していた [20]。同じ ^{9}Li-n 相互作用を用いて、ハイブリッド－TV模型計算も行われたが結果は全く悲観的なものであった [21]。その後、1993 年, Bohlen 等 [9] によって、^{10}Li の結合エネルギーだけなく励起共鳴状態についての新たな実験結果が報告された。^{10}Li の結合エネルギーに対する新たな観測データはより引力的 ^{9}Li-n 相互作用を示唆しており、新たなデータに基づいた精密な ^{9}Li+n+n 模型計算が期待された。

まず、我々は Bohlen 等による新しいデータに基づいて、^{9}Li-n 畳み込みポテンシャル (folding potential) を決める。^{10}Li の状態は基底状態から全て共鳴状態なので、複素座標スケーリング法を用いて計算する [22]。得られた ^{9}Li-n 相互作用を用いて、^{9}Li+n+n の結合エネルギーを計算し、その結果を Fig. 3 に示す [24]。この結果は、観測される^{11}Li の結合エネルギーを再現させるため ^{9}Li-n 相互作用を 2.75 % 強めた計算である。計算の枠組みは ^{4}He+n+n と同じで、その結合エネルギーの収束性の結果も ^{4}He+n+n の結果と非常によく似ている。従って、^{9}Li+n+n 系においても対相関が大変重要であることがわかる。しかし、すでに述べたように ^{10}Li の実験データを再現する ^{9}Li-n 相互作用を用いたのでは、観測される ^{11}Li の結合エネルギーが説明できず、およそ 1 MeV の不足となる [24]。

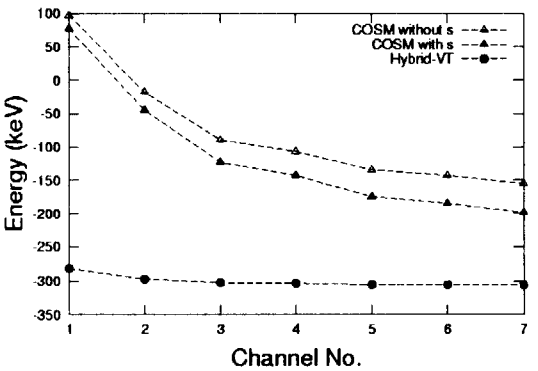

Figure 3: Bindind energy convergence of COSM and hybrid-TV model calculations of the ^{9}Li+n+n system.

一方、^{11}Liのハロー構造を説明するために, 外殻中性子の s-軌道配位が重要な役割が議論されてきた [26]。しかしながら、Li-アイソトープにおいて、なぜ s-軌道中性子配位が大きな結合エネルギーを得て、p-軌道配位と同程度のエネルギーになるのか納得の行く説明がない。そこで、我々は s-軌道がなぜ低エネルギー領域に出現するか新しい説明を試みる。その基本的アイディアは中性子の対相関に対するパウリ・ブロッキングである。同様なアイディアが、変形が重要になる Be-アイソトープにおいて、論じられているが [27, 28]、対相関に対するパウリ・ブロッキングは変形のない ^{9}Liコアにおいて重要になるのである。具体的に示すために、$[^9\mathrm{Li}((p_{3/2})^4_\nu)+\mathrm{n}]+[^9\mathrm{Li}((p_{3/2})^2_\nu(p_{1/2})^2_\nu)+\mathrm{n}]+[^9\mathrm{Li}((p_{3/2})^2_\nu(s_{1/2})^2_\nu)+\mathrm{n}]$ のチャンネル結合計算を実行する [25]。Fig. 4 に示すように、^{10}Li において、p-波の中性子はパウリ・ブロッキング効果として強い斥力ポテンシャルを受ける。一方、s-波を含む他の部分波中性子は非常に小さな効果しか受けない。^{9}Li コアの $(1s_{1/2})^2$ ペアリングに 対する s-波外殻中性子のパウリ・ブロッキングは外殻中性子が空間的に広がっているためには非常に小さい

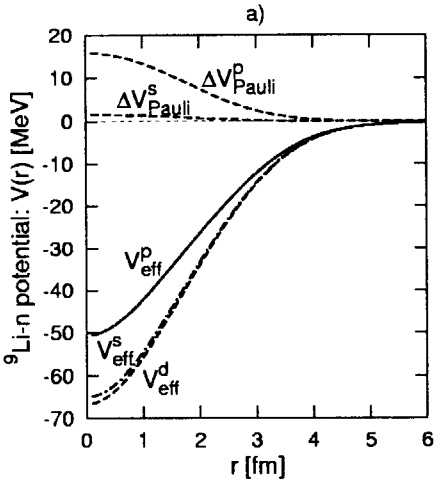

Figure 4: Effective ^{9}Li-n potentials and the Pauli-blocking potentials for s-, p- and d-wave neutrons.

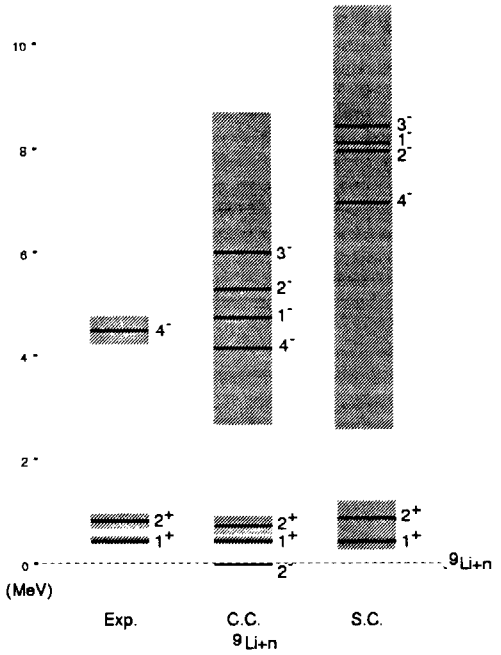

Figure 5: Energy levels of ^{10}Li.

ものになる。結果として、$p_{1/2}$-軌道中性子は浅い ^{9}Li-n ポテンシャルを受け、s-軌道および d-軌道中性子は深い ^{9}Li-n ポテンシャルを受けることが示された。この s-軌道中性子に対する深い ^{9}Li-n ポテンシャルのため、我々の^{10}Li の計算では中性子 $s_{1/2}$ 状態が仮想共鳴状態（virtual resonance）なる。また、^{9}Li コアに中性子対相関を取り入れた計算（チャンネル結合計算: cc）が、中性子対相関を取り入れない計算（シングル・チャンネル計算: sc）に比べて、Bohlen 等の 1^+ および 2^+ の実験結果をエネルギーだけでなく幅までよく説明することがわかる（Fig. 5）。

4 結論

不安定核の研究では、二体共鳴状態のみならず三体共鳴状態を研究対象にしなければならない。どの二体部分系も結合状態を持たないボロミーン系はそのような典型である。複素座標スケーリング法は多体系の束縛状態と同時に非束縛状態を統一的に扱う大変有用な方法であることが示されてきた。

この報告で、我々は、共鳴状態の行列要素を複素座標スケーリング法の枠組みで計算する方法を示した。その方法と拡張された完全系を用いて、遷移強度分布を共鳴状態からの寄与と連続状態からの寄与を分離して計算し、非束縛状態の性質を分析することを提案した。さらに、チャンネル結合系に対するヨースト関数法を用いて、共鳴状態の部分幅を計算する新たな方法を説明した。

^{4}He+n+n 系と^{9}Li+n+n 系について、複素座標スケーリング法を用いた不安定核の具体的分析結果の報告を行った。^{4}He+n+n 系では、三体共鳴状態が計算され、実験データとも対応する結果が得られることを示した。また、Li-アイソトープにおいて、^{9}Li コア内の対相関が外殻中性子の間の対相関と協同的に重要な役割を演ずることが論じられた。

References

[1] I. Tanihata, Nuc. Phys. **A488** (1988), 113c.

[2] J. Aguilar and J.M. Combes, *Commun. Math. Phys.* **22** (1971), 269. E. Balslev and J.M.Combes, *Commun. Math. Phys.***22** (1971), 280.

[3] K. Kato, T. Myo, S. Aoyama, K. Ikeda, 物理学会誌 52 巻 2 号 111.

[4] M. Homma, T. Myo and K. Katō, Prog. Theor. Phys. **97** (1997), 561.

[5] T. Myo, A. Ohnishi and K. Katō, Prog. Theor. Phys. **99** (1998), 801.

[6] H. Masui, S. Aoyama, T. Myo and K. Katō, inpress, Prog. Theor. Phys.

[7] S. Aoyama, S. Mukai, K. Katō and K. Ikeda, Prog. Theor. Phys. **93** (1995), 99; **94**, (1995), 343.

[8] J. Jänecke *et al*, Phys. Rev. **C54** (1996), 1070.

[9] H. G. Bohlen *et al*, Z. Phys. **344** (1993), 381.

[10] B. Gyarmati and T. Vertse, Nucl. Phys. **A160** (1971), 523.

[11] J. Humblet and L. Rosenfeld, Nucl. Phys. **26** (1961), 529; L. Rosefeld, Nucl. Phys. **26** (1961), 594
J. Humblet, Nucl. Phys. **A151** (1971), 225; **A187** (1972), 65.

[12] S.A.Sofianos and S.A.Rakityansky, J. Phys. A: Math. Gen. **30** (1997), 3725; *ibid.*, **31** (1998), 5149.

[13] N. Moiseyev and U. Peskin, Phys. Rev. A**42** (1990)255.

[14] Y. Suzuki and K. Ikeda, Phys. Rev. **C38** (1988),410.

[15] K. Ikeda, Nucl. Phys. **A538** (1992), 355c.

[16] H. Kanada, T. Kaneko, S. Nagata and M. Nomoto, Prog. Theor. Phys. **61** (1979), 1327.

[17] D. R. Thompson, M. LeMere and Y. C. Tang, Nucl. Phys. **A286** (1977), 53.

[18] A. Csótó, Phys. Rev. **C48** (1993), 165.

[19] K. Arai, Y. Suzuki and R. G. Lovas, Phys. Rev. **C59** (1999), 1432.

[20] Y. Tosaka and Y. Suzuki, Nucl. Phys. **A512** (1990), 46.

[21] Y. Tosaka, Y. Suzuki and K. Ikeda, Prog. Theor. Phys. **83** (1990), 1140.

[22] K. Katō and K. Ikeda, Prog. Theor. Phys. **89** (1993), 623.

[23] K. H. Wilcox *et al*, Phys. Lett. **B59** (1975), 142.

[24] S. Mukai, S. Aoyama, K. Katō and K. Ikeda, Prog. Theor. Phys. **99** (1998), 381.

[25] K. Katō T. Yamada and K. Ikeda, Prog. Theor. Phys. **101** (1999), 119.

[26] I. J. Thompson and M. V. Zhukov, Phys. Rev. **C49** (1994), 1904.

[27] H. Sagawa, B.A. Brown and H. Esbensen, Phys. Rev. Lett. **B309** (1993), 1.

[28] H. Esbensen, B.A. Brown and H. Sagawa, Phys. Rev. **C51** (1995), 1274.

16. Theory of Synthesis of Superheavy Elements

Yasuhisa Abe and Takahiro Wada*

Yukawa Institute for Theoretical Physics, Kyoto University, Kyoto 606-8502
**Department of Physics, Konan University, 8-9-1 Okamoto, Kobe 658-8501*

Abstract. The dynamical process of synthesizing superheavy elements is studied on the basis of the fluctuation-dissipation dynamics. A three-dimensional Langevin equation is used for the formation process of the superheavy compound nuclei in the spherical region. For the description of the surviving process, a one-dimensional Smoluchowski equation is adopted taking into account the temperature dependent shell correction energy and the competition between fission and neutron evaporations are described with the statistical model. Owing to the smaller hindrance for fusion, the fusion probability is larger for more asymmetric incident channels. On the other hand, such combinations lead the compound system to the relatively high excitation energy, comparing with when one uses the symmetric channel. In view of the Q-value of the reaction, the use of magic nuclei as target and projectile is preferable. The maximum residue cross section is obtained around the Bass barrier energy for the case of hot fusion reaction. The results show the importance of the use of neutron-rich beams and targets.

I INTRODUCTION

The superheavy elements were predicted to exist quasi-stably many years ago, based on our knowledge of the stability of nuclear systems, i.e., an additional stability due to the shell effect [1]. Theoretical studies on a center of the stability are still going on, in more and more refined ways [2]. But on the other hand, reaction theory for how to reach there is still missing, though the refined statistical studies have been made for the decay processes, assuming fusion cross sections. The systematic experiments performed empirically at GSI with the great efforts succeeded in synthesizing the elements up to with Z=112 [3]. They employed ^{208}Pb or ^{209}Bi as the target and found very narrow energy window for residues cross section peaks at sub barrier region in most cases [4]. The excitation energies of the compound nuclei formed are very small, so the reactions are called as "cold fusion". This is quite natural, for the purpose of obtaining larger survival probabilities. As is known well, excited nuclei have large fission decay widths, larger than neutron emission ones in heavier elements.

Recently, Dubna group has found events which are expected to be a signature for a synthesis of the element Z=114 with the collisions of ^{48}Ca + ^{244}Pu [5]. Subsequently, Berkeley group has reported that they have observed events for the element Z=118 with ^{86}Kr + ^{208}Pb [6]. Although there are many things to do experimentally for the confirmation, these experimental findings appear to open a new era for the synthesis of the superheavy elements.

We have been developing the theory [7] which should describe the whole process starting from a contact of incident ions, through an evolution of the excited composite system, and finally to fission with an extremely small probability for residues to be left for the superheavy elements. In the present talks, we briefly review the theory and give some recent results.

II THE REACTION PROCESSES

For the sake of simplicity, we discuss the whole process in two parts; formation of the compound nuclei and its decay, which follows the idea of the compound nucleus theory of reactions. Of course, in such heavy systems, it is not clear whether the theory is still valid or not.

Firstly, in decay process, the survival probability Γ_n/Γ_f should be maximized to obtain large residue cross sections. Since the fissility parameter of the superheavy elements is nearly equal to unity, the Γ_f is very large, then the survival probability is extremely small. Only the shell correction pocket gives rise to a quasi-stability against fission. Therefore, excitation energies of the compound nuclei formed are desired to be as low as possible, otherwise, the shell would be destroyed and thereby the stability by the shell correction energy would disappear. Of course, if we can synthesize extremely neutron-rich compound nuclei, a rapid cooling due to instantaneous neutron evaporations is helpful for a quick restoration of the shell correction energies.

In order to obtain compound nuclei in low excitation, we have to find projectile-target combinations whose interaction barrier top corresponds to low excitation energy of the compound nuclei, taking into account reaction Q-values. It is easy to find out such combinations, by extrapolating the systematic studies of fusion barrier or interaction barrier in lighter systems. In most cases, there are two regions of favorable combinations. For example, in the case of the compound nucleus Z=118 and N=176, one is around ^{86}Kr + ^{208}Pb, and the other is around ^{136}Xe + ^{158}Gd. They are related with N=50 and 82 closed shells in the projectiles, respectively. Actually, the former combination is that of Berkeley group's experiment. Such an argument, however, is not enough. There are dynamical effects in fusion process.

Secondly, in fusion process, it is well known that there exists the fusion hindrance in massive systems, which is described by the extra-push and the extra-extra-push energies [8]. This hindrance is considered to be due to the strong Coulomb repulsion as well as the strong energy dissipation into intrinsic motions of nucleons. The former requires a careful calculation of the potential energy surface in many degrees of freedom of the shape of the composite system, while the latter does the employment of Langevin or Kramers equation for the collective, i.e., the shape degrees of freedom. This is already well known in describing dynamically fission process of excited nuclei [10], which is required by the anomalous pre-scission neutron, gamma-ray multiplicities etc. Therefore, any combination of projectile and target around the above two regions is expected to suffer the hindrance, which means that much more energies than the barrier height would be required for the system to fuse. It is well known that the hindrance starts apparent at $Z_1Z_2 \sim 1800$ [9]. Therefore, we can avoid the hindrance by using lighter projectiles such as Dubna group's system. Naturally, excitation energies of the compound nuclei formed are relatively high, so they are called as "hot fusion", though it is not "hot".

Now, it is clear that in order to know optimum systems and optimum incident energies, we have to take into account the whole process, formation and decay, and to calculate residue cross sections by making products of the two factors over the promising systems. In the theory we are proposing, the evolutions of a composite system consisting of a projectile and a target in contact are described by the multi-dimensional Langevin equation, which accommodates all the possible processes not only into compact compound nucleus, but also into the reseparation corresponding to the so-called deep-inelastic collision and quasi-fission [11]. As for the decay of the compound nucleus, the dynamical evolution of fissioning motion is described by one-dimensional Smoluchowski equation which is a simplified version of Kramers equation and is valid for strong friction (energy dissipation) cases. Of course, neutron evaporations are taken into account, which give rise to a cooling and then to a time-dependent restoration of the shell correction pocket in the potential energy surface for the fissioning motion.

III THREE-DIMENSIONAL MODEL

We calculate the probability of the formation of spherical compound nucleus after the sticking of the target and projectile nuclei by the Langevin approach. The method of calculating the formation cross section with the Langevin equation is found in Ref. 12. When the incident energy is below the Bass barrier height [13], the barrier penetration probability is estimated in WKB approximation. After the formation of the spherical compound nuclei, a one-dimensional Smoluchowski equation is used along the symmetric fission path to estimate the survival probability including the temperature dependent shell correction energy.

We adopt the three-dimensional nuclear deformation space with the two-center parametrization [14]. The neck parameter ϵ is fixed to 1.0 in the present calculation, deformation parameters δ_1 and δ_2 of the colliding nuclei are taken to be equal, i.e., $\delta_1 = \delta_2 = \delta$. The collective coordinates are z_0 (distance between two potential centers), δ, and the mass-asymmetry α; $\alpha = (A_1 - A_2)/(A_1 + A_2)$, where A_1 and A_2 denote the mass numbers of the target and the projectile, respectively.

The multi-dimensional Langevin equation is given in the following form,

$$\frac{dq_i}{dt} = \left(m^{-1}\right)_{ij} p_j,$$
$$\frac{dp_i}{dt} = -\frac{\partial V}{\partial q_i} - \frac{1}{2}\frac{\partial}{\partial q_i}\left(m^{-1}\right)_{jk} p_j p_k - \gamma_{ij}\left(m^{-1}\right)_{jk} p_k + g_{ij} R_j(t), \quad (1)$$

where V is the potential energy, m_{ij} and γ_{ij} are the shape-dependent collective inertia and dissipation tensors, respectively. The normalized random force $R_i(t)$, is assumed to be a white noise, i.e., $\langle R_i(t)\rangle = 0$ and $\langle R_i(t_1)R_j(t_2)\rangle = 2\delta_{ij}\delta(t_1 - t_2)$. The strength of the random force g_{ij} is given by $\gamma_{ij}T = g_{ik}g_{jk}$, where T is the temperature of the compound nucleus. The potential is calculated as the sum of a generalized surface energy, Coulomb energy, and the centrifugal energy with the moment of inertia of the rigid body. Hydrodynamical inertia tensor is adopted with the Werner-Wheeler approximation for the velocity field, and the wall-and-window one-body dissipation [15] is adopted for the dissipation tensor. At t=0, each trajectory

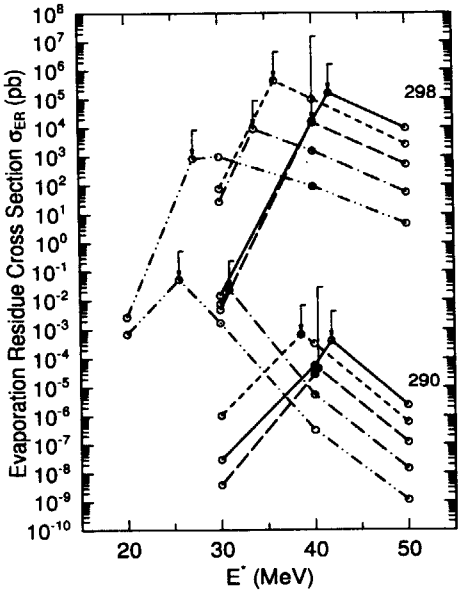

FIGURE 1. Excitation function of σ_{EV} forming $Z = 114$ with various values of α: $\alpha = 0.70$ (solid), 0.65 (short dashed), 0.60 (long dashed), 0.55 (dot-dashed), and 0.50 (dot-dot-dashed). Two groups of lines correspond to different mass number of the compound systems, $A = 298$ and 290. Arrows denote the corresponding Bass barrier energies.

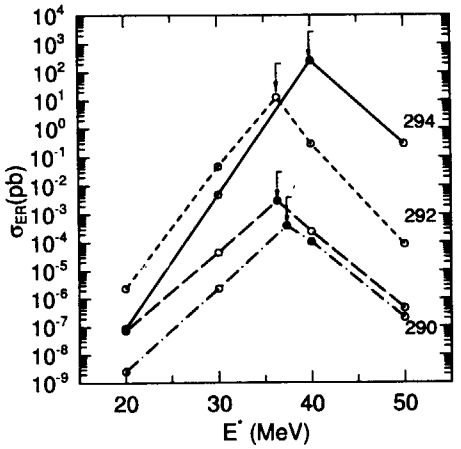

FIGURE 2. Excitation function of σ_{EV} for $Z = 114$. Figures attached to the lines denote the mass number of the compound systems. Solid line is for ^{258}Fm+^{32}Si, short dashed line for ^{244}Pu+^{48}Ca, long dashed line for ^{238}U+^{52}Ti, and dot-dashed line for ^{234}Th+^{56}Cr. Arrows denote the corresponding Bass barrier energies.

starts from z_0=1.6R_0 and δ=0 corresponding to the contact configuration with the initial velocity in the z_0 direction, where R_0 denotes the radius of the spherical compound nucleus.

In the surviving process, the evolution of the probability distribution $P(q,l;t)$ in the collective coordinate space is described with the Smoluchowski equation starting from the equilibrium shape,

$$\frac{\partial}{\partial t}P(q,l;t) = \frac{1}{\gamma}\left[\frac{\partial}{\partial q}\left\{\frac{\partial V(q,l;t)}{\partial q}P(q,l;t)\right\} + T\frac{\partial^2}{\partial q^2}P(q,l;t)\right]. \tag{2}$$

The angular momentum of the system is expressed by l. The temperature dependent shell correction energy is added to the macroscopic potential energy,

$$V(q,l;t) = V_{\rm macro}(q,l) + V_{\rm shell}(q)\Phi(t), \tag{3}$$

where $V_{\rm macro}$ is the same as that used in the previous stage and $V_{\rm shell}$ is the shell correction energy at $T = 0$. The temperature dependent factor $\Phi(t)$ is parametrized as $\Phi(t) = \exp\left(-aT^2(t)/E_d\right)$, following the work by Ignatyuk *et al.* [16]. The shell-damping energy E_d is chosen as 20 MeV. The compound nucleus is cooled down through particle evaporations, which is expressed in terms of the cooling curve $T(t)$ [17]. The process of calculating the evaporation cross section can be found in Ref. 7.

IV PRELIMINARY RESULTS

In our model space, there are two paths for the fusion reaction. One is essentially the reverse process of fission; two nuclei form a deformed mononuclear system and it changes its shape into a sphere along z_0 coordinate. The other is the path through the Bussinaro-Gallone saddle point along α coordinate. Except for a very asymmetric case, the latter process has only a very small contribution.

The formation probability becomes larger for more mass-asymmetric case. However, at the same time, the excitation energy that corresponds to the Bass barrier incident energy becomes higher due to smaller Q-value. The survival probability against fission strongly depends on the excitation energy of the compound system. When the neutron separation energy is not small enough, the survival probability decreases very rapidly with the excitation energy.

Figure 1 shows the calculated evaporation residue cross section with various incident channels forming the element $Z = 114$ with N=184 and $N = 176$. Five values of the mass-asymmetry parameter α are taken; α = 0.70, 0.65, 0.60, 0.55, and 0.50. In the figure, arrows denote the corresponding Bass barrier energies. In

the case of $\alpha = 0.70$, the formation probability is about 20% and it is of the order of 10^{-4} for $\alpha = 0.50$. It is seen that the lines are divided into two groups according to their neutron numbers. For $N = 184$ ($A = 298$), since the decrease of the survival probability with the excitation energy is small, strongly mass-asymmetric channels which have large formation probability have larger cross section. On the other hand, for $N = 176$ ($A = 290$), since the survival probability decreases rapidly, the resulting evaporation residue cross section is very small and less mass-asymmetric channels have larger cross section.

In Fig. 2, the excitation function of σ_{EV} is shown for four channels that can be studied experimentally, ^{258}Fm+^{32}Si, ^{244}Pu+^{48}Ca, ^{238}U+^{52}Ti, and ^{234}Th+^{56}Cr. Among them, the ^{244}Pu+^{48}Ca channel has been studied in FLNR, Dubna. It is seen that the cross section has a sharp peak around the Bass barrier energy and the maximum value becomes larger for more neutron-rich system. The absolute value of the cross section depends on the values of the parameters, which have not been thoroughly examined yet.

V REMARKS

The fluctuation-dissipation dynamics in the deformation parameter space is shown to be a necessary and an appropriate way to describe the fusion-fission process in heavy mass region. We use the multi-dimensional Langevin equation for the formation process and the Smoluchowski equation for the surviving process taking into account the particle evaporations and the temperature dependent shell correction energy. We apply this approach for the synthesis of superheavy elements and estimated the evaporation residue cross sections starting from the contact of two colliding nuclei. The process before the touching of the projectile and the target is to be studied. We only included the barrier-penetration effect within WKB approximation when the incident energy is lower than the Bass barrier. Other effects like the excitation during the approaching phase is not yet taken into account.

It is shown that the strongly asymmetric channel results in large formation probability, but it results in high excitation energy at the Bass barrier energy. Since the survival probability strongly depends on the neutron separation energy of the compound system, the use of the neutron-rich beam and target is highly desirable. The maximum cross section is expected around the Bass barrier energy for "hot-fusion" reaction. For the "cold-fusion" reaction channels, the statistical treatment is necessary to treat the competition between the fission and the neutron evaporation, because of the low excitation energy and the long life time of the neutron evaporation. This is now under progress.

ACKNOWLEDGEMENTS

The present talks are based on the collaboration with Dr. Y. Aritomo in Dubna, Prof. M. Ohta, Dr. T. Tokuda, and Mr. K. Okazaki from Konan University.

REFERENCES

1. P. Armbruster, Annu. Rev. Nucl. Sci., **35** (1985) 135; Y.T. Oganessian and Y.A. Lazarev, *Treatise on Heavy-Ion Science* (Plenum, 1985) pp.3-251; G. Münzenberg, Rep. Prog. Phys., **51** (1988) 57.
2. K. Rutz *et al.*, Phys. Rev. **C56** (1997) 238.
3. S. Hofmann *et al.*, Z. Phys. **A354** (1996) 229.
4. S. Hofmann, Rep. Prog. Phys., **61** (1998) 639.
5. Yu.Ts. Oganessian *et al.*, Nature, **400** (1999) 242.
6. V. Ninov *et al.*, Phys. Rev. Lett., **83** (1999) 1104.
7. Y. Aritomo, T. Wada, M. Ohta, and Y. Abe, Phys. Rev., **C55** (1997) R1011;
   Y. Aritomo, T. Wada, M. Ohta, and Y. Abe, Phys. Rev., **C59** (1999) 796.
8. W.J. Swiatecki, Nucl. Phys., **A376** (1982) 275.
9. K.-H. Schmidt and W. Morawek, Rep. Prog. Phys., **54** (1994) 949.
10. T. Wada, Y. Abe and N. Carjan, Phys. Rev. Lett. **70** (1993) 3538;
    Y. Abe et al., Phys. Reports **C275** (1996) 49.
11. T. Wada *et al.*, Nucl. Phys. **A654** (1999) 888c.
12. T. Tokuda, T. Wada, and M. Ohta, Prog. Theor. Phys., **101** (1999) 607.
13. R. Bass, *Nuclear Reactions with Heavy Ions* (Springer, 1980).
14. J. Maruhn and W. Greiner, Z. Phys., **251** (1972) 431;
    K. Sato, A. Iwamoto, *et al.*, Z. Phys., **A288** (1978) 383.
15. J.R. Nix and A.J. Sierk, Nucl. Phys., **A428** (1984) 161c.
16. A.V. Ignatyuk *et al.*, Sov. J. Nucl. Phys., **21** (1975) 255.
17. M. Ohta, Y. Aritomo, T. Tokuda and Y. Abe, Proc. of Tours Symp. on Nuclear Physics II (World Scientific, Singapore, 1995) p.480.

17. 超重元素合成のための重イオン融合反応

Heavy-ion fusion for synthesis of superheavy nuclei

池添 博、光岡 真一、西尾 勝久、Jun Lu、佐藤健一郎

Hiroshi IKEZOE, Shin-ichi MITSUOKA, Katsuhisa NISHIO, Jun Lu and Ken-ichiro SATO

原研 先端基礎研究センター

Advanced Science Research Center, JAERI

Keywords: Deformed Nuclei, Fusion, Evaporation residues, Statistical Model

Abstract: Evaporation residues produced in the fusion reactions of ^{60,64}Ni on ^{154}Sm and ^{76}Ge on ^{150}Nd were measured near Coulomb barrier energy by using JAERI-RMS. It was found that the fusion probability depends on the orientation of the deformed targets. When the projectiles collide at the tip of the deformed nuclei, the fusion probability is considerably reduced to the amount of 1/100 –1/1000 of the predictions. On the other hand, when the projectiles collide at the side of the deformed nuclei, the fusion occurs without any hindrance. This phenomenon was understood qualitatively by comparing the distance between mass centers of two colliding nuclei at the touching configuration with the position of the saddle point of the compound nucleus. When the distance is longer than the saddle position, the fusion is hindered and an extra-extra push energy is needed to evolve into the formation of the compound nucleus.

1. はじめに

最近ロシアのDubnaでZ=114、米国バークレーでZ=118の合成に関する報告があった[1,2]。Dubnaでは^{48}Ca+ ^{244,242}Pu融合反応で3nチャンネルを観測し、A=289と287からのα崩壊と核分裂を観測したと報告している。生成断面積は1 pbから4 pbである。この反応は励起エネルギーが30 - 35MeVで、熱い融合反応といわれる。一方バークレーでの実験では、^{86}Kr + ^{208}Pb融合反応で1nチャンネルでできるA=293のα崩壊を観測し、Z=118からZ=106に至る6個のα崩壊を検出したと報告している。この反応は冷たい融合反応と呼ばれ、生成断面積は2 pb程度であった。ドイツGSIでは冷たい融合反応を使ってZ=112の合成まで成功しており[3]、Z=102からZ=112に至る生成断面積の減少傾向からZ=118の場合、生成断面積はfb程度になると予想されていた。今回のバークレーの結果はこの傾向を完全に覆すもので、超重元素合成に大きな弾みを与える結果である。

熱い融合反応や冷たい融合反応の他に変形核同士の密着融合で超重元素を合成する可能性が理論的に提案されている[4]。この反応では、変形核の対称軸が互いにクロスする向きで衝突すると最もコンパクトな衝突形状ができ、融合しやすいと予想されている。さらに、衝突形状が軸対称性を持たないため、反応の過程で複合核を形成しないで核分裂過程へ向かう確率も小さいと予想されている。

この密着融合の可能性を探るために、希土類核の標的核に球形の入射核を当てて重イオンの融合確率が核の変形度や変形の向きにどのように依存するかを調べたので報告する。入射核が小さいとき変形核の長軸側で衝突するとクーロン障壁が低いため、この障壁を越えるに十分な入射エネルギーがあれば入射核は

容易に内部に入り融合する。たとえば、$^{16}O+^{154}Sm$ [5] や $^{40}Ar+^{154}Sm$ [6]などの場合がこれに当たる。これらの融合断面積データはサブバリアー領域で ^{154}Sm が変形していることによる融合断面積の増大を示している。もっと入射核が重くなった場合、すなわち入射核の原子番号 Z_1 と標的の原子番号 Z_2 の積 Z_1Z_2 が大きくなったとき、変形核を使った融合反応がどうなるのかに注目した。実験では $^{60,64}Ni+^{154}Sm$ 融合反応（複合核 $^{214,218}Th$）と $^{76}Ge+^{150}Nd$ 融合反応（複合核 ^{226}U）での生成核断面積を原研タンデム・ブースター加速器と反跳生成核分離装置 [7]を使って測定した。

2． 実験概要と実験結果

濃縮された ^{150}Nd と ^{154}Sm を１μmのアルミニウム箔に付け、約20 p nAの $^{60,64}Ni$、10 - 20 pnAの ^{76}Ge ビームで照射した。融合生成核はビーム方向に置かれた反跳生成核分離装置でビームから分離し、焦点面に置かれた２次元位置エネルギー検出器に埋め込まれた。２次元位置エネルギー検出器の前面にチャンネルプレート検出器を２台置いて生成核の飛行時間を測定し、飛行時間とエネルギーから生成核の質量を見積もり、反跳された標的核や散乱ビームから区別した。2 次元位置エネルギー検出器で観測されたα粒子のエネルギーと崩壊時間から生成核種が同定された。

融合反応における入射チャンネルの効果を引き出すためには出口チャンネル（蒸発過程）を正確に押える必要がある。そのために、同じ複合核を形成する異なる反応系で Z_1Z_2 の値が小さい反応系（$^{32}S+^{182}W \rightarrow ^{214}Th$ と $^{28}Si+^{198}Pt \rightarrow ^{226}U$）の融合生成核の測定も平行して行った。測定された核分裂断面積を図１に、生成核の断面積を図２－６に示す。

2．1 理論計算との比較

測定データは理論計算と比較された。融合断面積の計算は標的核や入射核の表面振動状態の励起（2^+および3^-状態）と標的核の変形（４重極および８重極変形）によるクーロン障壁の衝突角度依存性を考慮したチャンネル結合計算CCDEFコード [8]で行い、複合核の蒸発過程は統計モデルコードHIVAP [9]で計算した。CCDEFで計算された融合断面積は図１の実線で示されているように $^{32}S+^{182}W$ 反応および $^{28}Si+^{198}Pt$ 反応で測定された核分裂断面積とよい一致を示した。^{182}W（β_2=0.276、β_4=-0.089）と ^{28}Si（β_2=0.408、β_4=0）は変形しているため、計算値は球形の場合（点線）よりもサブバリアー領域で増大する（破線）。

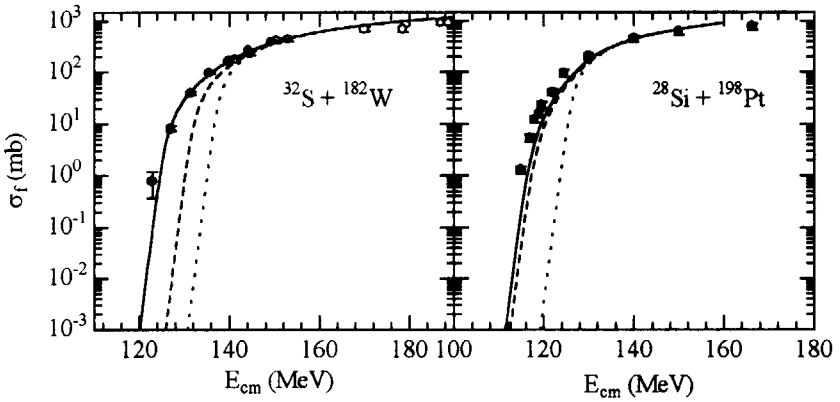

図１ 融合断面積の計算値と測定値（核分裂断面積で近似）。実線は核の変形と非弾性励起を考慮し、破線は変形度のみを考慮し、点線は球形の場合の計算結果を示す。

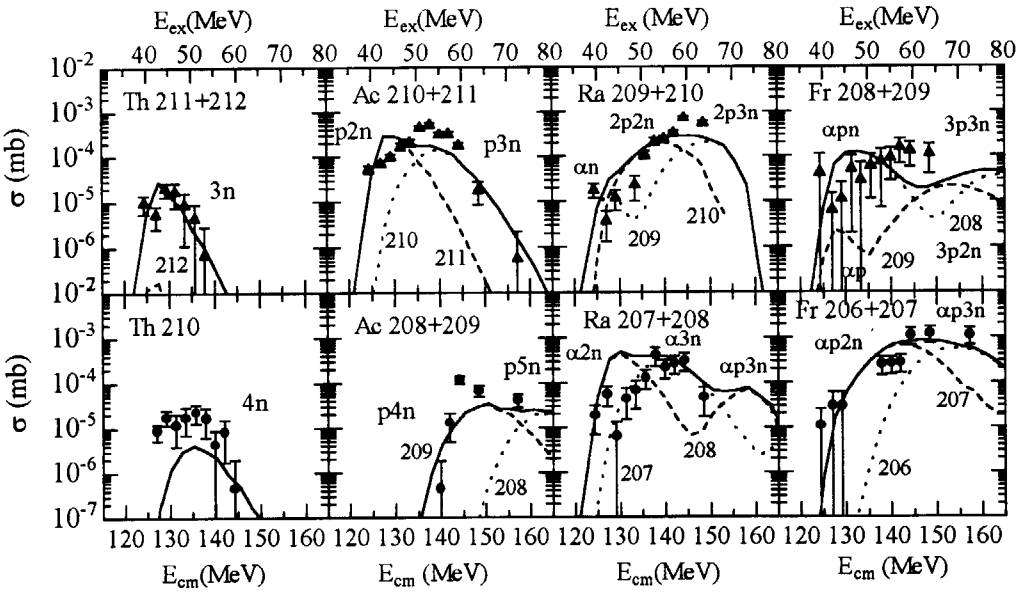

図２ $^{32}S+^{182}W$ 融合反応における蒸発残留核断面積（実線は計算値）。E_{ex} は励起エネルギー。

$^{32}S+^{182}W$ の場合は核の表面振動の励起を考慮すると融合断面積がさらに増大する（実線）。ここで示されているように、核の変形と表面振動状態の励起の効果はサブバリアー領域での核融合断面積（核分裂断面積で近似）の増大に寄与している。ただし、測定された核分裂断面積が複合核形成後の核分裂と複合核を形成しない準核分裂の両方を含んでいること注意しなければならない（実験的には区別できない）。複合核を形成しているかどうかは蒸発残留核（生成核）を測定して明らかになる。

CCDEF で計算された角運動量毎の融合断面積を HIVAP に入れて生成核の断面積を計算した。HIVAP 計算では、準位密度パラメータ a_n と a_f は文献[10, 11]にしたがって計算した。ただし、シェル減衰ファクターを 18 MeV を仮定した。また準位密度 $\rho(E^*)$ には回転や振動など集団運動の励起による準位密度増大も考慮した[12]。核分裂障壁 B_f は $B_f=B_{LD}-E_s$ で与えられる。ここで E_s はシェル補正エネルギーで B_{LD} は液滴モデル[13]で計算された。

（１）$^{32}S+^{182}W$ と $^{60,64}Ni+^{154}Sm$

図２に示されたように、$^{32}S+^{182}W$ 反応では生成核断面積の理論計算は測定データと良く一致している。バスバリアー（V_{Bass} = 135.9 MeV）以下のエネルギー領域で生成核が検出されており、原子核同士は完全に融合していることを示している。計算ではバスバリアー以下のエネルギーでの融合断面積は ^{182}W の変形、特に長軸側で ^{32}S が融合した場合に対応する。したがって、この測定データは ^{182}W 核の変形の効果がサブバリアーエネルギー領域で融合確率の増大に寄与している事を示している。

一方 $^{60}Ni+^{154}Sm$ 反応の場合（図３）、$E_{cm}\geqq 200$ MeV のエネルギー領域で計算値（破線）は測定データを再現しているが、バスバリアー（V_{Bass} = 192.8 MeV）近傍のエネルギー領域で期待される 2n、p2n、α、αn、α2n、αp、αpn チャンネルに対応する生成核の計算値が測定データより 100 - 1000 倍大きくなっている。統計モデルによるとこれらの生成核は主に ^{154}Sm の長軸側から ^{60}Ni が衝突してできる励起エネルギーの低い複合核の脱励起によって生成される。したがってこの測定結果は、このような低励起状態の複合核の形成が阻害されていることを示している。このことを裏付けるために、仮に衝突角度に依存したエキストラプッシュエネルギーを $\Delta E = 11(1-(\theta/90)^6)$ MeV と仮定して通常の障壁に加算したときの計算結果を

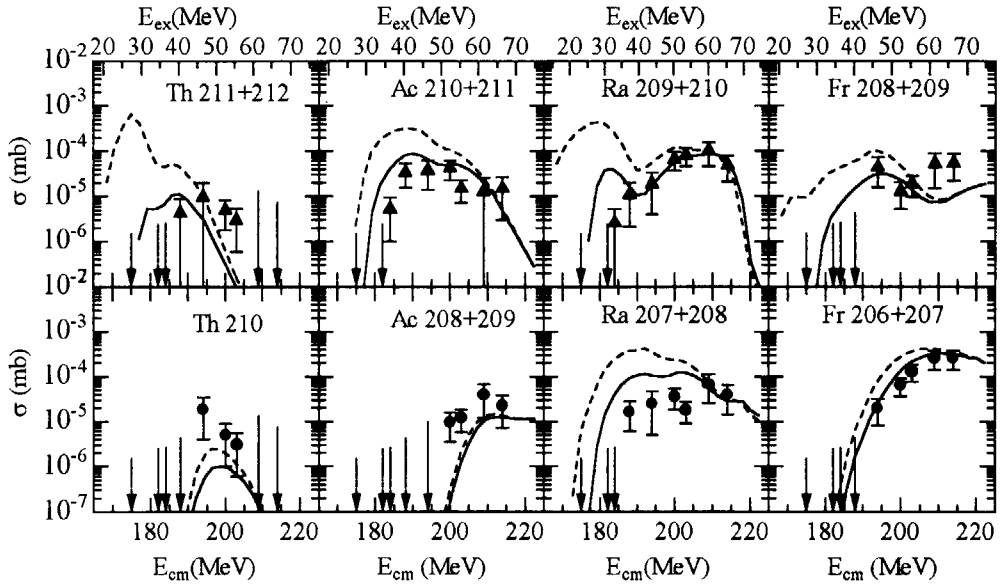

図３ ^{60}Ni＋^{154}Sm 融合反応における蒸発残留核断面積（矢印は測定値の上限値）。

図３の実線で示す。ここでθ＝０度は長軸方向、θ＝９０度は短軸方向である。計算結果は低エネルギー側で融合断面積が減少し測定データとよい一致を示している。ΔEのとり方はいろいろあり確定できないが、ここで言えることは長軸方向からの衝突で10 MeV以上のエキストラプッシュエネルギーが必要であり、短軸側からの衝突ではΔEは小さい（≅０）ということである。短軸側θ＝９０度でのクーロン障壁は198.8 MeVであり、E_{cm}≧200 MeVのエネルギー領域でデータが計算値と一致していることからも、短軸側での衝突では通常の融合障壁を越えれば融合することがわかる。

（２）　^{28}Si＋^{198}Pt と ^{76}Ge＋^{150}Nd 反応

図１に示したように、^{28}Si＋^{198}Pt 反応の融合断面積の計算値は核分裂断面積の測定値とほぼ一致して

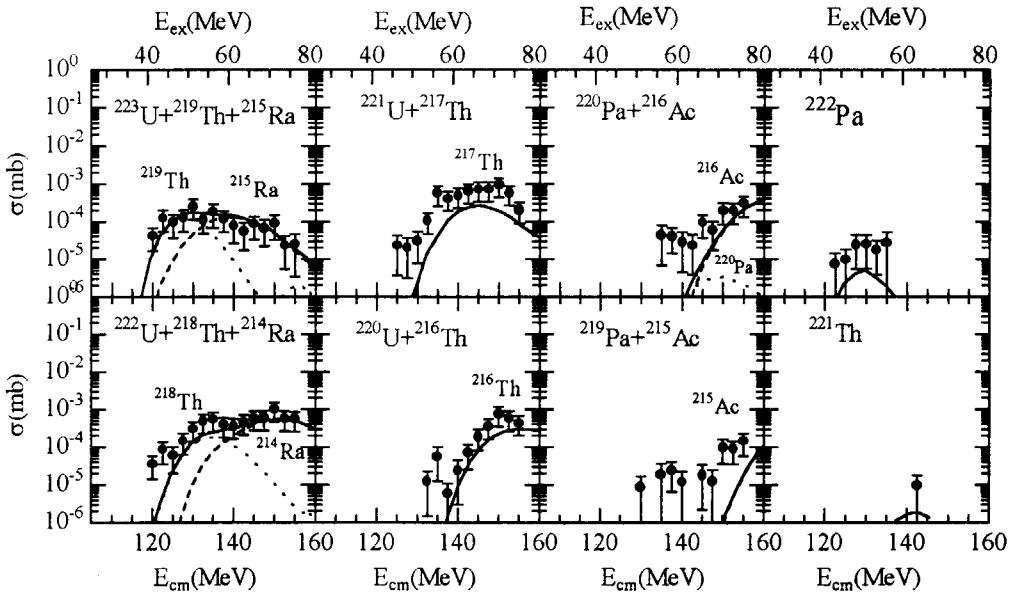

図４ ^{28}Si＋^{198}Pt 融合反応の蒸発残留核断面積（実線は計算値）。

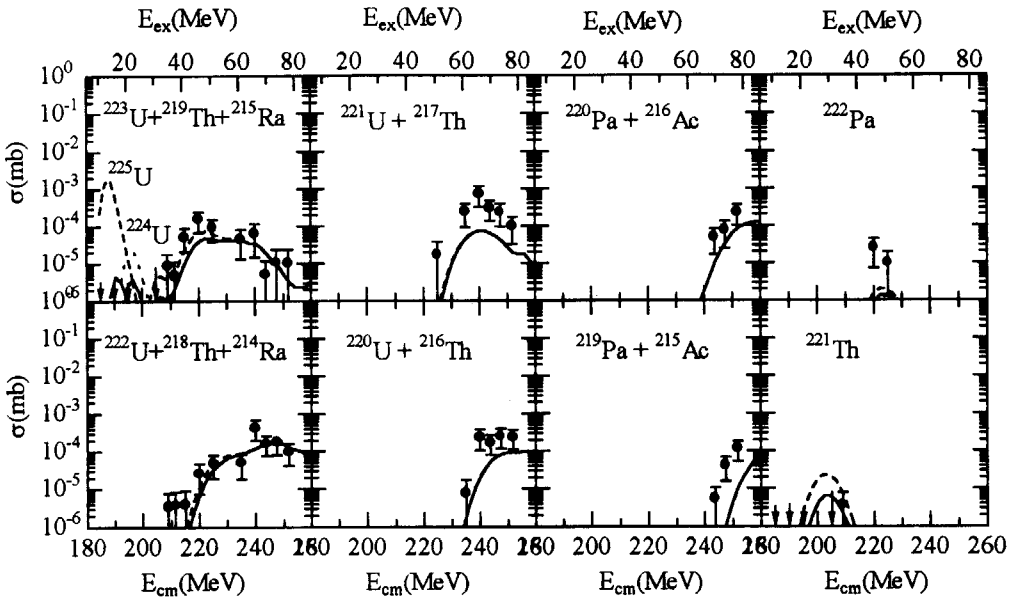

図５ $^{76}Ge+^{150}Nd$ 融合反応の蒸発残留核断面積（実線および破線は計算値）。

いる。すなわち ^{198}Pt の変形効果はサブバリアー領域で融合断面積に寄与している。さらに、生成核断面積の計算結果（図４の実線）は測定値とよい一致をしている。このことから、$^{28}Si+^{198}Pt$ 融合反応では $^{32}S+^{182}W$ 融合反応の場合と同様に、複合核を形成した完全融合反応であるといえる。

$^{76}Ge+^{150}Nd$ 反応の場合（図５）、$E_{cm} \geqq 210$ MeV では計算値（破線）は測定データと一致しているが、低エネルギー$E_{cm} \leqq 210$ MeV では $^{224,\ 225}U$ に対する計算値は測定上限値の 10 - 500 倍大きい。この低エネルギー領域は励起エネルギー20 MeV 程度に相当し、^{150}Nd の長軸側から ^{76}Ge が衝突した場合に対応する。ここでも $^{60}Ni+^{154}Sm$ の場合と同様に、融合確率が小さくなっている。仮に $\Delta E = 13\,(1-(\theta/90)^6)$ MeV のエキストラプッシュエネルギーを仮定すると実線で示したように、計算値は測定データと矛盾しなくなる。このことから ^{150}Nd の長軸側で ^{76}Ge が衝突する場合、13 MeV 程度のエキストラプッシュエネルギーが必要であるが、短軸側での衝突ではエキストラプッシュエネルギーは必要とせず、この位置でのクーロン障壁（214.4 MeV）を越えれば融合すると結論される。

２．まとめ

Z_1Z_2 が小さい反応系 $^{32}S+^{182}W$（$Z_1Z_2=1184$）や $^{28}Si+^{198}Pt$（$Z_1Z_2=1092$）の場合、入射核と変形した標的核との衝突角度に関係無く、複合核を形成した完全融合反応がおきる。$^{60,\ 64}Ni+^{154}Sm$ 反応($Z_1Z_2 = 1736$)や $^{76}Ge+^{150}Nd$ 反応（$Z_1Z_2 = 1920$）の場合のように Z_1Z_2 が大きくなると、変形核の長軸側での衝突では融合が著しく阻害されるが、短軸側での衝突では融合は阻害されない。このことは、２つの原子核が衝突したときの中心間距離 r/R_0（R_0：複合核の半径）と複合核のサドル点の位置を比較することで理解される。図６に示したように、$^{32}S+^{182}W$ 反応系や $^{28}Si+^{198}Pt$ 反応系では衝突角度によらず r/R_0 はサドル点の位置（太い実線[14]）より内部であるが、$^{60}Ni+^{154}Sm$ 反応系や $^{76}Ge+^{150}Nd$ 反応系では長軸側の衝突位置が複合核のサドル点より外に出ており、短軸側の衝突位置はサドル点の内部に位置する。したがって、短軸側での衝突では障壁を越えれば即融合するが、長軸側での衝突では融合障壁を越えてもさらにサドル点に達するためにエキストラプッシュエネルギーが必要になる。ここで得られた実験結果は、原子核同士の衝突した形状がよりコンパクトなものほど融合しやすいことを示しており、理論的に予想されている変形核同士の

密着融合の可能性を示唆するものである。

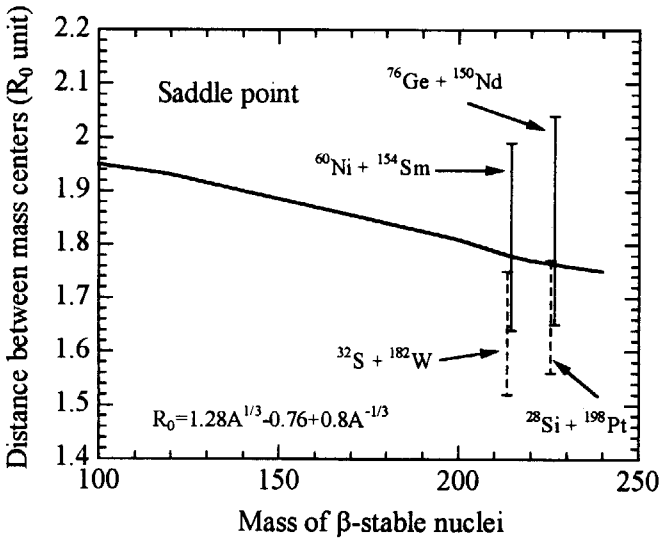

図6 複合核のサドル点と融合障壁の位置の関係。

参考文献

[1] Yu. Ts. Oganessian et al., Preprint JINR, E7-99-53.

[2] V. Ninov et al., Phys. Rev. Lett. 83 (1999) 1104.

[3] S. Hofmann, Rep. Prog. Phys. 61 (1998) 639.

[4] A. Iwamoto et al., Nucl. Phys. A 596 (1996) 329.

[5] R.G. Stokstad and E.E. Gross, Phys. Rev. C 23 (1981) 281.

[6] W. Reisdorf et al., Nucl. Phys. A 438 (1985) 212.

[7] H. Ikezoe et al., Nucl. Inst. And Meth. A 376 (1996) 420.

[8] J. Fernandez et al., Comp. Phys. Comm. 54 (1989)409.

[9] W. Reisdorf and M. Schädel, Z. Phys. A 343 (1992) 47.

[10] W. Reisdorf et al., Z. Phys. A 300 (1981) 227.

[11] A.V. Ignatyuk et al., Sov. J. Nucl. Phys. 21 (1975) 255.

[12] A.R. Junghans et al., Nucl. Phys. A 629 (1998) 635.

[13] S. Cohen et al., Ann. of Phys. 82 (1974) 557.

[14] G. Royer et al., Nucl. Phys. A 634 (1998) 267.

18. Deeply Bound Pionic States and Modifications of Hadrons

S. Hirenzaki
Department of Physics, Nara Women's University, Nara 630-8506, Japan

Abstract

We have studied the structure and formation of mesic atoms and mesic nuclei theoretically. The latest results on the deeply bound pionic atoms, the kaonic atoms and the sigma states are reported.

1 Deeply Bound Pionic Atoms

Pionic atoms are ones of the most interesting objects to study the behavior of the real pion in the nuclear medium. Especially, deeply bound pionic atoms, which can not be observed by the pionic x-ray spectroscopy, were expected to provide precise information on pion-nucleus interaction and/or pion effective mass in the nucleus. Theoretical investigations indicated that the deeply bound states were expected to be quasi-stable due to the repulsive s-wave interaction and to be observed by suitable reactions [1, 2]. Guided by the theoretical prediction, the (d,^{3}He) reaction on the ^{208}Pb target was performed at GSI and the pionic 2p state in Pb was observed successfully [3, 4]

Since the deepest 1s state was observed only as a skewed shape of the dominant peak due to the pionic 2p state formation, we tried to find better candidates theoretically to obtain clear signals of the pionic 1s state formation. We have concluded that the 1s state could be observed as a distinct peak structure in the ^{206}Pb(d,^{3}He) reaction because of the absence of the contributions from the $p_{1/2}$ neutron hole [5]. Very recently, the 1s state was observed experimentally, and the preliminary result was reported in PANIC99 [6].

The observed peak structure of 1s pionic state in the ^{206}Pb(d,^{3}He) reaction, however, comprises 2 subcomponents [5], namely $[(1s)_\pi \otimes (p_{3/2})_n^{-1}]$ and $[(1s)_\pi \otimes (f_{5/2})_n^{-1}]$. Uncertainties of the relative strength of these contributions will cause the systematic errors of the deduced binding energy and width of the 1s state.

In order to observe the deeply bound pionic 1s state as a clear peak which comprises only one component, we investigated theoretically the (d,^{3}He) reaction on the nucleus with $s_{1/2}$ neutron state in the valence orbit, such as Sn, Cd, Xe isotopes, at T_d=500 MeV, where the momentum transfer is almost zero [7]. We found that the $[(1s)_\pi \otimes (s_{1/2})_n^{-1}]$ configuration provides a dominant contribution and makes the largest peak in the spectrum. We expect to obtain the information of the deeply bound 1s pionic state very precisely from the ^{116}Sn(d,^{3}He) reaction at T_d=500 MeV. It is possible to perform this experiment at GSI [8].

2 Kaonic Atoms in a Chiral Unitary Model

We study kaonic atoms over the periodic table using a kaon selfenergy in the nuclear medium derived using a SU(3) chiral unitary model [9]. This model is quite successful in reproducing the scattering amplitude of meson-meson and the strangeness S=-1 meson-baryon reactions. In particular the properties of the $\Lambda(1405)$ resonance are well reproduced [10]. In the nuclear medium, the properties of this resonance are appreciably modified, and consequently leads to an attractive kaon nucleus selfenergy for densities higher than $\rho_0/10$. With this interaction we are able to reproduce shifts and widths of kaonic atoms over the periodic table [11].

We also investigate the region of deeply bound kaonic nuclear states which appear with very large widths in medium and heavy nuclei. At present it is known that a few kinds of kaon-nucleus optical potentials can reproduce the kaonic atom data well. Thus, it is desirable to observe the deeper bound states for getting further experimental information. Some of the deep atomic states, still unobserved, appear with narrower widths than the level distance, which makes them eligible for experimental observation. To such aim we make some estimates of the rates of formation in the (K^-, γ) reaction [11].

3 Mesic nuclei

Mesic nuclei, which are meson-nucleus bound states only with the strong interaction, will provide important information on meson properties in the nuclear medium. These properties have some relations to the chiral symmetry restoration of QCD vacuum in the nuclear medium. In this context, an experiment to search for bound nuclear states of η and ω mesons with the (d,^{3}He) transfer reaction was proposed based on the theoretical predictions [13].

The partial restoration of chiral symmetry implies (1) partial degeneracy of the scalar-isoscalar particle (σ meson) with the pion, and (2) decrease of the decay width of $\sigma \rightarrow \pi\pi$ due to the phase space suppression caused by (1). Thus, we may have a chance to observe the σ meson as a sharp resonance in the nuclear medium, thereby get an evidence of partial chiral restoration in nuclei [14].

We consider the σ meson embedded in nuclear matter based on the SU(2) linear σ-model and calculate the one-loop corrections to the self-energy for σ [15], which is used to investigate the σ eigenstates in finite nuclei. We find that there exist bound states of σ in nuclei in certain parameter range since the real part of the self-energy provides the strong attractive potential. Strikingly, even the eigenstates with the total energy below the 2π threshold may be formed in which the the σ cannot decay into $\pi\pi$ [16].

4 Summary

We have studied structure and formation of the mesic atoms and mesic nuclei, which are very interesting objects to observe meson properties at finite nuclear

densities. Recent discovery of the deeply bound pionic atoms proved that it is really possible to extend our research to deeper bound states, where we can see the medium effects clearly. In this paper, we have summarized current activities of meson-nucleus bound states research.

References

[1] H. Toki and T. Yamazaki, Phys. Lett. B213, 219 (1988).

[2] H. Toki, S. Hirenzaki, T. Yamazaki, and R. S. Hayano, Nucl. Phys. A501, 653 (1989).

[3] S. Hirenzaki, H. Toki, and T. Yamazaki, Phys. Rev. C44, 2472 (1991).

[4] T. Yamazaki *et al.*, Z. Phys. A355, 219 (1996).

[5] S. Hirenzaki and H. Toki, Phys. Rev. C55, 2719 (1997).

[6] A. Gillitzer *et al.*, Proceedings of the Particle and Nuclei International Conference (PANIC99), to be appear Nucl. Phys. A.

[7] Y. Umemoto, S. Hirenzaki, H. Toki, and K. Kume, in preparation.

[8] A. Gillitzer, R. S. Hayano, P. Kienle, T. Yamazaki, private communications.

[9] A. Ramos and E. Oset, nucl-th/9902036.

[10] E. Oset and A. Ramos, Nucl. Phys. A635, 99 (1998).

[11] S. Hirenzaki, Y. Okumura, H. Toki, E. Oset, and A. Ramos, in preparation.

[12] E. Friedman, A. Gal, and C. J. Batty, Nucl. Phys. A579, 518 (1994).

[13] R. S. Hayano, S. Hirenzaki, and A. Gillitzer, Euro. Phys. J. A, accepted.

[14] T. Hatsuda and T. Kunihiro, Phys. Rep. 247, 221 (1994).

[15] T. Hatsuda, T. Kunihiro, and H. Shimizu, Phys. Rev. Lett. 82, 2840 (1999).

[16] T. Hatsuda, S. Hirenzaki, T. Kunihiro, and H. Nagahiro, in preparation.

19. (K^-, N) 反応による K 中間子核の生成
Kaonic nuclei excited by the (K^-, N) reaction

岸本忠史
Tadafumi Kishimoto
Dept. of Phys., Osaka University, Toyonaka, Osaka, 560-0043, Japan

9月28日

要旨

We show that kaonic nuclei can be produced by the (K^-, p) and (K^-, n) reactions. The reactions are shown to have cross sections experimentally measurable. The observation of the kaonic nuclei gives a kaon-nucleus potential which answers the question on the existence of kaon condensation in dense nuclear matter especially neutron stars.

The kaon-nucleon interaction at low energy region is particularly important nowadays because of the current interrest in the dense nuclear matter in neutron stars where so-called kaon condensed state may be achieved by a strong attractive interaction [1, 2]. The existence of the kaon condensed state softens the equation of state (EOS) of nuclear matter in the neutron stars and reduces their calculated maximum mass above which the neutron stars become black holes. The observed mass distribution of the neutron stars agrees with the calculation with this softening [3]. The introduction of strange hyperons in the EOS gives a similar softening. Strangeness is essential in both cases although quantitative understanding of the EOS requires a knowledge of both the kaon-nucleon- and hyperon-nucleon interactions at high density [4]. The kaon-nucleon interaction, in particular, is known quite poorly experimentally.

Recently, effective kaon mass in dense nuclear matter has been derived by the Chiral SU(3) effective Lagrangian including $\bar{K}N$, $\pi\Sigma$, $\pi\Lambda$ systems[5]. Such a theoretical model reproduces well the $\Lambda(1405)$ as a $\bar{K}N$ bound state due to the strong $\bar{K}N$ attractive interaction [5, 6]. The $\bar{K}N$ interaction makes the K^- feel a strong attractive potential in nuclei which consequently leads to the existence of deeply bound kaonic nuclei. The $\Lambda(1405)$, however, can also be interpreted as a three-quark state with $\ell = 1$ excitation. In this case no attractive $\bar{K}N$ interaction is relevant and the deeply bound kaonic nuclei don't necessary exist.

Experimental data of K^- optical potential mostly come from kaonic atoms. The shifts and widths of atomic levels affected by the strong interaction were reproduced by introducing an appropriate optical potential in addition to the Coulomb interaction. Recent extensive analysis of kaonic X-ray data concludes that the potential is strongly attractive [7]. The derived depth is around -200 MeV which opens a possibility of kaon condensation at around three times normal nuclear density. Derivation of the optical potential from the kaonic atom data is, however, subtle since the atomic state is sensitive only to the phase shift of K^- wave function at the nuclear surface. The phase shift alone cannot determine the depth of the potential since the K^- wave function has an ambiguity in number of nodes in the nucleus especially when the potential depth

is quite deep. The strong imaginary part of the potential further obscures the nodes. Earlier studies with a different treatment of the nuclear surface gave much shallower potentials of -80 $\sim$ 90 MeV [7] which tend to exclude the kaon condensation in the neutron stars.

Heavy ion reactions have been studied to derive the K^- optical potential [8]. Enhanced K^- production in the reactions suggests a strong attractive interaction although quantitative argument requires understanding of details of the reaction mechanism [10].

The $\bar{K}N$ interaction has been derived from kaon scattering experiments. However, the available low-energy data are insufficient for unique multichannel analysis and the existence of $\Lambda(1405)$ makes the extrapolation of the amplitude below the threshold complicated[9]. Recent theoretical calculations on the kaon interaction in nuclei predict an attractive interaction although they are still controversial quantitatively and existence of kaon condensation in neutron stars is as yet inconclusive [11, 12].

If $\bar{K}$-nuclear potential is as attractive as derived from the kaonic atom stuides suggest [7], then deeply-bound kaonic nuclei should exist. The observation of kaonic nuclei gives directly the K^- optical potential and gives decisive information on the existence of kaon condensation in neutron stars. We show the general properties of the kaonic nuclei and that the (K^-, N) reaction can excite them with cross section experimentally measurable.

Energies and widths of kaonic nuclei are calculated with the potential given by the kaonic atom data. For the analysis of mesonic atoms the Klein-Gordon equation is usually used [7]. Here we use the Schrödinger equation with harmonic oscillator potential. It is a crude approximation although it is good enough for the present purpose. We are interested in gross structure of levels and an order-of-magnitude estimate of the cross section for the deeply bound state. For the moment we take the potential depth -200 MeV given by kaonic atom. It is roughly four times deeper than that for nucleon and the kaon mass is about half of that of a nucleon. Thus the major shell spacing ($\hbar\omega_K$) is $\sqrt{8}$ times the $40\mathrm{A}^{-1/3}$ frequently used for nucleon. Since the kaon has no spin, no spin dependent splitting has to be considered.

The $\hbar\omega_K$ is roughly 40 MeV, for instance, for the kaonic ${}^{28}_{K}\mathrm{Si}$ nucleus. The $1s$ state appears at around -140 ($\frac{3}{2}\hbar\omega_K - 200$) MeV bound, which is the deepest bound state ever observed in nuclear physics. If the potential shape is closer to the square-well it appears deeper. In order to observe the state its width has to be reasonably narrow. The width is given by the imaginary part of the potential, which decreases for the deeply bound state and is around 10 MeV [5, 7]. The narrow width is understandable since dominant conversion channels like $KN \to \pi\Sigma$ or $KN \to \pi\Lambda$ are energetically almost closed for such a deeply-bound state. Kaon absorption by two nucleons ($KNN \to YN$) gives little width since two nucleons have to participate to the reaction. Even though the width is twice wider the $1s$ state should be seen well separated since the next excited state ($1p$) is expected to appear 40 MeV higher.

The (K^-, N) reaction where a nucleon (N) is either a proton or a neutron is shown schematically in figure 1. The nucleon is knocked out in the forward direction leaving a kaon scattered backward in the vertex where the $K + N \to K + N$ takes place. This reaction can thus provide a virtual K^- or $\bar{K}^0$ beam which excites kaonic nuclei. This feature is quite different from other strangeness transfer reactions like (K^-, π), $(\pi^\pm, K^+)$ and (γ, K^+) extensively used so far. They primarily produce hyperons and thus are sensitive to states mostly composed of a hyperon and a nucleus.

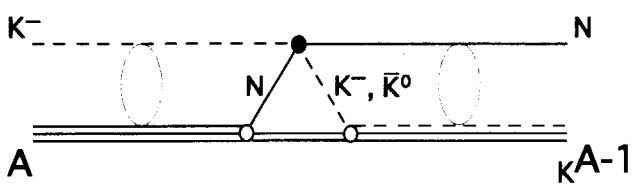

Figure 1
Diagram for the formation of kaonic nuclei via the (K^-, N) reaction. The kaon, the nucleon, and the nucleus are denoted by the dashed, thin solid and multiple lines, respectively. The kaonic nucleus is denoted by the multiple lines with the dashed line. The filled circle is the $KN \to KN$ amplitude while the open circles are the nuclear vertices. The bubbles represent distortion.

The momentum transfer, which characterizes the reaction, is shown in figure 2. It depends on the binding energy of a kaon. We are interested in states well bound in a nucleus ($BE = 100 \sim 150$ MeV). The momentum transfer for the states is fairly large ($q = 0.3 \sim 0.4$ GeV/c) and depends little on the incident kaon momentum for $P_K = 0.5 \sim 1.5$ GeV/c, where intense kaon beams are available. Therefore one can choose the incident momentum for the convenience of an experiment. It is a little beyond the Fermi momentum and the reaction has characteristics similar to the (π^+, K^+) reaction for hypernuclear production where so-called stretched states are preferentially excited [13].

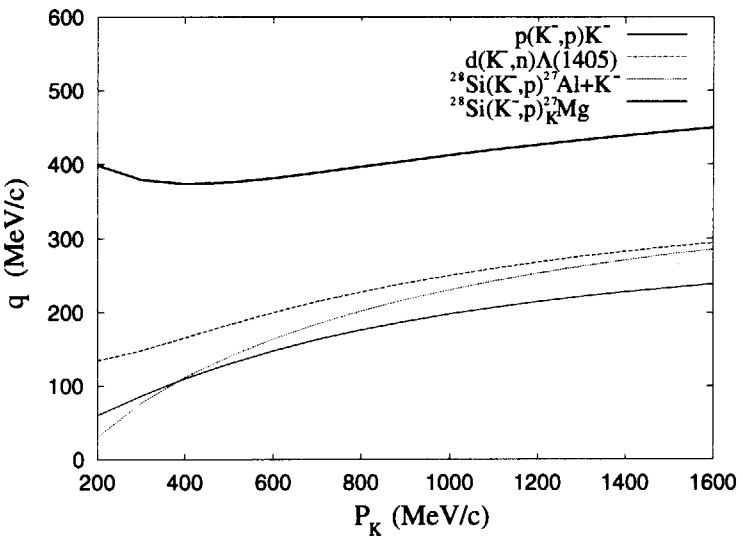

Figure 2
The momentum transfer of the (K^-, N) reaction at 0 degrees is shown for four reactions. Here binding energy of kaonic nucleus ${}^{27}_{K}$Mg is taken to be -150 MeV.

Recently deeply bound π^- atoms were observed by the $(d, {}^3\mathrm{He})$ reaction [14]. A small momentum transfer ($\sim 60 MeV/c$) was vital to excite the atomic states which were typically characterized by the size of the atomic orbits. If one wishes to excite kaonic atoms, a momentum transfer less than 100 MeV/c is desirable. It is achieved by kaon beams less than 0.4 GeV/c where available beam intensity is very small. The repulsive nature of the π-nucleus interaction allows no nuclear state although the strong attractive $\bar{K}$-nucleus potential makes kaonic nuclei exist. The (K^-, N) reaction can excite the deeply bound kaonic nuclei with large cross section in spite of the large momentum transfer of the reaction. For the excitation of nuclear states the momentum transfer is typically characterized by the Fermi momentum.

The (K^-, N) reaction on deuteron is the simplest reaction by which one can study the $\bar{K}N$

component of excited hyperons. The $d(K^-,p)$ reaction excites K^-n states which can only have $I=1$. On the other hand $d(K^-,n)$ reaction excites a K^-p state which can have either $I=1$ or $I=0$. Cross sections to the excited hyperons depend on their $\bar{K}N$ component. For instance, the well known $\Lambda(1405$ MeV) should be abundantly excited by the (K^-,n) reaction if it is a $\bar{K}N$ bound state with $I=0$ as usually believed. The $d(K^-,p)$ reaction, in particular, gives information on the K^-n interaction below the threshold, which plays decisive role on the kaon condensation in the neutron stars.

We adopt here the distorted wave impulse approximation (DWIA) to evaluate the cross section. The DWIA calculation requires: (a) distorted waves for entrance and exit channels, (b) two body transition amplitudes for the elementary (K^-,N) process, and (c) a form factor given by initial nuclear and kaonic-nuclear wave functions. Relevant formulas for the calculation can be found elsewhere [13].

The differential cross section in the laboratory system for the formation of kaonic nucleus is given by

$$\frac{d\sigma}{d\Omega} = \left(\frac{d\sigma}{d\Omega}\right)_{L,0^\circ}^{K^-N\to NK^-} N_{eff}. \tag{1}$$

It is given by the two body laboratory cross section multiplied by the so-called effective nucleon number (N_{eff}).

We first use the plane wave approximation to evaluate N_{eff}^{pw}. At 0 degrees, where only non-spin flip amplitude is relevant, N_{eff}^{pw} is given by

$$N_{eff}^{pw} = (2J+1)(2j_N+1)(2\ell_K+1)\begin{pmatrix} \ell_K & j_N & J \\ 0 & -\frac{1}{2} & \frac{1}{2} \end{pmatrix}^2 F(q). \tag{2}$$

In this equation we assumed that a nucleon in a j_N orbit is knocked out and a kaon enters in an ℓ_K orbit making transition from 0^+ closed shell target to a spin J state. Here the form factor $F(q)$ is given by the initial nucleon and final kaon wave functions as

$$F(q) = \left(\int r^2 dr R_K(r) R_N(r) j_L(qr)\right)^2, \tag{3}$$

where $L = J \pm \frac{1}{2}$ is the transferred angular momentum.

For an oscillator potential of radius parameter b, the radial wave function is

$$R_\ell(r) = c_\ell (r/b)^\ell e^{-r^2/2b^2} \tag{4}$$

for nodeless states, where $c_\ell = [2^{l+2}/b^3\sqrt{\pi}(2l+1)!!]^{1/2}$. In the present case it is enough to consider natural parity stretched states with $L = \ell_N + \ell_K$ since the transferred momentum q is larger than the Fermi momentum. The form factor (Eq. 4) is well known for the harmonic oscillator wave function [13] as

$$F(q) = \frac{(2Z)^L e^{-Z}}{[(2L+1)!!]^2} \frac{[\Gamma(L+3/2)]^2}{\Gamma(\ell_K+3/2)\Gamma(\ell_N+3/2)} \tag{5}$$

with $Z = (bq)^2/2$, where the radius parameter $b = \frac{m\omega}{\hbar}$ has to be replaced by

$$\frac{2}{b^2} = \frac{1}{b_N^2} + \frac{1}{b_K^2} \tag{6}$$

to account for the different radius parameters for the nucleon (b_N) and the kaon (b_K) where $1/b_K^2 = \sqrt{8}/b_N^2$. N_{eff}^{pw} is further reduced by the distortion of incoming and outgoing waves as

$$N_{eff} = N_{eff}^{pw} D_{eik} \ . \tag{7}$$

The distortion D_{eik} is estimated by the eikonal absorption where the imaginary parts of the K^- and proton optical potentials are given by their total cross sections with nucleons. At P_K= 1 GeV/c, total cross sections of K^--nucleon and p-nucleon are almost the same and we take both to be 40 mb. The small radius parameter b indicates larger cross sections through the high momentum component; we thus evaluated N_{eff} for $b_K = b_N$ also as the smallest value.

The cross section of the elementary reaction was given by the phase shift analysis of available data[15]. Here we need to consider only the non-spin flip amplitude (f) as explained above. Since the kaon and nucleon are isospin $\frac{1}{2}$ particles there are I=0 (f^0) and I=1 (f^1) amplitudes. The amplitudes for elastic and charge exchange scattering are represented by appropriate linear combinations of the isospin amplitudes as

$$f_{K^-n\to K^-n} = f^1 \ , \tag{8}$$

$$f_{K^-p\to K^-p} = \frac{1}{2}(f^1 + f^0) \ , \tag{9}$$

$$f_{K^-p\to \bar{K}^0 n} = \frac{1}{2}(f^1 - f^0) \ . \tag{10}$$

The c.m. (center-of-mass) differential cross section of the three reactions at 180° are shown in figure 3 as a function of incident kaon momentum. The cross sections depend on the incident momentum. For instance, the $K^-p \to K^-p$ reaction has a peak at around 1 GeV/c. We thus take 1 GeV/c for the incident kaon momentum. Since the target nucleon is moving in a nucleus, Fermi averaging has to be made for the two body cross section which smears the fine momentum dependence. The c.m. cross section is reduced by 20 to 30 % depending on models for this averaging. We take ~1.3 mb/sr as the c.m. cross section at 1 GeV/c.

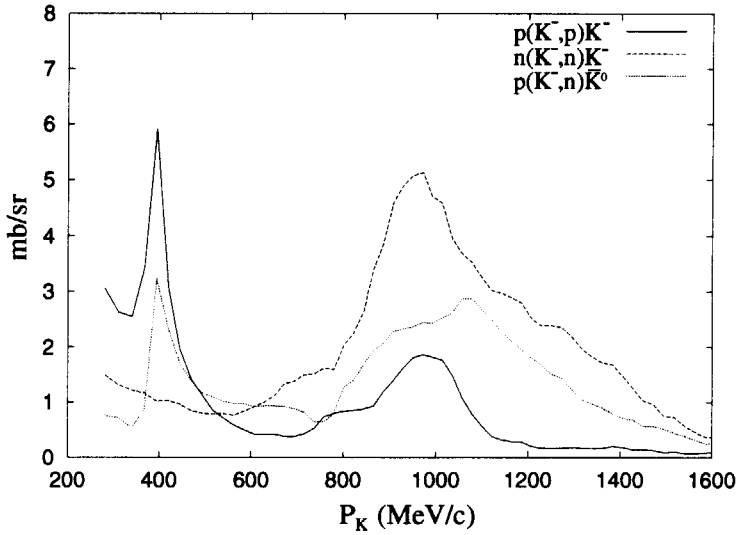

Figure 3
The c.m. differential cross sections of the three reactions are shown as a function of incident kaon lab momentum.

Here we consider I=0 symmetric nuclei as targets. The (K^-, p) reaction produces only an I=1 state; on the other hand the (K^-, n) reaction can produce both I=0 and 1 states. The $\bar{K}N$ system is strongly attractive in the I=0 channel though not so much in the I=1 channel. The

kaon-nucleus potential is an average of both channels and thus depends little on the total isospin of kaonic nuclei. Consequently we expect that the I=0 state produced by the (K^-, n) reaction appears at nearly the same excitation energy. The elementary cross section for the (K^-, n) reaction in eq (1) becomes the sum of the $K^-n \to K^-n$ and $K^-p \to \bar{K}^0n$ cross sections. The incoherent sum of the two cross sections may not be inappropriate for the evaluation since the K^- and $\bar{K}^0$ mass difference is considered to be large on a nuclear physics scale.

The cross section for the kaonic nuclear $1s$ states are shown in table 1. The (π^+, K^+) reaction for the hypernuclear production shows distinct peaks corresponding to series of major shell orbits especially for target nuclei with $j_n = \ell_n + 1/2$ orbit closed. We thus take ^{12}C and ^{28}Si for the present study.

nucleus	N_{eff}^{pw}	D_{eik}	$d\sigma/d\Omega$ μb/sr
^{12}C	0.055~0.26	0.25	100~490
^{28}Si	0.029~0.15	0.16	35~180

Table 1
Calculated laboratory differential cross sections of the $1s$ states excited by the (K^-, p) reactions at P_K=1 GeV/c for the ^{12}C and ^{28}Si targets. Range of values corresponds to the b parameter (see text)

The calculated cross sections turn out to be quite large which can compensate for a low intensity kaon beam. The large cross section comes from the large cross section of the elastic $K + N \to K + N$ reaction and from the transformation of c.m. system to laboratory system.

Feasibility of the experiment depends on backgrounds. Dominant backgrounds are nucleons from knock-out reactions, where kaons are scattered backward by the quasifree process. Since the nucleons associated with the deeply-bound kaonic nuclei are much more energetic, the knock-out reactions will not be a problem.

Kaon absorption by two nucleons in nuclei can generate energetic nucleons. The process has to involve another nucleon in addition to the (K^-, N) reaction. Thus one expects the process gives smaller cross section than that of the (K^-, N) reaction. The process can be interpreted as a spreading width of the kaonic nuclei.

A Λ produced in the forward direction by the quasifree (K^-, π) reaction provides an energetic nucleon. It would not be a serious background since no peak structure is expected.

From the experimental point of view energetic protons can be produced by knock-out reaction by pions which are contaminated in the kaon beam. This process however can be removed by the careful tuning of experimental condition.

It is shown that the (K^-, p) and (K^-, n) reactions can be used for the study of the kaonic nuclei. Study of the reaction requires intense low energy kaon beam for which the alternating-gradient synchrotron (AGS) of BNL and probably the proton synchrotron (PS) of KEK are particularly suitable. The beam momentum can be chosen by considering the cross section, beam intensity and momentum resolution of spectrometer. There are beam lines which provide K^- beam 0.5~2 GeV/c at BNL and KEK. The relatively broad width (~10 MeV) and simple structure of the state need spectrometers of only modest momentum resolution but wide momentum acceptance.

We demonstrated that the (K^-, p) and (K^-, n) reaction can be used to obtain direct information on the $\bar{K}N$ interaction in nuclear matter. The calculation employed here is rather crude although it is based on well-known general concepts in nuclear physics.

The anther is grateful to discussions with Professors A. Gal, Y. Akaishi, T. Tatsumi, and H. Toki. The anther thanks Dr. R. E. Chrien for careful reading of this manuscript.

参考文献

[1] D. B. Kaplan and A. E. Nelson, Phys. Lett., B175 (1986) 57

[2] G. E. Brown, Nucl Phys A574 (1994)217, G. E. Brown, M. Rho, Phys. Rep. 269 (1996) 333, C. H. Lee, Phys. Rep. 275 (1996) 255

[3] M. Prakash and J.M. Lattimer, Nucl.Phys. A639 (1998)433

[4] P. J. Ellis, R. Knorren, M. Prakash. Phys.Lett.B349 (1995)11

[5] T. Waas, N. Kaiser and W. Weise, Phys. Lett. B379 (1996) 34

[6] P. B. Siegel and W. Weise, Phys. Rev. C, 38 (1998)221

[7] C.J. Batty, E. Friedman, A. Gal. Physics Report 287 (1997) 385

[8] R. Barth at al., Phys. Rev. Lett. 78 4027 (1997)

[9] A. D. Martin, Nucl. Phys. B179 (1981) 33

[10] G.Q. Li, C.H. Lee, and G.E. Brown, Phys.Rev.Lett.79 5214 (1997); G.Q. Li, G.E. Brown, C.H. Lee, Phys.Rev.Lett.81 2177 (1998)

[11] A. Ramos and E. Oset, Nucl. Phys. A in press, XV Int. Conf. on "Particles and Nuclei" Uppsala, Sweden, 1999

[12] M. Lutz, Phys. Lett. B 426, 12 (1998)

[13] C. B. Dover, L. Ludeking and G. E. Walker, Phys. Rev. C22 (1980) 2073

[14] T. Yamazaki, et al., Z Phys. A 355, (1996) 219

[15] Gopal et al., Nucl. Phys. B119 (1977) 362

20. Charmed mesons in hadronic matter

Arata Hayashigaki †
Yukawa Institute for Theoretical Physics, Kyoto University, Kyoto 606-8502, Japan

Abstract:

For the "anomalous" J/ψ suppression in *Pb-Pb* collision announced by NA50 Collaboration I propose new mechanism accessible to the novel behavior of the data. The point of new idea is to focus on in-medium effects on the masses of mesons containing charmed quarks. In QCD sum rule analysis, I find that the D-meson involving one charmed quark feels more attractive force from the surrounding nucleons than the charmonium composed of two charmed quarks. As a result, it will appear that as the nucleon density increases, $D\bar{D}$ threshold in turn falls below higher-lying charmonium states (ψ', χ_c) which have the energy levels below the threshold in vacuum. Finally, also for the low-lying J/ψ state, a larger decay channel to the threshold could be opened up. Thus the mechanism can qualitatively explain some features of the anomalous J/ψ suppression without an advent of deconfinement phase.

Introduction

The NA50 Collaboration (CERN-SPS) has reported a strong suppression of J/ψ and ψ' production in *Pb-Pb* collision at 158 GeV per nucleon [1]. The suppression of J/ψ production (relative to Drell-Yan process) shows large discrepancy from conventional nuclear absorption models [2] exhibited by measurements from *p-A* up to *S-U* collisions. In particular, it seems to expose some characteristic suppression forms, which might be a first indication for color deconfinement [3]. The suppression form of $J/\psi(1S)$ shows the discontinuity around two points of the effective length L of nuclear matter over which the produced $c\bar{c}$ traverses. In contrast, the first excited state $\psi'(2S)$ seems to show only one discontinuity at smaller E_T value observed in the *S-U* collision. As is well known, the conventional attempts quantitatively encounter considerable difficulties to explain such peculiar behaviors. That is, such models allow only a gradual change from slight suppression in the *p-A* to strong suppression in the *Pb-Pb* collisions. On the other hand, once the local energy density exceeds certain threshold value in the heavy-ion collisions and an onset of deconfinement is switched on, the nature of deconfinement seems to give more satisfactory explanation for the anomalous data [4, 5]. This is based on the idea that if the deconfinement transition were of first order, the onset of a suppression will become discontinuous. But I feel that the suppression of χ_c-feeding effect introduced to explain double threshold structure of the data is not obvious in the plasma-based model, because the hadronization of $c\bar{c}$ system like the χ_c will not occur at a small central region of the collision where plasma bubbles are produced according to long formation time of $c\bar{c}$ resonances. Are such strong suppression phenomena peculiar to the phase transition? I suggest such phenomena could occur even in nuclear matter. Indeed, the formation time of charmonium is so long that final state interaction of the charmonium with nucleons or comovers will occur at the peripheral region of a nucleus (about a few times as large as normal matter density), although its magnitude

†E-mail: arata@yukawa.kyoto-u.ac.jp

of interaction depends on transverse momentum of the charmonium produced. Motivated by this point, it is reasonable as a first step to study matter effect at such a finite density. It was found in Ref.[6] that the light quark (u, d) condensates may be substantially reduced in medium and as a result light hadron masses would also decrease. On the other hand, if heavier quarks (s, c) feel so weaker interaction than the light quarks, the masses of mesons composed of heavy-light and heavy-heavy quarks may be expected to scale differently with density. In particular, the difference becomes larger with increasing the density. If it is the case of $|\delta m_\psi| < |\delta m_D|$, charmonia below the $D\bar{D}$ threshold in vacuum may rise above the threshold in matter. Therefore, the level crossing between the charmonium and the $D\bar{D}$ threshold can cause the abrupt decrease of J/ψ survival probability due to the decay to $D\bar{D}$ state. I advocate new mechanism to explain drastic change of the suppression which has ever been ruled out in normal nuclear absorption: $J/\psi + N \to D + \bar{D} + X$. This paper is composed as follows: First, in QCD sum rule analysis I make a detailed study of the mass modification for the J/ψ at finite density and second, a rough estimate of that for D-meson in terms of the same approach. In summary, I discuss the J/ψ suppression through these results.

In-medium effect for J/ψ

I calculate the medium modification of J/ψ on the basis of the relation between J/ψ-N scattering length and the mass shift [7, 8] through extending vacuum QCD sum rules (QSR's) to finite density [†]. First by applying QSR to J/ψ-N forward scattering amplitude, I evaluate the scattering length. The superposition of such elementary J/ψ-N elastic scattering at low energy affects the effective mass of J/ψ in nuclear matter. When one works in the dilute nucleon gas, one finds that the mass shift is linearly dependent on the density and the scattering length in the framework of QSR. In this approach with the Fermi gas model, in-medium correlation function (density ρ_N) is divided into vacuum part and static one-nucleon part near the normal matter density by applying OPE to the correlators at deep Euclidean region. That is, in the framework of QSR, in-medium correlation function can be approximated reasonably well to the linear density of nuclear matter that all nucleons are at rest:

$$\Pi^{\rm NM}_{\mu\nu}(q) \;=\; i\int d^4x e^{iq\cdot x}\langle {\rm T}J_\mu(x)J^\dagger_\nu(0)\rangle_{\rho_N} \simeq \Pi^0_{\mu\nu}(q) + \frac{\rho_N}{2M_N}T_{\mu\nu}(q), \qquad (1)$$

where $q^\mu = (\omega, \boldsymbol{q})$ is the 4-momentum of J/ψ ($J_\mu = \bar{c}\gamma_\mu c$). The one-nucleon part corresponds to the forward J/ψ-N scattering amplitude with the spin of nucleon averaged:

$$T_{\mu\nu}(\omega, \boldsymbol{q}) = i\int d^4x e^{iq\cdot x}\langle N(ps)|{\rm T}J_\mu(x)J^\dagger_\nu(0)|N(ps)\rangle, \qquad (2)$$

where $|N(ps)\rangle$ denotes the nucleon state with $p = (M_N, \boldsymbol{p} = \boldsymbol{0})$ and spin s normalized covariantly as $\langle N(\boldsymbol{p})|N(\boldsymbol{p}')\rangle = (2\pi)^3 2p^0\delta^3(\boldsymbol{p} - \boldsymbol{p}')$. By applying QSR to $T_{\mu\nu}$ directly, I can relate the scattering length extracted from the QSR for $T_{\mu\nu}$ with the mass shift, $\delta m_{J/\psi} = 2\pi\frac{M_N + m_{J/\psi}}{M_N m_{J/\psi}}\rho_N a_{J/\psi}$. For applying the dispersion relation to $T(\omega, \boldsymbol{q}) = T^\mu_\mu/(-3)$, I parametrize the spectral function such as $\rho(u, \boldsymbol{q} = \boldsymbol{0}) = a\,\delta'(u^2 - m^2_{J/\psi}) + b\,\delta(u^2 - m^2_{J/\psi}) + c\,\delta(u^2 - s_0)$, near the pole position of J/ψ. Here δ' is the first derivative of δ function

[†]For the detailed discussion of this section, refer to Ref.[9]. The similar QCD sum rule analysis was performed in Ref.[10].

with respect to u^2 and the parameter a is related to the spin-averaged scattering length $a_{J/\psi}$ as $a = 8\pi f_{J/\psi}^2 m_{J/\psi}^4 (M_N + m_{J/\psi}) a_{J/\psi}$, where the coupling $f_{J/\psi}$ and the J/ψ mass $m_{J/\psi}$ are defined by $\langle 0|J_\mu\ |J/\psi^{(h)}(q)\rangle = f_{J/\psi} m_{J/\psi}^2 \epsilon_\mu^{(h)}(q)$ with the polarization vector $\epsilon_\mu^{(h)}$. s_0 is the continuum threshold in vacuum. Moreover, among these parameters I impose the constraint from low energy theorem that in the low energy limit, $\omega \to 0$, $T(\omega, \mathbf{0})$ becomes equivalent to Born term $T^{\rm Born}(\omega, \mathbf{0})$ ($= 0$ for lack of charmed quarks inside a nucleon in this system). Finally, through the QSR I determine two unknown phenomenological parameters a and b. On the other hand, I give the following OPE expression for n-th derivative of $T_{\mu\nu}$ with respect to q^2, up to dimension-4 operators.

$$\frac{1}{n!}\left(\frac{d}{dq^2}\right)^n \frac{T^{\rm OPE}(q^2)}{q^2} = \frac{1}{3}\left[C_G^{(n)}(\xi)\left\{\left\langle\frac{\alpha_s}{\pi}G^2\right\rangle_N - 4\left\langle\frac{\alpha_s}{\pi}\mathcal{ST}(G_{0\sigma}^a G_{0\sigma}^a)\right\rangle_N\right\}\right.$$
$$\left. + \{D_1^{(n)}(\xi) - D_2^{(n)}(\xi) - D_3^{(n)}(\xi)\}\left\langle\frac{\alpha_s}{\pi}\mathcal{ST}(G_{0\sigma}^a G_{0\sigma}^a)\right\rangle_N\right], \qquad (3)$$

where $\xi = -q^2/4m_c^2$ (m_c; charmed quark mass 1.3 $\sim$ 1.35 GeV). $\mathcal{ST}$ means making the twist-2 operators symmetric and traceless in its Lorentz indices. The explicit forms of Wilson coefficient $C_G^{(n)}$, $D_1^{(n)}$, $D_2^{(n)}$ and $D_3^{(n)}$ are given in Ref. [9]. Eventually I evaluate the parameters in terms of the moment sum rule, $\widehat{T}^{(n)\,\rm ph}(\xi\ ;\ a, b) = \widehat{T}^{(n)\,\rm OPE}(\xi)$. Here I determine both n and q^2 to reproduce the experimental value of J/ψ bare mass by applying the moment sum rule to $\Pi_{\mu\nu}^0$. After inserting the sets of ξ and n obtained thus into the moment sum rule, I can determine unknown parameters a and b simultaneously. Here the values of other parameters are given in Ref. [9]. The direct application of moment sum rule to the forward J/ψ-N scattering amplitude supplies us the fascinating results for the J/ψ-N interaction, which is consistent with Ref.[10]. That is, the J/ψ-N scattering length $a_{J/\psi}$ indicates negative value (about -0.1 ± 0.02 fm). This result suggests that J/ψ-N interaction is very weakly attractive. Moreover the result gives very slight decreasing mass (about -4 to -7 MeV), about 0.1 to 0.2 % at normal matter density.

In-medium effect for D-meson

Next, as well as the above scheme I estimate the mass shift of D-meson through D-N scattering length. In this case, the pseudoscalar current ($J_5 = \bar{c} i\gamma_5 q$) is used for the D-meson, where q indicates massless light quarks. For simplicity, I don't take account of the isospin decomposition on the D-meson. Therefore, the in-medium mass of D-meson obtained by this analysis can be regarded as the isospin averaged result. The coupling f_D and the D-meson mass m_D are defined by $\langle 0|J_5\ |D(q)\rangle = i f_D m_D^2/m_c$ ($m_D = 1.87$ GeV). After applying the Borel transformation to the forward D-N scattering amplitude, I obtain that on the OPE side with $\nu = m_c^2/M^2$ (M; Borel mass) and the Whittaker function G,

$$B_M T^{\rm OPE}(q^2) = e^{-\nu}\left[-m_c\langle\bar{q}q\rangle_N - 2\left(1 - \frac{m_c^2}{M^2}\right)\langle q^\dagger i D_0 q\rangle_N\right.$$
$$+\frac{1}{12}\left\langle\frac{\alpha_s}{\pi}G^2\right\rangle_N + \frac{1}{3}\left\langle\frac{\alpha_s}{\pi}\mathcal{ST}(G_{0\sigma}^a G_{0\sigma}^a)\right\rangle_N$$
$$\left.\times\{-2 + G(1,2,\nu) + G(2,2,\nu) + 2G(2,3,\nu) + 2G(1,3,\nu)\}\right] \qquad (4)$$

and on the phenomenological side, if as before one assumes $T^{\rm Born} = 0$ [††],

$$B_M T^{\rm ph}(q^2) = a\left(\frac{1}{M^2}e^{-m_D^2/M^2} - \frac{s_0}{M^4}e^{-s_0/M^2}\right) + b\left(e^{-m_D^2/M^2} - \frac{s_0}{M^2}e^{-s_0/M^2}\right). \qquad (5)$$

As before I perform two-parameter fitting by means of OPE expanded up to dimension 4 including twist-2 operators. In fact, I can derive D-N scattering length a_D ($= -m_c^2 a/8\pi(M_N + m_D)f_D^2 m_D^4$) as a function of M^2 by removing the parameter b from both the matching equation of Eqs. (4) and (5) and its first derivative with respect to M^2. For coupling f_D and continuum threshold s_0, I adopt $f_D = 0.187$ GeV read off from a stable curve in the vicinity of $s_0 = 7.5$ GeV^2 using Borel sum rule of vacuum correlation function for the D-meson. This f_D value is very close to other calculations [11, 12] and experimental data (≤ 0.31 GeV). When one uses nucleon matrix elements for quark fields such as $\langle\bar{q}q\rangle_N = 5.3$ GeV and $\left\langle q^\dagger iD_0 q\right\rangle_N = 0.34$ GeV^2, comparatively stable curves of a_D are obtained at the reliable Borel mass region. To summarize the results for D-meson analysis, the D-N scattering length is -1.25 ± 0.05 fm. This result suggests that the D-N interaction is more attractive than the J/ψ-N interaction. I apply this result to effective mass of D-meson at normal matter density in the linear density approximation as before. Then the mass reduction is -83 ± 4 MeV, about 4 % of the total mass. I find this result leads to larger decrease than the charmonium. An origin of this mechanism originates in that on the OPE side, $m_c\langle\bar{q}q\rangle_N$ term is dominant for the D-meson in contrast to only gluon operator contribution for the charmonium. In Quark-Meson-Coupling model, this contribution will correspond to quark-σ meson coupling. Indeed, this model predicts the mass shift of D-meson becomes -60 MeV for the scalar potential at normal matter density [13].

Summary

Now I can come to some important conclusions through all the above results. If the mass modification of higher-lying charmonium states is very slight as well as the J/ψ in matter, the $D\bar{D}$ threshold falls below ψ' at the normal density and χ_c at twice as the normal density. These results could produce some important features relevant to recent NA50 experimental data. Namely, the behavior of level crossing may lead to the onset of discontinuous property for the suppression form. It is well known from p-A collision data that the J/ψ observed in nuclear collisions are directly produced only about 60% and the remainder comes from excited states ($\chi_c(1P)$, $\psi'(2S)$) with the ratio of 3 to 1 [14]. So the suppression of such feeddown effect from ψ' and χ_c to J/ψ could lead to direct decrease of J/ψ survival probability through the level crossings. First, the suppression of ψ' nearest to the $D\bar{D}$ threshold can be observed as the first very slight suppression of the J/ψ production. In fact, the ψ' data indicates a strong suppression even in cooler S-U collision. Next, three states of χ_c which is very close each other, induce the subsequent 2nd suppression through the level crossings. Finally, direct suppression due to the J/ψ itself can be observed as the 3rd suppression with further increase of the matter density. Thus the stair-shaped suppression form is not necessarily a phenomenon as far as deconfinement phase. From the point of view we should experimentally investigate whether or not one

[††]This implies one ignores the channels of D^+ or $D^0 + N \to \Lambda_c$ or Σ_c and so on. In the case of D^- or $\bar{D}^0$, since the anti-charm quark cannot couple to three quarks inside a nucleon by OZI rule, Born term will be zero.

of such level crossings could occur at least at normal matter density. To that end, I hope realization of the inverse kinematics experiments, in which the nuclear beam is incident on a hydrogen target, because this experiment can be feasible for measuring the decays of the charmonium and the D-meson [15] inside a nucleus. I can also suggest some observational consequences caused by such level crossings. One of them is to observe the change of decay width for the charmonium. In vacuum the resonances above $D\bar{D}$ threshold, for example ψ'' state have width of order MeV because of strong open charm channel. On the other hand, the resonances below the threshold have very sharp width of a few hundreds keV. So after the level crossing, the decay modes will change drastically at least one order of magnitude. The another is to observe the enhancement of D-meson at intermediate mass region of dilepton ($1.5 \leq M \leq 2.5$ GeV). In fact, such a dilepton enhancement was observed [16]. Thus I expect that the matter effect gives a considerable impact on the anomalous J/ψ suppression. Moreover it might be able to explain the anomalous suppression without an advent of deconfinement phase. Needless to say, in this case we must also perform the theoretical investigation of finite temperature effect [17, 18] to the mass modification in the future.

Acknowledgements

I would like to thank T. Hatsuda for useful discussions.

References

[1] L. Rammello et al., NA50 Collaboration, *Nucl. Phys.* **A638** (1998) 261c; M.C. Abreu et al., NA50 Collaboration, *Phys. Lett.* **450B** (1999) 456.

[2] C. Gershel and J. Hüfner, *Phys. Lett.* **207B** (1988) 253; D. Kharzeev, C. Lourenco, M. Nardi and H. Satz, *Z. Phys.* **C74** (1997) 307.

[3] T. Matsui and H. Satz, *Phys. Lett.* **178B** (1986) 416.

[4] R. Vogt, *Phys. Rep.* **310** (1999) 197.

[5] D. Kharzeev, M. Nardi and H. Satz, *hep-ph*/9707308; D. Kharzeev, *Nucl. Phys.* **A638** (1998) 279c.

[6] T. Hatsuda and T. Kunihiro, *Phys. Rev. Lett.* **55** (1985) 158; *Phys. Rep.* **247** (1994) 221.

[7] Y. Kondo and O. Morimatsu, *Phys. Rev. Lett.* **71** (1993) 2855.

[8] Y. Koike and A. Hayashigaki, *Prog. Theor. Phys.* **98** (1997) 631.

[9] A. Hayashigaki, *Prog. Theo. Phys.* **101** (1999) 923.

[10] F. Klingl, S. Kim, S.H. Lee, P. Morath and W. Weise, *Phys. Rev. Lett.* **82** (1999) 3396.

[11] T.M. Aliev and V.L. Eletskii, *Sov. J. Nucl. Phys.* **38**(6) (1983) 936.

[12] A.X. El-Khadra, A.S. Kronfeld, P.B. Mackenzie, S.M. Ryan and J.N. Simone, *Phys. Rev.* **D58** (1998) 014506.

[13] K. Tsushima, D.H. Lu, A.W. Thomas and R.H. Landau, *Phys. Rev.* **C59** (1999) 2824; A. Sibirtsev, K. Tsushima and A.W. Thomas, *nucl-th*/9904016.

[14] L. Antoniazzi et al., E705 Collaboration, *Phys. Rev. Lett.* **70** (1993) 383.

[15] G.A. Alves et al., *Phys. Rev. Lett.* **70** (1993) 722; M.J. Leitch et al., *Phys. Rev. Lett.* **72** (1994) 2542.

[16] M. Masera et al., HELIOS-3 Collaboration, *Nucl. Phys.* **A590** (1995) 93c; E. Scomparin et al., NA50 Collaboration, *Nucl. Phys.* **A610** (1996) 331c; M. Gazdzicki and C. Markert, *hep-ph*/9904441.

[17] R. Vogt and A. Jackson, *Phys. Lett.* **206B** (1988) 333.

[18] A. Sibirtsev, K. Tsushima, K. Saito and A.W. Thomas, *nucl-th*/9904015.

21. Quark Confinement and Color Monopoles in Quantum Chromodynamics

Hideo Suganuma, Kazahisa Amemiya and Hiroko Ichie

Research Center for Nuclear Physics (RCNP), Osaka University
Mihogaoka 10-1, Ibaraki, Osaka 567-0047, Japan
E-mail: suganuma@rcnp.osaka-u.ac.jp

We show the construction of the dual superconducting theory for the confinement mechanism from QCD in the maximally abelian (MA) gauge using the lattice QCD Monte Carlo simulation. We find that essence of infrared abelian dominance is naturally understood with the off-diagonal gluon mass $m_{\rm off} \simeq 1.2$GeV induced by the MA gauge fixing. In the MA gauge, the off-diagonal gluon amplitude is forced to be small, and the off-diagonal gluon phase tends to be random. As the mathematical origin of abelian dominance for confinement, we demonstrate that the strong randomness of the off-diagonal gluon phase leads to abelian dominance for the string tension. In the MA gauge, there appears the macroscopic network of the monopole world-line covering the whole system. We investigate the monopole-current system in the MA gauge by analyzing the dual gluon field B_μ. We evaluate the dual gluon mass as $m_B = 0.4 \sim 0.5$GeV in the infrared region, which is the lattice-QCD evidence of the dual Higgs mechanism by monopole condensation. Owing to infrared abelian dominance and infrared monopole condensation, QCD in the MA gauge is describable with the dual Ginzburg-Landau theory.

1. QCD and Dual Superconducting Theory for Confinement

Since 1974, quantum chromodynamics (QCD) has been established as the fundamental theory of the strong interaction, however, it is still hard to understand the nonperturbative QCD (NP-QCD) phenomena such as color confinement and dynamical chiral-symmetry breaking, in spite of the simple form of the QCD lagrangian

$$\mathcal{L}_{\rm QCD} = -\frac{1}{2}{\rm tr}G_{\mu\nu}G^{\mu\nu} + \bar{q}(i\not{D} - m_q)q. \qquad (1)$$

In particular, to understand the confinement mechanism is one of the most difficult problems remaining in the particle physics. As the hadron Regge trajectory and the lattice QCD simulation show, the confinement force between the color-electric charges is characterized by the *one-dimensional squeezing* of the color-electric flux and the universal physical quantity of the *string tension* $\sigma \simeq 1$GeV/fm.

As for the confinement mechanism, Nambu first proposed the *dual superconducting theory* for quark confinement, based on the electro-magnetic duality in 1974.[1] In this theory, there occurs the one-dimensional squeezing of the color-electric flux between quarks by the dual Meissner effect due to condensation of bosonic color-magnetic monopoles. However, there are *two large gaps* between QCD and the dual superconducting theory.[2]

(1) The dual superconducting theory is based on the *abelian gauge theory* subject to the Maxwell-type equations, where electro-magnetic duality is manifest, while QCD is a nonabelian gauge theory.

(2) The dual superconducting theory requires condensation of color-magnetic monopoles as the key concept, while QCD does not have such a monopole as the elementary degrees of freedom.

These gaps can be simultaneously fulfilled by the use of the *MA gauge fixing,* which reduces QCD to an abelian gauge theory. In the MA gauge, the off-diagonal gluon behaves as a charged matter field similar to $W_\mu^\pm$ in the Standard Model and provides a color-electric current in terms of the residual abelian gauge symmetry. As a remarkable fact in the MA gauge, color-magnetic monopoles appear as topological objects reflecting the nontrivial homotopy group $\Pi_2(\mathrm{SU}(N_c)/\mathrm{U}(1)^{N_c-1}) = \mathbf{Z}_\infty^{N_c-1}$, similarly in the GUT monopole.[3-6]

Thus, in the MA gauge, QCD is reduced into an abelian gauge theory including both the electric current j_μ and the magnetic current k_μ, which is expected to provide the theoretical basis of the dual superconducting theory for the confinement mechanism.

2. MA Gauge Fixing and Extraction of Relevant Mode for Confinement

In the Euclidean QCD, the maximally abelian (MA) gauge is defined by minimizing[2,6]

$$R_{\mathrm{off}}[A_\mu(\cdot)] \equiv \int d^4x \mathrm{tr}[\hat{D}_\mu, \vec{H}][\hat{D}_\mu, \vec{H}]^\dagger = \frac{e^2}{2}\int d^4x \sum_\alpha |A_\mu^\alpha(x)|^2, \tag{2}$$

with the $\mathrm{SU}(N_c)$ covariant derivative operator $\hat{D}_\mu \equiv \hat{\partial}_\mu + ieA_\mu$ and the Cartan decomposition $A_\mu(x) = \vec{A}_\mu(x)\cdot\vec{H} + \sum_\alpha A_\mu^\alpha(x)E^\alpha$. *In the MA gauge, the off-diagonal gluon components are forced to be as small as possible by the $SU(N_c)$ gauge transformation.* Since the covariant derivative $\hat{D}_\mu$ obeys the adjoint gauge transformation, the local form of the MA gauge fixing condition is derived as [2,6]

$$[\vec{H}, [\hat{D}_\mu, [\hat{D}_\mu, \vec{H}]]] = 0. \tag{3}$$

(For $N_c = 2$, this condition is equivalent to the diagonalization of $\Phi_{\mathrm{MA}} \equiv [\hat{D}_\mu, [\hat{D}_\mu, \tau^3]]$, and then the MA gauge is found to be a sort of the 't Hooft abelian gauge[3].) In the MA gauge, the gauge symmetry $G \equiv \mathrm{SU}(N_c)_{\mathrm{local}}$ is reduced into $H \equiv \mathrm{U}(1)_{\mathrm{local}}^{N_c-1} \times \mathrm{Weyl}_{\mathrm{global}}^{N_c}$, where the global Weyl symmetry is the subgroup of $\mathrm{SU}(N_c)$ relating the permutation of the N_c bases in the fundamental representation.[2,6]

We summarize abelian dominance, monopole dominance and extraction of the relevant mode for NP-QCD observed in the lattice QCD in the MA gauge.

(a) Without gauge fixing, all the gluon components equally contribute to NP-QCD, and it is difficult to extract relevant degrees of freedom for NP-QCD.

(b) In the MA gauge, QCD is reduced into an abelian gauge theory including the electric current j_μ and the magnetic current k_μ. The diagonal gluon behaves as the abelian gauge field, and the off-diagonal gluon behaves as the charged matter field. In the MA gauge, the lattice QCD shows *abelian dominance* for NP-QCD (confinement[6,7], chiral symmetry breaking[8], instantons[9,10]) : only the diagonal gluon is relevant for NP-QCD, while off-diagonal gluons do not contribute to NP-QCD. In the lattice QCD, there appears the *global network of the monopole world-line covering the whole system in the MA gauge.* (See Fig.3 (a).)

(c) The diagonal gluon can be decomposed into the "photon part" and the "monopole part", corresponding to the separation of j_μ and k_μ. In the MA gauge, the lattice QCD shows *monopole dominance* for NP-QCD: the monopole part ($k_\mu \neq 0$, $j_\mu = 0$) leads to NP-QCD, while the photon part ($j_\mu \neq 0, k_\mu = 0$) seems trivial like QED and does not contribute to NP-QCD.

Thus, by taking the MA gauge, the relevant collective mode for NP-QCD can be extracted as the color-magnetic monopole.[2,11]

3. Essence of Abelian Dominance : Off-diagonal Gluon Mass in MA Gauge

In this section, we study essence of abelian dominance for NP-QCD in the MA gauge in terms of the *generation of the effective mass $m_{\rm off}$ of the off-diagonal (charged) gluon by the MA gauge fixing.* In the SU(2) QCD partition functional, the mass generation of the off-diagonal gluon $A^\pm_\mu \equiv (A^1_\mu \pm iA^2_\mu)/\sqrt{2}$ in the MA gauge is expressed as[2,12]

$$\begin{aligned} Z^{\rm MA}_{\rm QCD} &= \int DA_\mu \exp\{iS_{\rm QCD}[A_\mu]\}\delta(\Phi^\pm_{\rm MA}[A_\mu])\Delta_{\rm PF}[A_\mu] \\ &= \int DA^3_\mu \exp\{iS_{\rm eff}[A^3_\mu]\} \int DA^\pm_\mu \exp\{i\int d^4x\ m^2_{\rm off}A^+_\mu A^\mu_-\}\mathcal{F}[A_\mu], \end{aligned} \tag{4}$$

with $\Phi_{\rm MA} \equiv [\hat{D}_\mu, [\hat{D}^\mu, \tau_3]]$, the Faddeev-Popov determinant $\Delta_{\rm FP}$, the abelian effective action $S_{\rm eff}[A^3_\mu]$ and a smooth functional $\mathcal{F}[A_\mu]$.

To investigate the off-diagonal gluon mass $m_{\rm off}$, we study the Euclidean gluon propagator $G^{ab}_{\mu\nu}(x-y) \equiv \langle A^a_\mu(x)A^b_\nu(y)\rangle$ in the MA gauge, using the SU(2) lattice QCD.[2,12] As for the residual $U(1)_3$ gauge symmetry, we impose the $U(1)_3$ Landau gauge fixing to extract most continuous gauge configuration under the MA gauge constraint and to compare with the continuum theory. The continuum gluon field $A^a_\mu(x)$ is extracted from the link variable as $U_\mu(s) = \exp(iaeA^a_\mu(s)\frac{\tau^a}{2})$. Here, the scalar-type gluon propagator $G^a_{\mu\mu}(r) \equiv \sum^4_{\mu=1}\langle A_\mu{}^a(x)A_\mu{}^a(y)\rangle$ is useful to observe the interaction range of the gluon, because it depends only on the four-dimensional Euclidean distance $r \equiv \sqrt{(x_\mu - y_\mu)^2}$.

We show in Fig.1(a) $G^3_{\mu\mu}(r)$ and $G^{+-}_{\mu\mu}(r) \equiv \sum^4_{\mu=1}\langle A^+_\mu(x)A^-_\mu(y)\rangle = \frac{1}{2}\{G^1_{\mu\mu}(r) + G^2_{\mu\mu}(r)\}$ in the MA gauge using the SU(2) lattice QCD with $2.2 \leq \beta \leq 2.4$ and the various lattice size ($12^3 \times 24$, 16^4, 20^4). Since the massive vector-boson propagator with the mass M takes a Yukawa-type asymptotic form as $G_{\mu\mu}(r) \sim \frac{M^{1/2}}{r^{3/2}}\exp(-Mr)$, the effective mass $m_{\rm off}$ of the off-diagonal gluon $A^\pm_\mu(x)$ can be evaluated from the slope of the logarithmic plot of $r^{3/2}G^{+-}_{\mu\mu}(r) \sim \exp(-m_{\rm off}r)$ as shown in Fig.1(b). The off-diagonal gluon $A^\pm_\mu(x)$ behaves as the massive field with $m_{\rm off} \simeq 1.2$ GeV in the MA gauge for $r \gtrsim 0.2$ fm.

Thus, *essence of infrared abelian dominance* in the MA gauge can be physically interpreted with the *effective off-diagonal gluon mass $m_{\rm off}$* induced by the MA gauge fixing.[2] Due to the effective mass $m_{\rm off} \simeq 1.2$GeV, the off-diagonal gluon $A^\pm_\mu$ can propagate only within the short range as $r \lesssim m^{-1}_{\rm off} \simeq 0.2$fm, and cannot contribute to the infrared QCD physics in the MA gauge, which leads to abelian dominance for NP-QCD.[2,12]

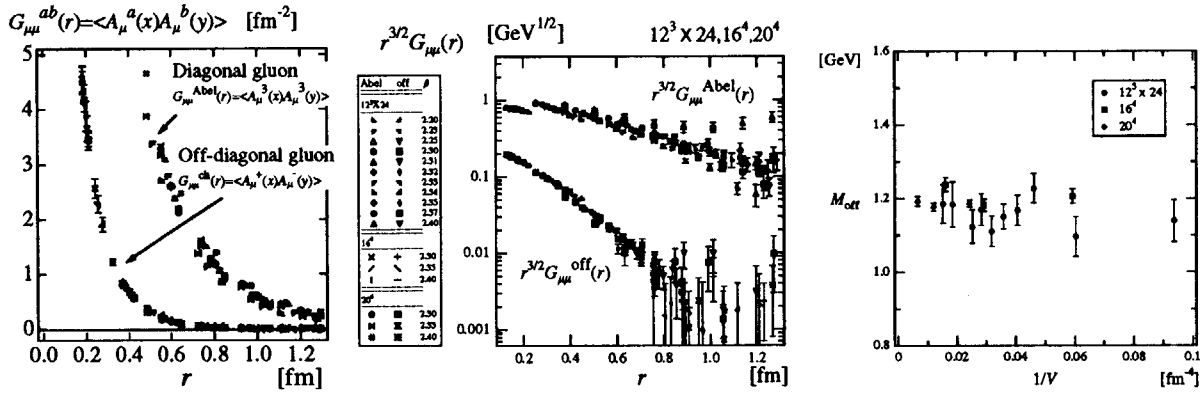

(a) (b) (c)

Figure 1. (a) The scalar-type gluon propagator $G^a_{\mu\mu}(r)$ as the function of the 4-dimensional distance r in the MA gauge in the SU(2) lattice QCD with $2.2 \leq \beta \leq 2.4$ and various lattice size ($12^3 \times 24$, 16^4, 20^4). (b) The logarithmic plot for the scalar correlation $r^{3/2}G^a_{\mu\mu}(r)$. The off-diagonal gluon propagator behaves as the Yukawa-type function, $G_{\mu\mu} \sim \frac{\exp(-m_{\rm off}r)}{r^{3/2}}$. (c) The effective off-diagonal gluon mass $m_{\rm off}$ extracted from the slope analysis, using each lattice with different β and volume ($12^3 \times 24$, 16^4, 20^4). The effective mass of the off-diagonal gluon $A^{\pm}_{\mu}$ can be estimated as $m_{\rm off} \simeq 1.2$GeV.

4. Randomness of Off-diagonal Gluon Phase as the Mathematical Origin of Abelian Dominance for Confinement

In the lattice QCD, the SU(2) link variable is factorized as $U_\mu(s) = M_\mu(s)u_\mu(s)$, according to the Cartan decomposition $\mathrm{SU(2)/U(1)_3 \times U(1)_3}$. Here, $u_\mu(s) \equiv \exp\{i\tau^3\theta^3_\mu(s)\} \in \mathrm{U(1)_3}$ denotes the abelian link variable, and the off-diagonal factor $M_\mu(s) \in \mathrm{SU(2)/U(1)_3}$ is parameterized as

$$M_\mu(s) \equiv e^{i\{\tau^1\theta^1_\mu(s)+\tau^2\theta^2_\mu(s)\}} = \begin{pmatrix} \cos\theta_\mu(s) & -\sin\theta_\mu(s)e^{-i\chi_\mu(s)} \\ \sin\theta_\mu(s)e^{i\chi_\mu(s)} & \cos\theta_\mu(s) \end{pmatrix}. \tag{5}$$

In the MA gauge, the *diagonal element* $\cos\theta_\mu(s)$ in $M_\mu(s)$ is maximized by the SU(2) gauge transformation and the "abelian projection rate" becomes almost unity as $R_{\rm Abel} = \langle\cos\theta_\mu(s)\rangle_{\rm MA} \simeq 0.93$ at $\beta = 2.4$. Using the lattice QCD simulation, we find the two remarkable features of the off-diagonal element $e^{i\chi_\mu(s)}\sin\theta_\mu(s)$ in $M_\mu(s)$ in the MA gauge.[2,6]

(1) The off-diagonal gluon amplitude $|\sin\theta_\mu(s)|$ is forced to be minimized in the MA gauge, which allows the approximate treatment on the off-diagonal gluon phase.

(2) The off-diagonal phase variable $\chi_\mu(s)$ is not constrained by the MA gauge-fixing condition at all, and tends to be random.

Therefore, $\chi_\mu(s)$ can be regarded as a *random angle variable* on the treatment of $M_\mu(s)$ in the MA gauge in a good approximation.

Now, we show the analytical proof of abelian dominance for the string tension or the confinement force in the MA gauge, within the random-variable approximation for $\chi_\mu(s)$

or the off-diagonal gluon phase.[2,6] Here, we use $\langle e^{i\chi_\mu(s)}\rangle_{\rm MA} \simeq \int_0^{2\pi} d\chi_\mu(s) \exp\{i\chi_\mu(s)\} = 0$. In calculating the Wilson loop $\langle W_C[U]\rangle \equiv \langle {\rm tr}\Pi_C U_\mu(s)\rangle = \langle {\rm tr}\Pi_C\{M_\mu(s)u_\mu(s)\}\rangle$, the off-diagonal matrix $M_\mu(s)$ is simply reduced as a c-number factor, $M_\mu(s) \to \cos\theta_\mu(s)\ \mathbf{1}$, and then the SU(2) link variable $U_\mu(s)$ is reduced to be a *diagonal matrix,*

$$U_\mu(s) \equiv M_\mu(s)u_\mu(s) \to \cos\theta_\mu(s)u_\mu(s), \tag{6}$$

after the integration over $\chi_\mu(s)$. For the $R\times T$ rectangular C, the Wilson loop $W_C[U]$ in the MA gauge is approximated as

$$\begin{aligned}\langle W_C[U]\rangle &= \langle {\rm tr}\Pi_{i=1}^L\{M_{\mu_i}(s_i)u_{\mu_i}(s_i)\}\rangle \simeq \langle \Pi_{i=1}^L \cos\theta_{\mu_i}(s_i)\cdot {\rm tr}\Pi_{j=1}^L u_{\mu_j}(s_j)\rangle_{\rm MA} \\ &\simeq \langle \exp\{\Sigma_{i=1}^L \ln(\cos\theta_{\mu_i}(s_i))\}\rangle_{\rm MA}\ \langle W_C[u]\rangle_{\rm MA},\end{aligned} \tag{7}$$

with the perimeter length $L \equiv 2(R+T)$ and the abelian Wilson loop $W_C[u] \equiv {\rm tr}\Pi_{i=1}^L u_{\mu_i}(s_i)$. Replacing $\sum_{i=1}^L \ln\{\cos(\theta_{\mu_i}(s_i))\}$ by its average $L\langle\ln\{\cos\theta_\mu(s)\}\rangle_{\rm MA}$ in a statistical sense, we derive a formula for the *off-diagonal gluon contribution to the Wilson loop* as[2,6]

$$W_C^{\rm off} \equiv \langle W_C[U]\rangle / \langle W_C[u]\rangle_{\rm MA} \simeq \exp\{L\langle\ln\{\cos\theta_\mu(s)\}\rangle_{\rm MA}\}, \tag{8}$$

which provides the relation between the *macroscopic* quantity $W_C^{\rm off}$ and the *microscopic* quantity $\langle\ln\{\cos\theta_\mu(s)\}\rangle_{\rm MA}$. Using the lattice QCD, we have checked this relation for large loops, where such a statistical treatment is accurate.[2,6]

In this way, the off-diagonal gluon contribution $W_C^{\rm off}$ obeys the *perimeter law* in the MA gauge, and then the off-diagonal gluon contribution to the string tension vanishes as

$$\sigma_{\rm SU(2)} - \sigma_{\rm Abel} \simeq -2\langle\ln\{\cos\theta_\mu(s)\}\rangle_{\rm MA} \lim_{R,T\to\infty} \frac{R+T}{RT} = 0. \tag{9}$$

Thus, *abelian dominance for the string tension*, $\sigma_{\rm SU(2)} = \sigma_{\rm Abel}$, can be demonstrated in the MA gauge within the random-variable approximation for the off-diagonal gluon phase. Also, we can predict the deviation between $\sigma_{\rm SU(2)}$ and $\sigma_{\rm Abel}$ as $\sigma_{\rm SU(2)} > \sigma_{\rm Abel}$, due to the *finite size effect* on R and T in the Wilson loop.[2,6]

5. The Structure of QCD-Monopoles in terms of the Off-diagonal Gluon

Let us compare the QCD-monopole with the point-like Dirac monopole. There is no point-like monopole in QED, because the QED action diverges around the monopole. The QCD-monopole also accompanies a large abelian action density inevitably, however, *owing to cancellation with the off-diagonal gluon contribution, the total QCD action is kept finite even around the QCD-monopole.*[2,6]

To see this, we investigate the structure of the QCD-monopole in the MA gauge in terms of the action density using the SU(2) lattice QCD.[2] From the SU(2) plaquette $P_{\mu\nu}^{\rm SU(2)}(s)$ and the abelian plaquette $P_{\mu\nu}^{\rm Abel}(s)$, we define the "SU(2) action density" $S_{\mu\nu}^{\rm SU(2)}(s) \equiv 1 - \frac{1}{2}{\rm tr}P_{\mu\nu}^{\rm SU(2)}(s)$, the "abelian action density" $S_{\mu\nu}^{\rm Abel}(s) \equiv 1 - \frac{1}{2}{\rm tr}P_{\mu\nu}^{\rm Abel}(s)$ and the "off-diagonal gluon contribution" $S_{\mu\nu}^{\rm off}(s) \equiv S_{\mu\nu}^{\rm SU(2)}(s) - S_{\mu\nu}^{\rm Abel}(s)$. In the lattice formalism, the monopole current $k_\mu(s)$ is defined on the dual link, and there are 6 plaquettes around the monopole. Then, we consider the average over the 6 plaquettes around the dual link,

$$S(s,\mu) \equiv \frac{1}{12}\sum_{\alpha\beta\gamma}\sum_{m=0}^{1} |\varepsilon_{\mu\alpha\beta\gamma}| S_{\alpha\beta}(s+m\hat{\gamma}). \tag{10}$$

We show in Fig.2(b) the probability distribution of the action densities $S_{\mathrm{SU(2)}}$, S_{Abel} and S_{off} around the QCD-monopole in the MA gauge. We summarize the results on the QCD-monopole structure as follows.

(1) Around the QCD-monopole, both the abelian action density S_{Abel} and the off-diagonal gluon contribution S_{off} are largely fluctuated, and their cancellation keeps the total QCD-action density $S_{\mathrm{SU(2)}}$ small.
(2) The QCD-monopole has an intrinsic structure relating to a large amount of off-diagonal gluons $A_\mu^\pm$ around its center, similar to the 't Hooft-Polyakov monopole.
(3) At the large-distance scale, off-diagonal gluons inside the QCD-monopole become invisible, and the QCD-monopole can be regarded as the point-like Dirac monopole.
(4) From the concentration of off-diagonal gluons around QCD-monopoles in the MA gauge, we can naturally understand the *local correlation between monopoles and instantons*. In fact, instantons tend to appear around the monopole world-line in the MA gauge, because instantons need full SU(2) gluon components for existence.[2,9]

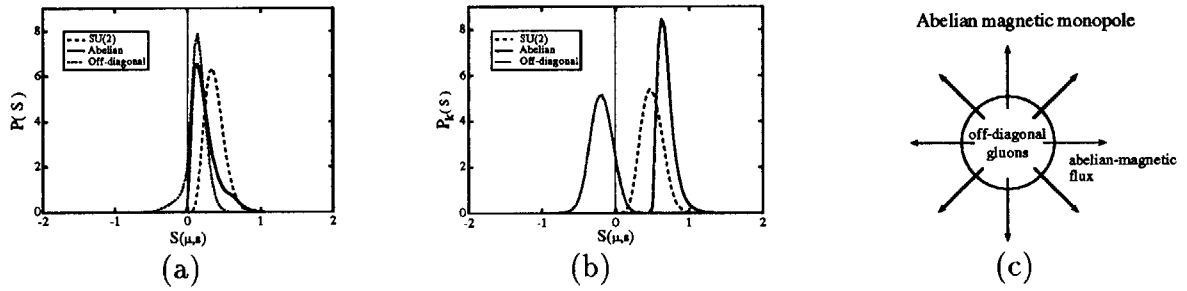

Figure 2. (a) The total probability distribution $P(S)$ on the whole lattice and (b) the probability distribution $P_k(S)$ around the monopole for SU(2) action density $S_{\mathrm{SU(2)}}$ (dashed curve), abelian action density S_{Abel} (solid curve) and off-diagonal gluon contribution S_{off} (dotted curve) in the MA gauge at $\beta = 2.4$ on 16^4 lattice. Around the QCD-monopole, large cancellation between S_{Abel} and S_{off} keeps the total QCD-action small. (c) The schematic figure for the QCD-monopole structure in the MA gauge. The QCD-monopole includes a large amount of off-diagonal gluons around its center.

6. Lattice-QCD Evidence of Infrared Monopole Condensation

In the MA gauge, there appears the global network of the monopole world-line covering the whole system as shown in Fig.3(a), and this monopole-current system (the monopole part) holds essence of NP-QCD[2,8,10,11]. We finally study the dual Higgs mechanism by monopole condensation in the NP-QCD vacuum in the MA gauge.

Since QCD is described by the "electric variable" as quarks and gluons, the "electric sector" of QCD has been well studied with the Wilson loop or the inter-quark potential, however, the "magnetic sector" of QCD is hidden and still unclear. To investigate the magnetic sector directly, it is useful to introduce the "dual (magnetic) variable" as the *dual gluon field* B_μ, which is the dual partner of the diagonal gluon and directly couples with the magnetic current k_μ.

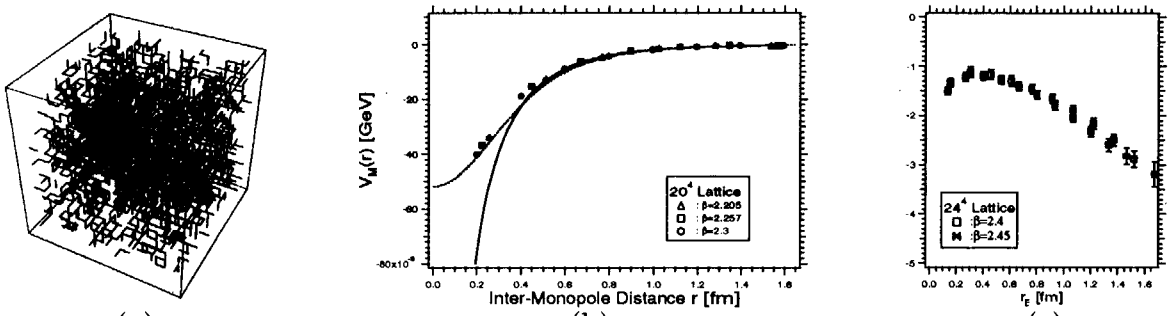

(a) (b) (c)

Figure 3. The SU(2) lattice-QCD results in the MA gauge. (a) The monopole world-line projected into $\mathbf{R}^3$ on the $16^3 \times 4$ lattice with $\beta = 2.2$ (the confinement phase). There appears the global network of monopole currents covering the whole system. (b) The inter-monopole potential $V_M(r)$ v.s. the 3-dimensional distance r in the monopole-current system on the 20^4 lattice. The solid curve denotes the Yukawa potential with $m_B = 0.5$GeV. The dotted curve denotes the Yukawa-type potential including the monopole-size effect. (c) The scalar-type dual-gluon correlation $\ln(r_E^{3/2}\langle B_\mu(x)B_\mu(y)\rangle)$ as the function of the 4-dimensional Euclidean distance $r_E \equiv \sqrt{(x-y)^2}$ on the 24^4 lattice.

Due to the absence of the electric current j_μ in the monopole part, the dual gluon B_μ can be introduced as the regular field satisfying $(\partial \wedge B)_{\mu\nu} = {}^*F_{\mu\nu}$ and the dual Bianchi identity, $\partial^{\mu *}(\partial \wedge B)_{\mu\nu} = j_\nu = 0$. By taking the dual Landau gauge $\partial_\mu B^\mu = 0$, the field equation is simplified as $\partial^2 B_\mu = k_\mu$, and therefore we obtain the dual gluon field B_μ from the monopole current k_μ as

$$B_\mu(x) = (\partial^{-2}k_\mu)(x) = -\frac{1}{4\pi^2}\int d^4y \frac{k_\mu(y)}{(x-y)^2}. \tag{11}$$

In the monopole-condensed vacuum, the dual gluon B_μ is to be massive, and hence we investigate the dual gluon mass m_B as the evidence of the dual Higgs mechanism.

First, we put test magnetic charges in the monopole-current system in the MA gauge, and measure the inter-monopole potential $V_M(r)$ to get information about monopole condensation. Since the dual Higgs mechanism is the screening effect on the magnetic flux, the inter-monopole potential is expected to be short-range Yukawa-type. Using *the dual Wilson loop* W_D as the loop-integral of the dual gluon,

$$W_D(C) \equiv \exp\{i\frac{e}{2}\oint_C dx_\mu B^\mu\} = \exp\{i\frac{e}{2}\iint d\sigma_{\mu\nu}{}^*F^{\mu\nu}\}, \tag{12}$$

the potential between the monopole and the anti-monopole can be derived as

$$V_M(R) = -\lim_{T\to\infty}\frac{1}{T}\ln\langle W_D(R,T)\rangle. \tag{13}$$

Here, $W_D(C)$ is the *dual version of the abelian Wilson loop* $W_{\rm Abel}(C) \equiv \exp\{i\frac{e}{2}\oint_C dx_\mu A^\mu\} = \exp\{i\frac{e}{2}\iint d\sigma_{\mu\nu}F^{\mu\nu}\}$ and we have set the test monopole charge as $e/2$.

We show in Fig.3(b) the inter-monopole potential $V_M(r)$ in the monopole part in the MA gauge.[2] Except for the short distance, the inter-monopole potential can be almost fitted

by the Yukawa potential $V_M(r) = -\frac{(e/2)^2}{4\pi}\frac{e^{-m_B r}}{r}$, after removing the finite-size effect of the dual Wilson loop. In the MA gauge, the dual gluon mass is estimated as $m_B \simeq 0.5$GeV from the infrared behavior of $V_M(r)$.

Second, we investigate also the scalar-type dual gluon propagator $\langle B_\mu(x)B_\mu(y)\rangle_{\rm MA}$ as shown in Fig.3(c), and estimate the dual gluon mass as $m_B \simeq 0.4$ GeV from its large-distance behavior.

From these two tests, the dual gluon mass is evaluated as $m_B = 0.4 \sim 0.5$ GeV, and this can be regarded as the lattice-QCD evidence for the dual Higgs mechanism by monopole condensation at the infrared scale.

7. Construction of DGL theory from lattice QCD in MA gauge

In the MA gauge, the off-diagonal gluon contribution can be neglected and monopole condensation occurs at the infrared scale of QCD. Therefore, the QCD vacuum in the MA gauge can be regarded as the dual superconductor described by the dual Ginzburg-Landau (DGL) theory, and quark confinement can be understood with the dual Meissner effect. The DGL theory can describe not only quark confinement [5] but also dynamical chiral-symmetry breaking (DχSB) by solving the Schwinger-Dyson equation for the quark field [5,13]. Monopole dominance for DχSB is also found from the analysis of the effective potential [14]. Using the DGL theory, we have studied the QCD phase transition (deconfinement [5,15] and chiral restoration [13]) at finite temperature, the QGP creation process in ultra-relativistic heavy-ion collisions [5,15], hadronization in the early universe [16], and glueball properties [17] systematically.

To summarize, the lattice QCD in the MA gauge exhibits *infrared abelian dominance* and *infrared monopole condensation*, and therefore the dual Ginzburg-Landau (DGL) theory[5,13–17] can be constructed as the infrared effective theory directly based on QCD in the MA gauge.[2,18]. as shown in Fig.4.

Acknowledgments

H.S. would like to thank Professor Yoichiro Nambu for useful discussions. K.A. and H.S. would like to thank Dr. Matsufuru for useful comments. We also thank to Professors H. Toki, O. Miyamura and H. Ejiri for continuous encouragements. H.S. is supported in part by Grant for Scientific Research (No.09640359) from Ministry of Education, Science and Culture, Japan. The lattice QCD simulations have been performed on sx4 at RCNP, Osaka University.

REFERENCES

1. Y. Nambu, *Phys. Rev.* **D10**, 4262 (1974).
2. H. Suganuma, H. Ichie, A. Tanaka and K. Amemiya, *Prog. Theor. Phys. Suppl.* **131**, 559 (1998).
3. G. 't Hooft, *Nucl. Phys.* **B190**, 455 (1981).
4. Z. F. Ezawa and A. Iwazaki, *Phys. Rev.* **D25**, 2681 (1982); **D26**, 631 (1982).

5. H. Suganuma, S. Sasaki and H. Toki, *Nucl. Phys.* **B435**, 207 (1995).
H. Suganuma, S. Sasaki, H. Toki and H. Ichie, *Prog. Theor. Phys. Suppl.* **120**, 57 (1995) and references therein.
6. H. Ichie and H. Suganuma, *Nucl. Phys.* **B548** (1999) 365;
Phys. Rev. **D60** (1999) 77501.
7. T. Suzuki and I. Yotsuyanagi, *Phys. Rev.* **D42**, 4257 (1990).
8. O. Miyamura, *Phys. Lett.* **B353**, 91 (1995).
9. M. Fukushima, H. Suganuma and H. Toki, *Phys. Rev.* **D60** (1999) in press.
M. Fukushima, S. Sasaki, H. Suganuma, A. Tanaka, H. Toki and D. Diakonov, *Phys. Lett.* **B399**, 141 (1997).
10. S. Sasaki and O. Miyamura, *Phys. Lett.* **B443**, 331 (1998);
Phys. Rev. **D59**, 94507 (1999).
11. K.-I. Kondo, *Phys. Rev.* **D57**, 7467 (1998); **D58**, 105016 (1998).
12. K. Amemiya and H. Suganuma, *Phys. Rev.* **D** (1999) in press.
13. S. Sasaki, H. Suganuma and H. Toki, *Prog. Theor. Phys.* **94**, 373 (1995);
Phys. Lett. **B387**, 145 (1996); *Prog. Theor. Phys. Suppl.* **129**, 227 (1997).
14. S. Umisedo, H. Suganuma and H. Toki, *Phys. Rev.* **D57**, 1605 (1998).
15. H. Ichie, H. Suganuma and H. Toki, *Phys. Rev.* **D52**, 2994 (1995); **D54**, 3382 (1996).
16. H. Monden, H. Ichie, H. Suganuma and H. Toki, *Phys. Rev.* **C57**, 2564 (1998).
17. Y. Koma, H. Suganuma and H. Toki, *Phys. Rev.* **D60**, 74024 (1999).
18. H. Suganuma, K. Amemiya, H. Ichie and A. Tanaka, *Nucl. Phys.* **A** (1999) in press.

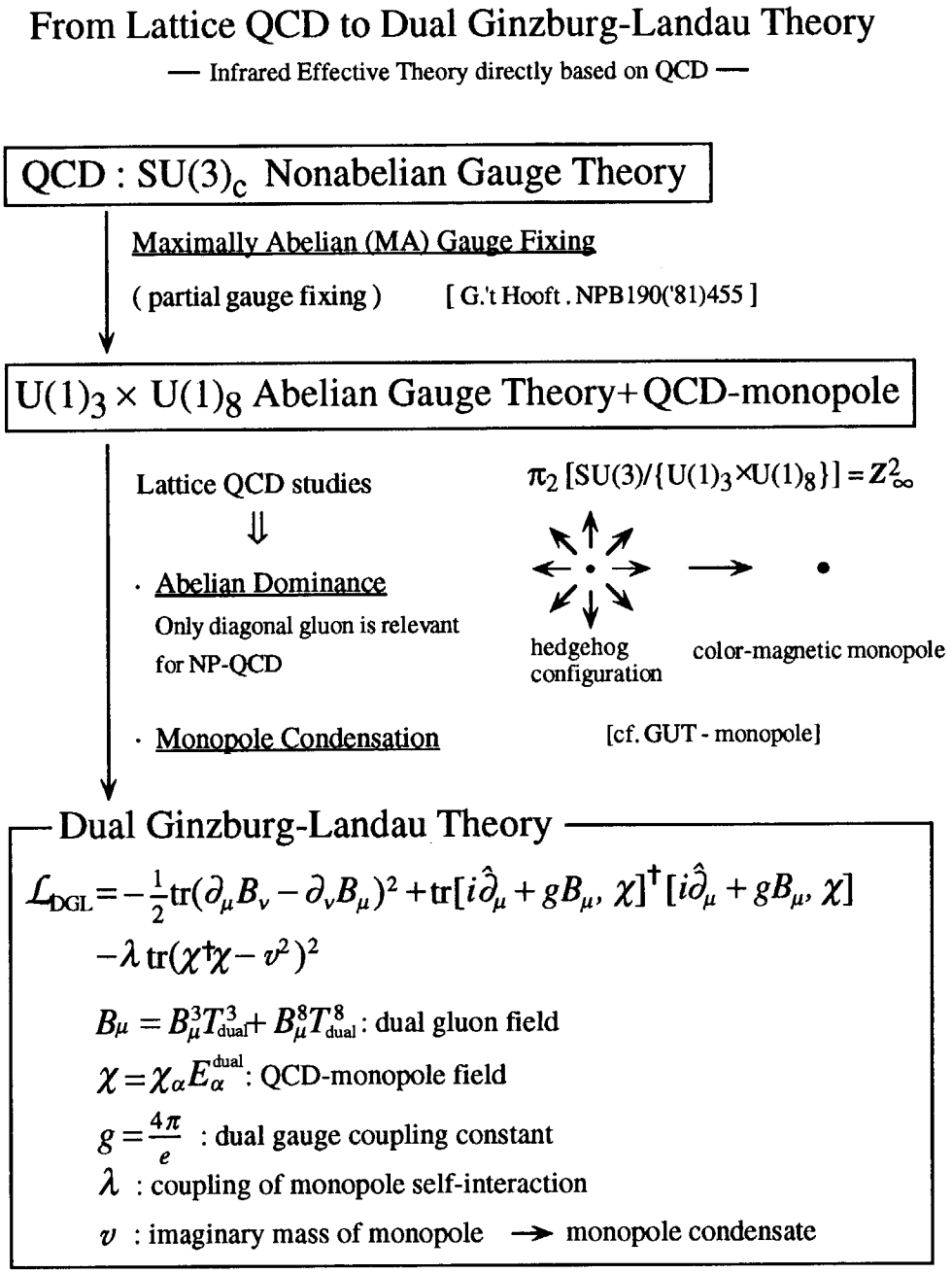

Figure 4. Construction of the dual Ginzburg-Landau (DGL) theory from the lattice QCD in the maximally abelian (MA) gauge.

22. 光円錐量子化法とその応用
– Past, Present and Near Future –

板倉 数記　阪大 RCNP

This talk is a brief overview of the light-front quantization as a new non-perturbative method and its application to hadron physics. Emphasis is put on the recent progress in describing the "vacuum physics" on the light front.

1 Light-Front Quantization

本稿では最近再び注目されている「光円錐量子化法 (Light-Front Quantization)」[1] を紹介し、そのハドロン物理への応用を議論する。QCD では閉じ込めによって全ての状態が束縛状態であるので、相対論的束縛状態を非摂動的に取り扱える光円錐量子化法を応用するのは非常に興味深い。以下ではその手法を導入するに至った動機を過去に遡って説明した後、最近になって発展してきた非摂動的な解析を自分の仕事を交えて概観し、さらに今後取り組むべき問題や応用可能な問題について触れる。さて、まず一番最初に光円錐量子化法の定義を明確にしておこう。光円錐量子化法とは、光円錐座標での x^+ すなわち

$$x^+ = (x^0 + x^3)/\sqrt{2} \tag{1}$$

を「時間」として取り扱い、正準量子化を行なう手法である。なお、その他の「空間」座標 $x^- = (x^0 - x^3)/\sqrt{2}$ と $x^i_\perp = x^1, x^2$ はそれぞれ「縦方向」と「横方向」と呼ばれる。例えば 3+1 次元スカラー場に対してなら $[\phi(x^+, \mathbf{x}),\ \pi(x^+, \mathbf{y})] = \frac{i}{2}\delta(x^- - y^-)\delta^{(2)}(x_\perp - y_\perp)$ なる「同時刻」交換関係を課すことになる。

2 Past [1949 – 1970's]

この手法の特徴を考える際、初めに考え出された時の純粋な動機を知ることは非常に重要である。x^+ を時間として量子化を行なうという突飛なアイディアはそもそも 50 年前に Dirac [2] によって提唱された。その時の彼の動機は「相対論と量子力学の融合」であった。さらに量子力学はハミルトン形式で書かれているので、「相対論とハミルトン形式の融合」と言い換えてもいい。普通の量子化は時間一定 (x^0 =constant) の超平面上で指定され、その面は回転や空間の平行移動のもとでは動かない (そのような運動の生成子 (ここでは 6 つ) を kinematical と呼ぶ) が、Lorentz 変換は時間を空間と混ぜるので明らかに Lorentz boost のもとでは動いてしまう。それゆえ、普通は静止系で得られた解から慣性系での解を得ることは容易ではない。その意味で相対論と量子論は相性が悪く、その幸福な融合が問題にされたのである。Dirac は相対論的系に最も「便利」なハミルトン形式を見つけるという形で問題設定をし、具体的には 10 個の Poincaré 生成子のうち、kinematical な生成子の数が最大になるような形式を探した。その結果、さらにある方向の boost を含んで全部で 7 つの kinematical な生成子を持つ枠組として "front form" を見つけたのである。実際、z 軸方向の Lorentz boost は光円錐座標に対しては ($\tanh\phi = \beta$)

$$x'^+ = \mathrm{e}^{\phi} x^+, \quad x'^- = \mathrm{e}^{-\phi} x^- \tag{2}$$

となり、$x^+ = 0$ なる超平面は不変である。この性質は非常に大きな意味を持っている。すなわち、光円錐量子化で時刻 $x^+ = 0$ において束縛状態を解き運動量 P の状態 $|P\rangle$ を得た時、その boost された状態 $|P'\rangle$ が $|P\rangle$ を使って容易に求めることができることを意味している。これは光円錐量子化法の特筆すべき利点である。特に複合粒子系であるハドロンにとっては非常に好ましい性質と言える。

もう一つの重要な側面としてパートン模型との関係について触れておこう。QCD およびパートン模型の発展の上で光円錐的な視点は様々な側面で現れてきた。まず、電子-核子の深非弾性散乱においては "Light-Cone Dominance" と呼ばれる状況があるが、それは hadronic tensor

$$W^{\mu\nu} = \frac{1}{4\pi}\int d^4x\ \mathrm{e}^{-iqx}\langle PS|[J^\mu(x), J^\nu(0)]|PS\rangle$$

の被積分関数が Bjorken 極限 ($Q^2 = -q^2 \to \infty,\ x_{\mathrm{bj}} = Q^2/2p\cdot q$: fixed) では $x^+ \sim 0, x_\perp \sim 0$ 付近が最も効くことをいう。また、そもそも Light-Cone gauge $A_- = 0$ で ($n^\mu = (1,0,0,-1)/2P$)

$$q(x_{\mathrm{bj}}) = \int \frac{d\lambda}{2\pi}\ \mathrm{e}^{i\lambda x_{\mathrm{bj}}}\langle PS|\bar\psi(0)\not{n}\psi(\lambda n)|PS\rangle$$

という量が「quark 数密度」として見なせるのは、いわゆる Infinite Momentum Frame(IMF) をとった時だけであることも注目して欲しい。なお、IMF は (少なくとも摂動論の範囲では) 光円錐量子化との同等性が示されている。以上のことから、光円錐上を出発点として深非弾性散乱を定式化すれば非常に自然な枠組ができると期待される。実際そのような試みは古くから存在するが、あくまでも摂動論の枠内での定式化であった。非摂動的領域までを見越しての定式化は最近の光円錐量子化自身の非摂動的手法の発展まで待たなくてはならなかった。このことについては 4 章で光円錐量子化の今後の可能性として議論する。

3 Present [1980's – 1990's]

光円錐量子化法における非摂動的な手法の開発は80年代中頃のPauliとBrodskyらの仕事を皮切りにして現在まで盛んに研究されている。単に「非摂動的」といっただけでは殆んど何も意味しないのでもう少し意味を限定すると、光円錐量子化での非摂動的な解析は大きく二つに分けられる。一つめは、光円錐量子化法の最大の利点である「真空の自明性」とその反映である「励起状態の記述の簡単さ」を応用した手法を開発していこうという流れであり、二つめは、対称性の自発的破れやトポロジカルな効果などのいわゆる「真空の物理」を光円錐量子化で記述する方法を探るという流れである。

3.1 "Vacuum Triviality" and How to Solve the LF Bound State Equation

光円錐量子化法の最大の利点は、この量子化では相互作用のある理論でも真空が摂動的に定義されたFock真空のままでよいという「真空の自明性」である。光円錐座標での分散関係 ($P^2 = 2P^+P^- - P_\perp^2 = M^2$)

$$P^- = \frac{P_\perp^2 + M^2}{2P^+} \tag{3}$$

の形から、「光円錐エネルギー」$P^- \geq 0$とすると、直ちに縦方向の運動量$P^+ \geq 0$が従う。つまり、$P^+ \neq 0$の粒子状態を使ってゼロ運動量状態を作ることができないため、Fock真空$|0\rangle$と混ざる状態が無く、もしメジャーゼロの$P^+ = 0$状態を無視できれば真空はFock真空のままという結論が得られる。

真空がFock真空で良いということは、さらにその上に作ったFock stateが励起状態に直接関与することを意味する。よって、一般にある励起状態はFock stateで次のように展開される。

$$|P^+, P_\perp, \lambda\rangle = \sum_{n,\lambda_i} \int \frac{dx_i d^2k_{\perp i}}{2(2\pi)^3} \Phi^{(n)}(x_i, k_{\perp i}, \lambda_i) |n;\ \{x_i P^+, k_{\perp i}, \lambda_i\}\rangle \tag{4}$$

ここで$\Phi^{(n)}(x_i, k_{\perp i}, \lambda_i)$と$|n;\{x_i P^+, k_{\perp i}, \lambda_i\}\rangle$は$n$体の波動関数とFock stateである。この状態を次の固有値方程式(Light-Front Bound State Equation, LFBSE)を解くことで求める ($H_{\rm LF} = P^-$)。

$$H_{\rm LF}|P^+, P_\perp, \lambda\rangle = \frac{P_\perp^2 + M^2}{2P^+}|P^+, P_\perp, \lambda\rangle \tag{5}$$

例えばメソンに対して行列表示をすると、次の無限次元固有値方程式を得る。

$$\left(M^2 - \sum_i \frac{k_\perp^2 + m_i^2}{x_i}\right)\begin{pmatrix}\Phi_{q\bar{q}} \\ \Phi_{q\bar{q}g} \\ \vdots\end{pmatrix} = \begin{pmatrix}\langle q\bar{q}|H_{\rm int}|q\bar{q}\rangle & \langle q\bar{q}|H_{\rm int}|q\bar{q}g\rangle & \cdots \\ \langle q\bar{q}g|H_{\rm int}|q\bar{q}\rangle & \langle q\bar{q}g|H_{\rm int}|q\bar{q}g\rangle & \\ \vdots & & \ddots\end{pmatrix}\begin{pmatrix}\Phi_{q\bar{q}} \\ \Phi_{q\bar{q}g} \\ \vdots\end{pmatrix} \tag{6}$$

この様な無限次元固有値方程式を解く方法もまた光円錐量子化法独特のものが考え出されており、以下に説明する3つの方法が有効であることが知られている。

- **DLCQ (Discretized Light-Cone Quantization)** [3]
  この手法の本質は単に「x^-方向を有限にする」だけだが、その威力はもの凄い。まずx^-を有限にし($-L \leq x^- < L$)、場には反周期的境界条件を課すことにすると、縦運動量は離散的になる。
  $$p_n^+ = \frac{\pi}{L}\left(n + \frac{1}{2}\right), \quad n \in \mathbf{Z}_{\geq 0} \tag{7}$$
  ここで$p_n^+ > 0$なので、Fock真空は完全に孤立し、他と混ざらない。さらにp_n^+が正であることから、全運動量$P^+ = \sum p_i^+$がある決まった値を与えるFock stateの数は有限(ある正の整数Nを正の整数で分割する場合の数)であり、行列の次元が有限になってしまう。その対角化は数値的には容易である。こうして結合定数の大きさに関係なく励起状態のスペクトルを得ることができる。実際1+1次元のQCDではメソン、バリオンの波動関数と質量を高励起状態まで求めることに成功している[4]。
- **LFTD (Light-Front Tamm-Dancoff approximation)** [5]
  この方法では無限次元のFock空間を有限粒子数の空間に限定する。さらに波動関数を有限個の基底で展開し近似すればLFBSEは有限次元になる。例えば(6)であれば$|\text{meson}\rangle = |q\bar{q}\rangle + |q\bar{q}g\rangle + |qq\bar{q}\bar{q}\rangle + \cdots$を初めの数項のみで近似し、さらにそれを有限個の基底で変分法的に解くことになる。この手法での近似の改良は、higher Fock statesを取り入れる方向と、基底の個数を増やす方向の2つになる。
- **Similarity Transformation** [6]
  この方法ではハミルトニアンを相似変換$S^\dagger H S = H'$によって徐々に対角化していく。ハミルトニアンの非対角成分$H_{ij} = \langle i|H|j\rangle$は一般にエネルギーの異なる状態間の結合を意味するので、非対角化部分を徐々に消す事ができれば各エネルギースケールが混ざりにくくなる。これは一種の「繰り込み」に相当する。そして、十分各エネルギー間の遷移が起こらないようなハミルトニアンを得ることができれば、そこでのTamm-Dancoff近似は、素朴に行なった場合よりもよい近似になると予想される。

3.2 "Vacuum Physics" on the Light Front

光円錐量子化法の最大の利点はその「真空の自明性」である。しかしQCDでの「カイラル対称性の自発的破れ」、「θ 真空」、「グルーオン凝縮」などの重要な性質は理論の真空が複雑な構造を持つことで通常は理解され、「真空の物理」と呼ばれる。では、これらの「真空の物理」は自明な真空構造をもつ光円錐量子化法ではどのようにして記述されるのだろうか。(3) 式をみると、「真空の自明性」の議論が破れる可能性があるのは $P^+ = 0$ モード（ゼロモード）についてだけであり、この部分に「真空の物理」の情報が押し込まれていると考えられている。このゼロモードの物理を取り扱うには次の3つの方法がある。

1. まともにゼロモードを取り扱う立場 [7]。DLCQ & 周期的境界条件で、直接ゼロモード自由度を扱う。
2. IR cutoff を導入してゼロモードを完全に排除する立場 [8]。(3) 式より、ゼロモード付近はエネルギーが発散することに注意。ゼロモードが持つはずの「非自明な真空」の情報は赤外発散に対する counter term が担うことになるので、非摂動的に繰り込みをする必要がある。
3. 光円錐直上から離れる立場 [9]。極限では光円錐量子化に一致するような量子化を考える。真空は自明ではなくなるが、真空の物理を議論することはできる。

このうち スカラー理論における自発的対称性の破れは 1. の方法でよく調べられており [10]、以下ではこの立場で南部 Jona-Lasinio 模型におけるカイラル対称性の破れを議論した我々の仕事を紹介しよう。スカラー理論でのやり方を利用するために、次の「カイラル湯川模型」を考える [11]。

$$\mathcal{L} = \bar{\Psi}_a(i\partial\!\!\!/ - m)\Psi_a + \frac{N}{2\mu^2}(\partial_\mu\sigma\partial^\mu\sigma + \partial_\mu\pi\partial^\mu\pi) - \frac{N}{2\lambda}(\sigma^2+\pi^2) - \sigma\bar{\Psi}_a\Psi_a - \pi\bar{\Psi}_a i\gamma_5\Psi_a, \tag{8}$$

ここで$\mu\to\infty$ の極限でσ とπ は補助場となりこの模型は南部 Jona-Lasinio 模型に帰着する。また、$1/N$ 展開を用いるために N 成分のフェルミオンΨ_a $(a=1,\ldots,N)$ を扱う。通常の枠組では $1/N$ 展開の主要項近似（フェルミオンの1ループ）の結果、$m=0$ のときに持つカイラル対称性は $\langle\sigma\rangle = -\frac{\lambda}{N}\langle\bar{\Psi}\Psi\rangle \neq 0$ によって自発的に破れることが容易に示せる。同じことを光円錐量子化で記述したい。そこでこの系を DLCQ で取り扱い、（スカラーに対して）周期的境界条件を課そう。するとゼロモード

$$\sigma_0(x_\perp) = \frac{1}{2L}\int_{-L}^{L} dx^-\ \sigma(x), \quad \pi_0(x_\perp) = \frac{1}{2L}\int_{-L}^{L} dx^-\ \pi(x) \tag{9}$$

をあからさまに扱えるようになる。さて、この系には光円錐量子化に特徴的な3つの拘束がある。フェルミオンの "bad component"ψ_- に対する拘束と2つのゼロモードに対する拘束である。

$$2i\partial_-\psi_-^a = (i\gamma^\perp\partial_\perp + m + \sigma - i\pi\gamma_5)\gamma^+\psi_+^a\ , \tag{10}$$

$$\left(\frac{\mu^2}{\lambda} - \partial_\perp^2\right)\begin{pmatrix}\sigma_0\\ \pi_0\end{pmatrix} - \frac{\mu^2}{N}\frac{1}{\sqrt{2}}\int_{-L}^{L}\frac{dx^-}{2L}\left[\psi_+^{a\dagger}\begin{pmatrix}-1\\ i\gamma_5\end{pmatrix}\gamma^-\psi_-^a + \psi_-^{a\dagger}\begin{pmatrix}-1\\ i\gamma_5\end{pmatrix}\gamma^+\psi_+^a\right] = 0 \tag{11}$$

ここで$\Psi = \psi_+ + \psi_-$, $\psi_\pm = \Lambda_\pm\Psi$, $\Lambda_\pm = \gamma^0\gamma^\pm/\sqrt{2}$. これらの拘束は、$\sigma_0$, π_0 および ψ_- が独立な自由度ではなく、スカラーの振動モードφ_σ, φ_πおよびフェルミオンの "good component" ψ_+によって書かれることを意味する。さて、ゼロモードを c 数部分と（正規順序化された）演算子部分に分けて書こう $\sigma_0 = \sigma_0^{(c)} + \sigma_0^{(op)}$, $\pi_0 = \pi_0^{(c)} + \pi_0^{(op)}$. もしこれらの c 数部分がゼロでないような解を求めることができたらそれは直ちに対称性の破れを与える。$\langle 0|\sigma|0\rangle = \sigma_0^{(c)} \neq 0$, $\langle 0|\pi|0\rangle = \pi_0^{(c)} \neq 0$. 従ってそのような解を見つけることが本質的であり、このアイディアの有効性はスカラー理論では確かめられている。そして、カイラル対称性の破れは、「ゼロモード拘束」を量子論的にかつ非摂動的に解くことで記述される。以下に我々の解析の結果をまとめる [11]。

- $1/N$ 展開の主要項でσに対するゼロモード拘束が次のギャップ方程式に帰着することが示される。

$$M - m = \lambda M\frac{\Lambda^2}{4\pi^2}\left\{2 - \frac{M^2}{\Lambda^2}\left(1 + \ln\frac{2\Lambda^2}{M^2}\right)\right\} \tag{12}$$

  ここで $M = m + \sigma_0^{(c)}$はフェルミオンの物理的質量である。この式を得る際、赤外発散の処理を慎重に行う必要がある（ここではパリティ不変な切断を導入）。ギャップ方程式の非自明な解 $(M \neq 0)$ を選ぶとカイラル対称性の破れた理論を得る。一方、自明な解 $(M = 0)$ はカイラル対称な理論を与える。
- カイラル対称性の破れた相と破れていない相でそれぞれ異なるラグランジアンを使い分けて、σ や πの質量を求めることができる。破れた相ではπ の質量は $m=0$ ではゼロになり、十分小さな $m\neq 0$ では Gell-Mann, Oakes, Renner 関係式を満たす。
- 光円錐上では対称性によらずに $Q_5^{\rm LF}|0\rangle = 0$ が成り立ってしまうので $\langle 0|\bar{\Psi}\Psi|0\rangle \neq 0$ と一見矛盾するように見えるが、それは破れた相でのカイラル変換が変更を受ける $[Q_5^{\rm LF}, \bar{\Psi}i\gamma_5\Psi] \neq 2i\bar{\Psi}\Psi$ ことで解決する。

- カイラルチャージ $Q_5^{\rm LF}$ は $m \to 0$ でも保存されないが、その原因がパイオンのゼロモードの特異的な振舞い $\pi_0 \sim 1/m$ に起因することが PCAC 関係式を通じてわかった。

なお、カイラル湯川模型 (8) を用いた間接的な方法でなく、南部 Jona-Lasinio 模型を直接解析しても破れを議論できることがわかっている [12]。その場合は ψ_- に対する複雑な拘束を解くことが重要になる。

4 Near Future [2000's −]

最後に光円錐量子化が今後取り組んでいくべき問題について触れる。まず、光円錐量子化法を用いれば QCD から構成子クォーク的描像が導けると期待されている [8]。そしてこの可能性をもう少し別の視点から見れば、深非弾性散乱の「非摂動的」な記述の枠組を自然に与えるものとしての光円錐量子化法が見えてくる。既に述べたように、深非弾性散乱にとってパートン描像が明白な光円錐上を出発点とすることは自然である。そしてごく最近、Harindranath らによって深非弾性散乱の「非摂動的」な記述を含む定式化がなされた [13]。光学定理 $W^{\mu\nu} = \frac{1}{2\pi}{\rm Im}T^{\mu\nu}$ によって $W^{\mu\nu}$ と関係づく virtual Compton 散乱の振幅 $T^{\mu\nu} = i\int d^4\xi\ {\rm e}^{iq\xi}\langle PS|T(J^\mu(\xi)J^\nu(0))|PS\rangle$ は Bjorken 極限において光円錐同時刻での 2 点関数で書けるので、それを出発点にすると、一般の場合はその同時刻面からのずれとして表される。すなわち、

$$T^{\mu\nu} = -\sum_{n=0}^{\infty}\left(\frac{1}{q^-}\right)^{n+1}\int d\xi^- d^2\xi_\perp\ {\rm e}^{iq\xi}\left\langle PS\middle|\left[\left(i\frac{\partial}{\partial\xi^+}\right)^n J^\mu(\xi),\ J^\nu(0)\right]_{\xi^+=0}\middle|PS\right\rangle. \tag{13}$$

つまり、この展開は光円錐エネルギーについての展開になっている。この記述の利点は全てが $\xi^+ = 0$ で評価できるということで、今まで述べてきた光円錐量子化法のハミルトン形式をこの行列要素を評価するのに直接利用することができる。すなわち、状態 $|PS\rangle$ は束縛状態の方程式 (5) を解いて与えればよい。そして、この枠組では高エネルギーから低エネルギーまでの深非弾性散乱を統一的に記述できると期待される。

応用可能な具体的な問題を挙げよう。例えば、パイオンの波動関数は Brodsky と Lepage の求めた $Q^2 \to \infty$ での形 $\phi_{\rm BL}(x) = \sqrt{3}f_\pi x(1-x)$ と Chernyak と Zhitnitsky が QCD 和則から求めた $Q^2 \sim (0.5{\rm GeV})^2$ での形 $\phi_{\rm CZ}(x) = 5\sqrt{3}x(1-x)(1-2x)^2$ は大きく異なり、現実の波動関数がどのような形であるか、あるいはどのようにしてこれらの 2 つの波動関数が関係つくのかなどの問題がある。これらの問題に対して光円錐量子化法での統一的な記述はまさにふさわしいと考えられる。前章の最後に触れた南部 Jona-Lasinio 模型では $1/N$ 展開の主要項の近似（平均場近似）では、$|\pi\rangle = |q\bar{q}\rangle$ で表され、パイオンの波動関数を具体的に求めることができる [12]。同じことを繰り込み可能な理論で行なえば高エネルギーから低エネルギーまでエネルギーが変化するときの波動関数の変化を議論できる。これは非摂動領域を含むため、通常の Q^2 発展とは異なることに注意して欲しい。つまり、摂動論では行けない領域にまで踏み込むことが原理的には可能なのである。

参考文献

[1] S. Brodsky, H. C. Pauli, and S. Pinsky, Phys. Rep. **301** (1998) 299.

[2] P. A. M. Dirac, Rev. Mod. Phys. **21** (1949) 392.

[3] H. C. Pauli and S. J. Brodsky, Phys. Rev. **D32** (1985) 1993; *ibid.* **D32** (1985) 2001.

[4] K. J. Hornbostel, S. J. Brodsky, and H. C. Pauli, Phys. Rev. **D41** (1990) 3814.

[5] R. J. Perry, A. Harindranath, and K. G. Wilson, Phys. Rev. Lett. **65** (1990) 2959.

[6] S.D.Glazek and K. Wilson, Phys. Rev. **D48** (1993) 5863, *ibid.* **D49** (1994) 4214.

[7] T. Maskawa and K. Yamawaki, Prog. Theor. Phys. **56** (1976) 270.

[8] K. Wilson, et al. Phys. Rev. **D49** (1994) 6720.

[9] For example, K. Hornbostel, Phys. Rev. **D45** (1992) 3781.

[10] T. Heinzl, et al., Z. Phys. C72 (1996) 353 and references therein.

[11] K. Itakura and S. Maedan, Prog. Theor. Phys. **97** (1997) 635; K. Itakura and S. Maedan, "*Dynamical Chiral Symmetry Breaking on the Light Front I. DLCQ Approach*" **hep-th/9907071**.

[12] K. Itakura, Prog. Theor. Phys. **97** (1997) 635; K. Itakura, Ph. D. Thesis (Univ. of Tokyo, Dec. 1996); K. Itakura and S. Maedan, "*Dynamical Chiral Symmetry Breaking on the Light Front II. NJL Model in the Continuum Approach*" (in preparation).

[13] A. Harindranath, R. Kundu, and W-M. Zhang, Phys. Rev. **D59** (1999) 094012, 094013.

23. Incident Energy Dependence of Collision Dynamics in A+A Reactions from AGS to SPS

Yasushi Nara
RIKEN BNL Research Center, Brookhaven National Laboratory, Upton, NY 11973 U.S.A
Advanced Science Research Center, Japan Atomic Energy Research Institute, Tokai, Naka, Ibaraki 319-11, Japan

Based on the hadronic transport model of JAM, I calculate the time evolution of particles, density, temperature and energy density for the heavy ion collision at the incident energies of AGS(11A GeV), JHF(25A GeV) and SPS(158A GeV). Microscopic calculations show that resonance matter with extremely large baryon density is created at AGS energy, while at JHF energy, quark matter with extremely large baryon density is suggested. At SPS energy, quark matter with large baryon density might be created.

I. INTRODUCTION

Heavy ion experiments at BNL-AGS and CERN-SPS have been performed motivating by the possible creation of QCD phase transition and vast body of systematic data such as proton, pion strangeness particles distributions, HBT correlation, flow, dileptons and J/ψ distributions have been accumulated including mass dependence and their excitation functions [1–3]. Data from forthcoming experiment at BNL-RHIC will soon become available.

In this work, I discuss the time evolution of matter which is created from high energy heavy ion collisions. To extract the properties of this matter, I use the microscopic transport model of JAM. Detailed description can be found in Ref. [5] and JAM is now available on web [4]. The purpose of this work is to find the differences in the matter produced from heavy-ion collisions at AGS, JHF, and SPS energies.

The article is organized in the following way. In section II, I summarize the main component of hadronic cascade model JAM. In section III, I first compare some JAM results to SPS data and discuss what is differences in the dynamics between AGS, JHF and SPS. In section,IV, I draw conclusions.

II. DESCRIPTION OF THE MODEL

In this section, I present the main features of the microscopic transport model of JAM. Relativistic Boltzmann equations for hadrons and their excitation states are solved on the computer in JAM. The main features in the Monet Carlo procedure are summarized as follows. (1) Nuclear collision is assumed to be described by the sum of independent binary hh collisions. Each hh collision is realized by the closest distance approach. In this work, no mean field is included, therefore the trajectory of each hadron is straight in between two-body collisions, decays or absorptions. (2) The initial position of each nucleon is sampled by the parameterized distribution of nuclear density. Fermi motion of nucleons are assigned according to the local Fermi momentum. (3) All established hadronic states, including resonances, are explicitly included with explicit isospin states as well as their anti-particles. All of them can propagate in space-time. (4) The inelastic hh collisions produce resonances at low energies while at high energies ($\gtrsim$ 4GeV in BB collisions $\gtrsim$ 3GeV in MB collisions and $\gtrsim$ 2GeV in MM collisions) color strings are formed and they decay into hadrons according to the Lund string model [6]. Formation time is assigned to hadrons from string fragmentation. Formation point and time are determined by assuming yo-yo formation point. This choice gives the formation time of roughly 1 fm/c with string tension $\kappa = 1$GeV/fm. (5) Hadrons which have original constituent quarks can scatter with other hadrons assuming the additive quark cross section within a formation time. The importance of this quark(diquark)-hadron interaction for the description of baryon stopping at CERN/SPS energies was reported by Frankfurt group [7,8]. (6) Pauli-blocking for the final nucleons in two-body collisions are also considered. (7) We do not include any medium effect such as string fusion to rope [9,7], medium modified cross sections and in-medium mass shift. All results which will be presented in this paper are those obtained from the free cross sections and free masses as inputs.

III. RESULTS

First, particle spectra calculated by JAM are compared with experimental data at SPS energies. A detailed comparison with AGS data can be found in Ref. [5]. Then calculated thermodynamical quantities at energies of AGS (10A GeV), JHF (25A GeV), and SPS(158A GeV) are presented in this section.

A. Comparison with sps data

I have calculated the system of Pb+Pb collision at SPS energies using the hadronic transport model of JAM 1.0, in order to show that this model accounts for gross features of heavy-ion collisions without any collective effect like string fusion or in-medium cross sections.

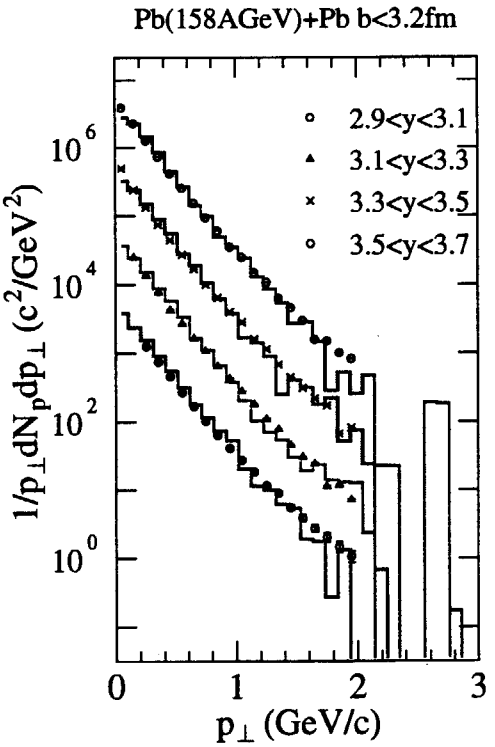

FIG. 1. The JAM calculation of transverse momentum distributions of negative charged particles ($\pi^-, K^-, \bar{p}$) for Pb + Pb collision at 158GeV/c with centrality 5%. Experimental data are taken from NA49 [10].

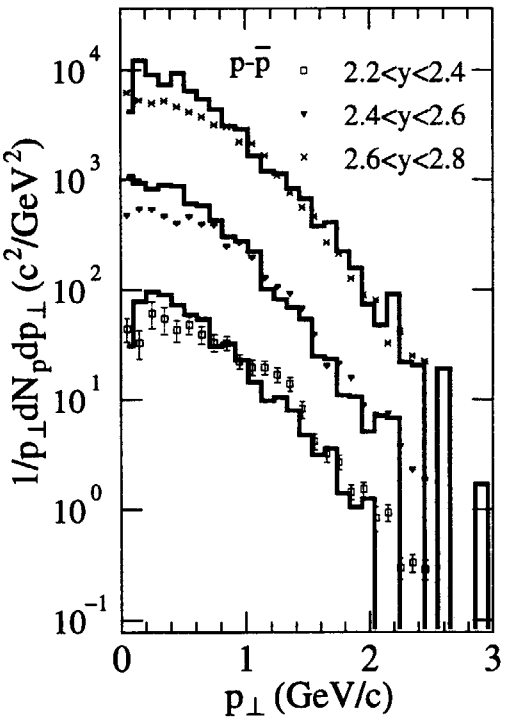

FIG. 2. The JAM calculation of transverse momentum distributions of net protons for Pb + Pb collision at 158GeV/c with centrality 5%. Experimental data are taken from NA49 [10].

In Fig. 1, JAM results of the transverse momentum distributions for negatively charged particles are compared to the NA49 data [10]. Transverse momenta of negatively charged particle are in good agreement with data.

Net proton transverse momentum distribution calculated by JAM is compared to experimental data of NA49 [10] in Fig. 2. Midrapidity protons at low momentum are slightly overpredicted in the model calculation. In order to reproduce data for Pb+Pb collisions, final state hadronic interaction is important. If we do not include meson-baryon and meson-meson collisions, the high momentum tail can not be reproduced within a hadronic transport approach.

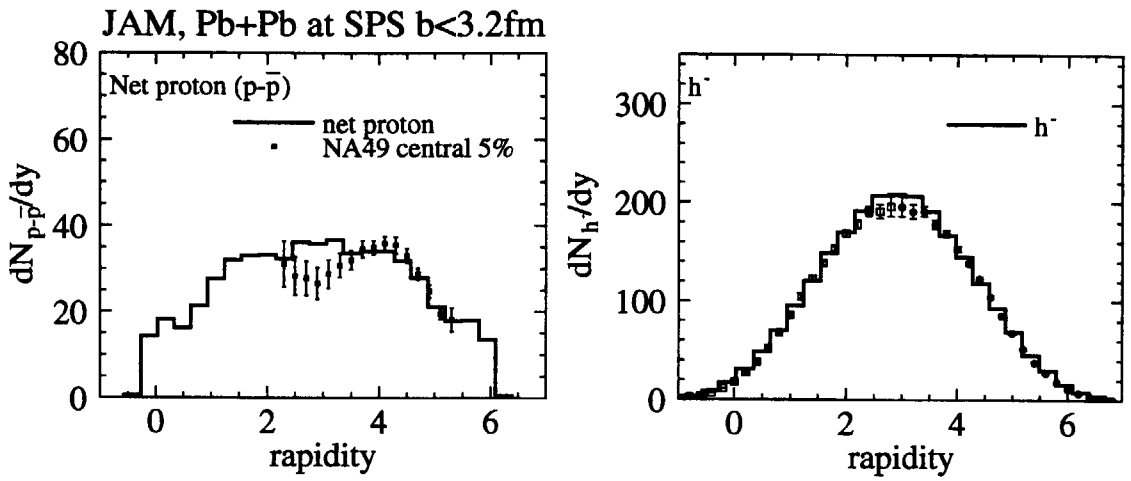

FIG. 3. Comparison of the rapidity distributions of net protons and negative particles for Pb+Pb collision at SPS energy between experimental data [10] and JAM calculations

I compare the data [10] on net proton and negative charged particle rapidity distributions in Fig. 3 for Pb+Pb collision at 158A GeV/c. The agreement is good for both negative particles and net protons. Secondary hadron-hadron interactions are not important for the rapidity distributions. The baryon stopping problem is one of the important element in nucleus-nucleus collisions. In order to reproduce baryon stopping at SPS energies with the phenomenological string model, the diquark breaking mechanism has to be included.

B. Dynamics from Hadronic transport model

Now I am going to see the time evolutions of thermodynamical values from hadronic cascade model. In the upper panel of Fig. 4, time evolution of nucleons, pions, their resonance states, and, constituent quarks which is attached at the end of strings are plotted for energies of 11.6, 25, and, 158AGeV. At the energy of 11AGeV/c, the degree of freedom is dominated by the excitations and evolution of resonances, however, above 25GeV energies, we can see that the number of quarks are larger than that of resonances.

In Fig. 4, the time evolution of temperature, pressure, baryon density, and energy density extracted from JAM simulations are plotted for the incident energies of 11.6A GeV/c (left), 25GeV (middle), and 158GeV/c (right). We define the temperature by the ratio of the pressure to the number density in the local rest frame, assuming that the local thermal equilibrium is always achieved for transverse motion. Here the pressure is defined by the two transverse diagonal component of the hadronic energy-momentum tensor. Theses quantities are extracted from the cascade simulation by using Gaussian smeared test particle method in a covariant way [11].

In the figures of temperature, we define two kind of temperature T and T_z. T is extracted from the transverse diagonal component of energy-momentum tensor, while T_z is obtained z-component of energy-momentum tensor. It is seen that those two temperatures become same at the certain point for all energies. That time is indicated by the vertical lines in the figure. This means that kinematical equilibrium is achieved. If we switch off secondary hadronic rescattering, systems do not equlibrate.

We see that pressures are almost the same for all incident energies, however, baryon densities at the equilibrated point are different, ρ_B/ρ_0 is about 5 at 11.6AGeV, 6 at 25GeV, and 4 at 158GeV. From this analysis, it is suggested that at 25AGeV, baryon density is the highest and the produced matter is dominated by the quark degree of freedom.

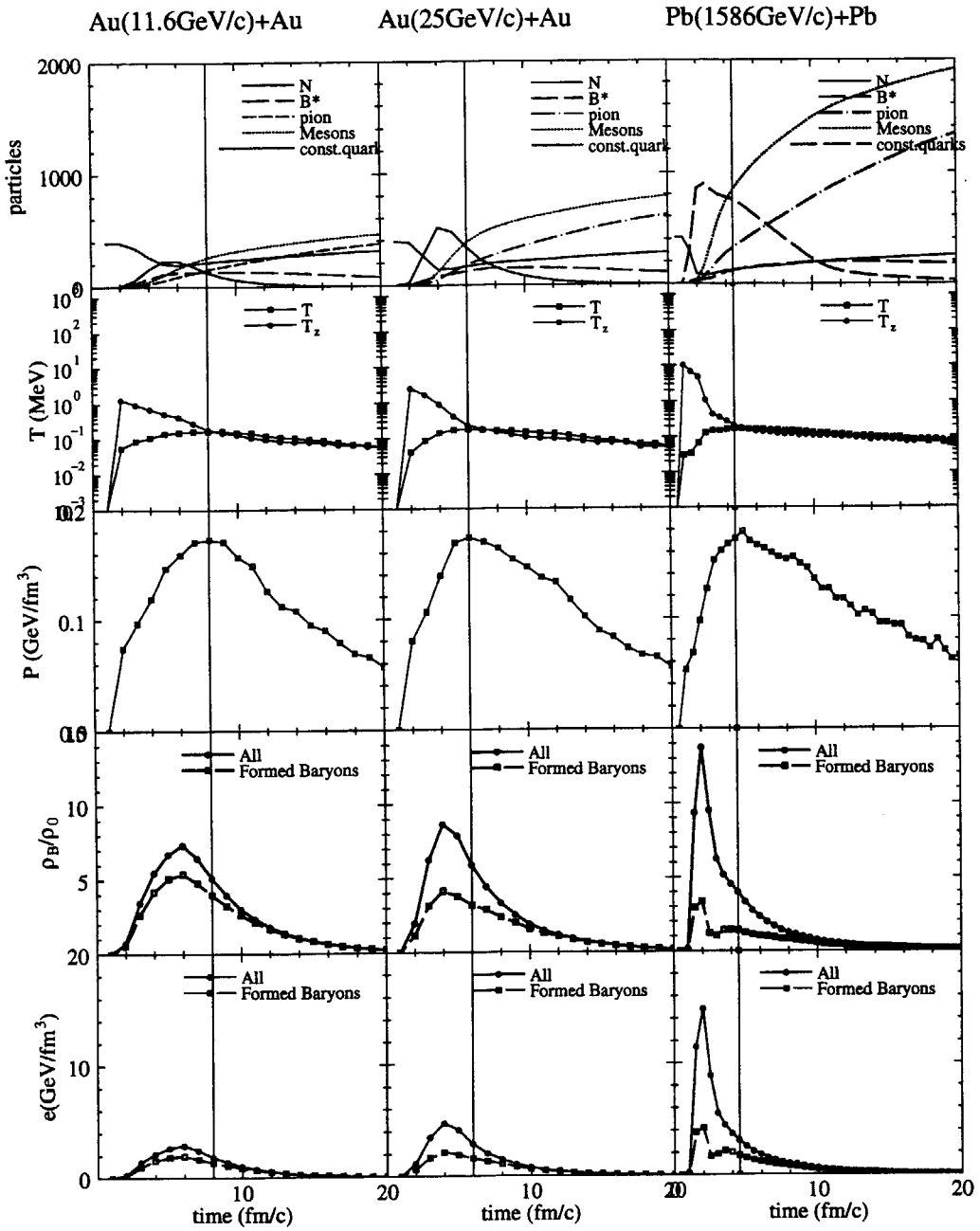

FIG. 4. The time evolution of particles, temperature, pressure, baryon density, and energy density extracted from JAM simulations are plotted for the incident energies of 11.6A GeV/c (left), 25GeV (middle), and 158GeV/c (right).

In Fig. 5, in order to see the path clearly, of the hot and dense matter, the T-ρ_B diagram is plotted. It is seen that later phase of the time evolution of the matter at AGS and JHF energies are quite similar, but baryon density at the initial phase at JHF is larger in comparison with AGS energies. At SPS, higher temperature and lower baryon density matter is predicted by this model calculation.

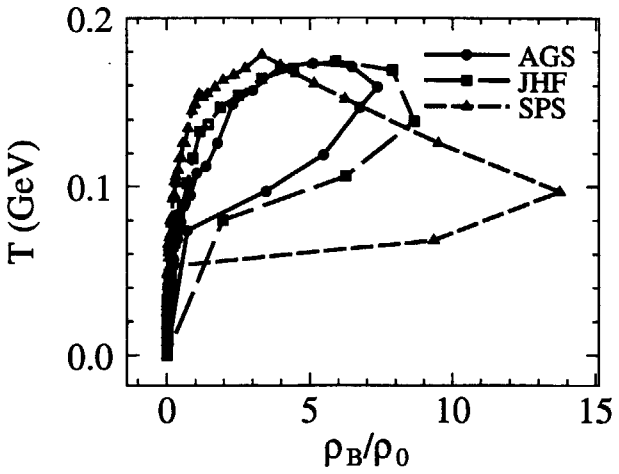

FIG. 5. Time evolution of baryon density and effective temperature in Au+Au at 11.6AGeV/c from 0 fm/c to 20 fm/c by 1.0 fm/c step, Au+Au at 25AGeV, and Pb+Pb at 158AGeV, respectively.

IV. SUMMARY

In summary, incident energy dependence of thermodynamic evolution was investigated with the microscopic transport model JAM. It is found that (1) at all incident energies, hadronic rescattering make the created hot and dense matter equilibrate, (2) at AGS energies, extremely large baryon density of hadronic resonance matter is produced, while at JHF energies, produced matter might be quark matter instead of resonance matter whose baryon density is larger than that of AGS energies, at SPS energies, quark matter, but baryon density is smaller than that of JHF.

---

[1] Proceedings of Quark Matter '96, *Nucl. Phys.* **A610**, 1c (1996).
[2] Proceedings of Quark Matter '97, *Nucl. Phys.* **A638**, 1c (1998).
[3] Proceedings of Quark Matter '99, to be published in *Nucl. Phys.* A.
[4] http://quark.phy.bnl.gov/~ynara/jam/.
[5] Y.Nara, N. Otuka, A. Ohnishi, K. Niita and S. Chiba, in press in Phys. Rev. C; nucl-th/9904059.
[6] T. Sjöstrand, *Comp. Phys. Comm.* **82**, 74 (1994); PYTHIA 5.7 and JETSET 7.4 Physics and Manual. *http://thep.lu.se/tf2/staff/torbjorn/Welcome.html.*
[7] H. Sorge, R. Mattiello, A. Jahns, H. Stöcker and W. Greiner, *Phys. Lett.* B **271**, 37 (1991); H. Sorge, L. Winckelmann, H. Stöcker and W. Greiner, *Z. Phys.* C **59**, 85 (1993).
[8] L.A. Winckelmann, S.A. Bass, M. Bleicher, M. Brandstetter, A. Dumitru, C. Ernst, L. Gerland, J. Konopka, S. Soff, C. Spieles, H. Weber, C. Hartnack, J. Aichelin, N. Amelin, H. Stöcker and W. Greiner, *Nucl. Phys.* **A610**, 116c (1996); nucl-th/9610033; S.A. Bass, M. Belkacem, M. Bleicher, M. Brandstetter, L. Bravina, C. Ernst, L. Gerland, M. Hofmann, S. Hofmann, J. Konopka, G. Mao, L. Neise, S. Soff, C. Spieles, H. Weber, L.A. Winckelmann, H. Stöcker, W. Greiner, C. Hartnack, J. Aichelin and N. Amelin, *Prog. Part. Nucl. Phys.* **41**, 225 (1998); nucl-th/9803035.
[9] K. Werner, *Z. Phys.* C **42**, 85 (1989); *Phys. Rev.* **232**, 87 (1993).
[10] NA49, *Phys. Rev. Lett.* **82**, 2471 (1999).
[11] C. Fuchs and H. H. Wolter, Nucl. Phys. **A589** (1995), 732.

24. Roles of the sigma meson in QCD and possible experiments to observe it

Teiji Kunihiro
Faculty of Science and Technology, Ryukoku University, Seta, Otsu, 520-2194, Japan

Abstract

Theoretical and phenomenological significance of the sigma meson (σ) in QCD is discussed: If the scalar-isoscalar meson with the mass 500-700 MeV exists, various empirical facts in hadron physics can be naturally accounted for, which otherwise would remain mysterious. We propose several experiments to produce and detect the σ in nuclei using nuclear and electro-magnetic projectiles. The recent CHAOS data which show a spectral enhancement near the 2 m_π threshold in the σ channel from the reactions A$(\pi, 2\pi)$A' where A and A' denotes nuclei is interpreted as a possible evidence of a partial restoration of chiral symmetry in nuclei.

1 Introduction

The particle representing the quantum fluctuation of the order parameter $\tilde{\sigma} \sim \langle (: \bar{q}q :)^2 \rangle$ is the σ meson. The σ meson is analogous to the Higgs particle in the Weinberg-Salam theory. The σ together with the pion constitutes a quartet of $SU_L(2) \otimes SU_R(2)$ symmetry in QCD.

Some effective theories[1, 2] including the ladder QCD[3] and Weinberg's mended symmetry[4] predict the σ meson mass $m_\sigma \sim$ 500-700 MeV: The Nambu-Jona-Lasinio(NJL) model[5] is now widely used as an effective theory for describing the chiral properties of QCD[2]. In this model, the chiral symmetry is realized linearly like the linear sigma models, hence the appearance of the σ meson is inevitable; one has the σ meson as well as the pions, and the chiral symmetry makes m_σ twice of the constituent quark mass $M_q \sim 335$ MeV as well as the pions are massless in the chiral limit [5], hence

$$m_\sigma \sim 2M_q \sim 670\text{MeV}. \tag{1}$$

The significance of this relation in the context of QCD was emphasized by us in [1].

If such a scalar meson with a low mass is identified, many experimental facts which otherwise are mysterious can be nicely accounted for in a simple way[2, 6]: (1) The correlation in the scalar channel as summarized by such a scalar meson can account for the $\Delta I = 1/2$ rule for the decay process $K^0 \to \pi^+\pi^-$ or $\pi^0\pi^0$ [7]. (2) In the meson-theoretical model for the nuclear force, a scalar meson exchange with the mass range 500$\sim$ 700 MeV is indispensable to fully account for the state-independent attraction in the intermediate range. (3) The collective excitation in the scalar channel as described as the σ meson is essential in reproducing the empirical value of the π-N sigma term $\Sigma_{\pi N} = \hat{m}\langle \bar{u}u + \bar{d}d \rangle$, the empirical value of which is reported to be 45 ± 10 MeV. (4) The convergence radius of the chiral perturbation theory is linked with the mass of the scalar meson.

Recent phase shift analyses of the π-π scattering in the scalar channel claim a pole of the scattering matrix in the complex energy plane with the real part $\mathrm{Re}m_\sigma$ = 500-700 MeV and the imaginary part $\mathrm{Im}m_\sigma \simeq$ 500MeV[8], although the possible coupling with glue balls with $J^{PC} = 0^{++}$ make the situation obscure. Our view about the identification of the scalar mesons is given in chapter 3 of ref.[2].

2 Experiments to produce the σ using nuclear targets

Since the σ meson is the fluctuation of the order parameter of the chiral transition, it will become a soft mode and induce characteristic phenomena associated with the chiral restoration in a hot and/or dense nuclear medium. Thus one may expect a better chance to see the σ meson in a clearer way in a hot and/or dense medium than in the vacuum[9, 2]. Such a behavior of the meson may be detected by observing two pions with the invariant mass around several hundred MeV in relativistic heavy ion collisions.

Some years ago, the present author proposed several experiments [6] to possibly produce the σ meson in nuclei, thereby to have a clearer evidence of the existence of the σ meson and also explore the possible restoration of chiral symmetry in the nuclear medium:

A (π, σ N) A′ The charged pion ($\pi^{\pm}$) is absorbed by a nucleon in the nucleus, then the nucleon emits the σ meson, which decays into two pions. To make a veto for the two pions from the rho meson, the produced pions should be neutral ones which may be detected through four γ's.

A (N, σ N) A′ N may be a proton, deuteron or ^{3}He, namely any nuclear projectile, which collides with a nucleon in the nucleus, then the incident particle will emit the σ meson, which decays into two pions. One may detect 4 γ 's from 2 π^0 which is the decay product of the σ. The collision with a nucleon may occur after the emission of the σ meson; the collision process is needed for the energy-momentum matching. In the detection, one may use the two leptons from the process. This is possible when the sigma has a finite three because of the scalar-vector mixing in the system with a finite baryonic density. This detection may gives a clean data, but the yield might be small.

Photo-σ production off a nucleus The γ ray is converted to the omega meson in accord with the vector meson dominance principle, if the particle has a finite three momentum. The omega meson may decay into the σ meson in the baryonic medium via the process $\omega \to \mathrm{N}\,\bar{\mathrm{N}} \to \sigma$. The σ will decay into two pions.

3 The spectral function in the $I = J = 0$ channel in the nuclear medium

When a hadrons is put in a nucleus, the hadron will couple strongly to various excitations in the system, such as nuclear particle-hole (p-h) and Δ-hole excitations, simultaneous excitations of them and mesons and so on. In general, the hadron may dissociate into complicated excitation to loose its identity in the nuclear medium. Thus the relevant quantity is the response function or spectral function of the system when the quantum numbers of the hadron are put in. A response function in the energy-momentum space is essentially the spectral function in the meson channel. If the coupling of the hadron with the environment is relatively small, then there may remain a peak with a small width in the spectral function, which correspond to the hadron; such a peak may be viewed as an elementary excitation or a quasi particle known in Landau's Fermi liquid theory for fermions. It is a difficult problem whether a many-body system can be treated as an aggregate of elementary excitations or quasi-particles interacting weakly with each other. Landau gave an argument that there will be a chance to describe a system as an assembly of almost free quasi-particles owing to the Pauli principle when the temperature is low. Then how will the decrease of m_σ in the nuclear medium[9] reflect in the spectral function in the sigma channel?

A calculation of the spectral function in the σ channel at finite T has been performed with the σ-2π coupling incorporated in the linear σ model[10]; it was shown that the enhancement of the spectral function in the σ-channel just above the two-pion threshold can be a signal of the decrease of m_σ, i.e., a softening; see also [11].

Recently, it has been shown [12] that the spectral enhancement associated with the partial chiral restoration takes place also at finite baryon density close to $\rho_0 = 0.17\text{fm}^{-3}$. Consider the propagator of the σ-meson at rest in the medium : $D_\sigma^{-1}(\omega) = \omega^2 - m_\sigma^2 - \Sigma_\sigma(\omega;\rho)$, where m_σ is the mass of σ in the tree-level, and $\Sigma_\sigma(\omega;\rho)$ is the loop corrections in the vacuum as well as in the medium. The corresponding spectral function is given by

$$\rho_\sigma(\omega) = -\pi^{-1}\text{Im}D_\sigma(\omega). \tag{2}$$

We parameterize the chiral condensate in nuclear matter $\langle\sigma\rangle$ as $\langle\sigma\rangle \equiv \sigma_0\ \Phi(\rho)$. In the linear density approximation, $\Phi(\rho) = 1 - C\rho/\rho_0$ with $C = (g_s/\sigma_0 m_\sigma^2)\rho_0$. Instead of using g_s, we use Φ as a basic parameter in the following analysis.

The spectral function together with $\text{Re}D_\sigma^{-1}(\omega)$ calculated with a linear sigma model are shown in Fig.1: The characteristic enhancements of the spectral function just above the $2m_\pi$. The mechanism of the enhancement is understood as follows. The partial restoration of chiral symmetry implies that m_σ^* approaches towards m_π. On the other hand, $\text{Re}D^{-1}(\omega)$ has a cusp at $\omega = 2m_\pi$. The cusp point goes up with the density and eventually hits the real axis at $\rho = \rho_c$ because $\text{Re}D^{-1}(\omega)$ increases associated with $m_\sigma^* \to 2m_\pi$. It is also to be

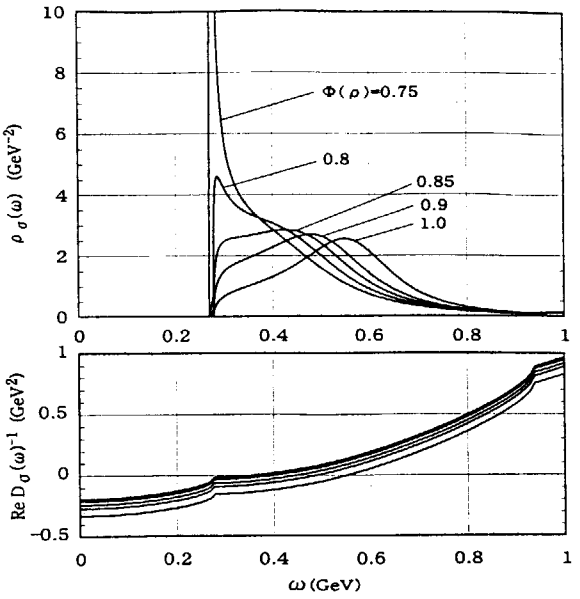

Fig.1 Spectral function for σ and the real part of the inverse propagator for several values of $\Phi = \langle\sigma\rangle/\sigma_0$ with $m_\sigma^{peak} = 550$ MeV. In the lower panel, Φ decreases from bottom to top.

noted that even before the σ-meson mass m_σ^* and m_π in the medium are degenerate,i.e., the chiral-restoring point, a large enhancement of the spectral function near the $2m_\pi$ is seen.

Recently CHAOS collaboration [13] measured the $\pi^+\pi^\pm$ invariant mass distribution $M^A_{\pi^+\pi^\pm}$ in the reaction $A(\pi^+, \pi^+\pi^\pm)X$ with the mass number A ranging from 2 to 208: They observed that the yield for $M^A_{\pi^+\pi^-}$ near the $2m_\pi$ threshold is close to zero for $A = 2$, but increases dramatically with increasing A. They identified that the $\pi^+\pi^-$ pairs in this range of $M^A_{\pi^+\pi^-}$ is in the $I = J = 0$ state. The A dependence of the the invariant mass distribution presented in [13] near $2m_\pi$ threshold has a close resemblance to our model calculation shown in Fig.1, which suggests that this experiment may already provide a hint about how the partial restoration of chiral symmetry manifest itself at finite density.

It should be mentioned that conventional nuclear many-body effects can cause an enhancement of the spectral function as seen in the CHAOS experiment[15, 16]. However, as emphasized in [16], such many-body effects solely is not sufficient to reproduce the enhancement seen in the experiment.

To confirm and understand the underlying mechanism of the threshold enhancement, the measurement of $2\pi^0$ and 2γ in experiments with hadron/photon beams off heavy nuclear targets is desirable. When σ has a finite three momentum, one can detect dileptons through the scalar-vector mixing in matter: $\sigma \to \gamma^* \to e^+e^-$. We remark that (d, ^{3}He) reaction is also useful to produce the excitations in the σ channel in a nucleus because of the large incident flux. The incident kinetic energy E of the deuteron in the laboratory system is estimated to be 1.1GeV $< E <$ 10 GeV, to cover the spectral function in the range $2m_\pi < \omega <$ 750 MeV. A recent theoretical investigation[14] shows a possibility of formation of sigma-mesic nuclei when the rate of the chiral restoration is considerable.

In conclusion, I thank T. Hatsuda, H. Shimizu, S. Hirenzaki and H. Nagahiro for their collaboration.

References

[1] T. Hatsuda and T. Kunihiro, Prog. Theor. Phys. **74** , 765 (1985).

[2] T. Hatsuda and T. Kunihiro, Phys. Rep. **247**, 221 (1994), and references therein.

[3] V. Elias and M. Scadron, Phys. Rev. Lett. **53**,1129 (1984).

[4] S. Weinberg, Phys. Rev. Lett., **65**, 1177 (1990).

[5] Y. Nambu and G. Jona-Lasinio, Phys. Rev. **122**,345 (1961).

[6] T. Kunihiro, Prog. Theor. Phys. Suppl. **120** , 75 (1995).

[7] E. P. Shabalin, Sov. Phys. J. Nucl. Phys., **48**, 172(1988); T. Morozumi et al, Phys. Rev. Lett., **65** , 404 (1990.

[8] Particle Data Group, Eur. Phys. J. **C** 363, 390 (1998). See also the recent analyses of σ: R. Kaminski et al, Phys. Rev. **D50**, 3145 (1994); S. Ishida et al., Prog. Theor. Phys. **95**, 745, **98**, 1005 (1997); N. A. Törnqvist and M. Roos, Phys. Rev. Lett. **76**, 1575 (1996); M. Harada, F. Sannino and J. Schechter, Phys. Rev. **D54**, 1991 (1996); J. A. Oller, E. Oset and J. R. Peláez, Phys. Rev. Lett. **80**, 3452 (1998); K. Igi and K. Hikasa, Phys. Rev. **D59**, 034005 (1999).

[9] T. Hatsuda and T. Kunihiro, Phys. Lett. **B 145**,7(1984); Phys. Rev. Lett. **55**, 158 (1985); Phys. Lett. **B185**, 304 (1987).

[10] S. Chiku and T. Hatsuda, Phys. Rev. **D58**, 076001 (1998).

[11] M.K. Volkov, E.A. Kuraev, D. Blaschke, G. Roepke and S. Schmidt, Phys. Lett. **B 424**, 235 (1998).

[12] T. Hatsuda, T. Kunihiro and H. Shimizu, Phys. Rev. Lett. **82**, 2840 (1999).

[13] F. Bonutti et al. (CHAOS Collaboration), Phys. Rev. Lett. **77**, 603 (1996).

[14] S. Hirenzaki, H. Nagahiro, T. Hatsuda and T. Kunihiro, contribution to PANIC 99.

[15] R. Rapp, et al, Phys. Rev. **C 59** (1999), R1237; see also Z. Aouissat, G. Chanfray, P. Schuck and J. Wambach, `nucl-th/9908076`.

[16] M. J. Vicente Vacas and E. Oset, `nucl-th/9907008`.

25. Nuclear matter in neutron star crust

Toshihiko Kido[a], Toshiki Maruyama[a], Koji Niita[b] and Satoshi Chiba[a]

[a]Advanced Science Research Center, Japan Atomic Energy Research Institute,
Tokai, Naka, Ibaraki, 319-1195 Japan

[b]Research Organization for Information Science & Technology,
Tokai, Naka, Ibaraki, 319-1106 Japan

Properties of nuclear matter below the nuclear saturation density is analized by numerical simulations with the periodic boundary condition. The equation of state at these densities is softened by the formation of cluster(s) internal density of which is nearly equal to the saturation density. The structure of nuclear matter shows some exotic shapes with variation of the density. Furthermore, it is found that the symmetry parameter $a_{\rm sym}(\rho)$ is not a linear function of density at low density region.

1. INTRODUCTION

The research for the property of nuclear matter has been attracting great attentions since the beginning of nuclear physics. By the discovery of neutron stars, the existence of giant nuclear matter became evident. The property of nuclear matter is essential to understand basic characteristics of neutron stars.

Various strange shaped (e.g. cylindrical, tabular) nuclear matter structures below the saturation density have been predicted by several macroscopic models which assume nuclear matter shapes [1–3] or Thomas Fermi calculation which deals with nuclear matter as a continuum [4]. These studies have shown that the structure is determined by the balance between surface tension and repulsive Coulomb force. As a result, the structure of stable nuclear matter changes from finite nucleus (sphere) to giant cluster (rod, plate, cylindrical-hole and spherical-hole) with increase of global density. Above the saturation density, the uniform structure is stable.

Recently, Maruyama *et al.* proposed a new approach for the study of nuclear matter [5]. This method is based on a microscopic treatment of particles, namely MD simulation. Therefore the effects of clusterization can be taken into account without any assumption of the structure. However, properties of finite nuclei, for instance radius and shape, were not well reproduced with the effective interaction employed by them.

The purpose of present study is to give more quantitative analysis of the nuclear structure in the low-density nuclear matter which is strongly related with the crust region of the neutron stars. We improve the effective nuclear interaction to reproduce the properties of the finite nuclei better than the previous calculation [5].

2. FRAMEWORK OF SIMULATION

We treat nucleons (protons, neutrons) as the constituent particles. Each particle is described by a gaussian wave packet characterized by the coordinate, the momentum and the width.

2.1. Interaction between particles

Our interaction contains Skyrme-type two-body and density dependent, symmetric, surface, momentum dependent term, and Pauli interaction which is an artificial repulsive one between two particles of the same kind. We determine the parameters of the nuclear potential to reproduce the bulk property of nuclear matter and the properties of stable nuclei, namely, binding energy and root-mean-square radius as shown in Figs. 1 and 2. Surface term which is newly added term make the surface property of nucleus smooth. Therefore the radii of stable nuclei are reproduced well.

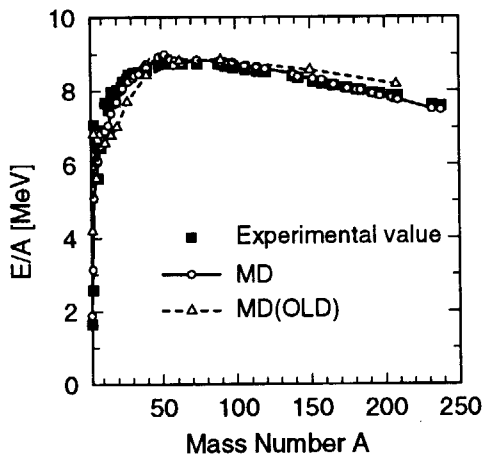

Figure 1: Binding energy of finite nuclei.

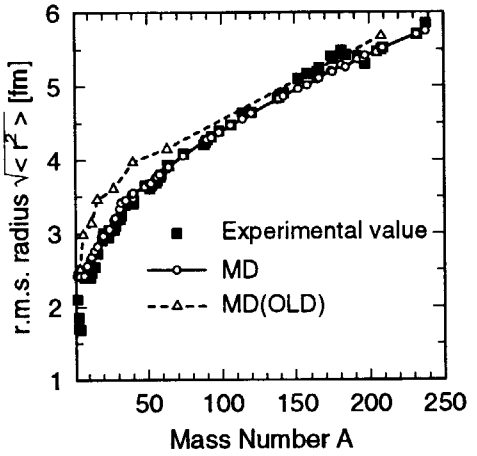

Figure 2: Root-mean-square radius of finite nuclei.

2.2. Simulation for infinite system

We simulate infinite system by employing the periodic boundary condition [6]. The volume containing the N particles is treated as the primitive cell of an infinite periodic lattice of identical cells. Each particle interacts with all other particles in the same cell and all particles in all other cells. The actual number of N in this paper is 3072.

Initial position and momentum of particles are given randomly, and we cool down or heat up the system by frictional cooling [7] or Metropolis sampling [8]. Finally, we get the ground state or the excited state with a certain temperature. Many calculations are carried out by changing the density ρ, proton fraction Z/A and temperature T of nuclear matter.

3. STRUCTURES OF NUCLEAR MATTER

Figure 3 shows the density dependence of symmetric matter structure. One box corresponds to the fundamental cell. At saturation density, uniform structure is stable.

However, as density becomes lower particles form clusters, showing that uniform structure become unstable. At $0.5\rho_0$, there appears the structure with cylindrical-holes. At $0.1\rho_0$, many spherical nuclei can be seen.

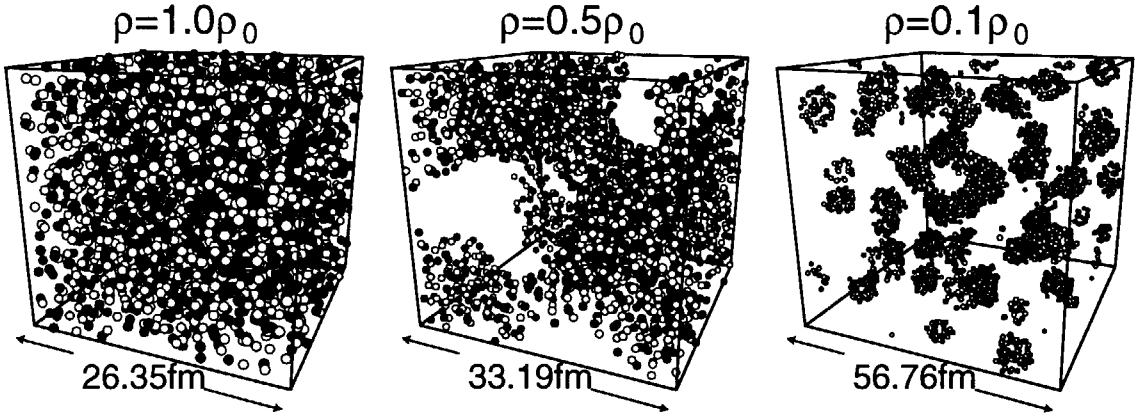

Figure 3: Examples of symmetric matter structure. Black circles denote protons and white are neutrons.

Figures 4 and 5 show the energy of symmetric matter and neutron matter, respectively. Our model reproduces the well known bulk property of symmetric matter at the region near saturation density (ρ_0). At low density region, our results deviate from the parabolic behavior. We find that the effect of clusterization softens the EOS. For the neutron matter EOS, our result agrees with RBHF calculation [9]. This fact give us a confidence that the interaction used in our simulation can well be applied for the study of neutron star matter which lies in between these two extreme conditions.

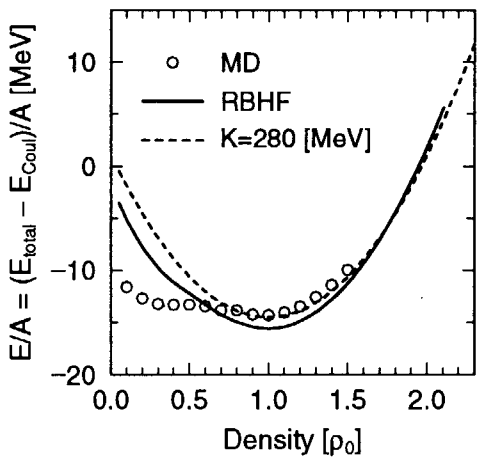

Figure 4: EOS of symmetric matter.

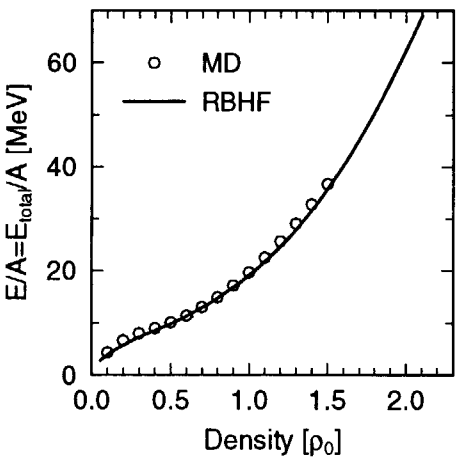

Figure 5: EOS of neutron matter.

Figure 6 shows the EOS of asymmetric matter. From the energy of asymmetric matter for several given densities, we estimate the density dependence of symmetry parameter $a_{\rm sym}(\rho)$ defined by the second derivative of $E(\rho,\alpha)/A$ over $\alpha = (N-Z)/A$ at $\alpha = 0$.

Figure 7 shows the density dependence of symmetry parameter in comparison with DBHF calculation [10]. We find the symmetry parameter is not proportional to density below the saturation density. This can be understood as the effect of clusterization.

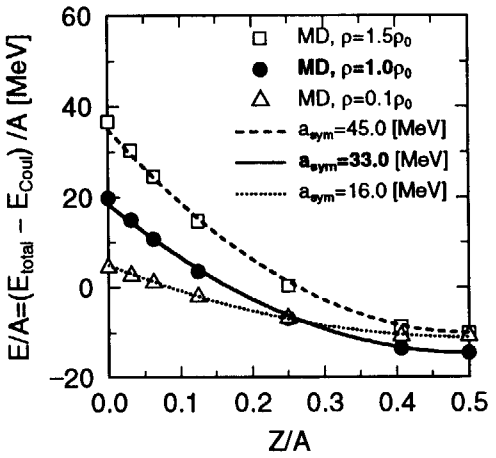

Figure 6: EOS of asymmetric matter.

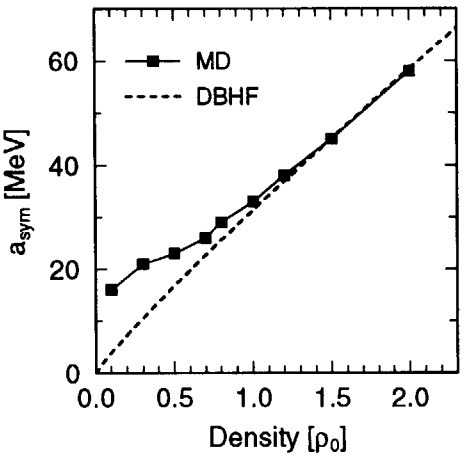

Figure 7: Density dependence of symmetry parameter.

4. SUMMARY

We have analyzed infinite system of nucleons by a molecular dynamics simulation with the periodic boundary condition. At extremely low temperature, the structure of nuclear matter below saturation density is not uniform and nucleons form $\rho \sim 1.0\rho_0$ aggregate(s). The density dependence of symmetry parameter for $\rho \leq \rho_0$ is not a linear function of ρ because of the effects of clusterization. Our results for finite temperature will be reported elsewhere. The EOS of neutron star matter is now under investigation!

REFERENCES

1. D.G. Ravenhall, C.J. Pethick and J.R. Wilson, Phys. Rev. Lett. 50 (1983) 2066.
2. M. Hashimoto, H. Seki and M. Yamada, Prog. Theor. Phys. 71 (1984) 320.
3. K. Oyamatsu, Nucl. Phys. A561 (1993) 431.
4. R.D. Williams and S.E. Koonin, Nucl. Phys. A435 (1985) 844.
5. T. Maruyama, K. Niita, K. Oyamatsu T. Maruyama, S. Chiba and A. Iwamoto, Phys. Rev. C57 (1998) 655.
6. D. Frenkel and B. Smit, "Understanding Molecular Simulation", Academic Press (1996).
7. L. Wilets, E.M. Henley, M. Kraft and A.D. Mackellar, Nucl. Phys. A282 (1977) 341.
8. N. Metropolis, A.W. Rosenbluth, M.N. Rosenbluth, A.H. Teller and E. Teller, J. Chem. Phys. 21 (1953) 1087.
9. K. Sumiyoshi, K. Oyamatsu and H. Toki, Nucl. Phys. A595 (1995) 327.
10. C.-H. Lee, T.T.S. Kuo, G.Q. Li and G.E. Brown, Phys. Rev. C57 (1998) 3488.

26. In-medium Properties of Antiproton in high energy reactions
高エネルギー原子核反応を用いた反陽子の媒質効果の研究

丸山 智幸
日本大学生物資源科学部

概 要

Using the RBUU approach we calculate the subthreshold production of antiprotons in the p- and d-nucleus reacitions done by the KEK-ps collaboration. Then we attempt to determine the depth of the anti-proton potential at the normal nuclear density from experimental data of these reacions. by introducing the

近年、数 GeV/u 以上のエネルギーを持つ加速器を用いた、ハドロンの性質に対する核媒質の効果を実験的に研究をしようという多くの試みがなされている。その中で、通常の理論値との差が非常に大きく、従って、大きな媒質効果の存在が最も期待されるものに反陽子がある。

JINR [1]、BEVELAC [2]、SIS [3] 等でおよそ 2GeV/u 程度のサブスレシュホールド・エネルギー領域での重イオンビームを用いた実験が行われたが、それらの実験における反陽子生成数は理論の予想をはるかに上回っていた。もし何らの媒質効果を仮定しなければ、第一機会衝突模型 [4] では実験値の 1/1000、多重衝突の効果を取り入れた BUU [5]、QMD [6] といった数値シミュレーション模型でも実験値の 1/10 しか説明できなかった。

ところで、反陽子の大きな媒質効果を予言する理論として、相対論的平均場理論 (RMFT) が存在する [7]。この RMFT では核子の波動関数は以下のような Dirac 方程式で示される。

$$\{\gamma^{\mu}(i\partial_{\mu} - U_{\mu}(x)) - (M - U_s(x))\}\psi(x) = 0. \tag{1}$$

上記の式で U_s はローレンツ・スカラー、U_{μ} は 4 元のローレンツ・ベクター・ポテンシャルを表す。静的な原子核内部では、核子に対してはスカラー場は引力であり、ベクター場の時間成分は斥力であり（空間成分は非常に小さくなる)、それらのポテンシャルの深さはおよそ 300 ~ 500MeV と非常に深いものである。ただし、この 2 種類の Dirac ポテンシャルは、非相対論的模型における中心力ポテンシャル U_c との対応は近似的に

$$U_c = -U_s + U_0 \tag{2}$$

で表され、互いに相殺する関係となっている。

さて、この模型を反陽子に適応すると従来の考えと大きく違う様相が見えてくる。U_s と U_0 を完全な一体場あるいは RMFT でよく行われている相対論的ハートリー (RH) 近似による平均場で

あると仮定すると、反陽子では，ベクター場の符号が逆転してしまい約700MeVという非常に強い引力場を感じることになってしまう。

ここで有効質量M^*を以下のように定義すると、

$$M^* = M - U_s, \tag{3}$$

原子核内部での陽子反陽子対生成のエネルギー敷地は$2M^*$となり、真空中での値$2M$の0.5～0.7倍と非常に小さいものになってしまう。もし、このことが正しいとするならば、陽子反陽子対は真空中よりも核媒質中でかなり生成されやすいこととなる。従って、通常考えられないくらい非常に多くの反陽子が生成されるという実験現象を、このDiracポテンシャルの効果による生成スレシュホールド・エネルギーによって説明できるのではないかと考えるのは極めて自然なことである。

ところで、Diracポテンシャルは、多核子系での自己エネルギーであり、RH近似で求まるような簡単な平均場ではない。例えば、Fock項まで考慮した計算では反陽子ポテンシャルはRHのものと比べかなり小さいものとなる[8]。現実的な原子核との相互作用においては核子との対消滅による反陽子の吸収が非常に大きく、従って、その吸収に対応するポテンシャルの虚数部分もまた大きいことになる。このことは1ボソン交換力による平均場では反核子の一体ポテンシャルを記述できないことを示しているが、さらに虚数部分から分散関係により実部分を予想すると、単純なGパリティー変換とは大きく異なり、RHで予想されるものよりもかなり小さいものと考える必要がある[9]。

さて、RMFTとBUUを組み合わせたRBUU法による反陽子生成の理論的解析がギーセン・グループ[9]とテキサス・グループ[10]で行われ、核子の感じる平均場が有効質量が$M^*/M = 0.65-0.7$と比較的深いときに、反陽子が強い引力を感じれば実験結果を説明できることを示した。ところが、反陽子ポテンシャルの強さ対する結論は大きく異なっている。テキサス・グループは反陽子のポテンシャルが上記のようなGパリティー変換で求めた深さ700MeV程度の非常に大きいものであったのに対して、ギーセン・グループの結果では深さが100～200MeVとそれほど大きいものではなかった。この違いは核子の感じる平均場に後者が運動量依存性[11, 12]を考慮しているのに対して、前者は考慮していないことから生じており、RBUUの計算に絞るならば後者の方により信頼が得られると言って良いであろう。

このような状況の中で日本のKEK-psグループがもう一つの興味深い実験結果を提示した[13]。このグループは陽子、重陽子、α粒子をビームとして、サブスレシュホールド・エネルギー領域での反陽子生成実験を行いそれらの比較を行った。すると、エネルギーが低くなるに従い、これらのビームを用いた反陽子生成数の違いが大きくなり、3.5GeV/uのビームエネルギーで陽子ビームでの生成数と比較して重陽子ビームの生成数は100倍、αビームではさらに10倍という驚くべき結果を示した。

この結果は当時のRBUUでは説明できるものではなかったが、テキサス側により不利なものであった。というのは、生成スレッシュホールド・エネルギーの大きな低下は、核子反核子対をより簡単に生成するため、生成数がビーム核種の核子数に比例してしまい、陽子入射と重陽子入射の

間の違いが2倍に近い程度の値になってしまうからである。

ところで3.5GeV/uという入射エネルギーは非常に小さいものであり、ポテンシャルの影響が全く無いとすれば、入射核のフェルミ運動を考慮したとしても反陽子を生成するのに十分なものではない。もし、陽子入射に関するスレシュホールド・エネルギーが存在するとすれば、重陽子のスレシュホールド・エネルギーはそれよりもわずかに小さいはずである。ならば、重陽子入射と陽子入射での反陽子生成数の比はそのエネルギーで発散するはずである。このように考えて行くと、KEK-psの実験結果はそれほど不思議なものではなく、入射エネルギー3.5GeVという値が核媒質中での反陽子生成スレシュホールド・エネルギーに近い状態にあることを示していると予想される。

そのような考察に沿って、ここでは、KEK-psの実験結果から逆に反核子ポテンシャルを決定するという試みを行ってみることにした。

計算はRBUU法を用いてRef.[9]と全く方法で行った。重陽子入射に関しては、テスト粒子の空間分布は陽子入射と同じものを用いて、運動量分布のみを現実的な分布になるように設定した。核子の平均場としては、NL6（飽和密度が$\rho_0 = 0.17$fm、束縛エネルギー$BE = 16$MeV、飽和密度での有効質量$M^*/M = 0.65$）を用い、高エネルギー入射核子に関しては$p + A$弾性散乱から求められた平均場の運動量依存性からの寄与も考慮した。また、反核子はベクター場を0とおき、スカラー場を

$$U_s(\bar{N}) = \tilde{c}_s U_s(N) \tag{4}$$

とし、飽和密度で$U_s(\bar{N}) = 0$ (case I)、$U_s(\bar{N}) = 100$ MeV (case II)の2種類のものを用いて両者を比較した。

図1に、Cu標的核に対する入射エネルギー$E_{in} = 3.5, 4.0, 5.0$GeVでの陽子入射（左側）と重陽子入射（右側）における反陽子生成断面積を示した。生成反陽子の散乱方向は0°（実験値は5°である。まず、陽子入射であるが、case Iの計算結果は全体に実験値を下回り、$E_{in} = 3.5$GeV/uでは一個も生成されなかった。これに対して、case IIの結果は実験値をよく再現している。しかしながら、重陽子に関しては両者の違いは非常に小さく、全体に実験値を下回っている。

次に生成反陽子運動量が1.5GeV/cの断面積について陽子入射と重陽子入射での比を計算し、実験値と比較してみよう。図2にその結果を示す。入射エネルギー$E_{in} = 3.5$GeV/uの場合に注目すると、case Iではより高い入射エネルギーですでに発散しており値が存在しないが、case IIでは逆に比が小さすぎる結果となっている。従って、この入射エネルギーでの結果に限るならば飽和密度での反陽子ポテンシャルは

$$U_s(\bar{N}, \rho = \rho_0) < 100\text{MeV} \tag{5}$$

となる。但し,より低いエネルギーではどちらのケースでも実験値を下回っている。

最後にまとめを書くことにする。ここでの仕事では、反核子ポテンシャル等による核子反核子対生成スレシュホールドエネルギーの核媒質内での変化が、KEK-ps実験で得られたp+AとD+Aの大きな差を説明できる可能性を示した。今回の結果では反核子ポテンシャルの飽和密度での深さは100MeV以下であると予想される。ただし、実験結果の入射エネルギー依存性が全て説明

できたわけではなく、ここでの計算の問題は重陽子入射での生成断面積が高いエネルギーで、すでに小さすぎることにある。われわれの結果は入射エネルギー $E_{in} = 5\text{GeV/u}$ での陽子入射と重陽子入射での生成断面積の比が $2-3$ とほぼ核子数の差で説明できる値になっている。Ref.sugaya で、平均場なしの第一機会衝突模型でこ入射のエネルギーでの生成数比がほぼ説明できることが示されている。このことは反陽子ポテンシャルだけではなく核子ポテンシャルの段階ですでに反陽子が生成しやすくなっていることを表している。現在のところ、この問題の解決方法は見出されていない。今後、この改良方法を考えながら最終的な結論にいたりたいと考えている。

参考文献

[1] A.A. Baladin et al., JETP Lett. **48** (1988) 137.

[2] J.B. Carrol et al, Phys. Rev. Lett. **48** (1989) 1829;
A. Shor et al., Phys. Rev. Lett. **63** (1989) 2192.

[3] A. Schroeter et al., Nucl. Phys. **A553** (1993) 775c.

[4] A. Shor et al., Nucl. Phys. **A514** (1990) 717.

[5] G. Batko et al., Phys. Lett. **B256** (1991) 331.

[6] S.W. Huang, G.Q. Li, T. Maruyama and A. Fässler, Nucl. Phys. **A547** (1992) 657.

[7] B. D. Serot and J. D. Walecka, The relativistic Nuclear Many Body Problem. In J. W. Negele and E. Voigt, editors, *Adv.Nucl.Phys.***Vol.16**, page 1, Plenum Press, 1986, and references therein.

[8] K. Soutome, T. Maruyama, K. Saito, Nucl. Phys. **A507** (1990) 731.

[9] S. Teis et al., Phys. Rev. **C50** (1994) 388.

[10] G.Q. Li wt al., Phys. Rev. **C49** (1994) 1139.

[11] K. Weber, et al., Nucl. Phys. **A539** (1992) 713.

[12] T. Maruyama et al., Nucl. Phys. **A573** (1994) 653.

[13] Y. Sugaya et al., Nucl. Phys. **A634** (1998) 115.

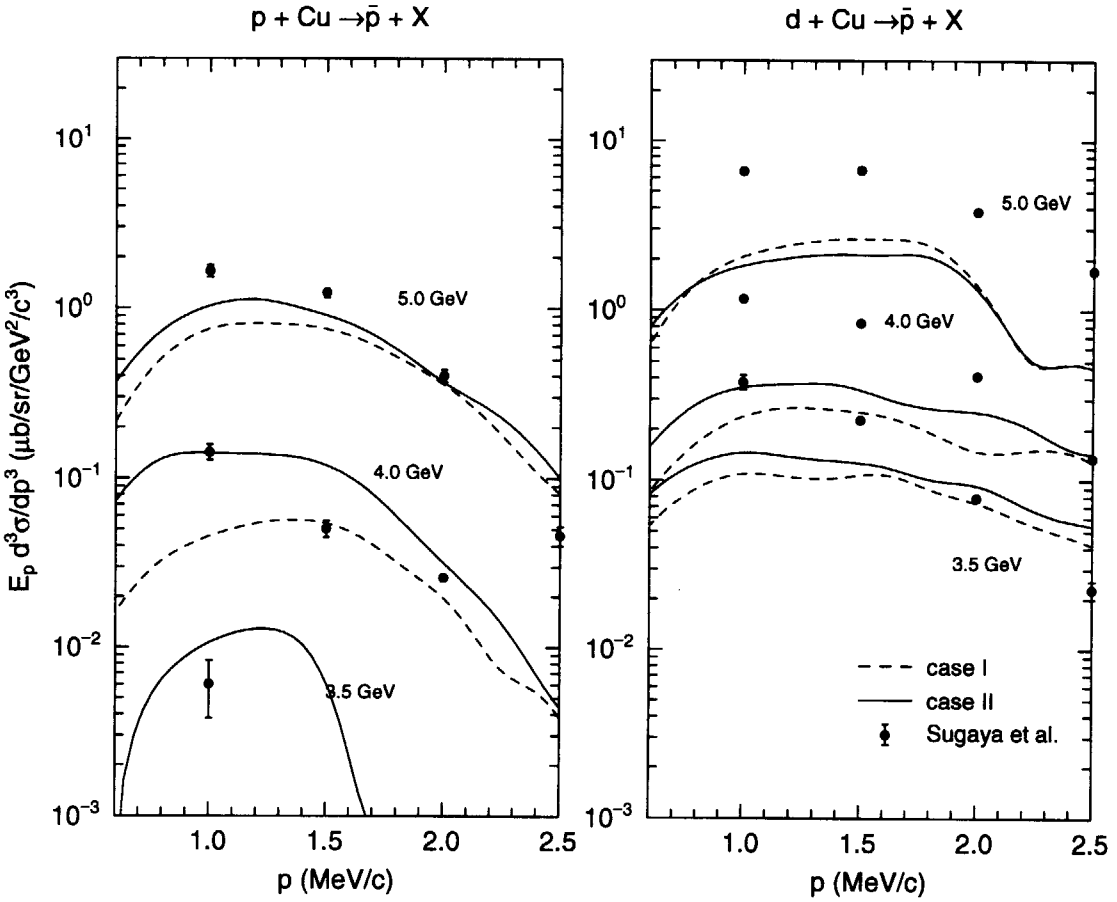

図 1: 陽子入射（左側）、重陽子入射（右側）における入射エネルギー 5.0, 4.0, 3.5 GeV/u での反陽子生成断面積。破線、実線は、それぞれ case I、case II の計算結果を、四角は実験結果を表す。

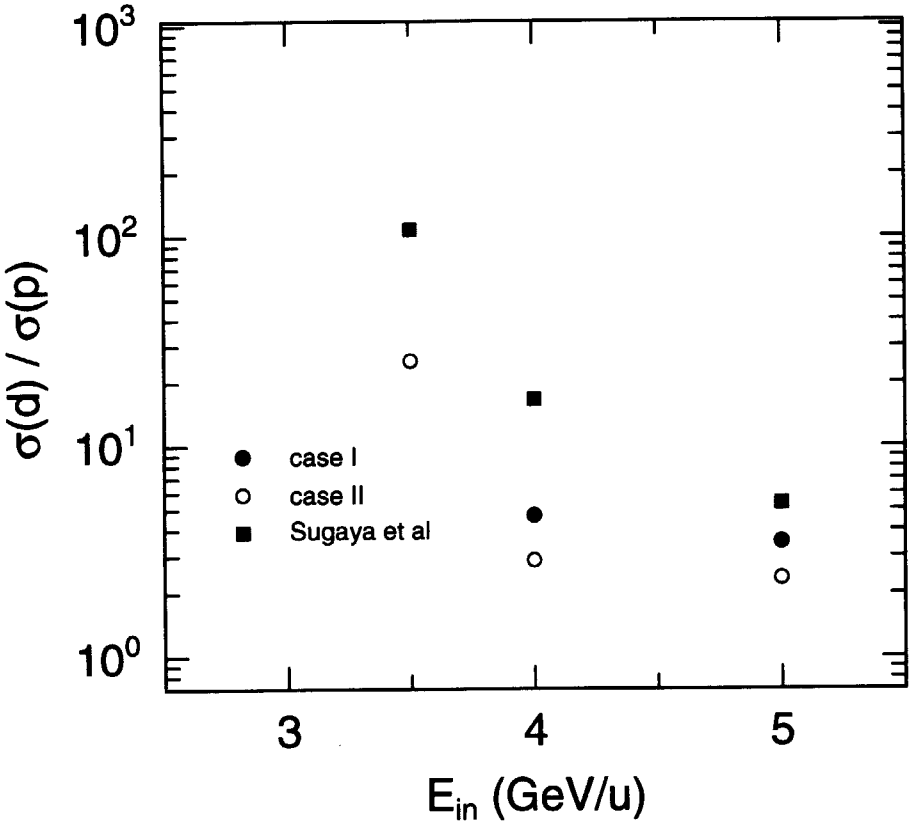

図 2: 運動量が 1.5GeV/c での生成反陽子の断面積陽子入射（左側）、重陽子入射（右側）の比を入射エネルギー依存の形で示した。白丸と黒丸丸はそれぞれ case I と case II の結果を表す。四角は実験結果。入射エネルギー 3.5 GeV/u では case I の計算結果は発散している。

27. Bound states of negative-energy nucleons in finite nuclei

G. Mao, H. Stöcker, and W. Greiner
Institut für Theoretische Physik der J. W. Goethe-Universität
Postfach 11 19 32, D-60054 Frankfurt am Main, Germany

We study the bound states of negative-energy nucleons in finite nuclei within the relativistic Hartree approach including the contributions of the Dirac sea to the source terms of the meson fields. The Dirac equations for the nucleon and the anti-nucleon are solved simultaneously. The single-particle energies of negative-energy nucleons are obtained through changing the sign of the single-particle energies of positive-energy anti-nucleons. Numerical results show that the bound levels of negative-energy nucleons vary drastically when the vacuum contributions are taken into account.

In spite of the great successes of the relativistic mean field (RMF) theory [1–4] and the relativistic Hartree approach (RHA) [5,6] in describing the ground states of nuclei, the arguments of introduction of strong Lorentz scalar (S) and time-component Lorentz vector (V) potential in the Dirac equation are largely indirect. So far, no evidence from experiments ensures the physical necessity. One usually compares the theoretical predictions only with the experimental data of the positive-energy sector, which is subject to a relatively small quantity stemming from the cancellation of two potentials $S+V$ (V is positive, S is negative.). While the dynamical content of the Dirac picture certainly lies with both the positive- and negative-energy sector, the study of the negative-energy sector enjoys an additional bonus: it provides us with a chance to determine the individual S and V! Due to the *G-parity*, the vector potential changes its sign in the negative-energy sector. The bound states of negative energy are sensitive to the sum of the scalar and vector field $S - V$. Combining with the information from the positive-energy sector, one may fix the individual values of the scalar and vector field.

The study of the negative-energy sector is extremely interesting for modern nuclear physics. If the potential of negative-energy nucleons is much weaker than what one expects or predicts by means of the RMF/RHA models, that is, the strong scalar and vector field are not necessary, one may question the validity of the models since some important physical ingredients, such as quantum corrections, correlation effects, three-body forces et al., are still missing in these phenomenological approaches. One may think about constituting a more elaborate model. Alternatively, if a deep potential of negative-energy nucleons is indeed observed, that is, the strong scalar and vector potentials are realistic, an interesting phenomena is that at certain density the negative energy of nucleons may turn out to be larger than the free nucleon mass, the system becomes unstable with respect to the nucleon–anti-nucleon pair creation [7]. On the other hand, as pointed out in Ref. [8], in high-energy relativistic heavy-ion collisions, the nucleons may be emitted from the deep bound states of negative energy due to dynamics. These can create a great number of nucleon-holes (i.e., anti-nucleons) in bound states. Such collective creation processes of anti-matter clusters have a large probability for the production of anti-nuclei, – and analogously also for multi-Λ, multi-$\bar{\Lambda}$ nuclei. These open two fascinating directions to extend the periodic system, i.e., to extend into the negative sector and into the multi-strangeness dimension, in addition to the islands of super-heavy nuclei. In order to reach the quantitative study of the above theoretical conjecture, a prerequisite is to know the exact potential depth of the bound states of negative energy. Up to now, no answers from experimental side or theoretical side are available.

We study the problem within the relativistic Hartree approach including the vacuum contributions. The starting point is the following effective Lagrangian for nucleons interacting through the exchange of mesons [1-3]

$$\begin{aligned}\mathcal{L} = &\bar{\psi}[i\gamma_\mu\partial^\mu - M_N]\psi + \frac{1}{2}\partial_\mu\sigma\partial^\mu\sigma - U(\sigma) \\ &-\frac{1}{4}\omega_{\mu\nu}\omega^{\mu\nu} + \frac{1}{2}m_\omega^2\omega_\mu\omega^\mu - \frac{1}{4}\mathbf{R}_{\mu\nu}\mathbf{R}^{\mu\nu} \\ &+\frac{1}{2}m_\rho^2\mathbf{R}_\mu\cdot\mathbf{R}^\mu - \frac{1}{4}A_{\mu\nu}A^{\mu\nu} + \mathrm{g}_\sigma\bar{\psi}\psi\sigma \\ &-\mathrm{g}_\omega\bar{\psi}\gamma_\mu\psi\omega^\mu - \frac{1}{2}\mathrm{g}_\rho\bar{\psi}\gamma_\mu\boldsymbol{\tau}\cdot\psi\mathbf{R}^\mu \\ &-\frac{1}{2}e\bar{\psi}(1+\tau_0)\gamma_\mu\psi A^\mu, \qquad (1)\end{aligned}$$

here U(σ) is the self-interaction part of the scalar field

$$U(\sigma) = \frac{1}{2}m_\sigma^2\sigma^2 + \frac{1}{3}b\sigma^3 + \frac{1}{4}c\sigma^4. \qquad (2)$$

Based on this Lagrangian, we have developed a relativistic model describing the bound states of negative energy in finite nuclei [9]. Instead of searching for the negative-energy solution of the nucleon's Dirac equation, we solve the Dirac equations for the nucleon and the anti-nucleon simultaneously. For each equation we look for only one solution, that is, the positive-energy solution. The single-particle energies of negative-energy nucleons are obtained through changing the sign of the single-particle energies of positive-energy anti-nucleons. The contributions of the Dirac sea to the source terms of the meson fields are evaluated by means of the derivative expansion [10] up to the leading derivative order for the one-meson loop and one-nucleon loop. Thus, the wave functions of anti-nucleons, which are used to calculate the single-particle energies, are not involved in evaluating the vacuum contributions to the scalar and baryon density which are, in turn, expressed by means of the scalar and vector field as well as their derivative terms [9]. The Dirac equation of the nucleon and the equations of motion of mesons (containing the densities contributed from the vacuum) are solved within a self-consistent iteration procedure [2]. Then, the Dirac equation of the anti-nucleon is solved with the known mean fields to obtain the wave functions and the single-particle energies of anti-nucleons. The space of anti-nucleons are truncated by the specified principal and angular quantum numbers n and j with the guarantee that the calculated single-particle energies of anti-nucleons are converged when the truncated space is extended.

TABLE I. Parameters of the RMF and the RHA models as well as the corresponding saturation properties.

	RMF		RHA	
	LIN	NL1	RHA0	RHA1
M_N (MeV)	938.000	938.000	938.000	938.000
m_σ (MeV)	615.000	492.250	615.000	458.000
m_ω (MeV)	1008.00	795.359	916.502	816.508
m_ρ (MeV)	763.000	763.000	763.000	763.000
g_σ	12.3342	10.1377	9.9362	7.1031
g_ω	17.6188	13.2846	11.8188	8.8496
g_ρ	10.3782	9.9514	10.0254	10.2070
b (fm^{-1})	0.0	12.1724	0.0	12.0435
c	0.0	−36.2646	0.0	−2.6656
ρ_0 (fm^{-3})	0.1525	0.1518	0.1513	0.1524
E/A (MeV)	−17.03	−16.43	−17.39	−16.98
m^*/M_N	0.533	0.572	0.725	0.788
K (MeV)	580	212	480	294
a_4 (MeV)	46.8	43.6	40.4	40.4

In the previous RHA calculations for the bound states of positive energy [5,6], the parameters of the model are fitted to the saturation properties of nuclear matter as well as the *rms* charge radius in ^{40}Ca. The *best-fit* routine within the RHA to the properties of spherical nuclei has not been performed yet. Thus, we first fit the parameters of Eqs. (1) and (2) within the RHA to the empirical data of binding energy, surface thickness and diffraction radius of eight spherical nuclei ^{16}O, ^{40}Ca, ^{48}Ca, ^{58}Ni, ^{90}Zr, ^{116}Sn, ^{124}Sn, and ^{208}Pb as has been done in Ref. [2] for the RMF model. We distinguish two different cases with (RHA1) and without (RHA0) nonlinear self-interaction of the

scalar field. The obtained parameters and the corresponding saturation properties are given in Table I. For the sake of comparison, two sets of the linear (LIN) and nonlinear (NL1) RMF parameters from Ref. [2] are also presented. One can see that the RHA gives a larger effective nucleon mass than the RMF does, which is mainly caused by the feedback of the vacuum to the meson fields, as can be seen from Eqs. (71) ~ (74) of Ref. [9]. When the effective nucleon mass decreases, the scalar density originated from the Dirac sea ρ_S^{sea} increases. It is negative and cancels part of the scalar density contributed from the valence nucleons ρ_S^{val}, which causes the effective nucleon mass to increase again. At the end, it reaches a balance value. In the fitting procedure, we have tried different initial values giving smaller effective nucleon mass. After running the code many times, all of them slowly converge to a large m^*.

In Table II we present the results of both positive- and negative-energy spectra of ^{16}O, ^{40}Ca and ^{208}Pb. The binding energy per nucleon and the *rms* charge radius are given too. The numerical calculations are performed within two frameworks, i.e., the RHA including the contributions of the negative-energy sector to the source terms of the meson fields and the RMF taking into account only the valence nucleons as the meson-field sources. The experimental data are taken from Ref. [11]. From the table one can see that all four sets of parameters can reproduce the empirical values of the binding energies, the *rms* charge radii and the single-particle energies of positive-energy proton states fairly well. For the E/A and the r_{ch}, the agreement between the theoretical predictions and the experimental data are improved from the LIN to the RHA0, RHA1 and NL1 set of parameters. For the spectra of positive-energy protons, due to large error bars, it seems to be difficult to queue up the different sets of parameters. However, because of the large effective nucleon mass, the RHA has smaller spin-orbit splitting (see $1p_{1/2}$ and $1p_{3/2}$ state) compared to the RMF. This situation can be improved through introducing a tensor coupling for the ω meson [2] which will be investigated in the future studies. For the negative-energy sector, no experimental

TABLE II. The single-particle energies of both positive- and negative-energy protons as well as the binding energy per nucleon and the *rms* charge radius in ^{16}O, ^{40}Ca and ^{208}Pb.

	RMF		RHA		
	LIN	NL1	RHA0	RHA1	EXP.
^{16}O					
E/A (MeV)	7.80	8.00	8.01	8.00	7.98
r_{ch} (fm)	2.59	2.73	2.62	2.66	2.74
POS. ENE.					
$1s_{1/2}$ (MeV)	42.99	36.18	32.21	30.68	40±8
$1p_{3/2}$ (MeV)	20.71	17.31	16.09	15.23	18.4
$1p_{1/2}$ (MeV)	10.85	11.32	12.98	13.24	12.1
NEG. ENE.					
$1\bar{s}_{1/2}$ (MeV)	821.30	674.11	413.62	299.42	
$1\bar{p}_{3/2}$ (MeV)	754.62	604.70	369.78	258.40	
$1\bar{p}_{1/2}$ (MeV)	755.43	605.77	370.36	258.93	
^{40}Ca					
E/A (MeV)	8.38	8.58	8.65	8.73	8.55
r_{ch} (fm)	3.36	3.48	3.39	3.42	3.45
POS. ENE.					
$1s_{1/2}$ (MeV)	51.21	46.86	38.64	36.58	50±11
$1p_{3/2}$ (MeV)	35.05	30.15	27.11	25.32	
$1p_{1/2}$ (MeV)	29.25	25.11	25.17	24.03	34±6
NEG. ENE.					
$1\bar{s}_{1/2}$ (MeV)	840.76	796.09	456.58	339.83	
$1\bar{p}_{3/2}$ (MeV)	792.36	706.36	424.85	309.24	
$1\bar{p}_{1/2}$ (MeV)	792.75	707.86	425.14	309.52	
^{208}Pb					
E/A (MeV)	7.83	7.89	7.96	7.93	7.87
r_{ch} (fm)	5.34	5.52	5.43	5.49	5.50
POS. ENE.					
$1s_{1/2}$ (MeV)	58.71	50.41	44.43	40.80	
$1p_{3/2}$ (MeV)	52.74	44.45	39.87	36.45	
$1p_{1/2}$ (MeV)	51.83	43.75	39.49	36.21	
NEG. ENE.					
$1\bar{s}_{1/2}$ (MeV)	830.16	717.01	476.61	354.18	
$1\bar{p}_{3/2}$ (MeV)	819.15	705.20	466.08	344.48	
$1\bar{p}_{1/2}$ (MeV)	819.22	705.28	466.13	344.52	

data are available. In all four cases, the potential of negative-energy nucleons is much deeper than the potential of positive-energy nucleons. On the other hand, one can notice the drastic difference between the RHA and the RMF calculations – the single-particle energies calculated from the RHA are about half of that from the RMF, exhibiting the importance of taking into account the Dirac sea effects. It demonstrates that the negative-energy spectra deserve a sensitive probe to the effective interactions. The spin-orbit splitting of negative-energy sector is so small that one nearly can not distinguish the $1\bar{p}_{1/2}$ and the $1\bar{p}_{3/2}$ state. This is because the spin-orbit potential is related to $d(S+V)/dr$ in the negative-energy sector and two fields cancel each other to a large extent. Nevertheless, the space between the $1\bar{s}$ and the $1\bar{p}$ state is still evident, especially for lighter nuclei. This might be helpful to separate the process of knocking out a $1\bar{s}_{1/2}$ negative-energy nucleon from the background – a promising way to measure the potential of the anti-nucleon in laboratory.

In summary, we have proposed to study the bound states of negative-energy sector which will provide us with a chance to judge the physical necessity of introducing strong scalar and vector potential in the Dirac picture. Due to the feedback of the vacuum to the meson fields, the scalar and vector fields decrease in the RHA. Numerical calculations show that the single-particle energies of negative-energy nucleons change drastically for the RMF and the RHA with different sets of parameters, while the single-particle energies of positive-energy nucleons remain in reasonable range. It is very important to have experimental data to check the theoretical predicted bound levels of negative energy. If the Dirac picture with the large potentials is valid for nucleon-nucleus interactions, a fascinating direction of future studies is to investigate the vacuum correlation and the collective production of the anti-nuclei in relativistic heavy-ion collisions. Experimental efforts in this direction are presently underway [12].

The authors thank P.-G. Reinhard, Zhongzhou Ren, J. Schaffner-Bielich, and C. Beckmann for stimulating discussions. G. Mao acknowledges the people at the Institut für Theoretische Physik der J. W. Goethe Universität for their hospitality. This work was supported by DFG-Graduiertenkolleg Theoretische und Experimentelle Schwerionenphysik, GSI, BMBF, DFG.

[1] B. D. Serot and J. D. Walecka, Adv. Nucl. Phys. **16**, 1 (1986).

[2] P.-G. Reinhard, M. Rufa, J. Maruhn, W. Greiner, J. Friedrich, Z. Phys. **A323**, 13 (1986); M. Rufa, P.-G. Reinhard, J.A. Maruhn, W. Greiner, M.R. Strayer, Phys. Rev. **C38**, 390 (1988).

[3] Y.K. Gambhir, P. Ring and A. Thimet, Ann. Phys. **198**, 132 (1990).

[4] Zhongzhou Ren, Z.Y. Zhu, Y.H. Cai, Gongou Xu, Phys. Lett. **B380**, 241 (1996).

[5] C.J. Horowitz and B.D. Serot, Phys. Lett. **B140**, 181 (1984).

[6] R.J. Furnstahl and C.E. Price, Phys. Rev. **C40**, 1398 (1989); Phys. Rev. **C41**, 1792 (1990).

[7] I.N. Mishustin, L.M. Satarov, J. Schaffner, H. Stöcker and W. Greiner, J. Phys. G: Nucl. Part. Phys. **19**, 1303 (1993).

[8] W. Greiner, Heavy Ion Physics **2**, 23 (1995).

[9] G. Mao, H. Stöcker, and W. Greiner, Int. J. Mod. Phys. **E8**, 389 (1999).

[10] I.J.R. Aitchison and C.M. Fraser, Phys. Lett. **B146**, 63 (1984); O. Cheyette, Phys. Rev. Lett. **55**, 2394 (1985); C.M. Fraser, Z. Phys. **C28**, 101 (1985); L.H. Chan, Phys. Rev. Lett. **54**, 1222 (1985).

[11] J.H.E. Mattauch, W. Thiele, and A.H. Wapstra, Nucl. Phys. **67**, 1 (1965); D. Vautherin and D.M. Brink, Phys. Rev. **C5**, 626 (1972); H. de Vries, C.W. de Jager, and C. de Vries. At. Data Nucl. Data Tables **36**, 495 (1987).

[12] R. Arsenescu and the NA52 collaboration, J. Phys. **G25**, 225 (1999).

国際単位系（SI）と換算表

表1　SI基本単位および補助単位

量	名称	記号
長さ	メートル	m
質量	キログラム	kg
時間	秒	s
電流	アンペア	A
熱力学温度	ケルビン	K
物質量	モル	mol
光度	カンデラ	cd
平面角	ラジアン	rad
立体角	ステラジアン	sr

表2　SIと併用される単位

名称	記号
分，時，日	min，h，d
度，分，秒	°，′，″
リットル	l，L
トン	t
電子ボルト	eV
原子質量単位	u

1 eV=1.60218×10^{-19}J

1 u=1.66054×10^{-27}kg

表3　固有の名称をもつSI組立単位

量	名称	記号	他のSI単位による表現
周波数	ヘルツ	Hz	s^{-1}
力	ニュートン	N	m·kg/s^2
圧力，応力	パスカル	Pa	N/m^2
エネルギー，仕事，熱量	ジュール	J	N·m
工率，放射束	ワット	W	J/s
電気量，電荷	クーロン	C	A·s
電位，電圧，起電力	ボルト	V	W/A
静電容量	ファラド	F	C/V
電気抵抗	オーム	Ω	V/A
コンダクタンス	ジーメンス	S	A/V
磁束	ウェーバ	Wb	V·s
磁束密度	テスラ	T	Wb/m^2
インダクタンス	ヘンリー	H	Wb/A
セルシウス温度	セルシウス度	℃	
光束	ルーメン	lm	cd·sr
照度	ルクス	lx	lm/m^2
放射能	ベクレル	Bq	s^{-1}
吸収線量	グレイ	Gy	J/kg
線量等量	シーベルト	Sv	J/kg

表4　SIと共に暫定的に維持される単位

名称	記号
オングストローム	Å
バーン	b
バール	bar
ガル	Gal
キュリー	Ci
レントゲン	R
ラド	rad
レム	rem

1 Å=0.1nm=10^{-10}m

1 b=100fm^2=10^{-28}m^2

1 bar=0.1MPa=10^{5}Pa

1 Gal=1cm/s^2=10^{-2}m/s^2

1 Ci=3.7×10^{10}Bq

1 R=2.58×10^{-4}C/kg

1 rad=1cGy=10^{-2}Gy

1 rem=1cSv=10^{-2}Sv

表5　SI接頭語

倍数	接頭語	記号
10^{18}	エクサ	E
10^{15}	ペタ	P
10^{12}	テラ	T
10^{9}	ギガ	G
10^{6}	メガ	M
10^{3}	キロ	k
10^{2}	ヘクト	h
10^{1}	デカ	da
10^{-1}	デシ	d
10^{-2}	センチ	c
10^{-3}	ミリ	m
10^{-6}	マイクロ	μ
10^{-9}	ナノ	n
10^{-12}	ピコ	p
10^{-15}	フェムト	f
10^{-18}	アト	a

（注）

1．表1－5は「国際単位系」第5版，国際度量衡局1985年刊行による。ただし，1 eVおよび1 uの値はCODATAの1986年推奨値によった。

2．表4には海里，ノット，アール，ヘクタールも含まれているが日常の単位なのでここでは省略した。

3．barは，JISでは流体の圧力を表わす場合に限り表2のカテゴリーに分類されている。

4．EC閣僚理事会指令ではbar，barnおよび「血圧の単位」mmHgを表2のカテゴリーに入れている。

換算表

力	N(=10^{5}dyn)	kgf	lbf
	1	0.101972	0.224809
	9.80665	1	2.20462
	4.44822	0.453592	1

粘度　1Pa·s(N·s/m^2)=10 P(ポアズ)(g/(cm·s))

動粘度　1m^2/s=10^{4}St(ストークス)(cm^2/s)

圧力	MPa(=10bar)	kgf/cm^2	atm	mmHg(Torr)	lbf/in^2(psi)
	1	10.1972	9.86923	7.50062×10^3	145.038
	0.0980665	1	0.967841	735.559	14.2233
	0.101325	1.03323	1	760	14.6959
	1.33322×10^{-3}	1.35951×10^{-3}	1.31579×10^{-3}	1	1.93368×10^{-2}
	6.89476×10^{-3}	7.03070×10^{-2}	6.80460×10^{-2}	51.7149	1

エネルギー・仕事・熱量	J(=10^7 erg)	kgf·m	kW·h	cal(計量法)	Btu	ft·lbf	eV
	1	0.101972	2.77778×10^{-7}	0.238889	9.47813×10^{-4}	0.737562	6.24150×10^{18}
	9.80665	1	2.72407×10^{-6}	2.34270	9.29487×10^{-3}	7.23301	6.12082×10^{19}
	3.6×10^6	3.67098×10^5	1	8.59999×10^5	3412.13	2.65522×10^6	2.24694×10^{25}
	4.18605	0.426858	1.16279×10^{-6}	1	3.96759×10^{-3}	3.08747	2.61272×10^{19}
	1055.06	107.586	2.93072×10^{-4}	252.042	1	778.172	6.58515×10^{21}
	1.35582	0.138255	3.76616×10^{-7}	0.323890	1.28506×10^{-3}	1	8.46233×10^{18}
	1.60218×10^{-19}	1.63377×10^{-20}	4.45050×10^{-26}	3.82743×10^{-20}	1.51857×10^{-22}	1.18171×10^{-19}	1

1 cal= 4.18605J（計量法）

= 4.184J（熱化学）

= 4.1855J（15℃）

= 4.1868J（国際蒸気表）

仕事率　1 PS(仏馬力)

= 75 kgf·m/s

= 735.499W

放射能	Bq	Ci
	1	2.70270×10^{-11}
	3.7×10^{10}	1

吸収線量	Gy	rad
	1	100
	0.01	1

照射線量	C/kg	R
	1	3876
	2.58×10^{-4}	1

線量当量	Sv	rem
	1	100
	0.01	1

（86年12月26日現在）

PROCEEDINGS OF THE SYMPOSIUM ON FRONTIER NUCLEAR PHYSICS (FRONP99) AUGUST 2–4, 1999, JAERI, TOKAI, JAPAN